November 2012

Determining the Impact of Climate Change on Insurance Risk and the Global Community

Phase I: Key Climate Indicators

Sponsored by:

American Academy of Actuaries' Property/Casualty Extreme Events Committee
Casualty Actuarial Society
Canadian Institute of Actuaries
Society of Actuaries

Prepared by

Solterra Solutions
www.solterrasolutions.com

Foreword

How climate change will affect society is a complex question, and the answer depends on the temporal and spatial scales over which one is concerned, the entities of interest, judgment criteria, and the desired level of certainty. Assessing the potential impacts of climate change on insurance is similarly complex. In addition, climate change—given its potential for systemic impact—can dramatically alter the risk management landscape. The Casualty Actuarial Society, Canadian Institute of Actuaries, Society of Actuaries, and the American Academy of Actuaries' Property/Casualty Extreme Events Committee have responded to this emerging risk by collaboratively commissioning committees to recommend, support, and perform research on climate change and assess the potential risk management implications for the insurance industry.

To paraphrase the CAS definition of an actuary, he/she is a professional skilled in the analysis, evaluation, and management of the financial implications of future contingent events and as such has practical knowledge of how these various risks interact with each other and the environment in which these risks occur. As actuaries, our key roles as risk advisors require us to be knowledgeable in many complex areas. Our professional societies hold a commitment to contribute to the well being of society as a whole, and are dedicated to research, education, and advancing the profession. With these considerations in mind, it becomes our professional responsibility to understand the latest in climate change science and develop actuarially sound approaches to managing the potential implications of climate change risk factors. This means that we need to engage in interdisciplinary communications and contribute to discussions about risks to society associated with climate change. Once we have recognized the issues associated with climate change, we can begin to evaluate and quantify these risks as they pertain to our individual industries and businesses. Climate change, by definition, affects society's key resource base, the environment. The broad consensus of climate scientists on the nature and scope of climate change implies that there could be serious impacts on our industry, affecting each sector in different ways, at different spatial and temporal scales, and of varying financial magnitudes.

The CAS Climate Change Committee is the parent committee of the Climate Index Working Group (CIWG). The report that follows is the product of Phase I of the work, which was commissioned by the actuarial organizations and prepared by Solterra Solutions, with input from the CIWG. Phase I is a synthesis of a vast and rapidly growing body of scientific knowledge on climate change with a focus on potential impacts to society and the insurance industry. The CIWG fostered collaboration among the representatives of the various actuarial societies and the climate scientists at Solterra Solutions to create the current report. The actuaries in the working group are grateful for the extensive education Solterra Solutions patiently provided to us on the current state of climate change science and for their diligence in creating a comprehensive literature survey of the science. As a group, we have integrated ideas, established common ground, and educated one another on our areas of expertise and primary questions of concern to produce this report. It is our hope that this research better positions us as actuaries to fulfill our missions.

The Climate Index Working Group: Doug Collins, Tanya Havlicek, Caterina Lindman, Vijay Manghnani, Jason Pessel, Ronora Stryker

Table of Contents

Executive Summary

Since 2005, severe weather and climatological events accounted for 85% to 90% of natural hazards resulting in claims of property damage or personal injury, according to global totals (Munich Re, 2012). Prompted by evidence of recent increases in damages due to such events and longer-term climate trends, this report presents a summary of the most recent data from the area of climate change research. This effort is intended to inform both the worldwide community of actuaries, business leaders, and the general public of the weight of scientific evidence regarding the Earth's climate and the changes it is undergoing.

Scientists studying the Earth's climate system, which encompasses the entirety of the atmosphere, land surface and oceans, have developed a sophisticated understanding of how this system operates and varies over a wide range of time scales. Over the last several decades, these researchers[1] have discovered that additional changes are occurring, on both regional and global scales that exceed what is to be expected from natural climate variability alone. In the case of surface air temperature, this phenomenon has come to be known as *global warming*, but similar directional changes have been measured for many other climate variables, including ocean temperature, sea level, precipitation, sea ice extent and thickness, soil moisture, and others. The main changes that have occurred, synthesized from a large body of long-term data published in peer-reviewed scientific publications, are the following:

- *Global mean surface temperatures have risen by three-quarters of a degree Celsius (1.3 degrees Fahrenheit) over the last 100 years (1906–2005). Further, the rate of warming over the last 50 years is almost double that over the last 100 years.*
- *The 16 warmest years on record occurred in the 17-year period from 1995 to 2011.*
- *Land regions have warmed at a faster rate than the oceans, which is consistent with the known slower rate of heat absorption by seawater.*
- *Average Arctic temperatures increased at almost twice the global average rate in the past 100 years.*
- *The thickness and areal extent of Northern Hemisphere snow cover and Arctic sea ice has decreased steadily over the last 30 years, in response to this enhanced polar warming. The last decade (2002-2011) contains the 9 lowest recorded extents of annual minimum Arctic sea ice. 2012 is presently tracking at record low levels.*

[1] Anderegg et al (2010) examined a database of 1,372 climate researchers to reveal that: i) 97-98% supported the United Nations Intergovernmental Panel on Climate Change (IPCC) 4th Assessment Report finding that most of the warming observed over the latter part of the 20th century was a consequence of human activities; ii) Those researchers who disagreed with this notion had a significantly lower scientific expertise and prominence as measured by their total number of climate publications and the times these publications were cited by other researchers.

- *The area of glaciers has been decreasing worldwide since the 1960s, as has the thickness of the vast Greenland and Antarctic ice sheets over the past two decades.*

- *Global average sea level has been rising at a rate of approximately 3 mm (1/8") per year over the past two decades. About half of this rise is due to the expanded volume of sea water under increased temperatures, and the other half to the melting of land ice.*

- *Regionally, changes in climate variables can be significantly higher or lower than the global average. To give two examples relating to sea-level rise (SLR): (1) in the Southwestern Pacific Ocean, home to numerous low-lying island communities, the rate of SLR is almost 4 times the global mean value; and (2) at two-thirds of measurement stations along the continental shores of the United States, SLR has led to a doubling in the annual risk of what were considered "once-in-a-century" or worse floods.*

- *Clear evidence has emerged that ecosystems are responding to strong regional warming, e.g., with leaf onset and fruit ripening shifting to earlier in the year and bird and insect populations shifting their ranges poleward.*

- *Over the past five decades, the frequency of abnormally warm nights has increased, and that of cold nights decreased, at most locations on land. Further, the fraction of global land area experiencing extremely hot summertime temperatures has increased approximately ten-fold over the same period.*

- *A significant increase in the frequency of heavy precipitation events has been observed in the majority of locations where data are available, and particularly in the eastern half of North America and Northern Europe, where there is a long record of observations.*

Climate experts explain the global warming phenomenon using scientific principles relating to the Earth's thermal balance and the known history of greenhouse gas amounts in the atmosphere. This has allowed independent simulation of these characteristics using complex computer models of the climate system, driven by the known history of industrial emissions of these gases. These models successfully reproduce the observed features of historical climate change noted above. This has prompted an exploration of possible future states of the climate system, using the same models driven by various industrial emissions scenarios based on assumptions of socio-economic variables such as population, economic policies, and technological development. Broadly speaking, global climate models project a continuation of the above historical trends in climate variables, including the following:

- *A larger increase in temperature over land than over ocean, and in polar regions compared to lower latitudes.*

- *Continuing or accelerating losses of ice and snow over ocean and land.*

- *An overall strengthening of the hydrological cycle, leading to precipitation increases at mid-to-high latitudes and decreases in low latitudes.*

- *An increase in the frequency of hot extremes worldwide, and increased frequency of drought in normally dry regions and extreme rainfall/flooding in normally wet regions.*

- *A slight decrease in the frequency of tropical cyclones, but an increase in their average intensity and destructive potential.*

The implications of these wide-ranging and rapid changes in climate for human populations, their economic and societal structures, and the ecosystems on which they depend are an object of concern, and several examples of such impacts are detailed in the report. Moreover, there is a perceived need to quantify the risk posed by a changing climate to human health and capital, an area traditionally the domain of insurers and actuaries. By making use of the detailed climate observations of the past century, simplified representations of the changes in many climate variables can be formulated. These are referred to as *climate indices*. The report presents numerous examples of such indices, with the main conclusions:

- *Various indices can be constructed, using either observed data or model projections, which adequately reflect changes in the underlying climate variable(s).*

- *A composite index, carrying information from many individual climate variables and standardized with respect to climate variability, can be formulated which would suit the needs of both actuaries and the public at large. This is termed the Actuaries Climate Change Index™, or ACCI™ for short.*

- *Such an index could carry information regarding the occurrence of climate extremes, as well as more gradual changes in mean quantities.*

- *The index could be calculated on individual regions of interest, provided sufficient high-quality data are available.*

- *Finally, with the addition of socioeconomic data, the ACCI can form the basis of a more targeted index that reflects the risk to populations and capital due to climate change (the Actuaries Climate Risk Index™, or ACRI™).*

1. Introduction: Extreme Weather, Climate Science and Societal Context

Determining the Impact of Climate Change on Insurance Risk and the Global Community–Phase I responds to a request from the American Academy of Actuaries' Property/Casualty Extreme Events Committee, the Canadian Institute of Actuaries (CIA), the Casualty Actuarial Society (CAS), and the Society of Actuaries (SOA) to synthesize the extensive and rapidly growing body of knowledge on climate and climate change as it relates to possible impacts on human society. While human-induced climate change is driven largely by global agents, referred to as climate forcings—primarily increases in carbon dioxide, other greenhouse gases, and sulfate aerosols emitted by industrial activity—it is the regional/local response to these forcings that may adversely affect quality of life, including morbidity and mortality (interconnections between regions may present further challenges). Specifically, an insurer might be interested in reducing exposure and risk to claims associated with changes in the statistics of extreme weather, which are expected to occur under global warming.

This report provides a review of the most current published scientific research in a number of specific areas, namely:

(1) Worldwide temperature and precipitation trends
(2) Temperature and precipitation extremes, including heat waves and floods
(3) Arctic sea ice, snow cover and permafrost degradation
(4) Changes in land-based glaciers
(5) Sea-level rise
(6) Wildfires and pest outbreaks
(7) Hurricane intensity and frequency, including storm surges
(8) Droughts

This review is intended to lay the foundation for the development of an Actuaries Climate Change Index (ACCI). The goal of such an index is threefold: first, to summarize in a quantitative and most succinct manner possible the vast amount of research that has emerged on the above topics; second, to assist policymakers, risk professionals, and the public at large in managing the potential impacts of climate change; and third, to form the basis of a more targeted index that illustrates the specific risks of climate change to the insurance sector.

We first introduce the report by discussing the links between natural disasters, weather, and climate-related disasters, and the insurance industry. After discussing the difference between weather and climate, we discuss the scientific method, and the concept of scientific uncertainty as it relates to climate change. We note that an individual's personal experience with weather events (as opposed to climate) is important evidence supporting their belief in global warming. Since we will be extensively referring to the assessment reports produced by the Intergovernmental Panel on Climate Change, we provide a brief discussion of its mandate. Finally, we close by reviewing the goals of the present report.

1.1 Natural disasters and the insurance industry

In 2011, a record $380 billion worth of economic losses ($105 billion of insured losses) occurred worldwide as a consequence of natural disasters, shattering the previous record of $220 billion set in 2005 (Munich Re, 2012)[1]. While 61% (~$230 billion) of these losses occurred as a consequence of geophysical events (including the most economically costly natural disaster ever—the $200 billion Japan earthquake/tsunami on March 11, 2011), severe weather and climatological events accounted for nearly $150 billion. These included flooding in Thailand ($40 billion), US ($4.6 billion), Australia ($2.8 billion), multiple storm/tornado events in the US (>$32.5 billion), drought in the southern US, ($8 billion), and Hurricane Irene, whose damage was spread across Canada, the US and a number of Caribbean islands (**Figure 1.1**).

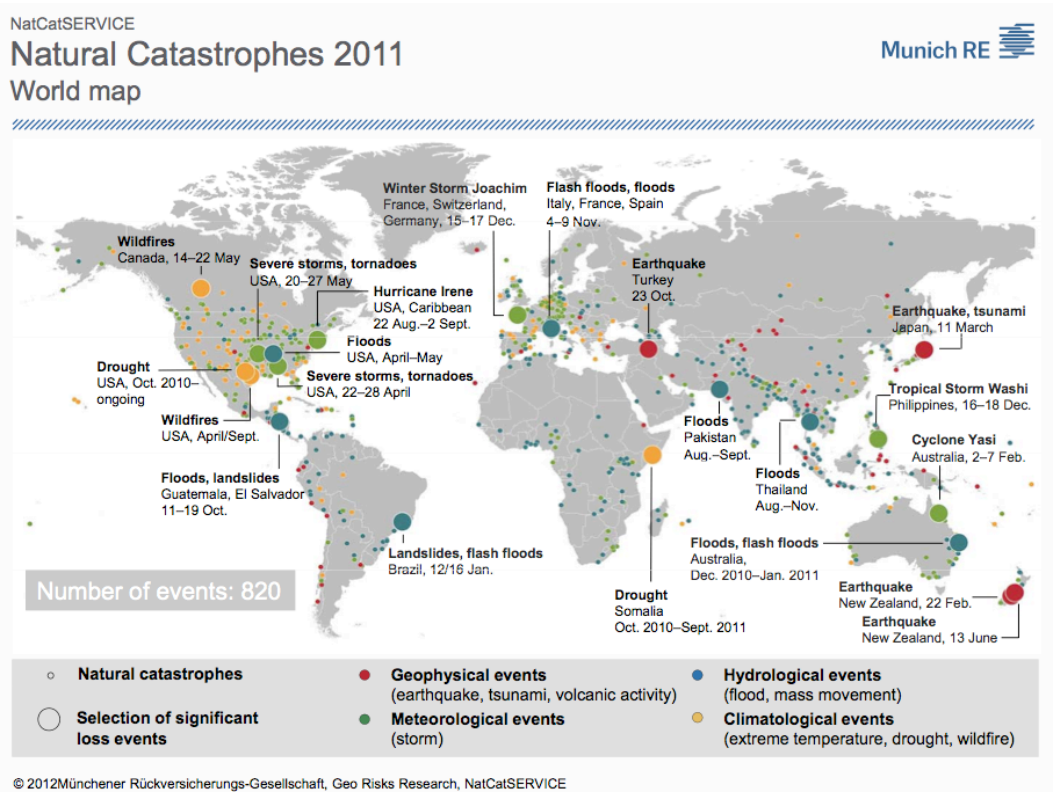

Figure 1.1. Map of global natural catastrophes in 2011. *Source:* Munich Re (2012).

By number, severe weather and climatological events accounted for 85% to 90% of natural hazards resulting in property damage or personal injury each year since 2005, according to Munich Re's NatCatSERVICE database (Munich Re, 2012). The remainder of the loss events recorded over this time were earthquakes. While the latter display no apparent trend, Munich Re (2012) presents compelling evidence suggesting a trend towards an increasing total number of weather-related catastrophes since the 1980s (**Figure 1.2**)[2]. Clearly, understanding the extent to

[1] Munich Re data is cited as it is a world-wide compilation of insurance industry information.
[2] In this section, we adopt the definition of "catastrophe" employed by Munich Re (2011): namely, an event incurring more than 20 fatalities or greater than a specified threshold value of overall economic losses, where the latter

which this trend is significant and/or related to human activity is a matter of some importance to the insurance and reinsurance industries. As regards the first question, there is an ongoing need for risk assessment regarding the insurance of property in regions that might be increasingly (or decreasingly) vulnerable to natural catastrophes in the future. Such an assessment should consider both trends in the amount of property exposed to damages as well as the number and strength of events doing the damage. With regard to the second point, should human activity or development decisions be identified as playing a decisive role in the damages resulting from climate change, then there could be implications for liability insurance.

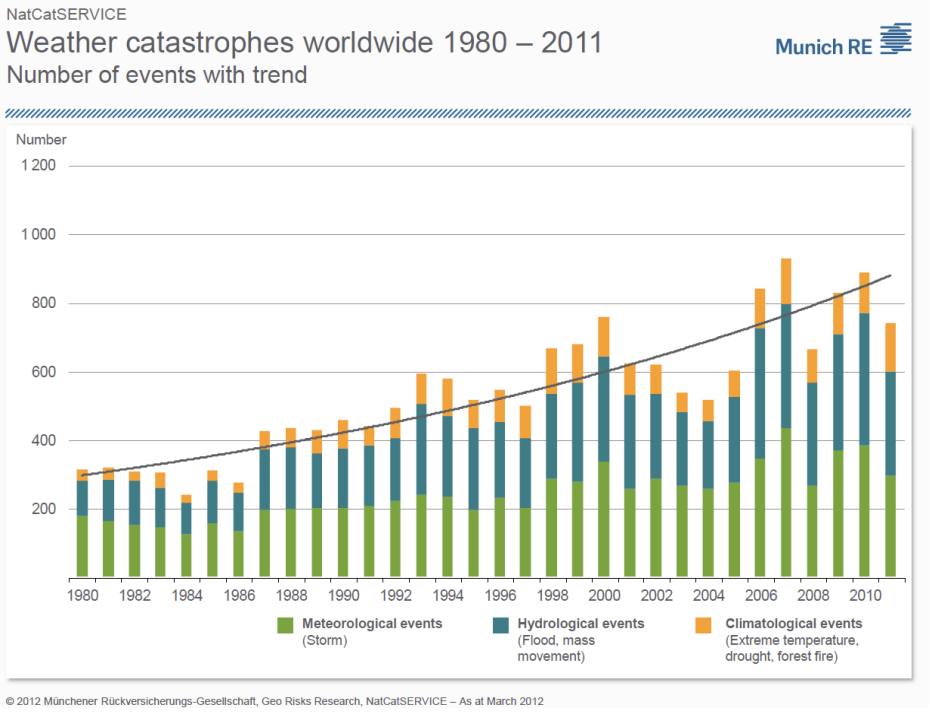

Figure 1.2. Global weather-related catastrophes that have occurred annually from 1980-2011. *Source:* Munich Re (2012).

Note that the distribution of insured losses would be slightly different from that of economic losses. According to Swiss Re[1], weather related events have a huge impact on the global economy, and that cost is growing steadily. As indicated in **Figure 1.3**, there has been an approximately 4-fold increase in CPI-adjusted losses between the early 1980s and 2007-2011.

The situation in the United States is of particular concern both because of the high value of the property exposed to damages as well as the vulnerability of this property to changes in climate. Over the period 1980 to 2011, there have been 134 weather/climate events with economic costs of more than one billion dollars (**Table 1.1**). Fourteen of these occurred in 2011 (**Figure 1.3**). Since 1980, 33% of the events have arisen from severe storms (including tornados), 23% from

increases with time due to inflation. In the 2000s, for example, a monetary threshold of US$50 million was used, which increased to US$60 million in the 2010s.

[1] http://www.swissre.com/rethinking/climate/fostering_discussion_climate_change_risks.html, accessed September 2012

tropical cyclones (hurricanes), 12% from flooding, 12% from drought, 8.2% from wildfires, 7.5% from winter storms and 4.5% from freezing events. Ranked in terms of consumer price index (CPI)-adjusted 2012 dollars, tropical cyclones ($420 billion) and drought ($210 billion) are the causes of the most costly weather/climate-related catastrophes in the United States (Table 1.1). Despite 2011 yielding the most independent catastrophes, the largest economic damages occurred in 2005 as a consequence of Hurricane Katrina making landfall on U.S. Gulf Coast (Fig. 1.3).

Table 1.1. Breakdown by type of billion-dollar weather/climate disasters in the United States from 1980 to 2011.

Disaster Type	# Events	% frequency	CPI-adjusted damages (billions of dollars)	% Damage
Severe storm	44	32.8%	96.1	10.9
Tropical cyclone	31	23.1%	417.9	47.4
Flooding	16	11.9%	85.1	9.7
Drought	16	11.9%	210.1	23.8
Wildfire	11	8.2%	22.2	2.5
Winter storm	10	7.5%	29.3	3.3
Freeze	6	4.5%	20.5	2.3
Total	**134**	**100%**	**881.2**	**100%**

[a]Total damages are in consumer-price-index-adjusted 2012 dollars. *Source:* http://www.ncdc.noaa.gov/billions/.

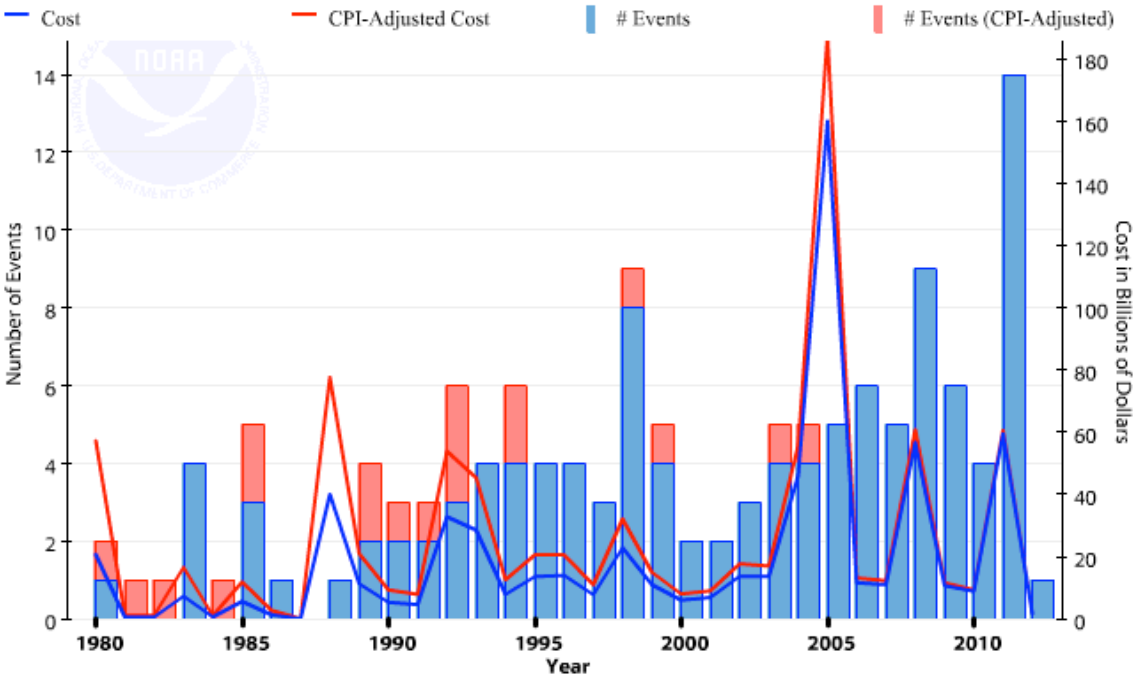

Figure 1.3. Total number of billion-dollar weather/climate disasters in the U.S. (*bars*) and their net cost (*line*) per year from 1980 to March 2012. The blue bars and the blue line are based on the cost of the disaster in the year that it occurred. Red includes additional events that occur when all costs are consumer-price-index-adjusted to 2012 dollars. *Source:* http://www.ncdc.noaa.gov/billions/.

Since 1980, the Southeast and Midwest U.S. states have experienced the greatest number of billion-dollar weather/climate disasters (**Figure 1.4**). This is not unexpected since these are the regions most susceptible to the impact of Atlantic hurricanes and most conducive to the formation of strong tornadoes. In addition, these regions include the dry, subtropical portion of the United States that, as outlined in Section 6, is likely to experience increased incidence of drought and wildfire outbreaks.

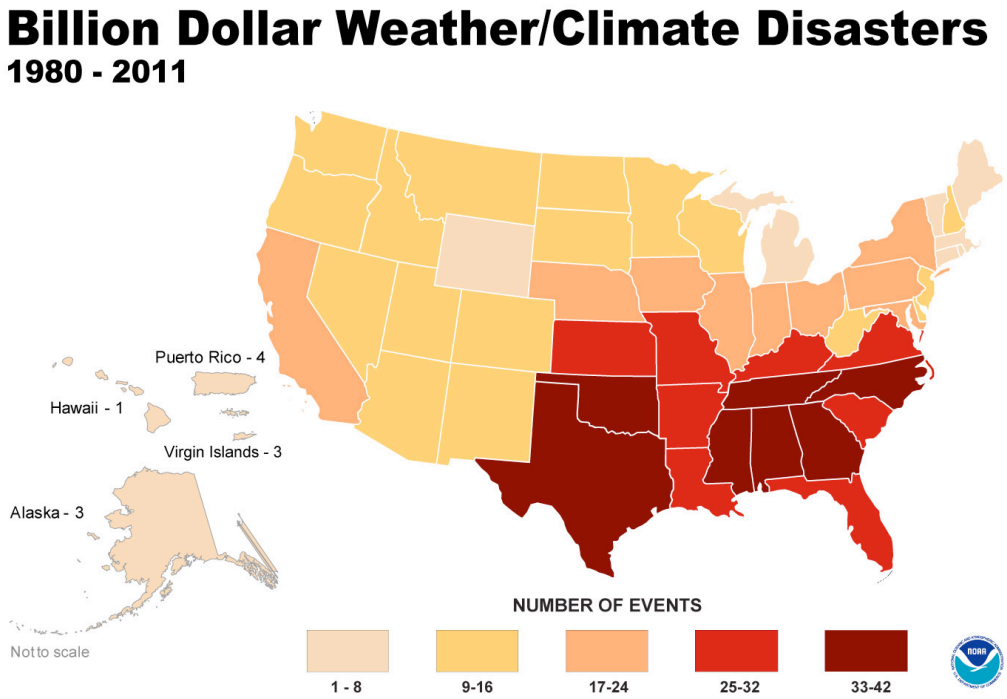

Figure 1.4. Map showing the distribution of billion-dollar weather/climate disasters in the United States from 1980 to 2011. The map shows where the damages associated with each of the 134 billion-dollar events listed in Table 1.1 were located. A single billion-dollar disaster can be distributed across, and hence included in the data for, several states. *Source:* http://www.ncdc.noaa.gov/billions/.

1.2 Weather and climate

Weather is the state of the atmosphere at a particular time and place. Climate, on the other hand, gives the likelihood of occurrence of a particular weather event. Another way of looking at climate is that it is the statistics of weather. Climate is what you expect; weather is what you get. It's important to recognize that when climate scientists make projections of future changes in climate, they are not making long-range weather predictions. Instead, they are making predictions of the change in the statistics of weather. In climate prediction, we examine how the shape of the distribution of a particular aspect of weather, such as temperature or precipitation, changes in the future. We might make predictions of the change in mean temperature or the change in the likelihood of occurrence of a particular extreme precipitation event.
An example is provided in **Figure 1.5.** Each of the three panels shows two curves: a present-day curve ("Previous climate") and a future climate curve ("New climate"). The present-day curve is

centered around the "Average" temperature, with the average temperature also being the most probable temperature you would get in the present-day climate. There is an equal probability in the present-day climate that you could have warmer than average or cooler than average temperatures. That is, the area under the present-day curve is the same to the left and to the right of the average temperature. The tails of the present-day distribution have low values of probability. These are the extreme high and low temperatures.

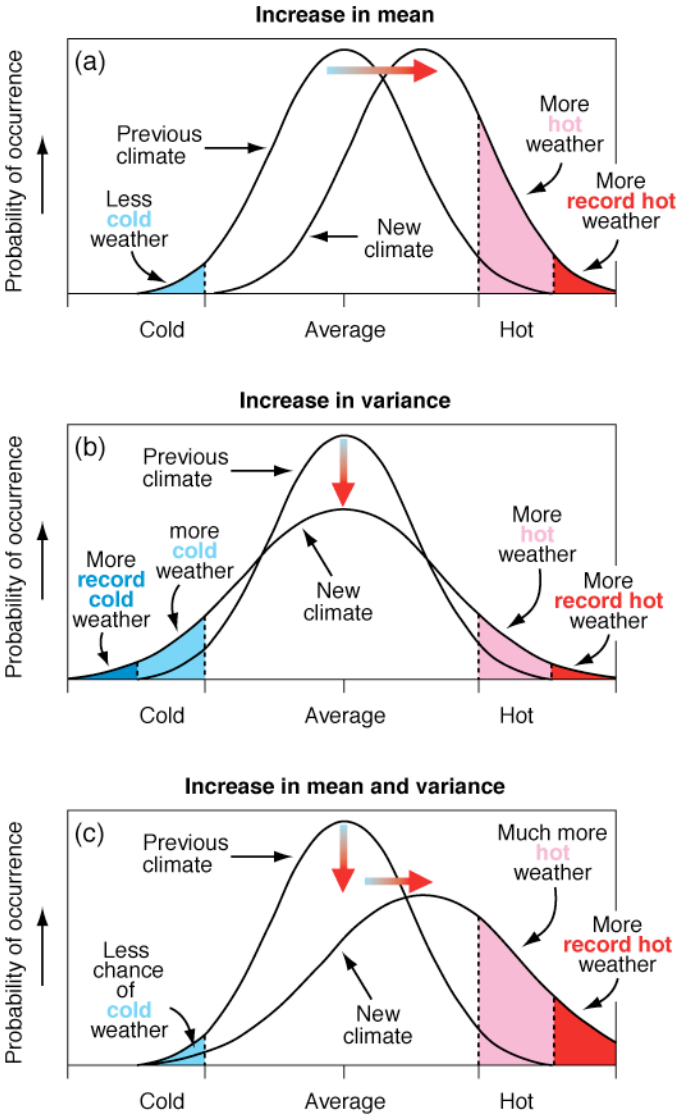

Figure 1.5. Schematic diagram showing a sample distribution of temperature in the present climate as well as how it might change in future. The horizontal axis shows temperatures ranging from cold to hot, while the vertical axis shows the probability of occurrence of these temperatures. Panel (a) shows an example where the average (or mean) temperature warms but the shape of the distribution (or variance) does not change in the future climate. Panel (b) shows an example where the average temperature does not change but the distribution spreads out in the future climate. Panel (c) shows an example where both the average temperature and the temperature distribution change in the future climate. *Source:* Folland et al. (2001).

Fig. 1.5a shows an example of climate change where average (or mean) temperature warms,[1] but the width of the distribution (or the variance, often measured by its square root, known as the standard deviation) does not change in the future climate. Fig. 1.5b gives an illustration of what one might expect if the average temperature did not change, but the variance increased. In this case the distribution is wider even though the most probable temperature remains the same. Here we expect both more record hot and more record cold temperatures. One would say that the weather has become more variable. Fig. 1.5c gives an example with both the mean and the variance increasing. In this case, the shift of the entire distribution to higher temperature leads to much more hot and record hot weather, but less cold weather than in the previous climate. As shall be demonstrated later in the report, this is the case best supported by observations of the real climate system.

1.3 Science and scientific uncertainty

By way of the scientific method, scientists seek to develop an understanding of a particular phenomenon consistent with all known observations of it. A scientist cannot simply ignore data if they do not support a theory; rather, s/he will seek either to modify the theory so that the data are explainable or determine if an error occurred in the collection of the data or their interpretation. When it comes to dissemination of their findings, scientists generally document their research in scientific journals, which are typically published by national or international scientific societies or academic publishers. Common to all reputable journals is a process known as peer review, wherein publications submitted to journals are subjected to an anonymous evaluation process undertaken by other scientists having known expertise in the area addressed by the paper. This process goes a long way toward preventing sloppy or biased work (e.g., pieces having an ideological stance) from appearing in the scientific literature. Peer review is therefore a form of quality control exercised by the scientific community at large, and it plays a key role in establishing the long-term legitimacy and advance of scientific knowledge.

The concept of scientific uncertainty is poorly understood by the public. Scientific uncertainty has two categories: reducible (or epistemic) uncertainty, which is associated with an incomplete understanding of the system; and irreducible (or aleatoric) uncertainty, which is linked to inherent randomness. The existence of scientific uncertainty is often legitimately used as a reason for not rapidly moving forward with some particular initiative. For example, drug companies cannot simply introduce a new drug into the general population without first undertaking several phases of highly controlled clinical trials. These companies must reduce the scientific uncertainty in the potential effects of this new drug on a diversity of people. But there are also many examples where the concept of scientific uncertainty has been misused in an attempt to stall the introduction of regulatory policies. Take, for example, smoking as a cause of cancer. For years the concept of scientific uncertainty was used to confuse the public about the link between smoking and various forms of cancer. A similar story unfolded with respect to chlorofluorocarbons (CFCs) and the depletion of the stratospheric ozone layer. Eventually,

[1] While the terms "climate change" and "global warming" are often used interchangeably, they are distinguished in this report as follows. *Climate change* refers to broad changes in many different aspects of the climate system, from upper air to sub-surface ocean temperatures to precipitation, cloud cover, etc. *Global warming*, however, refers only to the increase in surface air and ocean temperatures averaged over the entire planet.

however, the discovery and growth of the Antarctic ozone hole proved enough of a concern that major industrialized nations committed to the Montreal Protocol banning the use of CFCs by all relevant industries.

We constantly make decisions in the face of uncertainty. We eat food without knowing exactly where it came from or who handled it on its way to the supermarket shelf. We drive to work without knowing who else will be on the roads. We go to colleges and universities not knowing exactly what will happen in class today. We are constantly assessing the risk versus reward of our actions in the face of uncertainty. The theory of turbulence provides another example. There are many aspects of turbulence that are still not well understood today. Yet over the years, the scientific community has developed a fairly good understanding of the bulk properties of turbulence. We may not be able to predict exactly where turbulent air motions will take a dandelion seed as it sails in the air, but that doesn't prevent us from getting in an airplane, whose design requires an understanding of the bulk properties of turbulence.

The risks of this flawed view of scientific uncertainty are embedded in the United Nations Framework Convention on Climate Change (UNFCCC), to which the U.S. and 194 other nations are parties. Specifically, Article 3.3 of the UNFCCC expresses the precautionary view that some existing level of uncertainty is not a reason for inaction. While the Article was mainly directed at those tasked with developing international policy instruments, it is particularly relevant to the notion of insuring against climate-related hazards. Indeed, the use of insurance instruments as a means of pecuniary protection against climate-induced losses can be viewed as being highly resonant with this core statement of the UNFCCC.

1.4 The Intergovernmental Panel on Climate Change (IPCC)

In 1988, the World Meteorological Organization (WMO) and the United Nations Environment Programme (UNEP) established the IPCC as a means to assess global climate change. The IPCC is governed by United Nations regulations with the following mandate (reaffirmed in 2006 at its twenty-fifth session):

> The role of the IPCC is to assess on a comprehensive, objective, open and transparent basis the scientific, technical and socio-economic information relevant to understanding the scientific basis of risk of human-induced climate change, its potential impacts and options for adaptation and mitigation. IPCC reports should be neutral with respect to policy, although they may need to deal objectively with scientific, technical and socio-economic factors relevant to the application of particular policies.

The IPCC oversees three Working Groups (WGI, WGII, and WGIII) that assess different aspects of global warming and climate change. In the Fourth Assessment Report (AR4), the specific mandates of these working groups were:

> *WGI:* assesses the scientific aspects of the climate system and climate change;

WGII: assesses the scientific, technical, environmental, economic and social aspects of the vulnerability (sensitivity and adaptability) to climate change of, and the negative and positive consequences (impacts) for, ecological systems, socio-economic sectors and human health, with an emphasis on regional, sectoral and cross-sectoral issues;

WGIII: assesses the scientific, technical, environmental, economic and social aspects of the mitigation of climate change.

Another way to think of these groups is that WGI describes the problem of global warming, WGII details its consequences, and WGIII assesses what we can do about it.

A common misconception is that the IPCC Working Groups undertake their own independent research, collect their own data, or monitor the climate system. This is not the case—they exclusively provide an assessment of the peer-reviewed scientific literature, although they may make passing reference to non-peer-reviewed technical reports. Web sites and newspaper opinion pieces/editorials are typically not used in the assessment, as they have not passed the standards set by the peer-review system.

The IPCC has published four comprehensive assessments of climate change and a number of special reports on a variety of topics. The 1st Assessment Report (1990) was influential in the formation of the United Nations Framework Convention on Climate Change (UNFCCC), which currently has 194 member states, including Canada and the United States. The 2nd Assessment Report (1996) had a great impact on the negotiations leading up to the adoption of the Kyoto Protocol to the UNFCCC at the Third Conference of Parties in 1997. The 3rd Assessment Report was completed in 2001, and the 4th Assessment Report in 2007.

The IPCC does not make policy recommendations to governments but rather assesses our current understanding of the scientific, socio-economic, technological, and environmental aspects of climate change. The reports provide input into the national and international negotiations aimed at developing policy to deal with global warming.

1.5 Goal of the report

In recognition of the importance of assessing climate and weather related risk upon the insurance and reinsurance sectors, this report provides a review of the latest developments in climate science. The goal of this report is to lay the foundation for the development of the ACCI, which is intended to illustrate various aspects of climate change in an accurate and succinct manner. The report does not attempt to provide a climate risk assessment nor does it undertake a detailed summary of projected climate change over North America or any other region.

An index is an effective means of summarizing and subsequently illustrating changes through time of an aggregate measure of a particular issue or concept. For example, the consumer price index referred to above is a standardized indicator of consumer prices and hence inflation. Climate indices can be constructed to illustrate, for example, the aggregate impact or occurrence

frequency of climate or weather extremes. Such climate indices might be modified to account for local vulnerability or insured risk to climate and weather related disasters.

We begin our analysis in the next section with a discussion of global-scale indicators of climate change. We focus on changes at the regional scale in Section 3 and move on to examine climate and weather extremes in Section 4. Section 5 contains a review of the development and use of existing climate indices. In Section 6 we provide a brief assessment of current literature concerning projected future climate change. The extensive literature review of prior sections is used in Section 7 to provide a strategy and framework for the development of the ACCI for use by the Index Working Group led by the Climate Change Committee of the CAS, American Academy of Actuaries' Property/Casualty Extreme Events Committee, CIA and SOA.

2. Global Climate Change Indicators

This section and the next provide a current summary of the state of scientific knowledge on global and regional climatic indicators. By these are meant properties of the climate that are either potentially observable over the majority or entirety of the globe (e.g., surface temperature, precipitation, sea level) or are bellwethers of global or systematic regional climate change (e.g. Arctic sea ice, glaciers, wildfires, storms). The most valuable resource for such a wide-ranging summary are the knowledge synthesis reports of the Intergovernmental Panel on Climate Change (IPCC), the most recent of which, the 4th Assessment Report (AR4) was published in 2007 (the next report is due in 2013). In this summary we draw from two volumes of the AR4, *Working Group I: The Scientific Basis* (AR4-WGI) and *Working Group II: Impacts and Adaptation* (AR4-WGII). Much information for the U.S. specifically is obtained from two reports, *Climate Change Indicators for the United States* (EPA, 2010) and *Global Climate Change Impacts in the United States* (U.S. Global Change Research Program, 2009). Additional information is presented from more recent syntheses, including the U.S. National Research Council report on *Climate Stabilization Targets: Emissions, Concentrations, and Impacts over Decades to Millennia* (2011) the IPCC *Special Report on Climate Extremes* (SREX, 2012), and many peer-reviewed meta-analyses and research articles. Thus, each of the following subsections begins with a description of the climate indicator and how it is measured, followed by its status as summarized in AR4-WGI, and concludes with an update based on more recent research.[1] The observational results cited in the report are in standard SI (metric) units, consistent with international scientific practice. In some cases where results for the United States alone are shown, imperial units are used. Conversion tables are provided in Appendix B. Finally, unless stated otherwise, an uncertainty range in any figure cited denotes the 5% to 95% confidence interval.

2.1 Climate change versus climate variability

Before commencing our summary of global climate indicators, it is wise to confront straightaway what James Hansen, one of the world's best known climate scientists, has called "the greatest barrier to public recognition of human-made climate change": namely, the natural variability of climate. The climate system, which comprises the atmosphere, oceans, land surface, and cryosphere (snow and ice-covered land or ocean), is an enormously complex dynamical system that exhibits a variety of regular, irregular, and forced behaviors. The scientific instruments used to collect weather and climate data are by necessity also complex; but for our present purpose we may conceive of all of these as a simple radio receiver with a dial used to filter out all but the frequencies, or "stations," of interest. In any given location at a specific moment, most frequencies along the dial contain little more than random weather, or climate "noise." But at certain frequencies, regularities become apparent: on the daily time scale, temperatures increase and decrease as day turns to night, while the same occurs on the annual timescale, more

[1] The reason for the emphasis given to results from the IPCC AR4 and subsequent reports is the following. These detailed assessment exercises, which take place every 6 years, effectively add another round of extensive peer review to climate and related impacts research that has already met the same standard for individual scientific journals. In the assessment process, individual studies are placed in context with related results, and the level of consistency between different studies can be ascertained, an important criterion for the overall acceptance of scientific results.

noticeably the further one is from the equator. These stronger "signals" that emerge from the static noise as the radio knob turns are the primary interest of the climate scientist, and distinguishing them from the noise is an ever-present task. Indeed, the climatologist learns early on that characterizing the noise is as important as discerning the signal.

The significance of the climate change signal, which emerges at decadal to century timescales, compared to the pervasive noise of natural climate variability present at all frequencies, is widely misunderstood. One often hears statements in the media or in public discourse along the lines of, "Climate is changing and has always changed, and therefore trends detected around the world today are no different from ever-present climate variability." It is essential that the public, their elected representatives, and the media understand that the conclusions reached by climate scientists and published in peer-reviewed journals account for the background static of climate variability, and that the signals they are drawing attention to are as strong compared to the background climate variability as is your favorite radio station to the static elsewhere along the dial.

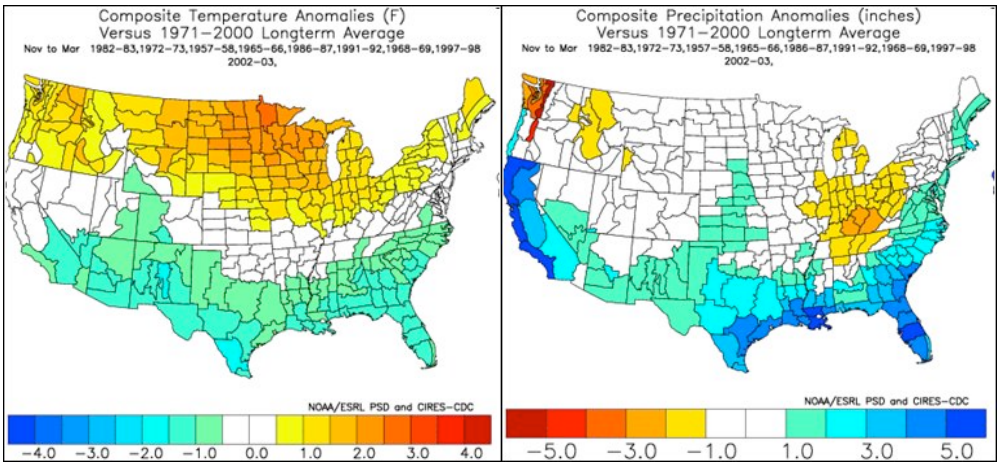

Figure 2.1. *Left:* Surface air temperature anomalies, i.e., departures from long-term means (November to March, relative to the 1971-2000 average), for the continental United States during El Niño years. *Right:* Precipitation anomalies for the same months and years. *Source:* U.S. National Oceanic and Atmospheric Administration (NOAA).

Climate variability is much more complex than just weather, because it occurs on fairly long timescales as well. The most prominent behavior of this type is the El Niño-Southern Oscillation (ENSO), which alternates in a semi-regular way between two phases: El Niño or La Niña. A strong ENSO phase is associated with a prevailing pattern of sea surface temperature (SST) in the tropical Pacific Ocean, which can have a profound influence on continental climates. All else being equal, El Niño years tend to produce warm temperature anomalies on land, while La Niña years tend to produce cold anomalies. **Figure 2.1** shows how much surface air temperature and precipitation deviate from long-term mean values over the continental United States during El Niño years. Wintertime temperatures tend to be considerably higher than average in the northern U.S., and below average in the south. Deviations in winter precipitation behave in an approximately opposite manner, but are generally small in the north. These departures are strong enough to be misunderstood as "climate change," if one were using data over a sufficiently short time span. But climatologists typically use much longer periods (usually 30 years) over

which to characterize the prevailing climate variability, and then measure any remaining changes against *that*.

In March 2012, an early spring heat wave affected much of North America, with over 15,000 daily high temperature records broken in the U.S. alone in March. According to a NOAA bulletin issued on April 9, 2012:

> The average temperature of 51.1 degrees F was 8.6 degrees above the 20th century average for March and 0.5 degrees F warmer than the previous warmest March in 1910. Of the more than 1,400 months (or more than 116 years) that have passed since the U.S. climate record began, only one month, January 2006, has seen a larger departure from its average temperature than March 2012.

This event is all the more remarkable as it occurred during La Niña, not El Niño, conditions. This initial digression is only to point out that the results which follow are to be understood in the context of the ever-changing background climate, and to focus due attention on certain trends—truly significant "signals"—in the various indicators.

2.2 Surface temperature

The thermometer record of land-surface air temperature (hereafter SAT) extends back several centuries in Europe and North America. However, the global coverage of such data is small prior to about 1850, which thus serves as the starting point for most analyses of large-scale temperature variability and change. Global datasets for SAT have been painstakingly assembled from daily thermometer readings at thousands of measurement stations taken since 1850, with incomplete or erroneous data being removed in the process (**Figure 2.2**). These are complemented by thousands more measurements of SST taken from ocean-going ships over this period. The resulting data set, which comprises part of the Global Historical Climatology Network (GHCN), provides global coverage, albeit with variable data density in different regions (Durre et al. 2010).

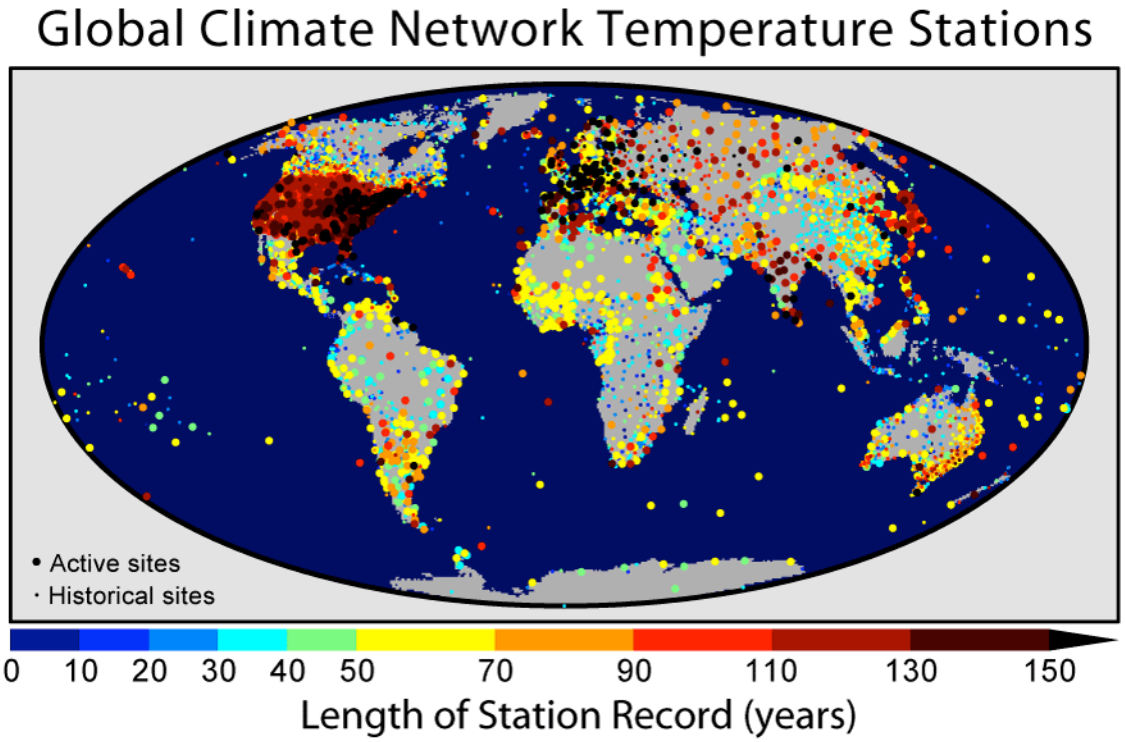

Figure 2.2. The map shows the 7,280 fixed temperature stations in the Global Historical Climatology Network (GHCN) catalog color-coded by the length of the available record. Sites that are actively updated in the database (2,277) are marked as "active" and shown in large symbols; other sites are marked as "historical" and shown in small symbols. In some cases, the "historical" sites are still collecting data but due to reporting and data processing delays (of more than a decade in some cases) they do not contribute to current temperature estimates. This image shows 3,832 records longer than 50 years, 1,656 records longer than 100 years, and 226 records longer than 150 years. The longest record in the collection began in Berlin in 1701 and is still collected in the present day. *Source:* Wikipedia. Figure created by Robert A. Rohde from published NOAA data.

It is important to emphasize that this process has been conducted independently by many research groups, resulting in several slightly different versions of the global temperature evolution from 1850 to present, as can be seen in **Figure 2.3** (in the figure,[1] the NCDC data are based upon the GHCN coverage shown in Fig. 2.2, while the other curves are based upon slightly different distributions). These quality-controlled datasets constitute what is arguably one of the most heavily scrutinized knowledge bases in all of science.

The principal conclusions based on these data summarized in the IPCC AR4-WGI are as follows (cited verbatim, but with figures in Fahrenheit added):

1) *Global mean surface temperatures have risen by 0.74 ± 0.18°C (1.33 ± 0.32°F) when estimated by a linear trend over the last 100 years (1906–2005). The rate of warming over the last 50 years is almost double that over the last 100 years (0.13°C ± 0.03°C vs. 0.07°C ± 0.02°C per decade).*

[1] This figure, and all others reproduced from the IPCC AR4, is reproduced with permission and accompanied by the original caption, as a condition of open access. See: http://www.ipcc.ch/publications_and_data/publications_and_data_figures_and_tables.shtml#.T2wOX8zgKfQ

2) *Land regions have warmed at a faster rate than the oceans.*

3) *Urban heat island effects are real but local, and have not biased the large-scale trends.*

4) *Average Arctic temperatures increased at almost twice the global average rate in the past 100 years.*

5) *The temperature increases are consistent with observed changes in the cryosphere and oceans.*

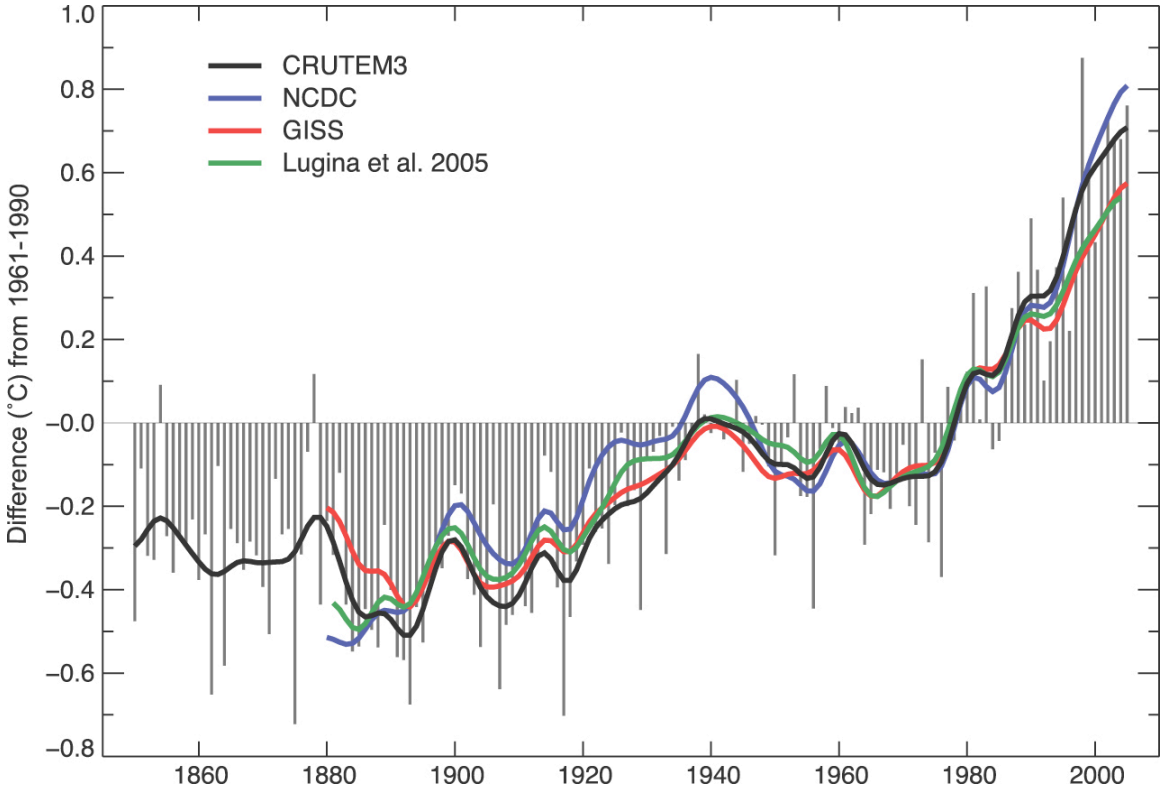

Figure 2.3. Annual anomalies of global land-surface air temperature (°C), 1850 to 2005, relative to the 1961 to 1990 mean for CRUTEM3 updated from Brohan et al. (2006). The smooth curves show decadal variations (see Appendix 3.A). The black curve from CRUTEM3 is compared with those from NCDC (Smith and Reynolds, 2005; blue), GISS (Hansen et al., 2001; red) and Lugina et al. (2005; green). *Source:* IPCC AR4-WGI, Figure 3.1 (2007).

Some further conclusions from AR4-WGI which are relevant for this study are the following:

6) *From 1979-2005, the linear, combined SAT and SST trend was 0.17 ± 0.05 °C (0.31 ± 0.09°F) per decade globally, and 0.24 ± 0.07 °C (0.43 ± 0.13°F) in the Northern Hemisphere alone.*

7) *11 of the 12 warmest years on record occurred from 1995 to 2006.*

In light of more recent data (**Figure 2.4**), the latter statement can be amended to "the 16 warmest years on record occurred in the 17-year period from 1995 to 2011." Fig. 2.4 shows that many of the warmest anomalies coincide with El Niño years, as might be expected.

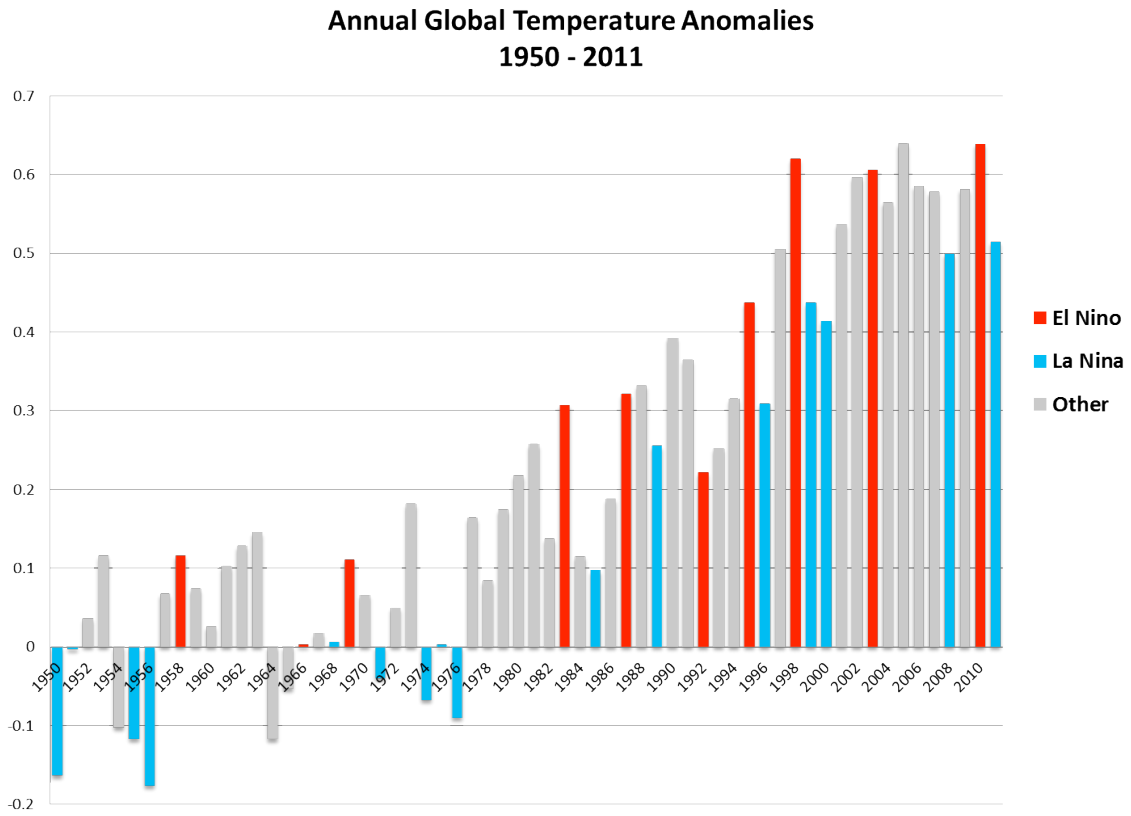

Figure 2.4. Annual global temperature anomalies since 1950, with strong El Niño and La Niña years indicated. *Source:* NOAA.

2.3 Carbon dioxide and its effect on global temperature

The cause of the global SAT increase over the last 150 years has been intensively investigated. The rapid rise in atmospheric carbon dioxide (CO_2) concentration over the same period, revealed by the analysis of bubbles trapped in polar ice and by direct air sampling since the 1950s, is shown alongside this temperature change in **Figure 2.5**. The two curves are roughly coincident, and analogues can be found in the ancient temperature and ice-core records. The close agreement is no accident: indeed, the well-understood mechanism of the greenhouse effect dictates that such a correspondence must hold.

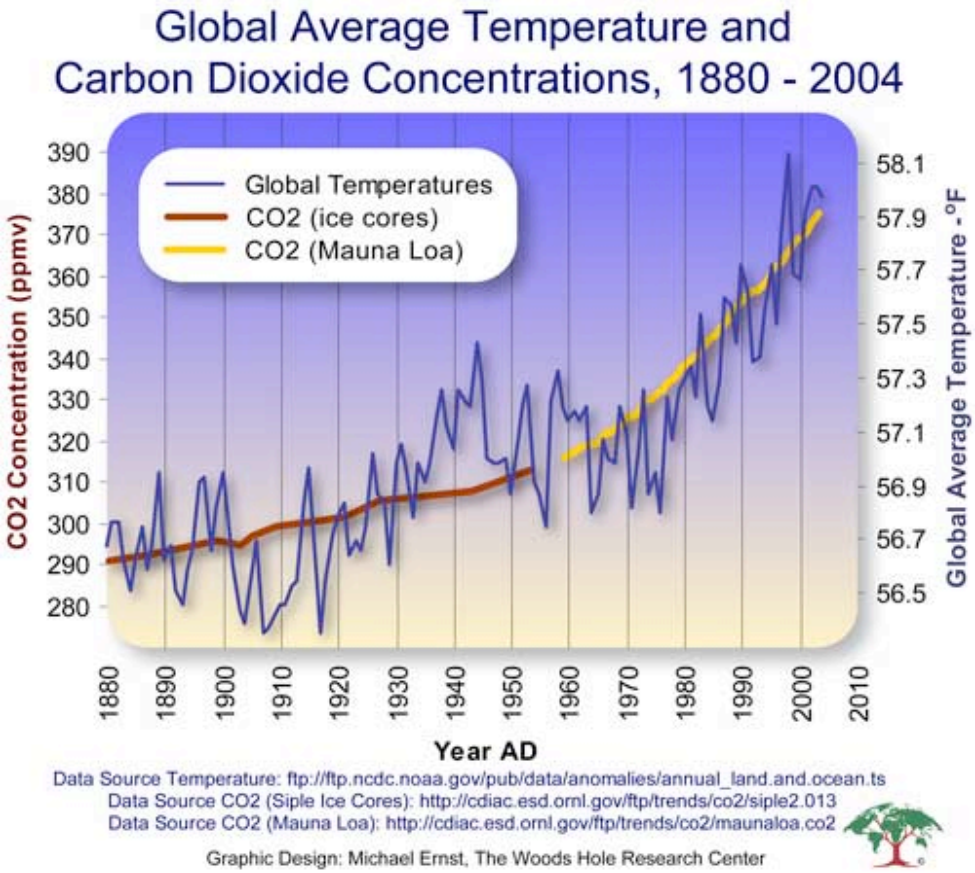

Figure 2.5. Global annual average CO_2 rise (left-hand axis, in parts per million) superimposed on the global average SAT increase (right-hand axis, in degrees Fahrenheit), as measured over both land and oceans. While there is a clear long-term warming trend, successive individual years do not necessarily show a temperature increase, and some years show greater changes than others. These year-to-year fluctuations in SAT are due to natural processes, such as the effects of ENSO and the eruption of large volcanoes. Note also the scales along the vertical axes, which indicate that the relative change in SAT is considerably smaller than that in CO_2. *Sources:* As indicated.

Comprehensive global climate models (GCMs) that simulate the 1850-to-present period using the observed CO_2 increase as input, along with similar increases in other greenhouse gases (such as methane, nitrous oxide, and chlorofluorocarbons) and industrial sulfate emissions, can reproduce the temperature rise, to within the error of the measurements. Not only can such models replicate global temperature change, they also explain observed regional patterns of change and seasonality (Sec. 3.1). The same models run with only naturally changing factors such as solar variability, and volcanoes fail to produce any systematic surface temperature change (**Figure 2.6a**). In particular, satellite measurements of solar energy received at the top of the atmosphere made since 1978 do not indicate any systematic trends (**Figure 2.6b**); this is worth noting as those who dispute human-caused warming have often pointed to the Sun as a proximate cause of the temperature rise.

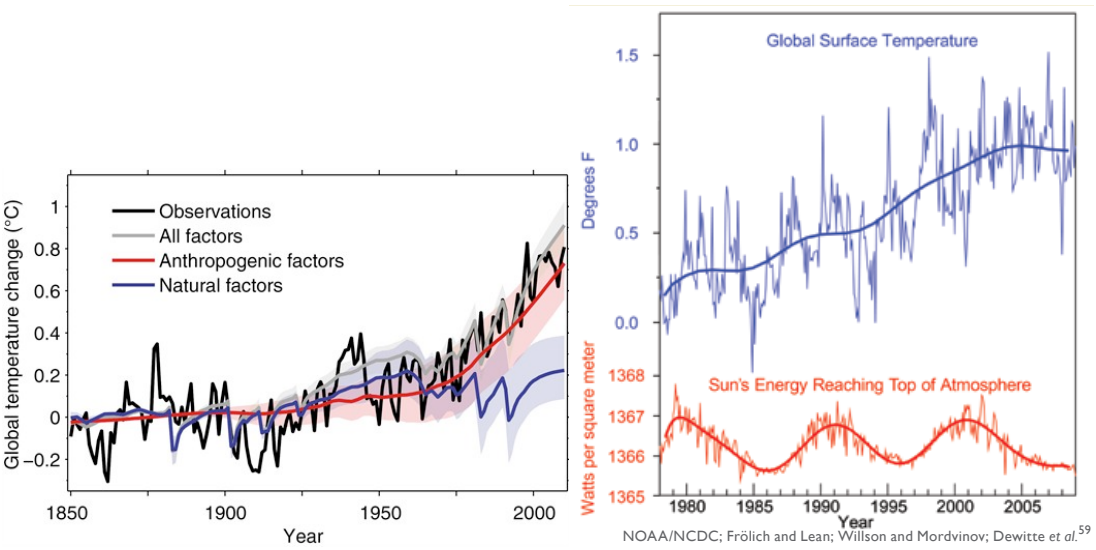

Figure 2.6. *Left:* Attribution of global SAT change to human-caused and natural factors. *Source:* Huber and Knutti (2012). *Right:* Global SAT change (*top*) contrasted with solar energy received at the Earth as measured by satellite (*bottom*). The latter has followed its natural 11-year cycle of small ups and downs, but with no net increase. *Source:* Karl et al. (2009).

It is also important to recognize the delayed effect of CO_2 emissions on climate. Newly added CO_2 to the atmosphere is only partly absorbed by the land and ocean, and the time scale for total absorption is on the order of thousands of years. Climate model studies show that even if fossil fuel emissions were to immediately cease, both CO_2 concentration and global mean temperatures would remain well above preindustrial levels for hundreds of years (Matthews and Caldeira, 2008; Eby et al., 2009).

2.4 Precipitation

All else being equal, increased heating at the Earth's surface increases evaporation, especially over the oceans, and thus enhances the moisture-holding capacity of the atmosphere at a rate of about 7% per °C (as predicted by underlying theory—i.e., the Clausius-Clapeyron relation—and in close accord with observations; AR4-WGI, Ch. 3.4.2). Both theory and observations suggest that, even in the presence of changing background temperature in the atmosphere, relative humidity remains approximately unchanged. This implies that the weather systems which transport this increased moisture around the atmosphere may release this moisture either in the form of more frequent precipitation events, or relatively more heavy rainfall episodes. These precipitation extremes are addressed in Section 4. Here we review observations of changes in global precipitation amount under the warming documented in Sec. 2.2 above.

Global precipitation anomalies, derived from the GHCN data set and referenced to the base period of 1961-90, are shown in **Figure 2.7**. Due to large interannual variability, no significant linear trend is apparent in these data. However, it is worth noting that 13 of the last 17 years feature positive global precipitation anomalies, coinciding with all but one of the SAT anomalies over the same period (Sec. 2.2). This is suggestive of a connection to global warming, but not conclusive, given the large year-to-year variability in precipitation which is, like temperature,

strongly influenced by the phase of ENSO.

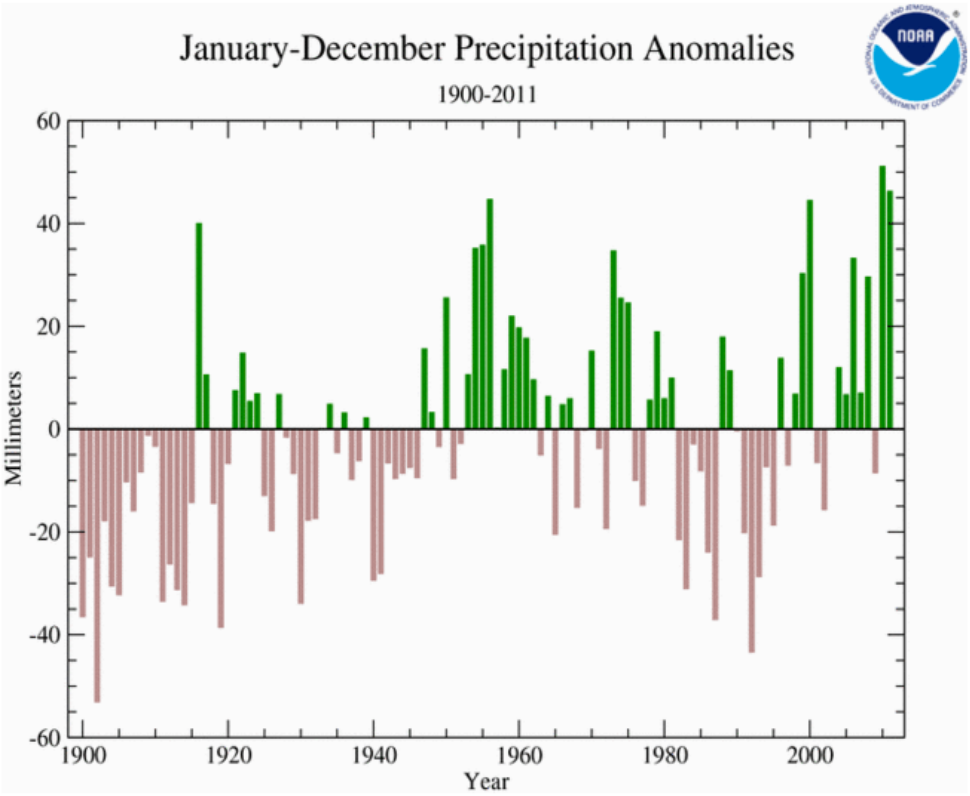

Figure 2.7. Global precipitation anomalies with respect to 1961-90 normals. *Source:* NOAA; http://www.ncdc.noaa.gov/sotc/global/2011/13.

Despite the absence of a strong global signal, many individual regions feature significant trends in precipitation. These are reviewed below in Sec. 3.2.

2.5 Sea-level rise

Sea level is a sensitive indicator of climate change, as it responds to global warming both directly, via the heating and consequent expansion of seawater, and indirectly, via the loss of land-based ice due to increased melting.[1] According to the AR4-WGI, "there is strong evidence that global sea level gradually rose in the 20th century and is currently rising at an increased rate, after a period of little change between AD 0 and AD 1900" (AR4-WGI Ch. 5, p. 409). Two independent means of measuring sea level are available. Tidal gauges measure relative sea level at points along the coast, while satellite instruments (radar altimeters) measure absolute sea level over nearly the entire ocean surface. Measurements of relative sea level include contributions from ocean thermal expansion and runoff from land ice melt, while absolute sea level data contain the additional effects of local crustal displacement, post-glacial "rebound," and even local wind

[1] Note that melting sea ice does not contribute to sea level rise, as the ice was already floating. This is in accord with Archimedes' principle, which holds that any floating object displaces its own weight of fluid.

patterns. The former two effects can be removed by simultaneous measurements over nearby land surfaces. Many tidal gauges have collected data for more than 100 years, while satellite measurements began in the early 1990s.

The long-term tidal gauge measurements indicate that global mean, relative sea level has risen by an average of 1.7-1.8 mm per year during the 20th century (Church and White, 2011), while satellite data indicate a higher mean rate of relative sea-level rise (SLR) of 3.2 ± 0.4 mm per year during the 1993-2010 period (Church and White, 2011; Cazenave and Remy, 2011). This amounts to a total, global average, relative SLR since 1880 of approximately 20 cm or 8 inches. Continuing SLR is virtually guaranteed in the coming decades, due to warming that will occur as the ocean adjusts to the thermal forcing from existing greenhouse gas levels (Sec. 2.3).

Figure 2.8 shows the latest available data on global, relative SLR. The rate of SLR since 1993 displayed in the figure is near the upper end of sea-level projections from comprehensive global climate models used in the AR4-WGI (Church and White, 2011). A significant, increasing trend of ocean heat content determined from temperature measurements has also been established, and more than half of the observed SLR from1993-2003 is attributed to thermal expansion (AR4-WGI, Fig. 5.15).

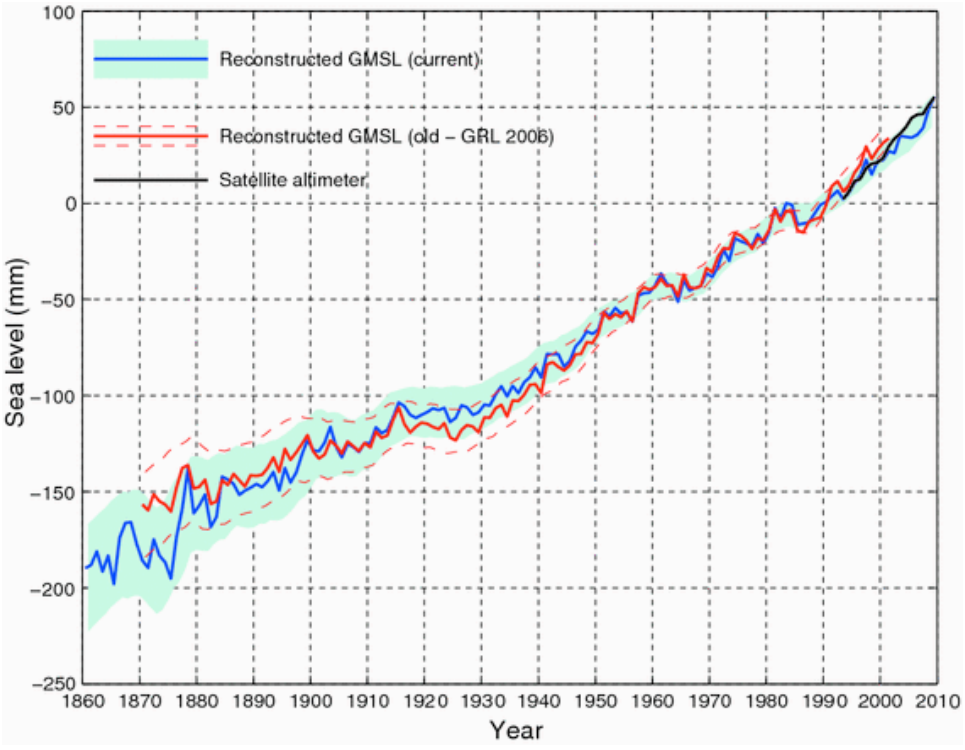

Figure 2.8. Global average sea level from 1860 to 2009 as estimated from the coastal and island sea-level data (*blue*). The one standard deviation uncertainty estimates plotted about the low-passed sea level are indicated by the *shading*. The Church and White (2006) estimates for 1870–2001 are shown by the *red solid line* and *dashed magenta lines* for the 1 standard deviation errors. The series are set to have the same average value over 1960–1990 and the new reconstruction is set to zero in 1990. The satellite altimeter data since 1993 is also shown in *black*. *Source:* Church and White (2011).

2.6 Arctic sea ice, snow cover and permafrost

Over the past three decades, surface air temperatures in the Arctic have risen approximately three times faster than the global average rate of warming. This would be expected to lead to a reduction in the amount ice, snow, and permafrost, although the exact rate of change can only be determined from direct observations, which we now review.

2.6.1 Arctic sea ice

Reliable, continuous measurements of Arctic sea ice extent[1] are obtained from passive microwave satellite observations, which exist from 1979 to present. Over the period 1979-2006, annual mean ice extent decreased at an average rate of 3.4 ± 0.2% per decade, while the September minimum sea ice extent declined at a faster rate of 8.4 ± 1.4% per decade (Comiso and Nishio 2008). The last decade (2002-2011) featured the nine lowest values of Arctic sea ice extent ever recorded (Fetterer 2012). A dramatic decline occurred in September 2007, when the annual minimum sea ice extent was reduced to about 39% of its climatological average value. Although the rate of decrease has slowed somewhat in the years since, the trend in sea ice extent has now reached −12.0% per decade, and the current level lies three standard deviations below the mean value of the 1968-96 period (Meier 2012; **Fig. 2.9**). The observed June to October sea ice extent in the last 5 years lies well outside the natural variability in this quantity, as characterized by observations in the 1979-2000 period falling between the 2nd and 98th percentiles (i.e., two standard deviations below and above the mean; **Figure 2.10**).

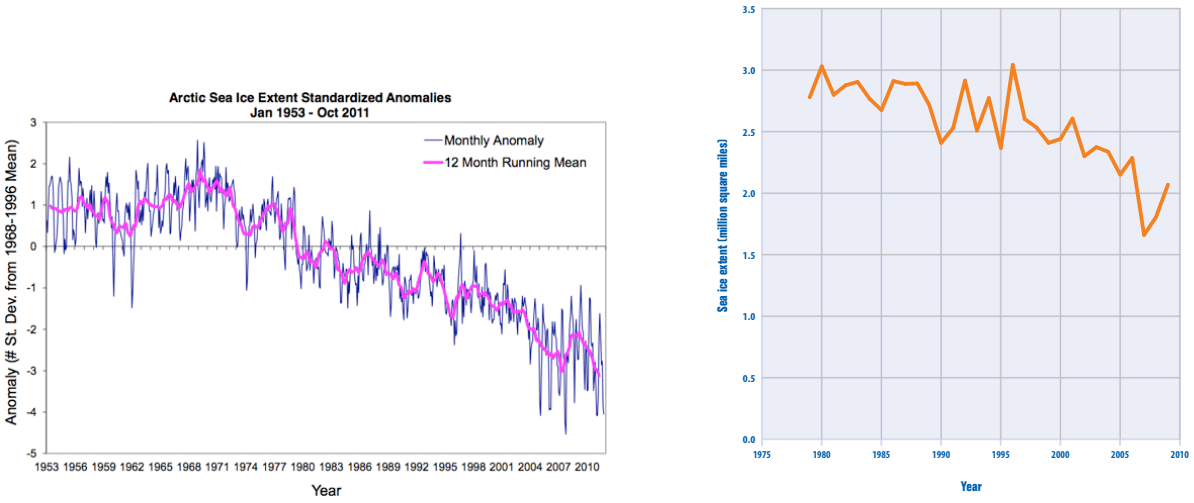

Figure 2.9. *Left:* Sea ice extent departures from monthly means for the Northern Hemisphere. For January 1953 through December 1979, data were obtained from the UK Hadley Centre and are based on operational ice charts and other sources. For January 1979 through October 2011, data are derived from passive microwave (SMMR/SSM/I). Image by Walt Meier and Julienne Stroeve, National Snow and Ice Data Center (NSIDC), University of Colorado, Boulder. *Right:* Absolute values of annual mean sea ice extent, since the beginning of the satellite record. *Source:* U.S. National Snow and Ice Data Center (NSIDC); http://nsidc.org/cryosphere/sotc/sea_ice.html.

[1] The terms "extent" and "area" (or "cover") are both used to describe sea ice, but they have different definitions; see Appendix A. In this report, we use the term "extent," as it is less prone to observational errors.

Multi-year sea ice, the thickest ice that persists for at least two summers, has also been declining. A recent study by Comiso (2012) based on the same satellite data reveals a decline of 17.2% per decade in the thickest sea ice. The largest recent decline in multi-year sea ice occurred in 2008, when it was reduced to 55% of its climatological areal coverage.[1]

As a result of the loss of the multi-year sea ice, average sea ice thickness over the Arctic likewise exhibited a substantial decline in the latter half of the 20th century. Recently declassified ice thickness records from U.S. Navy submarines using upward-looking sonars, covering 38% of the Arctic Ocean and spanning 1958-2000, reveal "an astonishing decrease of 1.75 m in thickness" (a decline of 48%) between 1980 and 2000 (Rothrock et al. 2008; Kwok and Rothrock 2009). Combining these results with laser altimeter measurements from satellites (Kwok et al. 2009) allowed Kwok and Rothrock to conclude that a long-term trend of sea ice thinning has occurred over much of the Arctic Ocean, which is even more pronounced than the previously mentioned decline in sea ice extent.

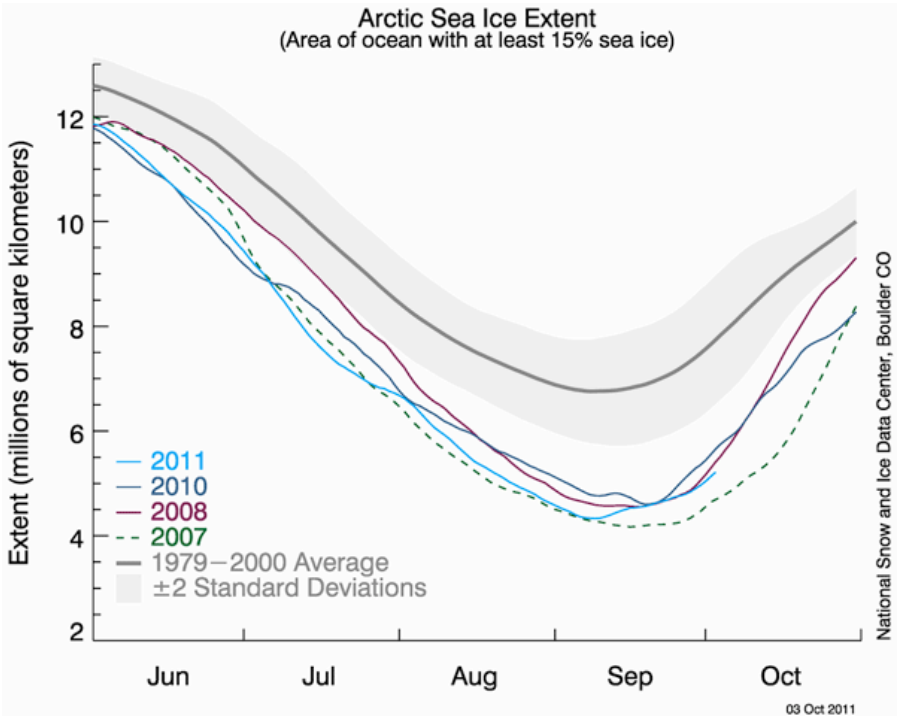

Figure 2.10. This graph compares 5-day running means for Arctic sea ice extent (area of ocean with ice concentration of at least 15 percent) for the long-term mean (1979-2000), the record low (2007), and the extents for 2008, 2010, and 2011. Sea ice extent was second-lowest in 2011, and experienced a rapid freeze-up after reaching its minimum in early September. *Source:* NSIDC, University of Colorado, Boulder, http://nsidc.org/cryosphere/sotc/sea_ice.html.

Due to the warmer Arctic Ocean, trends toward earlier sea ice melt and later freeze-up have been detected nearly everywhere in the Arctic. Over the last 30 years, the mean melt season over the

[1] A helpful visualization can be found at: http://www.nasa.gov/topics/earth/features/thick-melt.html

Arctic ice cover has increased by about 20 days (Markus et al., 2009).

According to the U.S. National Snow & Ice Data Center (NSIDC), which maintains year-round scientific analysis and daily image updates of Arctic sea ice:

> … warming conditions and wind patterns have been the main drivers of the steeper decline since the late 1990s. Sea ice may not be able to recover under the current persistently warm conditions, and a tipping point may have been passed where the Arctic will eventually be ice-free during at least part of the summer (Lindsay and Zhang 2005).

In contrast to the Arctic, Antarctic sea ice extent exhibits a weak, net positive trend of 0.9 ± 0.2% since 1979 (Comiso and Nishio 2008). Significant growth in extent in the Ross and Weddell Seas is nearly balanced by marked sea ice loss along the Antarctic Peninsula. These trends are consistent with corresponding local trends in sea and air surface temperature. Near the Antarctic Peninsula, significant breakup of ice shelves has occurred since the late 1980s, with the most notable being the collapse of the Larsen-B ice shelf in 2002 (AR4-WGI, Chapter 4). Although isolated studies are starting to emerge, there is currently no information on large-scale Antarctic sea ice thickness change. Changes in the much larger Antarctic (land) ice sheet are documented below in Section 2.7.2.

The mention of the term "tipping point" in the NSIDC statement is an unsettling prospect that deserves further elaboration. The impression one might gain from examining historical data on global climate indicators is one of gradual, unidirectional change; however, experience with other highly complex physical and biological systems indicates that "surprises" can occur when certain thresholds in controlling variables are exceeded. In a review of elements of the climate system that may prove susceptible to such transitions on relatively short timescales, Lenton et al. (2008) ranked Arctic sea ice as the current leading candidate for such behavior, based on the recent observations summarized above. The basic physical principle of positive ice-albedo feedback that underlies the response of floating ice to increased infrared heating at the surface is well understood, and its magnitude has been quantified in contexts ranging from the simplest energy balance models to fully coupled ocean-atmosphere 3-D general circulation models with an interactive sea ice component. The notion that this feedback operates at some level is undisputed; only its magnitude in the presence of other physical changes is uncertain.

Another reason for concern along these lines is the fact the observed rate of Arctic sea ice decline actually exceeds that simulated in the most complex state-of-the-art climate models (**Figure 2.11**), indicating that the models may be lacking some aspects of sea ice description that are important for describing melt rates.[1] Improving sea ice models is an active area of research, but the important point for our present purpose is that the predictions of sea ice loss in such models should be considered a lower limit to the actual sea ice loss that will be realized.

[1] Recent work by Rampal et al. (2011) found that compared to observations, most models underestimate sea ice thinning and the subsequent increase in drift velocity.

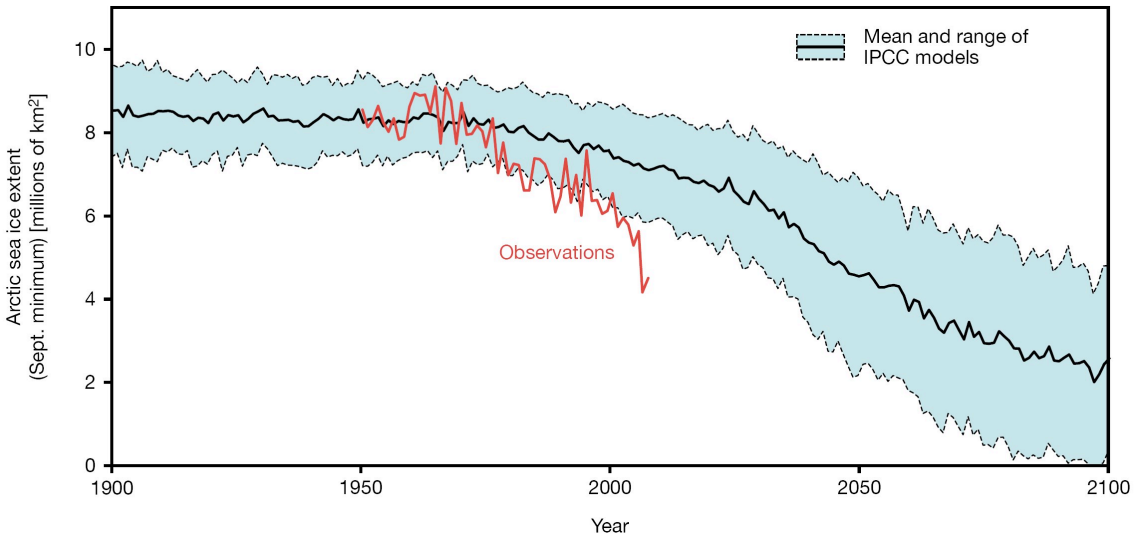

Figure 2.11. Arctic September sea ice extent (millions of km²) from observations (*red line*) and 13 IPCC AR4-WGI climate models, together with the multi-model ensemble mean (*solid black line*) and range of model results (*blue shading*). *Source:* Allison et al. (2009).

2.6.2 Snow cover, spring thaw and permafrost

Like sea ice, snow cover extent (SCE) is a sensitive indicator of climate change due to the existence of snow-albedo feedback, which works in an analogous manner to ice-albedo feedback, but over bare or vegetated ground. According to the AR4-WGI:

> Snow cover has decreased in most regions, especially in spring and summer. Northern Hemisphere (NH) snow cover observed by satellite over the 1966 to 2005 period decreased in every month except November and December, with a stepwise drop of 5% in the annual mean in the late 1980s. In the Southern Hemisphere, the few long records or proxies mostly show either decreases or no changes in the past 40 years or more. Where snow cover or snowpack decreased, temperature often dominated; where snow increased, precipitation almost always dominated (AR4-WGI, Ch. 4, p. 339).

Brown and Robinson (2011) updated the time series of Northern Hemisphere (NH) average SCE by combining NOAA satellite and in situ observations. They found significant reductions over the past 90 years, with an accelerated decrease during the last 40 years. The changes were largest in March and April, which featured an 8% lower SCE (~0.8 million km² per decade) over the 1970-2010 period compared to 1922-70 (**Figure 2.12**). Reduced spring SCE is also manifested as a shorter snow season, which declined by 5.3 days per decade since 1972–1973 due to earlier spring snowmelt (Choi et al., 2010).

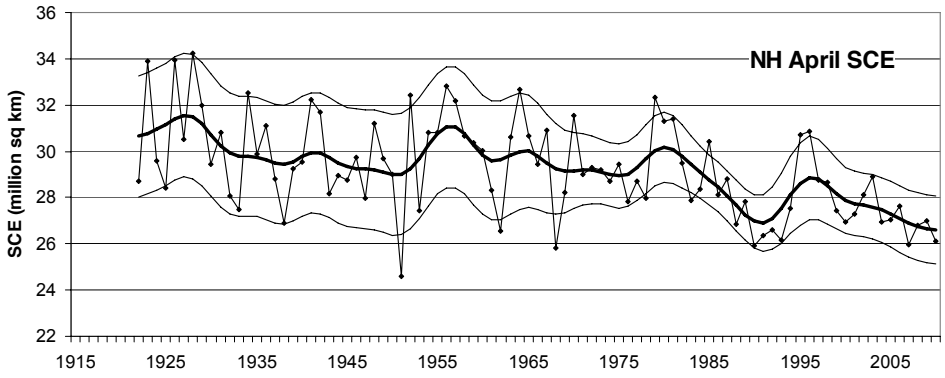

Figure 2.12. Northern Hemisphere April snow cover extent estimated from NOAA satellite data. Smooth curves are 13-term filtered values of the mean and 95% confidence interval (excludes Greenland, which averages 2.16 × 10^6 km^2).

The observed decline in SCE is likely due to warmer air temperatures, and Brown and Robinson (2011) demonstrate a strong negative correlation of NH spring SCE with NH mid-latitude air temperatures. However, they also note that changes in atmospheric circulation may also have contributed.

Increasing air temperatures over NH continents have raised ground temperatures as well. Permafrost, areas of soil or rock where the temperature remains below 0°C for long periods. underlie about one-quarter of the terrestrial surface of the Northern Hemisphere, and are very sensitive to thermal changes. The temperature at the base of the "active layer," which overlays permafrost and thaws in summer, has increased by up to 3°C since the 1980s in the Arctic (AR4-WGI, Sec. 4.7.3.2). Furthermore, according to the AR4-WGI:

> [t]he permafrost base has been thawing at a rate ranging up to 0.04 m per year in Alaska since 1992 and 0.02 m per year on the Tibetan Plateau since the 1960s. Permafrost degradation is leading to changes in land surface characteristics and drainage systems.
>
> The maximum extent of seasonally frozen ground has decreased by about 7% in the NH from 1901 to 2002, with a decrease in spring of up to 15%. Its maximum depth has decreased about 0.3 m in Eurasia since the mid-20th century. In addition, maximum seasonal thaw depth over permafrost has increased about 0.2 m in the Russian Arctic from 1956 to 1990. Onset dates of thaw in spring and freeze in autumn advanced five to seven days in Eurasia from 1988 to 2002, leading to an earlier growing season but no change in duration.

These results are summarized graphically in **Figure 2.13**.

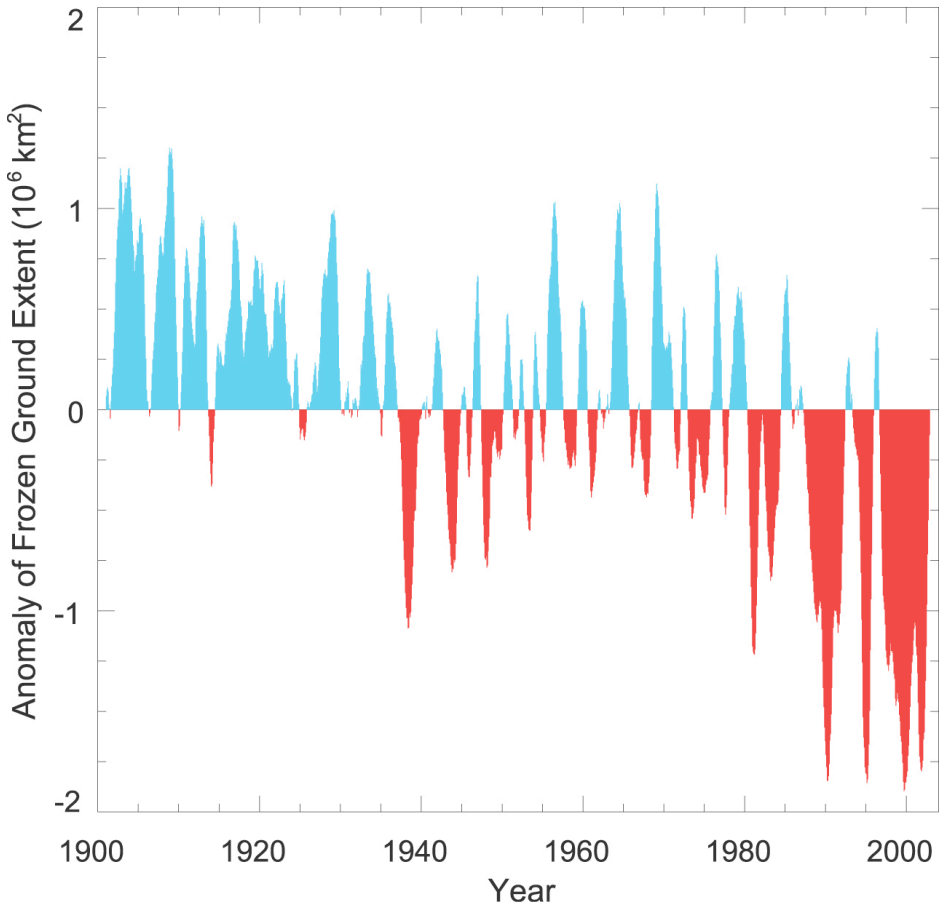

Figure 2.13. Historical variations in the monthly areal extent (in millions of square km) of seasonally frozen ground (including the active layer over permafrost) for the period from 1901 through 2002 in the NH. The positive anomaly (blue) represents above-average monthly extent, while the negative anomaly (red) represents below-average extent. The time series is smoothed with a low-pass filter (after Zhang et al., 2003). *Source:* AR4-WGI, Figure 4.22.

Nearly all ground transportation and civil infrastructure at sufficiently high northern latitudes overlays permafrost, and destabilization of these areas is clearly detrimental from both an economic and safety perspective. Numerous examples of the degradation and failure of roads, buildings, pipelines and other structures have now been documented in Siberia, Alaska, the Yukon, and other areas (e.g., see *Climate Change, Permafrost, and Impacts on Civil Infrastructure,* U.S. Arctic Research Commission Permafrost Task Force Report, 2003).

Permafrost also functions as a storage reservoir for large quantities of frozen methane, both on land and beneath the ocean floor. As these areas warm, it is expected that this methane will be liberated as a gas and escape to the atmosphere, where it acts as a potent greenhouse gas (with about 25 times the warming effect per molecule as CO_2, over the timescale of decades to centuries; AR4-WGI, Table 2.14). While this represents a potential positive feedback effect of some concern (Sec. 2.6.1), there are few observations to date indicating that previously frozen methane is being released (e.g., Shakhova et al. [2010]).

Information on changes in snow cover and permafrost in the Southern Hemisphere has been slow to emerge, and thus no significant trends have been documented to date.

2.7 Continental ice: Glaciers and ice sheets

2.7.1 Glaciers and ice caps

According to the NSIDC, glaciers store about 69% of the world's freshwater, and represent an important source of freshwater for a significant fraction of the world's population. Central Asian countries are dependent on seasonal glacier melt water for irrigation and drinking supplies, while in Norway, the Alps, and the Pacific Northwest of North America, glacier runoff is used to generate hydroelectric power. Glacier fluctuations can be reconstructed back to the peak of the last ice age about 21,000 years ago using a variety of scientific methods. The transition from that state to the early Holocene epoch (about 12,000 to 6,000 years ago) was marked by a widespread warming, prompting a drastic general ice retreat with intermittent periods of re-advances. The maximum glacier extents in many mountain ranges over the entire Holocene (12,000 years ago to present) are marked by moraines that date from the Little Ice Age (LIA, early 14th to mid-19th century).

Glacier length change measurements, available since the late 19th century, show a general glacier recession from the positions of the LIA moraines worldwide. These results were reviewed in AR4-WGI and in the World Glacier Monitoring Service (WGMS) report, *Global Glacier Changes: Facts and Figures* (Zemp et al., 2008), the first-ever worldwide inventory of glaciers and ice caps which includes an analysis of glacier trends. For larger glaciers, the overall retreat is commonly measured in kilometers, and in hundreds of meters for smaller glaciers. Within this general trend, strong glacier retreat was observed in the 1920s and 1940s, followed by stable or advancing conditions around the 1970s, and again drastic glacier retreats after the mid-1980s. The surface areas of individual glaciers in the tropics (e.g., Irian Jaya, Indonesia, and Kibo-Kilamanjaro and Rwenzori in Africa) exhibit some of the strongest declines, by about 80% of their 1900 areas (AR4-WGI, Sec. 4.5.3). On shorter (decadal) timescales, deviations from these global trends are found in many regions, due to high variability in glacier fluctuations.

Direct field measurements of the change in glacier surface elevation between two dates and subsequent estimation of the glacier's area and snow density yield an important quantity called the glacier *mass balance*. The mass balance corresponds to the mean thickness change (in units of meters of water equivalent: m w.e.) and can be compared directly between different glaciers and/or world regions. **Figure 2.14** shows the global average glacier mass balance as a function of time, from 1955-2005, while **Figure 2.15** gives a breakdown by region. In the former figure, an acceleration of mass loss since the mid-1980s is evident, consistent with the results for glacier retreat noted above. Fig. 2.15 shows that the largest mass losses per unit area occurred in Patagonia, Alaska and northwest USA, and southwest Canada. In the decade 1996-2005, all major glaciated regions except Antarctica show a decrease in glacier mass balance (Zemp et al., 2008).

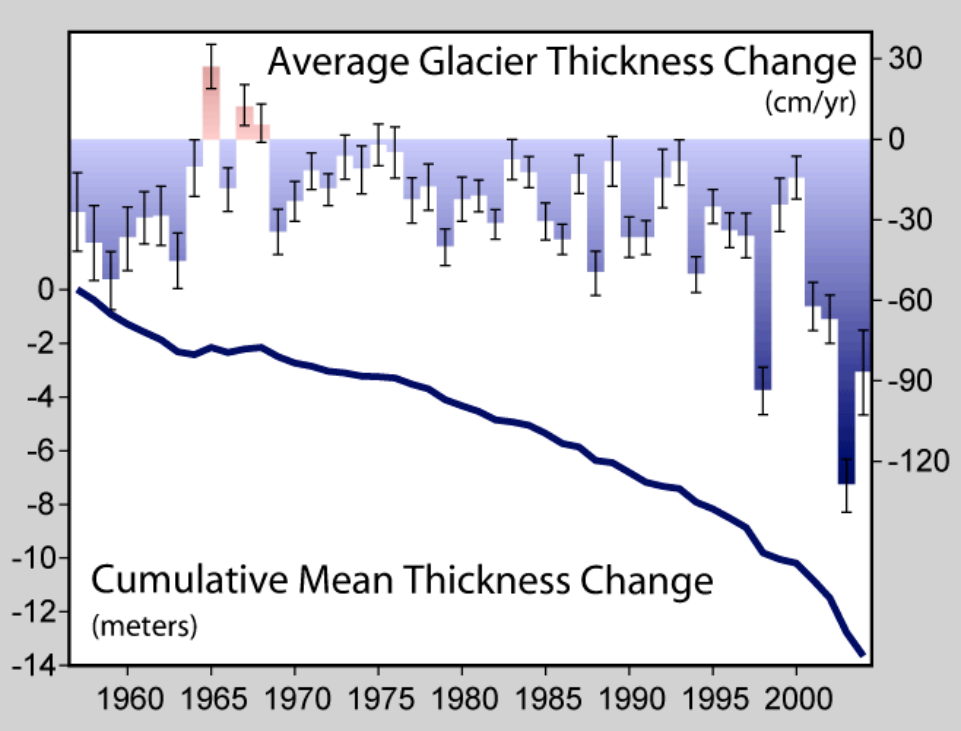

Figure 2.14. Average changes in the thickness of mountain glaciers, shown as both annual changes and the accumulated change since the late 1950s. *Source:* R. Rodhe (2006), http://www.globalwarmingart.com/, prepared from published data archived at the World Glacier Monitoring Service at the NSIDC.

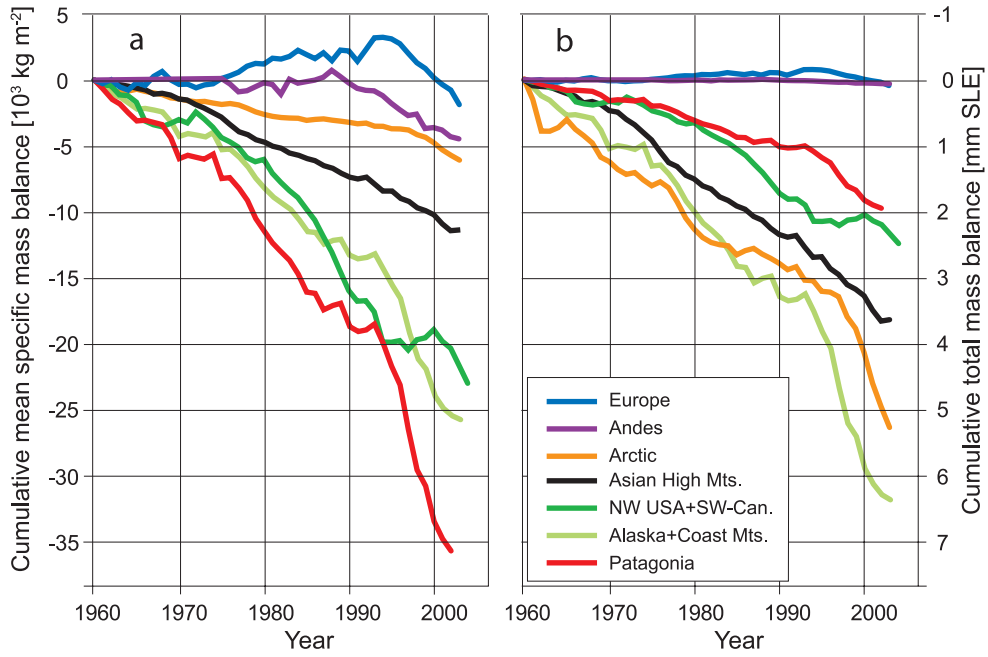

Figure 2.15. Cumulative mean specific mass balances (a) and cumulative total mass balances (b) of glaciers and ice caps, calculated for large regions (Dyurgerov and Meier, 2005). Mean specific mass balance shows the strength of climate change in the respective region. Total mass balance is the contribution from each region to sea level rise. *Source:* AR4-WGI, Figure 4.15. "mm SLE" refers to "millimeters of sea level equivalent."

2.7.2 Greenland and Antarctic ice sheets

The Earth's most massive ice monuments, the Greenland and Antarctic ice sheets, have displayed both increases and declines in recent decades, according to the AR4-WGI:

> Thickening of high-altitude, cold regions of Greenland and East Antarctica, perhaps from increased snowfall, has been more than offset by thinning in coastal regions of Greenland and West Antarctica in response to increased ice outflow and increased Greenland surface melting (AR4-WGI, Ch. 4, FAQ 4.1)

Much of our knowledge about these ice sheets has been obtained only recently, since the launch of the Gravity Recovery and Climate Experiment (GRACE) satellite in 2002. This satellite provides routine measurement of the Earth's gravity field and its temporal variability. Information on changes in the mass distribution of the ice sheets and underlying rock can be obtained after correcting for the effects of tides, atmospheric loading, and other factors. Velicogna (2009) presented results for the two ice sheets from 2002-2009, reproduced here in **Figure 2.16**. Both ice sheets display a clear decline in ice mass over this period, with an accelerating trend in recent years.

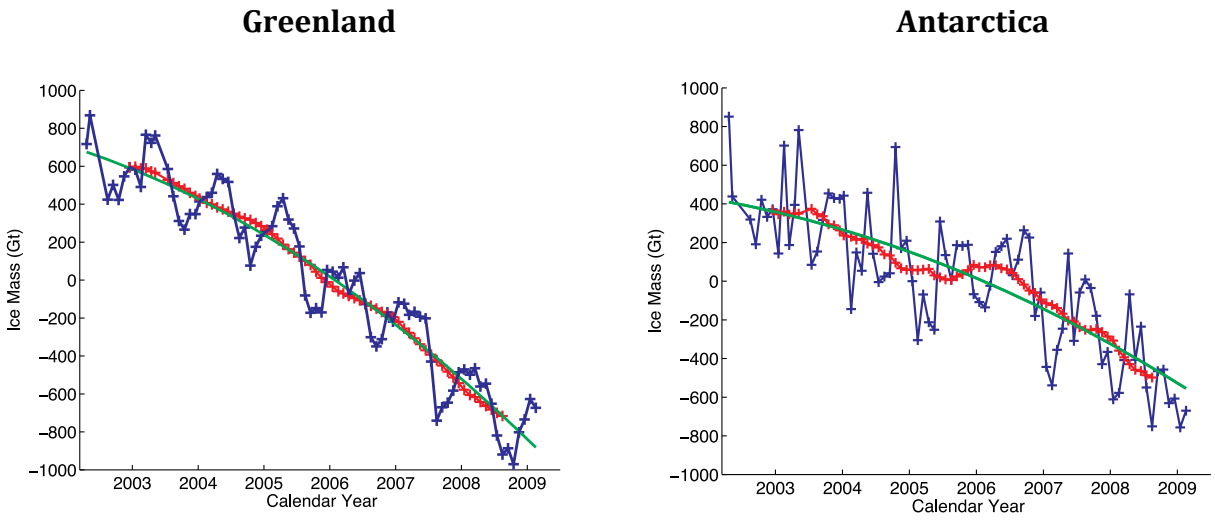

Figure 2.16. Time series of ice mass changes (gigatons) estimated from GRACE monthly mass solutions for the period from April 2002 to February 2009 for the Greenland (*left*) and Antarctic (*right*) ice sheet. Unfiltered data are blue crosses. Data filtered for the seasonal dependence using a 13-month window are shown as red crosses. The best-fitting quadratic trend is shown (green line). The GRACE data have been corrected for leakage and GIA. *Source:* Velicogna (2009).

Other measurement techniques, such as radar and laser altimetry and examination of aerial photographs and satellite images, confirm these results. For example, Cook et al. (2005) found that 87% of the 244 glaciers on the West Antarctic Peninsula and adjacent islands have retreated over the last six decades (WGMS). Several prominent ice shelves in this region, which represent the termination of inland glaciers at the sea, have collapsed over the past decade (e.g., the Larsen-

B ice shelf in 2002). Similar collapses in the adjacent Amundsen Sea are likely the result of thinning ice shelves from a warm underlying ocean (Jacobs et al., 2011).

2.7.3 Associated sea-level rise

In the AR4-WGI, it was estimated that the melting of glaciers and ice caps contributed 0.77 ± 0.22 mm per year to SLR between 1991 and 2004, with a smaller contribution from the Greenland and Antarctic ice sheets, 0.2 ± 0.1 mm per year and 0.2 ± 0.35 mm per year, respectively.

The more recent GRACE data have allowed these ice sheet trends to be updated. Velicogna (2009) estimated a total SLR contribution of 7.7 ± 1.4 mm (about 1 mm/yr) from the two ice sheets between 2002 and 2009, two-thirds of which comes from Greenland. Several recent estimates using independent measurements are roughly in line with this. Compared to the annual rate of total SLR cited in Sec. 2.5, ice sheet melting contributed about one-third of global SLR. There is also evidence that the rate of melting of the Greenland and Antarctic ice sheets has accelerated in recent years (Rignot et al., 2011). To gain some perspective for the absolute values, we note that these figures are very small compared with the potential SLR from a complete melting of the Greenland and Antarctic ice sheets, which are estimated as 7.3 m and 56.6 m, respectively. Melting of the West Antarctic ice sheet alone would contribute approximately 4.8 m of this (Bamber et al., 2009). However, most experts believe that the prospect of such catastrophic ice sheet loss in the 21st century is remote (Sec. 6).

2.8 Forest disturbance: Wildfires, pests, and climate-induced mortality

Increased temperature over land, with larger increases in high northern latitudes and continental interiors, might be expected to increase the incidence of forest fires for several reasons. First, increased evapotranspiration leads to drier forests. Second, warming enhances convection over land, leading to increased storm activity and lightning strikes (the cause of 85% of fires in North America). And third, as the growing season lengthens, so does the fire season. Coincident increases in precipitation may also occur in some areas, but their magnitude is likely not as important as their timing during the fire season (Flannigan and Harrington, 1988). The increasing occurrence of drought during the fire season has been linked to some of the largest wildfires (Sec. 4.4; Krawchuk and Moritz, 2011).

Globally, there are few studies of trends in forest fire occurrence or affected area. Mouillot and Field (2005) assembled a fire history reconstruction for the 20th century for 14 regions worldwide, based on fire data for the 1980s and 1990s and back-extrapolation of land use practices and local studies, such as tree ring analysis, for previous decades. Over the past few decades, their findings indicate that area burned has decreased in Australia, Eastern Asia, the Eastern U.S., and South American temperate forests, increased slowly in boreal North America, Europe, and South Asia, and increased dramatically in Southeast and Central Asia and South American tropical forests. In the latter forests, fires are an infrequent element of the natural disturbance regime, and the increase is largely due to deforestation to prepare land for agriculture.

The boreal forests of North America are the best studied fire regime on the planet, and studies by

Littell et al. (2009), Westerling and Bryant (2008), and others have demonstrated that climate variability along with vegetation type and elevation are important regulating factors for the area burned in wildfires. **Figure 2.17** (left) shows the observed area burned for the entire historical record (1916-2003) and that predicted by empirical models that take climate data over more recent decades (temperature, precipitation, and wind) and these environmental factors into account.

Westerling et al. (2011) noted a correlation between the number of large (> 200 ha) fires versus average March through August temperature anomalies in Western U.S. forests from 1972-2008, as depicted in **Figure 2.17** (right). Thus, provided that warm anomalies occur over dry, forested regions, one might expect the incidence of the largest fires to increase under global warming.

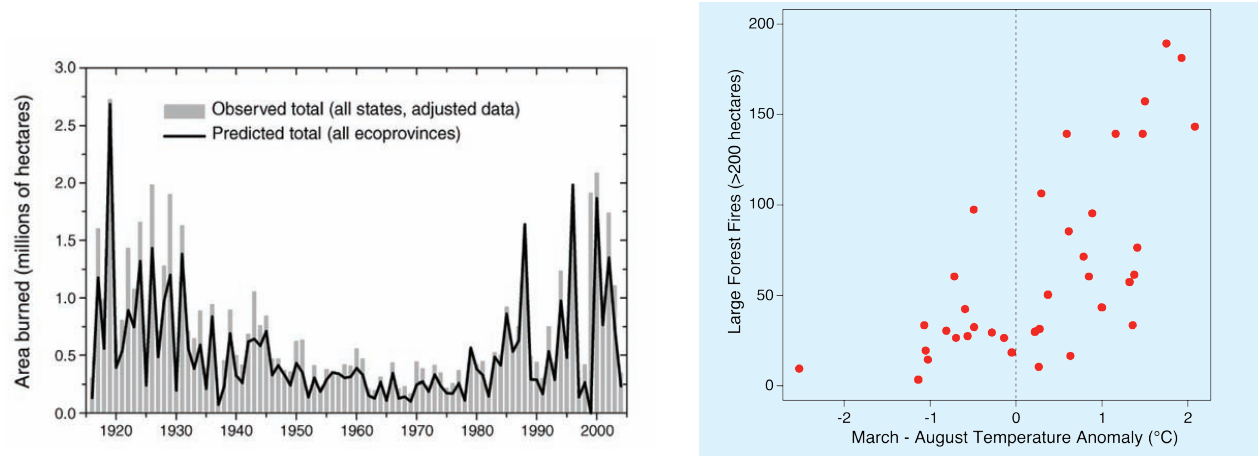

Figure 2.17. *Left:* Observed and reconstructed wildfire area-burned for 11 Western U.S. states (*bars*) and reconstructed (*line*) for the period 1916-2004. *Source:* Littell et al. (2009). *Right:* The number of large forest wildfires (*vertical axis*) versus average March through August temperature anomalies (*horizontal axis*) for 1972-2008 in Western U.S. forests. Anomalies were constructed subtracting the long-term mean for 1972-1990. Fires are all large (> 200 ha) fires reported by the United States' Bureau of Indian Affairs, National Park Service, and Forest Service as burning in forests. All fires were classified as "action" fires on which suppression was attempted (fires used to manage vegetation were excluded). *Source:* Westerling (2012). Also see Westerling et al. (2006) and Westerling et al. (2011) for data and methodology.

Gillett et al. (2004) showed that the area burned by forest fires in Canada has increased over the past 40 years, coincident with warming summer temperatures. They further demonstrated that human-induced climate change had a detectable influence on the area burned by Canadian forest fires over that period.

Furthermore, it is generally acknowledged among experts in forest inventories and tree mortality that historical and current drought episodes coupled with elevated temperatures have contributed to the recent increase in widespread fires and bark-beetle outbreaks in the U.S. Southwest region (Williams et al., 2010 and references therein). In that region, after 15 months of depleted soil water content in 2002-2003, drought, unusually high temperatures, and associated bark-beetle infestations killed more than 90% of the dominant, overstory tree species, *Pinus edulis*. The dieback was reflected in changes in a satellite index of vegetation greenness across the

region, extending over approximately 12,000 km^2 (Breshears et al., 2005). An experimental study of the same species subjected to similar conditions led Adams et al. (2009) to the conclusion that "carbon starvation"—through increased respiration, which is an exponential function of temperature—likely affected dieback more than water stress.

While the devastating effect of fires is well known, it has been estimated that forest insects annually cause 1.3 to 3 times the damage of forest fires to timber volumes across Canada (Haughian et al., 2012; Volney and Fleming, 2000), and can affect 10 times as much area (CCFM, 2011). A warmer, drier climate is expected to favor increased growth rates and over-winter survival of many insect pest species. Indeed, as reported by Kurz et al. (2008):

> The current outbreak of mountain pine beetle in western Canada is an order of magnitude greater in area than previous outbreaks owing to the increased area of susceptible host (mature pine stands) and favourable climate… An expansion in climatically suitable habitat for the mountain pine beetle, including reduced minimum winter temperature, increased summer temperatures and reduced summer precipitation, during recent decades has facilitated expansion of the outbreak northward and into higher elevation forests. This range expansion, combined with an increase in the extent of the host, has resulted in an outbreak of unprecedented scale and severity. By the end of 2006, the cumulative outbreak area was 130,000 km^2 (many stands being attacked in multiple years), with tree mortality ranging from single trees to most of a stand in a single year.

In this example, climate change is not the entire story: the early 20th century forestry industry policy of fire suppression also exacerbated the problem, by allowing the buildup of large amounts of dry fuel which increased the severity of uncontrollable fires. Also, according to the Canadian Council of Forest Ministers (2011), the area affected by the mountain pine beetle has been decreasing since reaching a peak in 2007.

Finally, some types of forest disturbance are more indirectly connected to climate, but are nevertheless significant. For example, in 2005 Hurricane Katrina killed or severely damaged over 320 million large trees as it crossed over the Gulf States of the southeastern U.S. As these trees decompose over subsequent years, it has been estimated that they will release an amount of carbon dioxide equivalent to that taken up by all U.S. forests in a year (Kunkel et al., 2008).

3. Regional and Seasonal Climate Change

The changes in global average, annual mean climate variables discussed above are made up of the sum of seasonally varying changes over all the planet's disparate regions. Global, annual mean variables are smoothed versions of their regional and seasonal components, and thus mask higher magnitude changes that are of interest for local climate change impacts. A simple mathematical example of computing an average from two numbers illustrates the point. Consider the two data sets [1, 3] and [-99, 103]. The average of each is +2, but the components of each set are significantly different.

Even as the global and annual mean surface air temperature (SAT) has increased over the past few decades, there are regions where it has decreased, or where the changes are indistinguishable from natural variability over that period. Thus, the term "global warming" has never meant "temperature is increasing everywhere on the globe," but rather, "while in some in regions SAT has decreased, it has increased by a larger amount elsewhere." The same is true of all other climate variables, and hence it is worth delving deeper into exactly where the largest changes are being experienced, and in which climate indicators.

3.1 Surface air temperature

At each point on the Earth's surface where measurements exist (Fig. 2.2), the evolution of surface temperature looks roughly like one of the curves of global SAT shown in Fig. 2.3. Beginning with the irregularly spaced data shown in Fig. 2.2, climate researchers find it useful to construct a uniform grid of area-averaged measurements, known as a *gridded* data set. This allows coherent patterns of regional temperature change and associated trends to be more easily identified.

Linear trends in SAT displayed on a grid generated from the GHCN data for the periods 1901-2005 and 1979-2005 are shown in **Figure 3.1** from the IPCC AR4-WGI. For the purpose of this review, two important conclusions can be drawn from Fig. 3.1. First, over areas with sufficient data, almost all trends are statistically significant at the 5% level, meaning that they are unlikely to arise from natural climate variability alone. In layman's terms, one would say they represent "real" changes to the pre-industrial climate. Second, the map for the more recent period (Fig. 3.1, right) shows that there are very few areas over land where negative temperature trends are seen. Hence, over 1979-2005 the annual average warming is truly global in extent. It is also clear that warming has occurred more rapidly over some regions than others: Central and eastern Asia and northern Canada particularly stand out.

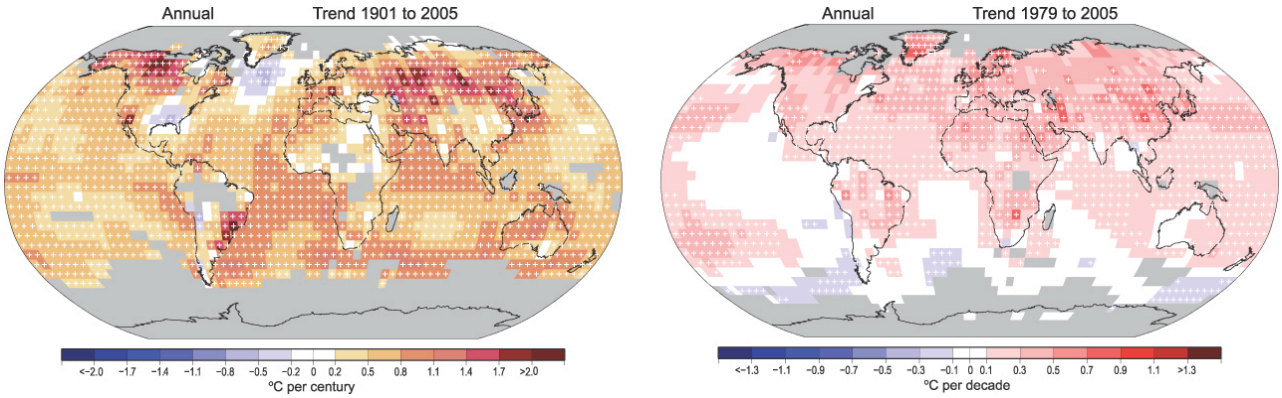

Figure 3.1. Linear trend of annual temperatures for 1901 to 2005 (left; °C per century) and 1979 to 2005 (right; °C per decade). Areas in grey have insufficient data to produce reliable trends. The minimum number of years needed to calculate a trend value is 66 years for 1901 to 2005 and 18 years for 1979 to 2005. An annual value is available if there are 10 valid monthly temperature anomaly values. The data set used was produced by NCDC from Smith and Reynolds (2005). Trends significant at the 5% level are indicated by white + marks. *Source*: AR4-WGI, Figure 3.9.

There is also considerable variation of SAT trends with season, as can be seen in **Figure 3.2**, which is constructed from the publicly available NASA-GISS surface temperature analysis, also based on GHCN station data (Hansen et al., 2010; Appendix B: List of Online Resources). While the absolute changes are largest at high latitudes, it should be noted that, over land, SAT variability also increases steadily as one approaches the poles. Hence, to determine whether these regional trends are statistically significant, one also needs to consider interannual variability. This aspect is incorporated in Section 4.1 on temperature extremes.

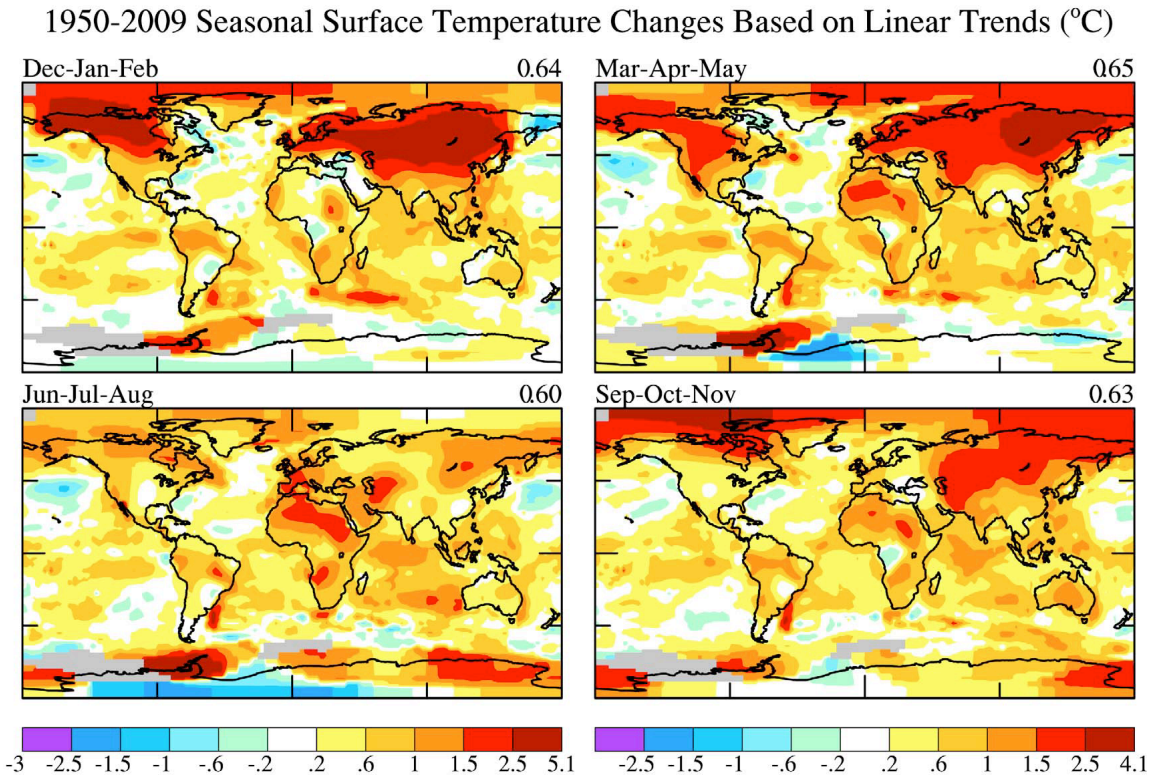

Figure 3.2. Maps of SAT changes for the four seasons for the period 1950-2009 (Hansen et al., 2010). Numbers to the upper right of each panel are the global average SAT change.

In Canada and the United States, annual mean temperature has increased in most locations over recent decades, as shown in **Figure 3.3**. In the U.S., the SAT increase is approximately 2°F over the last century, but the warming has not been uniform over the country. Moderate to strong warming of up to 4°F has occurred in the western half of the country and the U.S. Northeast, while cooling of up to 1°F occurred over some southeastern states. As Fig. 3.3 shows, regional differences in the SAT change are even larger in Canada, with a notable warming-to-cooling gradient from west to east.

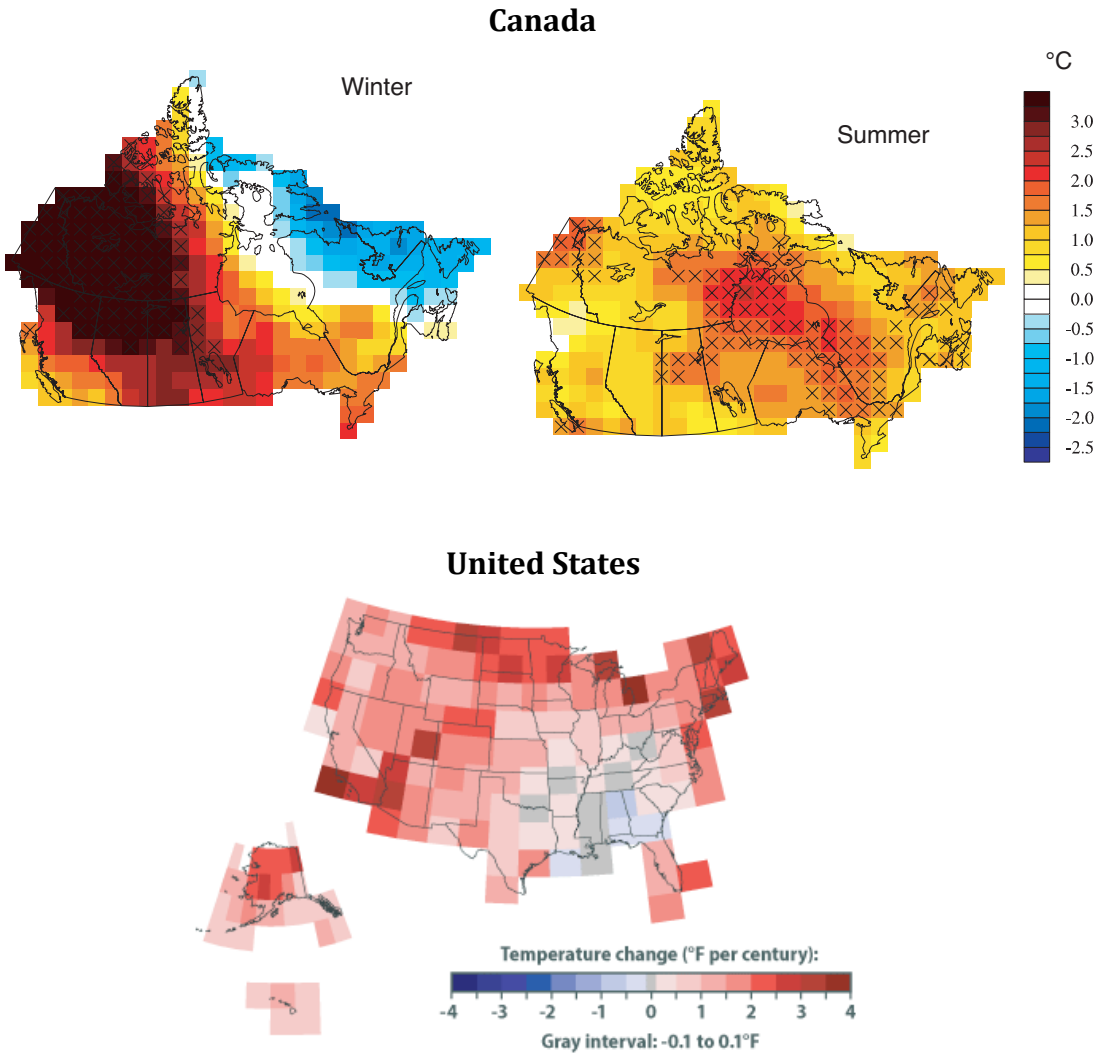

Figure 3.3. *Top:* Change in winter (*left*) and summer (*right*) mean temperatures in Canada from 1950–2003. Grid squares with trends statistically significant at 5% are marked by crosses. Units are °C. *Source:* Zhang et al. (2000), updated to 2003 by Hengeveld et al. (2005). *Bottom:* Rate of annual mean temperature change in the U.S. from 1901 to 2008 (since 1905 for Hawaii, and 1918 for Alaska). Units are °F per century. *Source:* NOAA-NCDC (2009).

On a much smaller scale, land-use effects related to increasing urbanization have been linked to increased temperatures and decreased diurnal temperature range, compared to surrounding rural areas. This *urban heat island* effect is important for understanding the character of temperature extremes experienced in urban areas, as will be discussed later in Sec. 4.1. However, it is worth noting that despite the large number of meteorological stations located near urban centers, many analyses have concluded that the slightly higher rate of urban warming has not strongly biased the above estimates of worldwide warming trends over recent decades (AR4-WGI, p. 244).

In small regions undergoing rapid development such as eastern China, urban warming is likely to make up a larger fraction of the overall SAT trend (upwards of 20%, according to Yang et al., 2011), and may have contributed up to 0.1°C/decade to the SAT trend in China as a whole, over the last few decades (compared to a total trend of ~0.7°C/decade). However, this has had little

impact on the hemispheric or global scale trends.

3.2 Precipitation and streamflow

The worldwide pattern and trends of precipitation change are constructed in the same way as for temperature, although the data are considerably more limited in time and location. **Figure 3.4** shows the pattern of precipitation anomalies in the GHCN data set, both for the entire 20th century, and 1979-2005, relative to the 1961-90 base period.

In contrast to the lack of a trend found in mean precipitation (Sec. 2.2, Fig. 2.7), statistically significant changes are detected in several regions at the century time scale, notably:

1) increases of 5%–20% over much of North America, Europe and Asia;

2) larger increases of 20%–40% over southernmost South America and Australia;

3) decreases of 20%–40% and higher in north and western Africa and the Sahel.

Over the past few decades, some of these trends appear to have reversed. For example, Sahel rainfall recovered in the 1990s, while a drying pattern was established on the Indian sub-continent. Here it should be understood that 'drying' refers strictly to 'meteorological drought,' a significant deficit of precipitation as compared with climatological normals. In addition, in the mid-to-high latitudes where average winter temperatures hover close to 0 °C for long periods, more precipitation now falls as rain than snow, owing to rising temperatures in these regions (AR4-WGI, p. 258). This has been demonstrated in particular for western Canada (**Figure 3.5**; Zhang et al., 2000) and the northern half of the United States (Feng and Hu, 2007).

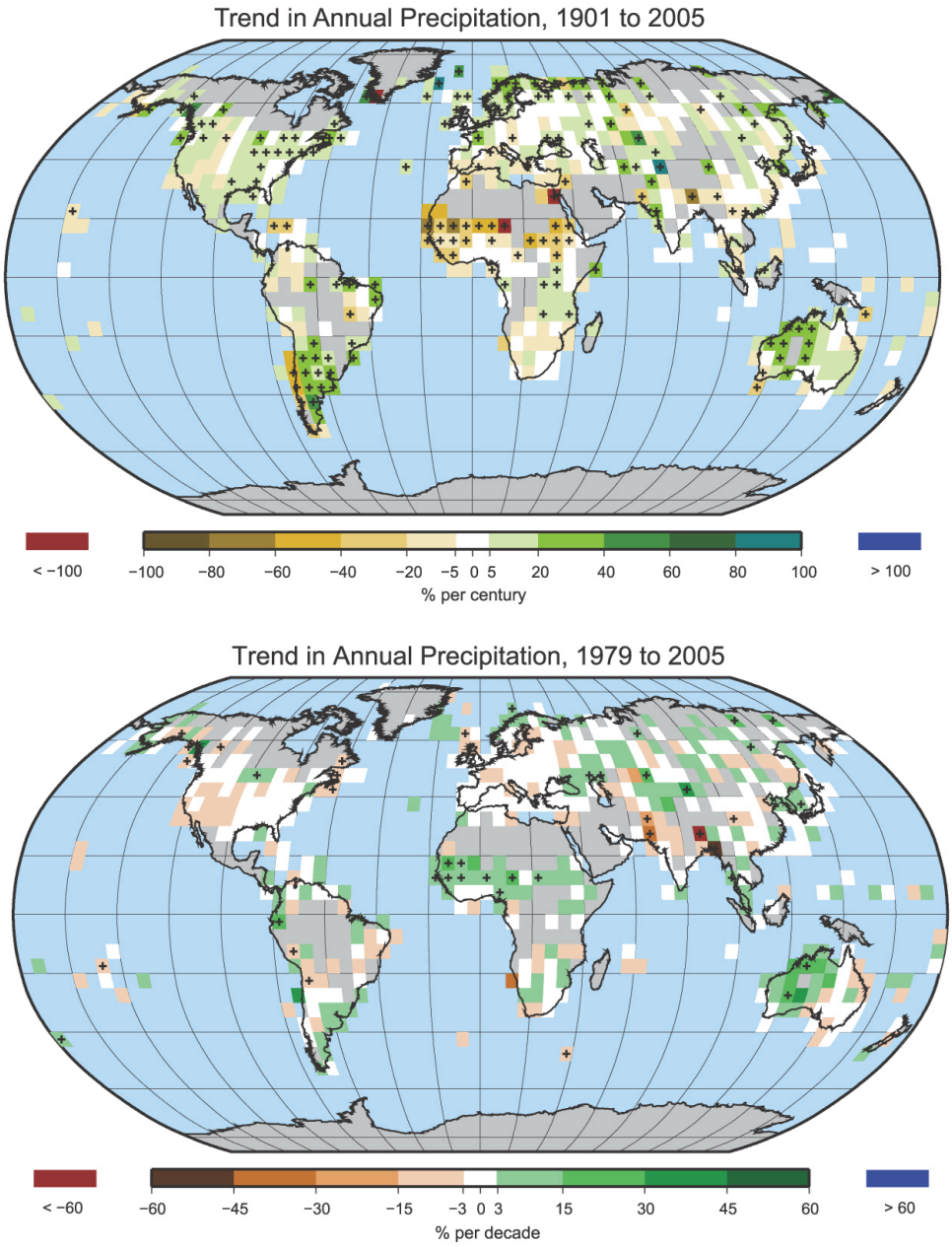

Figure 3.4. Trend of annual land precipitation amounts for 1901 to 2005 (*top*, % per century) and 1979 to 2005 (*bottom*, % per decade), using the GHCN precipitation data set from NCDC. The percentage is based on the means for the 1961 to 1990 period. Areas in grey have insufficient data to produce reliable trends. The minimum number of years required to calculate a trend value is 66 for 1901 to 2005 and 18 for 1979 to 2005. An annual value is complete for a given year if all 12 monthly percentage anomaly values are present. Note the different color bars and units in each plot. Trends significant at the 5% level are indicated by black + marks. *Source:* AR4-WGI, Figure 3.13.

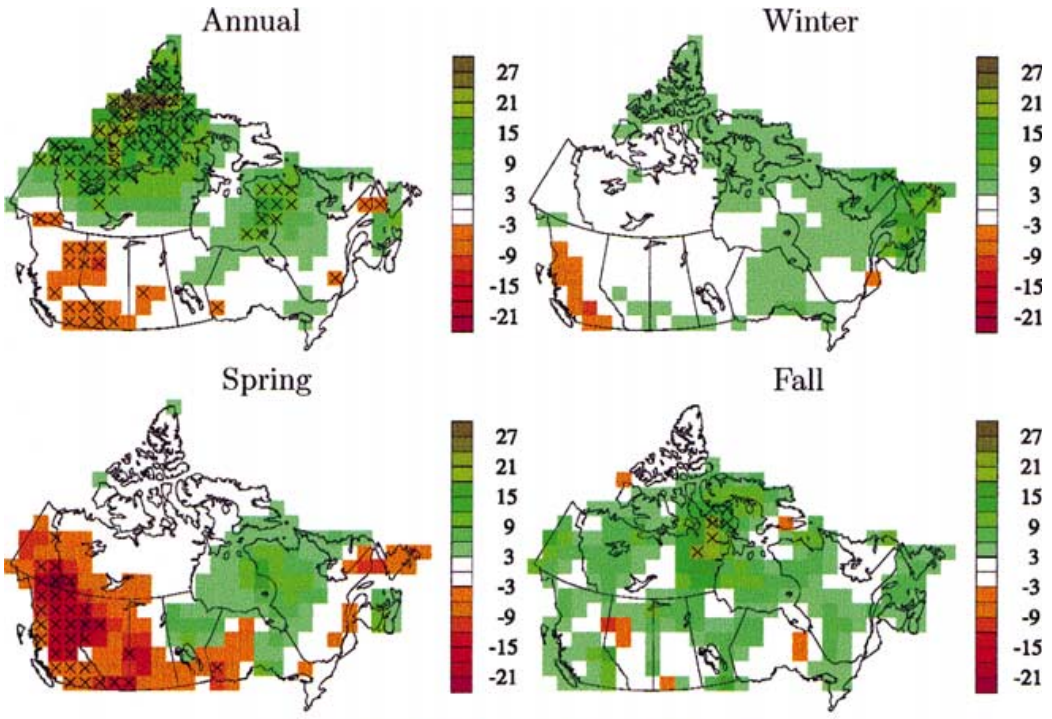

Figure 3.5. Change in the ratio of snow to rain in Canada over the 1950-98 period. White areas have insufficient data, while crosses indicate 95% significance. *Source:* Zhang et al. (2000).

Over Canada and the United States, annual mean precipitation has increased by about 5% over the past 50 years, with an overall increasing magnitude toward the north. While in Canada precipitation increased nearly everywhere (there were 21 more days with precipitation in 2003 than in 1950, according to a fitted linear trend), in the U.S. both the magnitude and sign of the change are highly variable across the nation (**Figure 3.6**). Reductions of up to -25% are seen in the Southeast and Northwest U.S., -40% in the Southwest, and increases of up to +25% in the North-central and Northeast states. This variable regional pattern of change is also seen on other continents in the mid-latitudes, e.g. in the Mediterranean region (Hoerling et al., 2012).

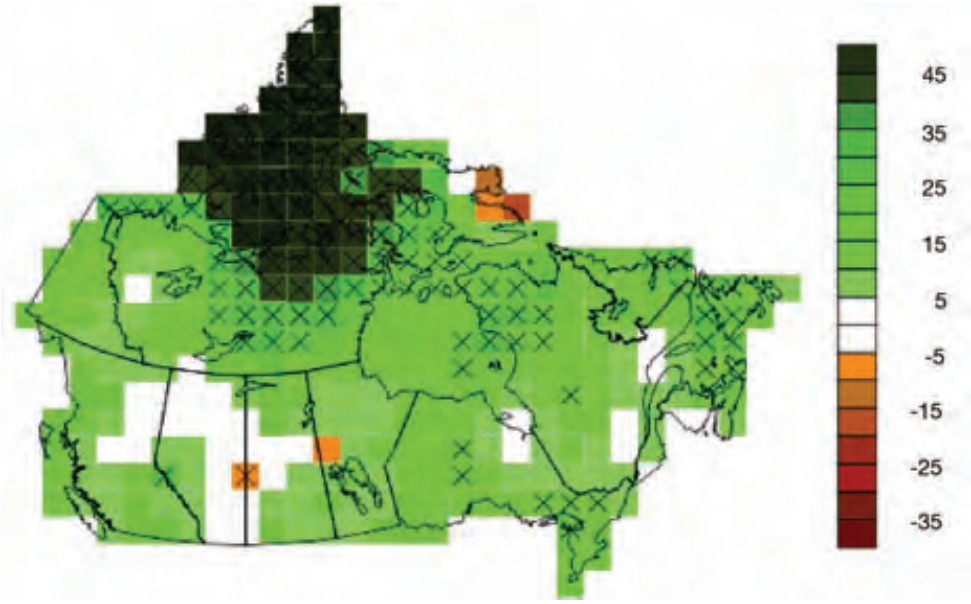

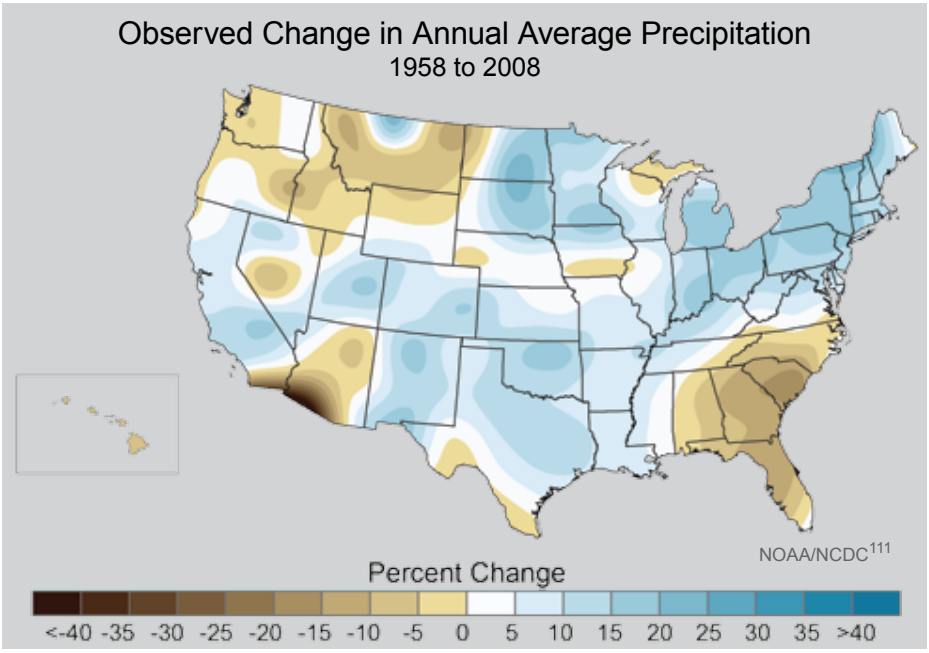

Figure 3.6. *Top:* Percentage change in annual mean precipitation in Canada over the 1948-2003 period. White areas have insufficient data, while crosses indicate 95% significance. *Source:* Zhang et al. (2000), updated to 2003 by Hengeveld et al. (2005). *Bottom:* Percentage change in annual mean precipitation in the U.S. over the period 1958-2008. *Source:* Karl et al. (2009).

It is worth noting that, just as for temperature, precipitation may be normalized by its standard deviation. The Standardized Precipitation Index (SPI; McKee, 1993) is defined as the number of standard deviations that observed cumulative precipitation deviates from the climatological

average. The SPI for the continental U.S.A. under drought and non-drought conditions is shown in Figure 4.12 of the following section.

Streamflow records are available for most of the world's major rivers. Many major rivers are affected by the construction of large dams and reservoirs and changes in adjoining land-use, so any trends that are found must be interpreted with caution. Nevertheless, according to the AR4-WGI, since rapid warming began in the 1970s there is evidence of earlier snowmelt and earlier peak streamflow in the western (~20 days earlier) and northeastern (~14 days earlier) USA (Karl et al., 2009; **Figure 3.7**). Also, earlier breakup of river ice in the Russian Arctic and in numerous Canadian rivers has been recorded. Streamflow in the Yellow River in China decreased significantly in the second half of the 20th century, even after increased human water consumption was accounted for. Coincident temperature increases were found in this basin, while precipitation showed little change, suggesting that evaporation has been increasing (AR4-WGI, p. 264).

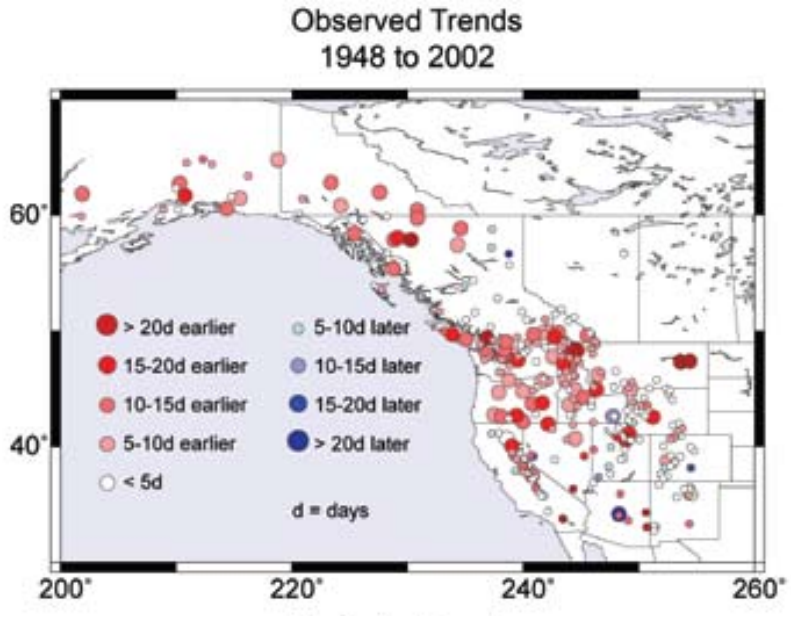

Figure 3.7. Changes in runoff timing in snowmelt-driven streams from 1948 to 2002 with red circles indicating earlier runoff, and blue circles indicating later runoff. *Source:* Karl et al. (2009), after original in Stewart et al. (2005).

Among other impacts, these results have important consequences for hydroelectric power generation. The latter is very sensitive to changes in precipitation and river discharge. It has been estimated that for every 1 percent decrease in precipitation there is a 2 to 3 percent drop in streamflow (Karl et al., 2009). Because water often flows through multiple power plants in a river basin, a decline in streamflow leads to stronger decreases in power generation. In the Colorado River Basin, e.g., every 1 percent decrease in streamflow results in a 3 percent drop in power generation (Bull et al., 2007).

3.3 Sea-level rise

Figure 3.8 shows the pattern of regional, absolute SLR over the global ocean obtained via satellite altimetry (Sec. 2.5). The trends are highly variable over the globe, an important factor to consider when evaluating regional impacts of SLR.

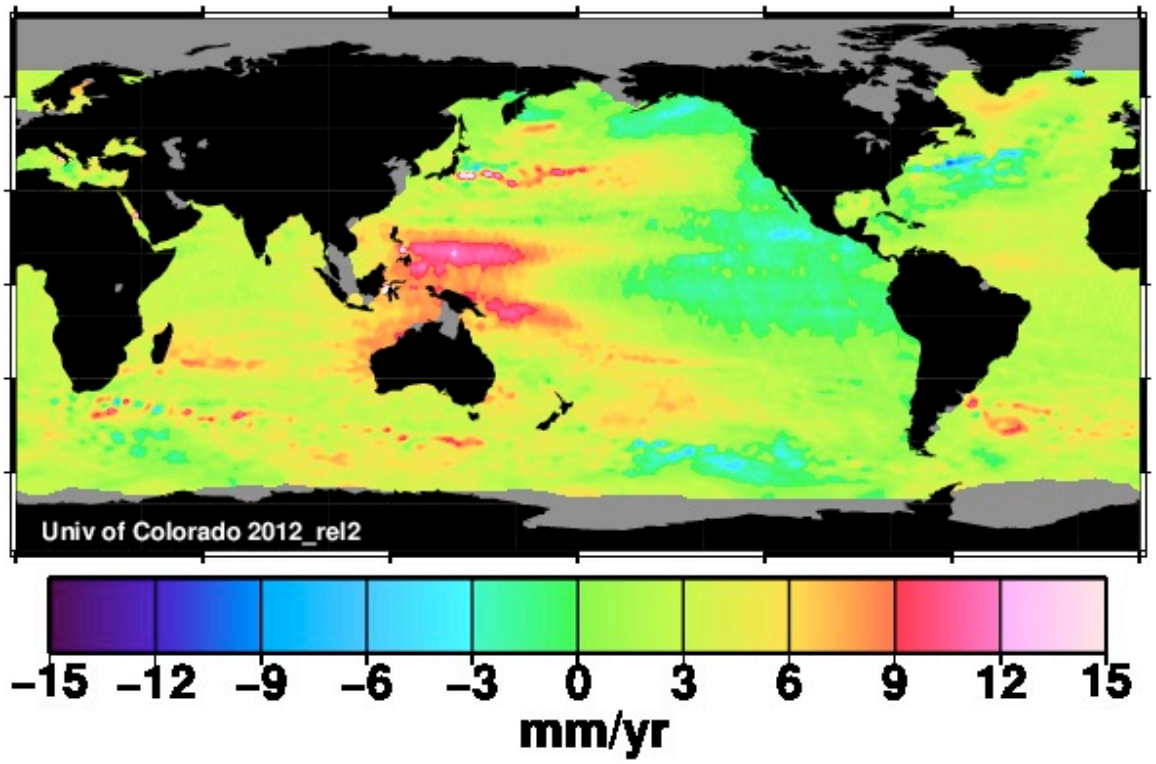

Figure 3.8. Geographic distribution (latitude versus longitude) of linear trends in mean sea level (mm per year) for 1993 to 2012 based on TOPEX/Poseidon satellite altimetry. *Source:* http://sealevel.colorado.edu/content/map-sea-level-trends.

Ongoing tidal gauge measurements provide complementary information at the local scale, and these are shown for sites with the longest, quality-controlled records in **Figure 3.9.** Positive relative sea-level anomalies were recorded in most locations in 2010, with the largest magnitudes in Japan and the eastern U.S. seaboard. Notable decreases are apparent in Scandinavia and the Baltic, and along the Gulf of Alaska.

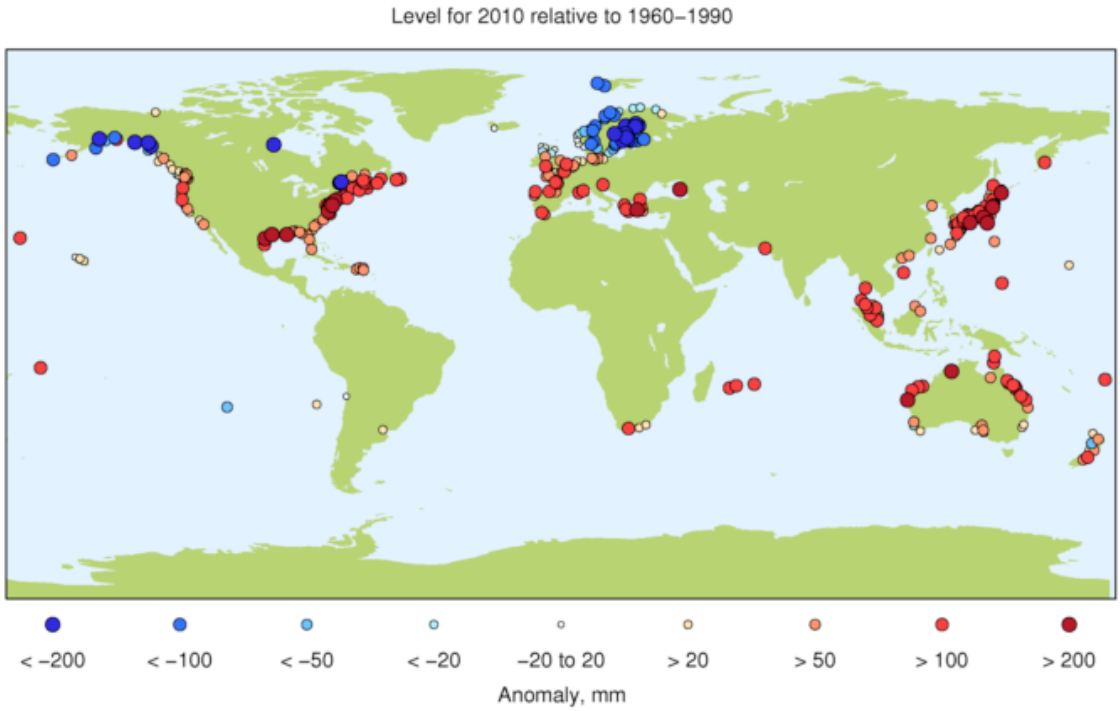

Figure 3.9. Relative sea-level anomalies for 2010, generated from a worldwide network of tide gauges, demonstrates how sea level varies from year to year when compared with the long-term (1960-90) average at a particular site. *Source*: UK Permanent Service for Mean Sea Level (PSMSL). http://www.psmsl.org/products/anomalies/.

Sea-level changes are regularly monitored at the national level by most maritime nations. Trends for the United States between 1958 and 2008 are shown in **Figure 3.10**. Relative sea level rose along much of the U.S. coastline over this period, particularly the Mid-Atlantic coast and parts of the Gulf coast, where some stations registered increases of more than 8 inches. Meanwhile, relative sea level fell at some locations in Alaska and the Pacific Northwest. In this area of the Pacific, Fig. 3.8 shows that absolute SLR is near zero or negative; but where sea level has risen, land elevation has evidently also risen faster.

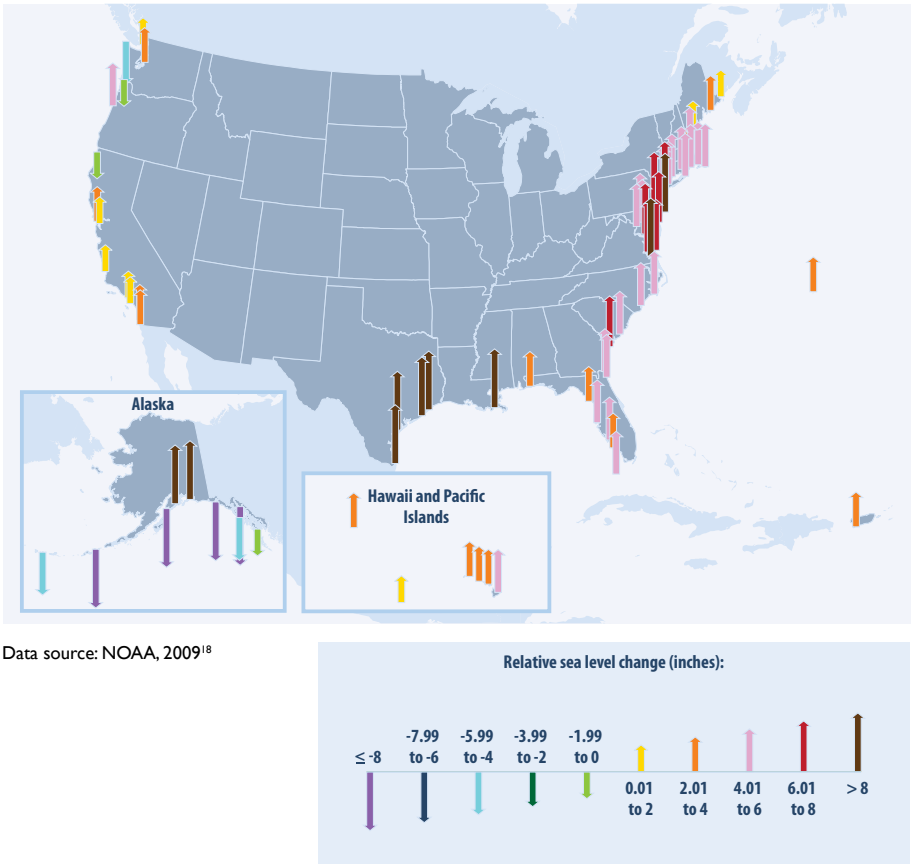

Data source: NOAA, 2009[18]

Figure 3.10. Changes in relative sea level from 1958 to 2008 at tidal gauge stations along U.S. coasts. Relative sea level accounts for changes in sea level as well as land elevation. *Source*: NOAA (2009).

It stands to reason that regional SLR, in combination with the regular occurrence of tides and seasonal storms, will lead to increased risk of flooding in coastal areas. To illustrate this, we focus on the situation in the U.S., which has recently been evaluated in detail in the recent report issued by the organization Climate Central, *Surging Seas* (Strauss et al., 2012a). The main concern is an increase in the magnitude and/or frequency of storm surges. Storm surges are a coastal phenomenon associated with offshore low pressure weather systems, such as tropical or extratropical cyclones (Sec. 4.3). High winds associated with the storm push on the sea surface, causing water to pile up higher than the ordinary sea level. If a storm surge coincides with a rising tide, severe coastal flooding can result (**Figure 3.11**). Historically, most casualties resulting from tropical cyclones occur during the storm surge.[1]

[1] The Galveston Hurricane of 1900, a Category 4 hurricane that struck coastal Texas, packed a devastating storm surge; between 6,000 and 12,000 lives were lost, making it the deadliest natural disaster ever to strike the United States (Hebert and Taylor, 1983).

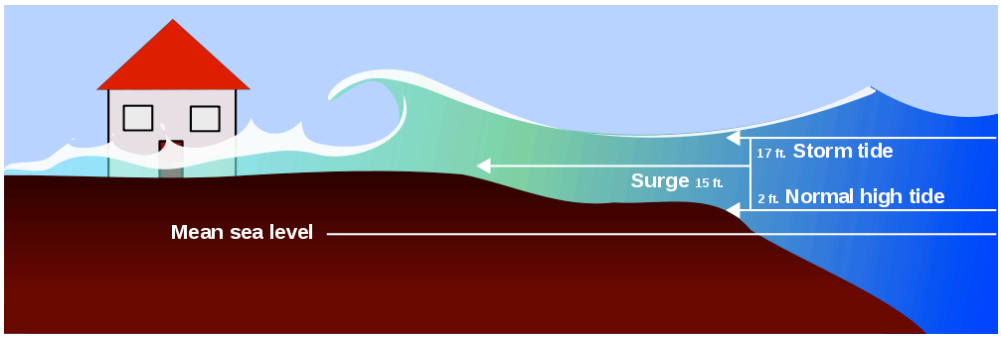

Figure 3.11. An illustration comparing mean sea level, normal high and storm tide, and storm surge. *Source:* Wikimedia Commons, accessed 03/27/2012.

The recent studies summarized by Strauss et al. (2012) found that, at two-thirds of the 55 tide gauge stations distributed around the coastal U.S. that were analyzed, SLR from warming has already at least doubled the annual risk of "once-in-a-century" or worse floods.[1] That is, at these locations, a 1% risk of flooding in any given year has become a 2% risk.

How is it that the seemingly modest rises in sea level recorded to the present can lead to significantly increased risk of catastrophic floods? The Climate Central report states:

> The increases in odds come despite the fact that sea level rise from warming, over the next two decades and over the last century, is better measured in inches than in feet. In many places, only inches separate the once-a-decade flood from the once-a-century one; and separate the water level communities have prepared for, from the one no one has seen. Critically, a small change can make a big difference, like the last inch of water that overflows a tub. Sea level rise is raising the launch pad for storms and high tides, and being experienced by the ever-more frequent occurrence of extreme high water levels during these events long before the ocean reaches damaging heights permanently. (p.4)

With regard to flooding, estimates of relative SLR alone are not informative in and of themselves; what matters is the amount of SLR relative to typical flood levels at a given location. In a region such as the Florida coastline along the northeastern Gulf of Mexico, ten-foot storm surges are sometimes seen, and thus ten inches of SLR may not necessitate unprecedented adaptation measures for those communities. Such measures may be necessary, however, in a coastal city that has only ever experienced two-foot surges.

Due to the inevitability of future warming, the flood probabilities cited above will increase further, even without assuming any change in the frequency and/or intensity of major landfalling storms (Sec. 4.3). Exposure of U.S. populations and property to future SLR was assessed in detail by Strauss et al. (2012a); these results are reviewed in Section 6.

[1] The calculation behind this result and the others cited here is based on the assumption that 90% of historical SLR is caused by warming, either directly through thermal expansion of sea water or indirectly via glacier melt. The remaining 10% would be due to ongoing, post-glacial adjustment of the Earth's crust.

3.4 El Niño-Southern Oscillation (ENSO)

As mentioned in Sec. 2.1, the phase of ENSO has a significant effect on temperature and precipitation in many areas adjacent to the Pacific Ocean and beyond. Hence, considerable attention has been focused on changes in ENSO itself, as measured by monitoring SST variability in the central equatorial Pacific (known as the NINO3 index). It was noted in the AR4-WGI that substantial variability in ENSO has occurred over the period of instrumental data, with strong events from the late 19th century through the first quarter of the 20th century and again after 1950. A notable shift to generally above-normal SSTs in the central and eastern Pacific around 1976-77 signaled a tendency toward more prolonged and stronger El Niño episodes (Trenberth et al., 2007). The NINO3 index indicates a trend toward more frequent or stronger El Niño episodes over the past 50 to 100 years (Vecchi and Wittenberg, 2010), which may have contributed to the warming trend in wintertime SAT over the western and mid-western U.S. in recent decades (Figs. 2.1 and 3.3).

There is also evidence of a tendency for the more intense recent El Niño episodes to be centered more toward the central equatorial Pacific than in the east Pacific (Yeh et al., 2009; Lee and McPhaden, 2010). This phenomenon has been linked to different patterns of rainfall and other climatic variations in Australia and the mid-latitudes (Wang and Hendon, 2007; Weng et al., 2009), relative to the east Pacific-centered El Niño events.

3.5 Ecosystem response to regional temperature change

According to the AR4 Working Group II report (AR4-WGII, 2007):

> The overwhelming majority of studies of regional climate effects on terrestrial species reveal consistent responses to warming trends, including poleward and elevational range shifts of flora and fauna. Responses of terrestrial species to warming across the Northern Hemisphere are well documented by changes in the timing of growth stages (i.e., phenological changes) especially the earlier onset of spring events, migration, and lengthening of the growing season. Changes in abundance of certain species, including limited evidence of a few local disappearances, and changes in community composition over the last few decades have been attributed to climate change (very high confidence) (AR4-WGII, Ch. 1, Executive Summary).

The magnitude, timing and character of climate change affects the Earth's diverse species in myriad ways. Provided habitats are not strongly disturbed, organisms such as insects with short life cycles may adapt relatively quickly by shifting their geographical ranges or reproductive timing. But other species may lag behind patterns of temperature change, for example, or find their habitats degraded or disappearing as a consequence of it (e.g., polar bears).

The literature on ecological change is vast, and such studies far outnumber those on physical climate changes in many world regions, particularly in Europe and the U.S. In the AR4-WGII, the relation between studies of biological systems showing significant changes between 1970 and 2004 and corresponding temperature changes from the GHCN data was examined. In Europe and

the U.S., the percentage of significant biological changes consistent with a regional warming signal were found to be 89% and 92%, respectively (AR4-WGII, Fig. 2.9).

The above figures are heavily supported by data on the biological side, especially in Europe. A massive meta-analysis project (COST725) used a network of more than 125,000 observational series of various phases in 542 plant and 19 animal species in 21 European countries, spanning the 1971-2000 period. As summarized in AR4-WGII (see **Figure 3.12**):

> Overall, the phenology of the species (254 national series) was responsive to temperature of the preceding month, with spring/summer phases advancing on average by 2.5 days/°C and leaf colouring/fall being delayed by 1.0 day/°C. The aggregation of more than 100,000 trends revealed a clear signal across Europe of changing spring phenology with 78% of leaf unfolding and flowering records advancing (31% significantly (sig.)) and only 22% delayed (3% sig.) … Fruit ripening was mostly advanced (75% advancing, 25% sig.; 25% delayed, 3% sig.).

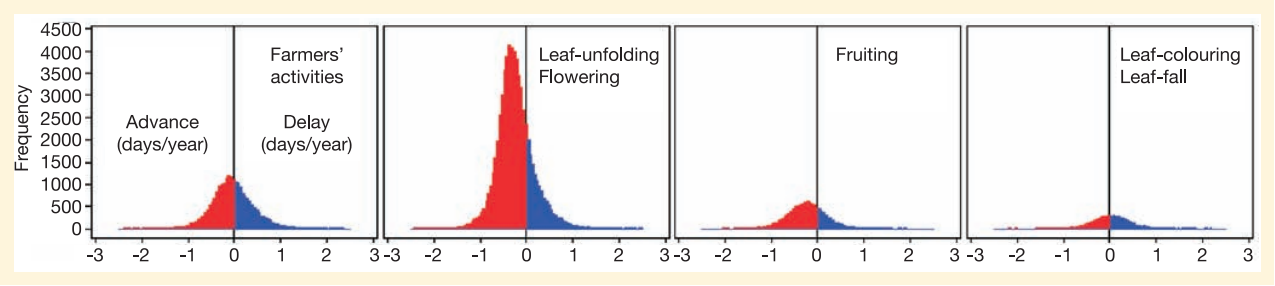

Figure 3.12. Frequency distributions of trends in phenology (in days/year) over 1971 to 2000 for 542 plant species in 21 European countries. *Source:* AR4-WGII, Fig. 1.6. Original figure from Menzel et al. (2006).

One meta-analysis of global scope (Root et al., 2003) found that 143 studies out of over 2,500 articles examined showed significant changes in species characteristics over the last 30 years. Of these, about 80% of the species were changing in the direction expected with warming. The types of changes included advances in the timing of spring events by about 5 days/decade and species expanding their ranges poleward and to higher elevations. Another meta-analysis of migratory bird arrival dates showed that 39% were significantly earlier and only 2% significantly later for the date of first arrival (Lehikoinen et al., 2004). The average latitude of over 300 common species of birds in North America has shifted northward by about 35 miles (56 km) in the past 40 years (**Figure 3.13**).

Finally, a recent study of European bird and butterfly populations found that these communities are responding to warming continental temperatures by shifting their ranges northward, birds by about 21 km per decade and butterflies by a remarkable 63 km per decade (Devictor et al., 2012). This suggests that different species cope with the same temperature change at differing rates, complicating predator-prey relationships, for example.

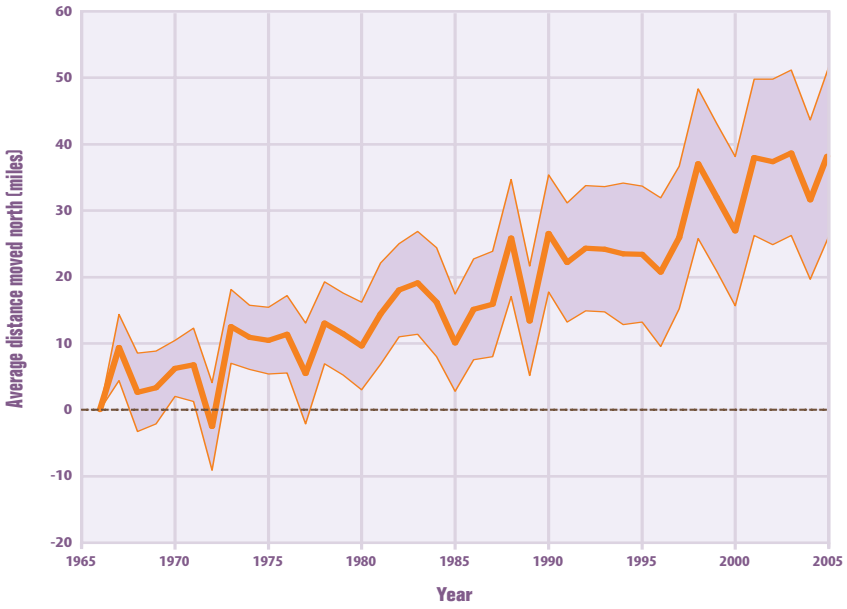

Figure 3.13. Annual change in latitude of bird center of abundance for 305 widespread bird species in North America from 1966 to 2005. Each winter is represented by the year in which it began (for example, winter 2005–2006 is shown as 2005). The shaded band shows the likely range of values, based on the number of measurements collected and the precision of the methods used. *Source:* U.S. EPA, *Climate Change Indicators in the U.S.* (2010), using original data from the National Audubon Society (2009), www.audubon.org/ bird/bacc/index.html.

4. Climate Extremes and Extreme Weather

The recently released special IPCC report, *Managing the Risks of Extreme Events and Disasters to Advance Climate Change Adaptation* (2012) (hereafter SREX), synthesizes and assesses all available published evidence on the nature of climate extremes and their changes over the historical record. We begin this section with the SREX assessment of changes in various climate variables and associated phenomena, which employs standardized language to express the level of uncertainty in those changes. Thus, available evidence is described as limited, medium, or robust; the consistency of evidence from different sources as low, medium, or high; and an overall level of confidence in the results is expressed using five qualifiers: very low, low, medium, high, and very high. Where the overall level of confidence is high or very high, an assessment of likelihood is also made, according to the following probability-based scale:

Virtually certain: 99–100% probability
Very likely: 90–100% probability
Likely: 66–100% probability
About as likely as not: 33–66% probability
Unlikely: 0–33% probability
Very unlikely: 0–10% probability
Exceptionally unlikely: 0–1% probability

Note, for example, that one may have "high confidence" (meaning that there is a large body of consistent evidence on a topic or question) in a conclusion stating that certain climatic events are "exceptionally unlikely" (meaning that the evidence suggests such events are historically rare and/or unlikely to occur in future). The assessments of changes in climate indicators are as follows, based on the period since 1950, and cited verbatim from the report (SREX Table 3.1):

Temperature: *Very likely* decrease in number of unusually cold days and nights at the global scale. *Very likely* increase in number of unusually warm days and nights at the global scale. *Medium confidence* in increase in length or number of warm spells or heat waves in many (but not all) regions. *Low or medium confidence* in trends in temperature extremes in some subregions due either to lack of observations or varying signal within subregions.

Precipitation: *Likely* statistically significant increases in the number of heavy precipitation events (e.g., 95th percentile) in more regions than those with statistically significant decreases, but strong regional and subregional variations in the trends.

El Niño and other modes of variability: *Medium confidence* in past trends toward more frequent central equatorial Pacific El Niño-Southern Oscillation (ENSO) events. Insufficient evidence for more specific statements on ENSO trends. *Likely* trends in Southern Annular Mode.

Tropical cyclones: *Low* confidence that any observed long-term (i.e., 40 years or more) increases in tropical cyclone activity are robust, after accounting for past changes in observing capabilities.

Extratropical cyclones: *Likely* poleward shift in extratropical cyclones. *Low* confidence in regional changes in intensity.

Droughts: *Medium* confidence that some regions of the world have experienced more intense and longer droughts, in particular in southern Europe and West Africa, but opposite trends also exist.

Floods: *Limited to medium* evidence available to assess climate-driven observed changes in the magnitude and frequency of floods at regional scale. Furthermore, there is *low* agreement in this evidence, and thus overall *low* confidence at the global scale regarding even the sign of these changes. *High* confidence in trend toward earlier occurrence of spring peak river flows in snowmelt- and glacier-fed rivers.

Extreme sea level and coastal impacts: *Likely* increase in extreme coastal high water worldwide related to increases in mean sea level in the late 20th century.

Other physical impacts: *Low* confidence in global trends in large landslides in some regions. *Likely* increased thawing of permafrost with likely resultant physical impacts.

Before reviewing these areas in more detail, it is important to distinguish between extreme behavior of climate variables and extreme weather events, especially with respect to the seeking of causal explanations of one or the other. Extreme weather events usually result from a combination of factors, and all are unique in some respects, making it difficult to attribute an extreme event to a single cause (e.g., "Hurricane X," or "Last week's heat wave …was due to global warming."). For example, the summer 2003 European heat wave was associated with a combination of a persistent high-pressure system (which limited cloudiness), abnormally dry soil (which reduced evaporation and cooling at the surface), and a number of other factors (García-Herrera et al., 2010).

With this in mind, it is likely more productive to frame the problem in a probabilistic manner, by considering the frequency of the occurrence of certain extreme weather events, and whether this has been changing compared to a chosen climatology. This places extreme weather events on nearly the same footing as climate extremes, at least for variables such as temperature, allowing both to be evaluated against "normal" conditions (i.e., climatology). An example of this is a week-long heat wave, which can either be viewed as a single climate extreme or a collection of sequential daily hot weather events. Statistically speaking, they are indistinguishable, and we will refer to both as "climate extremes" in what follows.

As reviewed below, evidence exists for changes in the frequency of many types of climate extremes over recent decades. Furthermore, the cause of those changes is also of interest. While individual weather events are difficult to attribute to specific causes, the situation for climate extremes is somewhat different. As explained in the SREX:

> [C]limate models can sometimes be used to identify if specific factors are changing the likelihood of the occurrence of extreme events. In the case of the 2003 European heat wave, a model experiment indicated that human influences more than doubled the likelihood of having a summer in Europe as hot as that of 2003, as discussed in the AR4. The value of such a probability-based approach – "Does human influence change the likelihood of an event?" – is that it can be used to estimate the influence of external factors,

such as increases in greenhouse gases, on the frequency of specific types of events, such as heat waves or cold extremes. The same likelihood-based approach has been used to examine anthropogenic greenhouse gas contribution to flood probability (SREX, FAQ 3.2, p.127).

The results from several studies of this type are reviewed in the following subsections.

4.1 Temperature Extremes

The regional surface air temperature (SAT) trends shown in Fig. 3.1 establish that, over the past century and over most of the land surface, mean annual temperatures have increased by an amount larger than that expected from natural climate variability alone. While the mean is a useful statistical quantity, humans and other living things are not particularly sensitive to changes in annual or monthly mean temperature. Rather, organisms are more responsive to the extremes of the distribution of SAT, from extremely low to extremely high values, and to large variations occurring within a short span of time. Extremely hot conditions in summer and freezing temperatures in winter are particularly noticeable, and can have concrete societal impacts.

As mentioned in Sec. 3.1 above, absolute changes in seasonal temperature over the last few decades should be placed in the context of natural variability, which varies strongly over the Earth's surface, and between land and ocean (SAT variability is generally lower over oceans). The variability in any quantity is commonly expressed as the standard deviation, usually denoted by σ. For a variable such as temperature that is approximately normally distributed (i.e., according to a bell curve), there is a straightforward relation between the change, ΔT, expressed in units of σ, and the corresponding percentile of the distribution. A calculated ΔT of $+1\sigma$, for example, corresponds to the 84th percentile of the distribution, a Δ of $+2\sigma$ to the 98th percentile, and a Δ of $+3\sigma$ to the 99.9th percentile. In the latter case, less than 0.1% of the values of Δ would be expected to be larger than the change in question, making it a very exceptional value indeed. The ratio $\Delta T/\sigma$, called the *standardized temperature anomaly (*or *standardized temperature index*), is a dimensionless measure of change. Such a quantity can be defined for any climate variable, as discussed further in Section 5.

Recent work by Hansen et al. (2012), based on the NASA-GISS surface temperature analysis, uses the standardized anomaly of SAT to demonstrate the significance of regional warming over the last decade. These authors examined the regional pattern of SAT change by season, with a focus on Northern Hemisphere summer, and drawing particular attention to extremes in the frequency distribution of temperature. **Figure 4.1**, taken from this analysis, shows the standardized SAT anomaly over land for a selection of individual summer seasons (June-Aug).

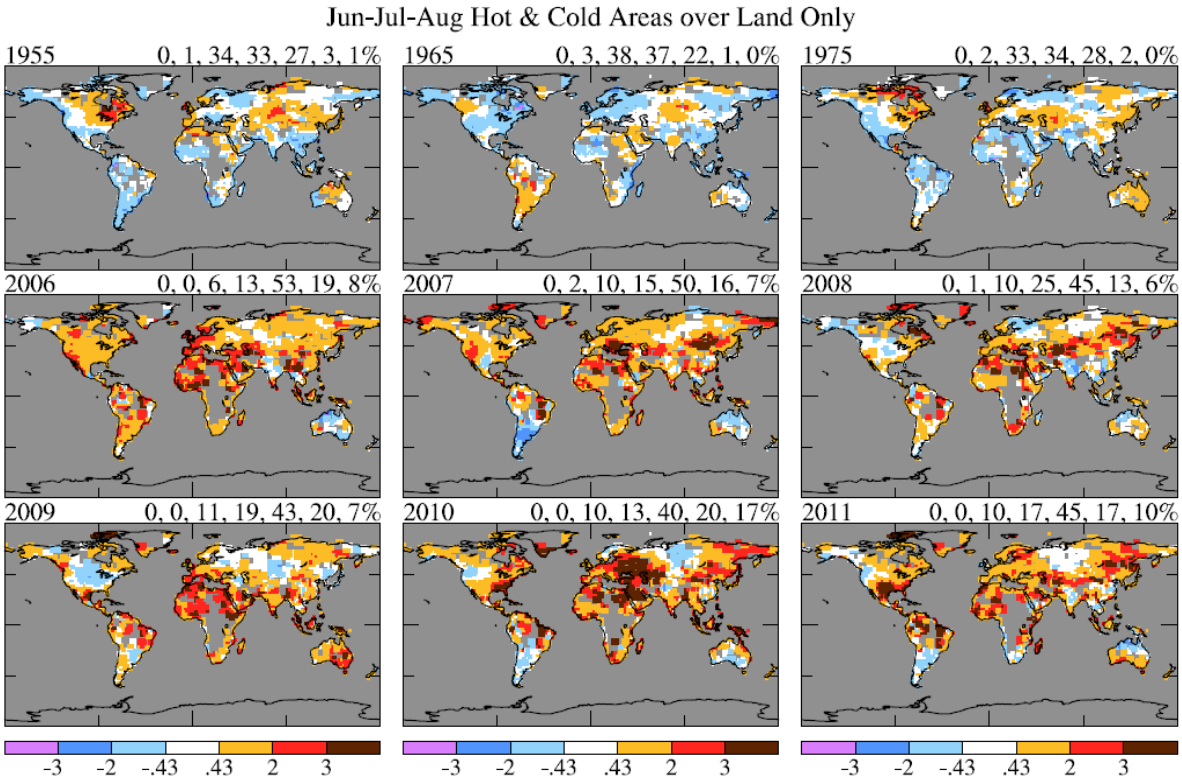

Figure 4.1. Jun-Jul-Aug surface temperature anomalies over land in 1955, 1965, 1975 and 2006-2011 relative to 1951-1980 mean temperature in units of the local standard deviation of temperature. The numbers above each map are the percent of surface area covered by each of the categories in the color bar. *Source:* Hansen, Sato and Ruedy (2012).

The most striking message conveyed by Fig. 4.1 is the following. Anomalies greater than +3σ, which cover much less than 1% of the land area in the base period (here 1951-1980), occupy between 6-17% of the land from 2006-2011, a more than ten-fold increase. Interestingly, these +3σ summers have not occurred predominantly at high latitudes, as might be expected from the results shown in Fig. 3.1, but are rather more common in the mid-latitudes and tropics. This becomes apparent only after folding in the effects of local natural variability.

Summing the total area covered by colder- and warmer-than-average anomalies, Hansen et al. (2012) constructed the time series shown in **Figure 4.2.** The sharp increase in warmer-than-average land areas in summer over the last 50 years is characterized by the authors as a "loading of the climate dice," inasmuch as the chance of such events occurring has increased from 2 in 6 in the 1950s to 4 in 6 in the last decade. The authors explain:

> Hansen et al. (1988) represented the climate of 1951-1980 by colored dice with two sides colored red for "hot", two sides blue for "cold", and two sides white for near average temperatures. With a normal distribution of temperatures the dividing point would be at 0.43σ to achieve equal (one third) chances of being in each of these three categories in the period of climatology (1951-1980). ...[Fig. 4.2] confirms that the global occurrence of "hot" anomalies (seasonal mean temperature anomaly exceeding +0.43σ has approximately reached the level of 67% required to make four sides of the dice red, with

the odds of either an unusually "cool" season or an "average" season now each approximately corresponding to one side of the six-sided dice. However, the loading of the dice over land area in summer is even stronger ([Fig. 4.2], lower row) (Hansen et al., 2012).

Fig. 4.2 also shows that over Northern Hemisphere land, the area fraction of "very hot" summer SAT anomalies has increased from negligible values in 1951-80 to nearly one-third in the last decade. In other words, seasonal warming that was once described as "hot" (+0.43σ) is now "very hot" (+2σ), corresponding to a 2 in 6 chance upon rolling the climate die.

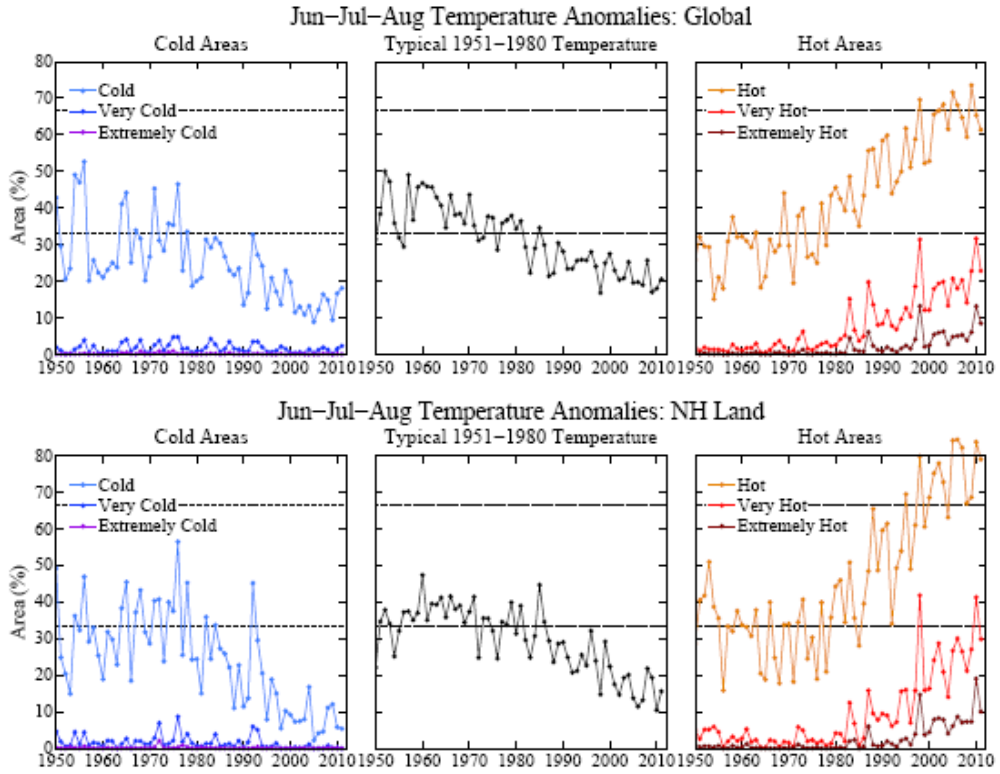

Figure 4.2. Area of the world (in percent) covered by temperature anomalies from Fig. 4.1 in categories defined as hot (+0.43σ), very hot (+2σ), and extremely hot (+3σ), with analogous divisions for cold anomalies. Dashed horizontal lines indicate areas of 33% and 67%, corresponding to climate dice with two and four sides colored red, respectively (see text for details). *Source:* Hansen et al. (2012).

Moving from seasonal to daily timescales, similar trends are seen in daily extreme temperatures across the globe. Extremes are defined here as lying below the 10th (cold) or above the 90th (warm) percentile of the long-term climatological distribution of SAT. As **Figure 4.3** shows, the frequency of warm days/nights has been generally increasing (+0.7/+1.4% per decade globally) while that of cold days/nights has decreased (-0.6/-1.2 % per decade) in most world regions. Generally speaking, nighttime SAT has been increasing faster than daytime SAT. Note that this is precisely what is expected under increased greenhouse gas concentrations, since the atmosphere emits more infrared radiation down to the surface. Consistent with this, the frequency of colder-

than-average nights has been declining more rapidly than colder-than-average days. Consequently, the length of the frost-free season has increased in most continental locations, leading to an earlier onset of spring.

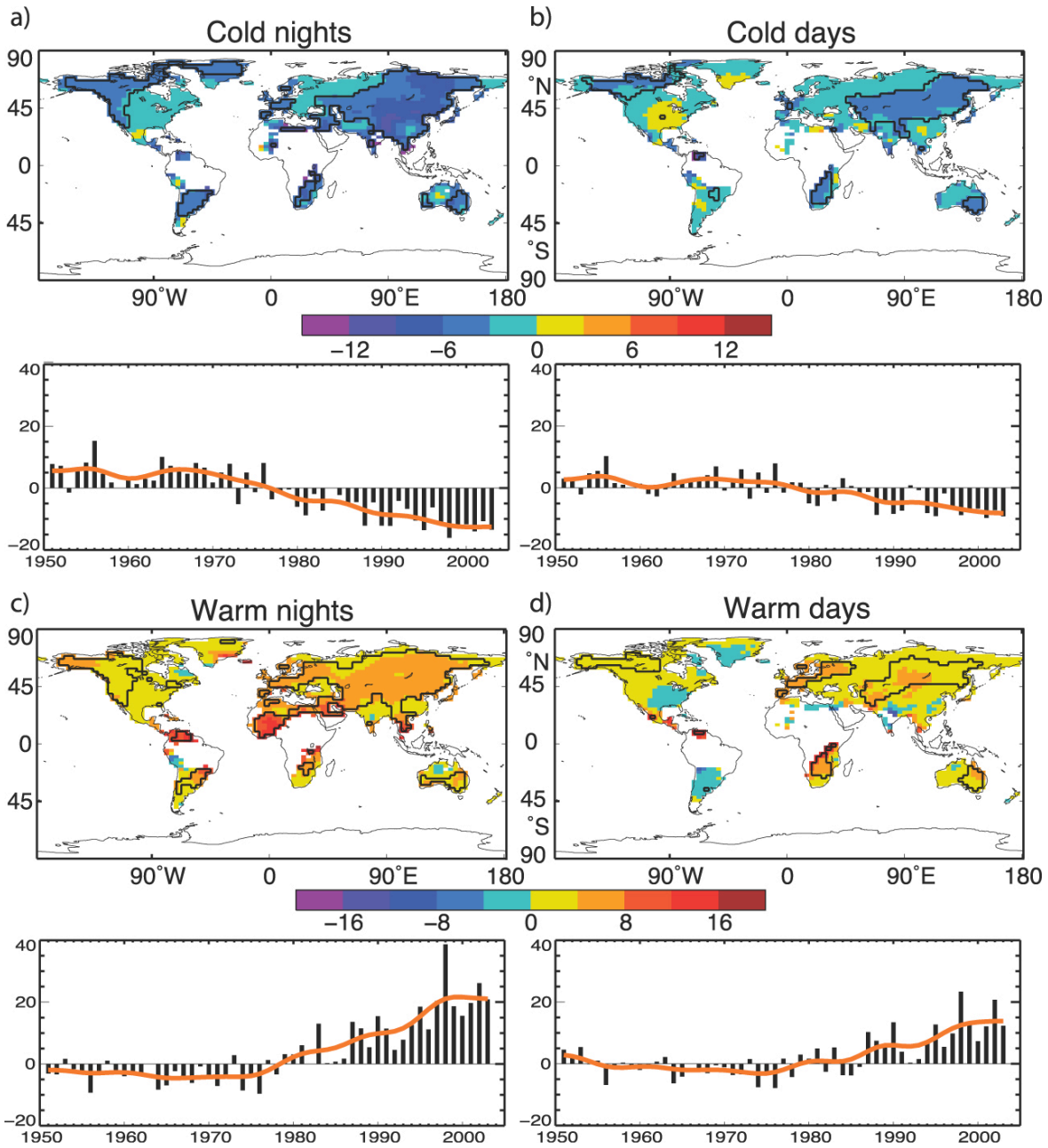

Figure 4.3. Observed trends (days per decade) for 1951 to 2003 in the frequency of extreme temperatures, defined based on 1961 to 1990 values, as maps for the 10th percentile: (a) cold nights and (b) cold days; and 90th percentile: (c) warm nights and (d) warm days. Trends were calculated only for grid boxes that had at least 40 years of data during this period and had data until at least 1999. Black lines enclose regions where trends are significant at the 5% level. Below each map are the global annual time series of anomalies (with respect to 1961 to 1990). The orange line shows decadal variations. Trends are significant at the 5% level for all the global indices shown. *Source:* AR4-WGI, FAQ 3.3, Fig. 1, adapted from Alexander et al. (2006).

In Canada and the U.S. in particular, similar trends in cold and warm nights are apparent (**Figure 4.4**), with considerable regional differences in the magnitude of change.

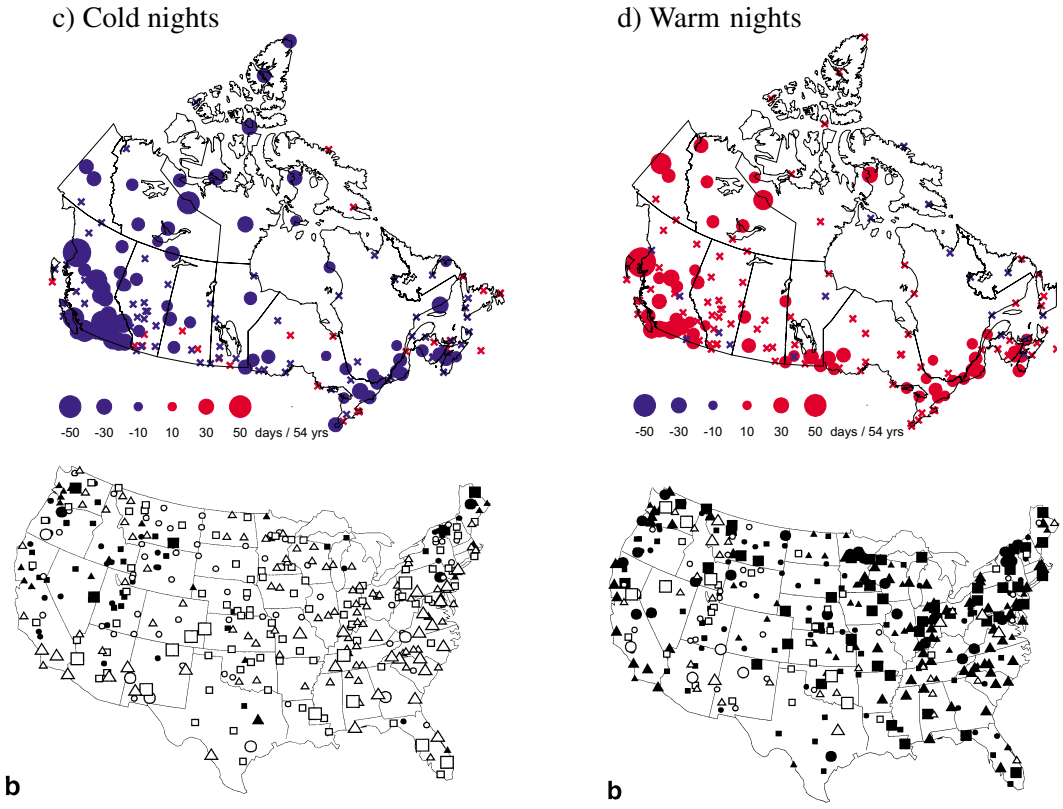

Figure 4.4. Trends in cold (*left*) and warm (*right*) nights for Canada from 1950–2003 (*top*) and the U.S. from 1960-96 (bottom). In the top panels, blue and red dots indicate trends significant at the 5% level. The size of the dots is proportional to the magnitude of the trend (in units of days per 54 years). Crosses denote non-significant trends. In the bottom panels, trends significant at the 5% level are indicated by large symbols, with filled (open) symbols for positive (negative) trends. The symbols also classify the stations as urban (*triangle*); suburban (*square*); or rural (*circle*). *Sources:* Vincent and Mekis (2006) (*top*); Degaetano and Allen (2002) (*bottom*).

In Figs. 4.1 and 4.3, Europe stands out as a region where extreme warm summertime temperatures have been occurring more frequently over the past decade. Establishing these as statistically significant phenomena is aided by the exceptionally long record of SAT observations in central Europe, where daily data extend back to the 1860s in major centers, and temperature reconstructions to 1500. As shown in **Figure 4.5**, the summers of 2003 and 2010 were the warmest in 510 years, both exceeding +3σ of the 1970-99 mean value, while three other summers in the decade exceeded +2σ. The decade as a whole stands well above any other 10-year period since 1500 (Fig. 4.5, lower left). Moreover, compared to the previous 500 years, the areal extent of the overheated (+3σ) regions has more than doubled in the last decade (Fig. 4.5, lower right).

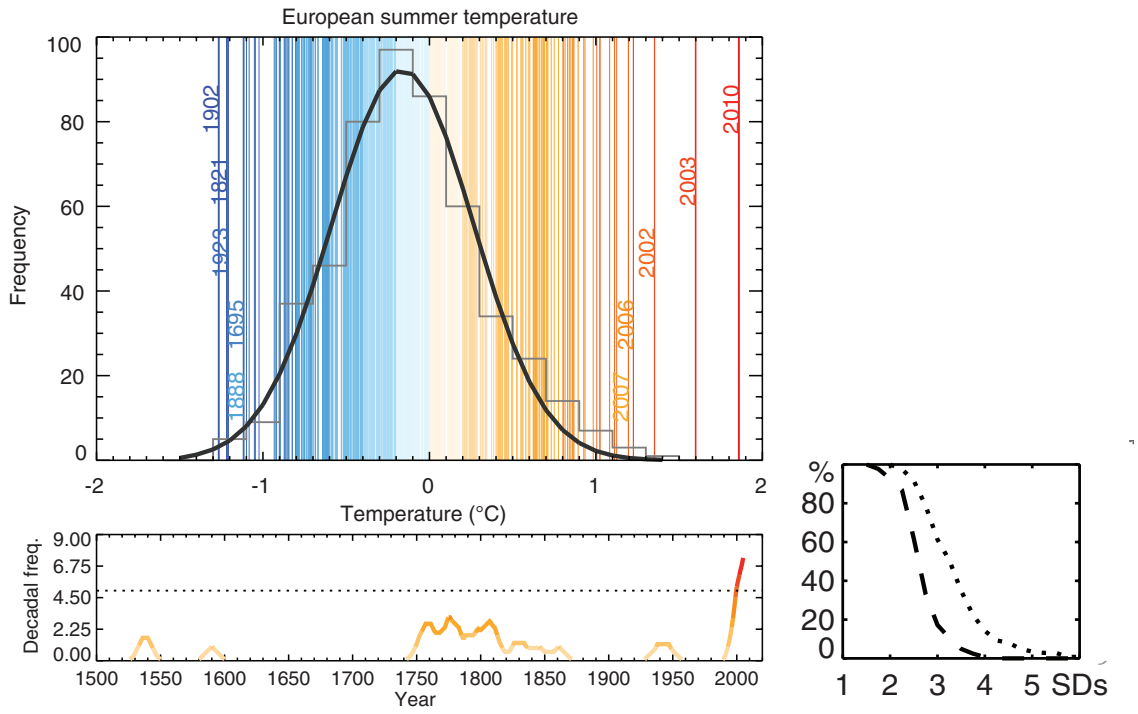

Figure 4.5. *Top:* European summer temperatures for 1500–2010. Statistical frequency distribution of best-guess reconstructed and instrument-based European ([35°N, 70°N], [25°W, 40°E]) summer land temperature anomalies (degrees Celsius, relative to the 1970–1999 period) for the 1500–2010 period (vertical lines). The five warmest and coldest summers are highlighted. Gray bars represent the distribution for the 1500–2002 period, with a Gaussian fit in black. Data for the 2003–2010 period are from Hansen et al. (1999). *Bottom left:* The running decadal frequency of extreme summers, defined as those with temperature above the 95th percentile of the 1500–2002 distribution. A 10-year smoothing is applied. Dotted line shows the 95th percentile of the distribution of maximum decadal values that would be expected by random chance. *Lower right:* The difference between the percentage of European areas with summer maxima abovethe given temperature (in SDs) for the 1500–2000 (*dashed line*) and 1500–2010 (*dotted line*) periods. *Source:* Barriopedro et al. (2011).

Stott et al. (2004) pointed out that the question of "whether the 2003 heatwave was caused, in a simple deterministic sense, by a modification of the external influences on climate—for example, increasing concentrations of greenhouse gases in the atmosphere" is ill-posed, "because almost any such weather event might have occurred by chance in an unmodified climate. However, it is possible to estimate by how much human activities may have increased the risk of the occurrence of such a heatwave." The authors did this by conducting two types of GCM simulations over central and southern Europe; the attribution method is described in more detail below in Sec. 4.6 for the case of flood risk.

The most notable outcome of the Stott et al. study was that extremely hot summers (defined as those having a SAT in the 1990-99 period > 1.6°C above the 1961-90 summer mean), which were 1-in-1000 year events in simulations with natural (solar and volcanic) forcing, only became 1-in-250 year events in the simulations including anthropogenic (increasing greenhouse gas, aerosol, and ozone) forcing. Equivalently, extreme summer temperatures were always larger in the latter simulations for a given occurrence frequency (return period). On the basis of further analysis, the authors concluded: "… there is a greater than 90% chance that over half the risk of European

summer temperatures exceeding a threshold of 1.6 [°C] is attributable to human influence on climate."

Finally, it is worth noting some of the deleterious consequences of temperature extremes of this magnitude for human society and ecosystems in general. According to a recent study, episodes of extreme heat in the United States cause more deaths than floods, hurricanes, and tornadoes combined (Hartzet al., 2012). As noted by Hayhoe et al. (2010) and others, within human populations at highest risk (i.e., infants, the elderly and infirm), heat-related mortality depends on both the apparent temperature (a combination of SAT and humidity) and on its persistence above a threshold value deemed to be hazardous. There is also some evidence that mortality rates in urban settings are correlated with diurnal temperature range, and that modifiers such as seasonality and socio-economic status may be important (Lim 2012).

In central Europe in the summer of 2003, there were nine consecutive days during which the maximum daily temperature exceeded 35°C (95°F). As a result of this confluence, heat-stress related mortality rose sharply in western and central Europe and was linked to around 70,000 heat-related deaths (Robine et al., 2008). The bulk of the increased mortality occurred in France, as depicted in **Figure 4.6**.

Subsequent research has shown that extended warm and dry conditions in 2003 also perceptibly slowed vegetation growth in Europe (as detected in satellite observations; Ciais et al., 2005), increased area burned in wildfires (nearly half a million hectares burned in Portugal; **Figure 4.7**), and caused extensive agricultural losses (~36% decline in annual maize production in Italy, 25% drop in fruit harvests in France). Total (uninsured) economic loss for the agriculture sector in the European Union were estimated at **€**13 billion, with **€**4 billion in France alone (Sénat, 2004).

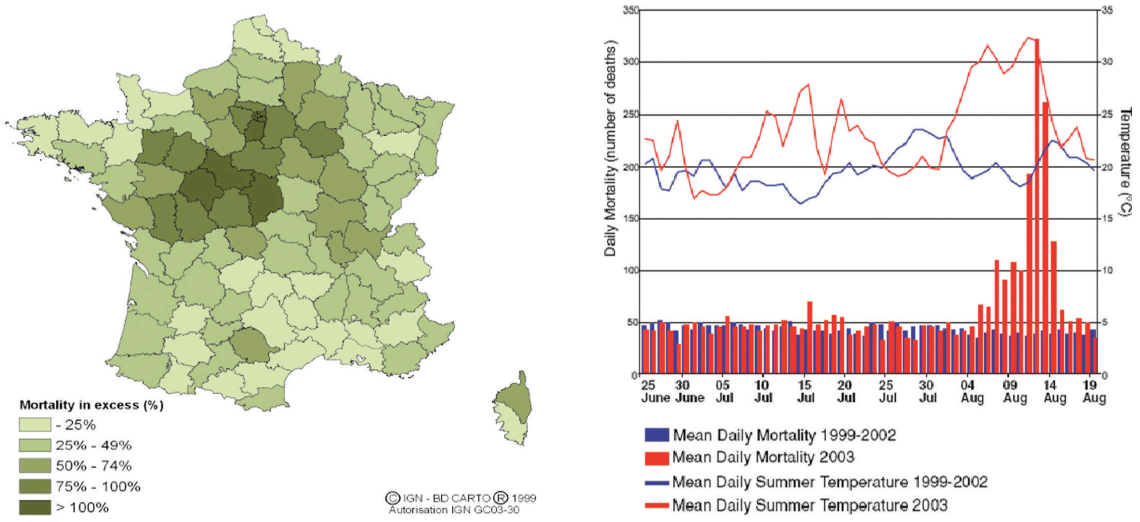

Figure 4.6. *Left:* Excessive mortality (%) per French Department for the period 1 – 15 August 2003 by comparison with the average 2000–2002 (adapted from Institut de Veille Sanitaire [2003]). *Right:* Increase in daily mortality in Paris during the heat wave in early August (Vandentorren and Empereur-Bissonnet, 2005). *Source*: AR4-WGII, Confalonieri et al. (2007).

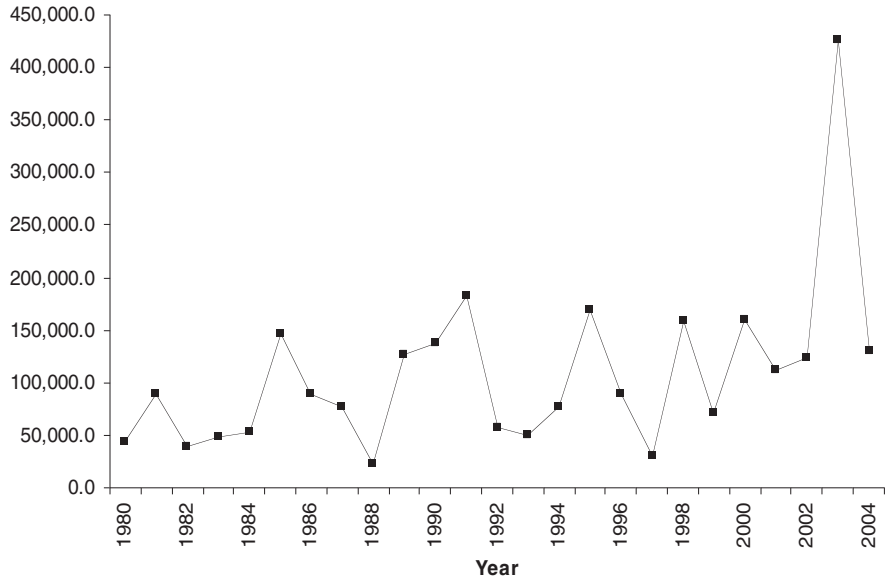

Figure 4.7. Annual values of total area burned (vertical axis, in hectares) between 1980 and 2004 compiled by the Portuguese Forest Institute (DGRF). The wildfire scars were evaluated based on visual interpretation and on-screen digitizing of data from the MODIS satellite instrument. The minimum mapping unit (i.e., the size of the smallest fire scars mapped) is 100 hectares. *Source*: García-Herrera et al. (2010).

The European heat wave of 2010, which was centered on western Russia, was in fact more intense and covered a larger area than that in 2003. In Russia alone, the death toll was ~55,000, wildfires burned more than 1 million hectares, and total economic losses were estimated at about U.S. $50 billion (Barriopedro et al., 2011). Ongoing analyses will be able to better place this event in perspective with the 2003 heat wave.

The threat to agriculture from heat stress is clearly a serious one, given the interlinked nature of the world food supply through trade. Lobell et al. (2012) used nine years of satellite measurements of wheat growth in northern India, one of the most intense wheat cultivation areas on the planet, to measure the rate of wheat senescence (progression from plant maturity to death) as a function of temperature. The authors found that senescence accelerates following exposure to temperatures greater than 34°C, resulting in a significantly reduced growing season (by 8-10 days), and hence lower crop yields (by 15-20%).

Livestock are also at risk. For example, in the U.S. Northeast, dairy ranks as the most economically important contributor to the agricultural sector, bringing in $3.6 billion annually. The optimal temperature for milk production ranges from 40°F to 75°F (4.4°C to 24°C), depending on humidity. Currently, some areas of New York and Pennsylvania, where over 80% of production occurs, experience more than 20 days a year with daily maximum SAT over 90°F. Warming summer temperatures are already having negative effects on dairy operations. Increasing intensity and frequency of heat stress, which depresses milk production and birthing rates in cows, is taking a huge financial toll on dairy farmers: around $2.4 billion for U.S. farmers overall and more than $80 million for Northeastern U.S. farmers in 2002 (Frumhoff et al., 2007; St. Pierreet al., 2003). At the same time, dairy operations should see some benefit from decreased heating costs in winter; but this does not appear to have been documented.

4.2 Precipitation Extremes

Rainfall statistics for many areas of the globe were summarized in the AR4-WGI. Significant trends were found at many NH locations in the proportion of very wet days (95th percentile) in recent compared to earlier decades (**Figure 4.8**). Further, the magnitude of the trend from 1979-2003 is about twice that from 1951-2003 (AR4-WGI, p. 302, Table 3.6).

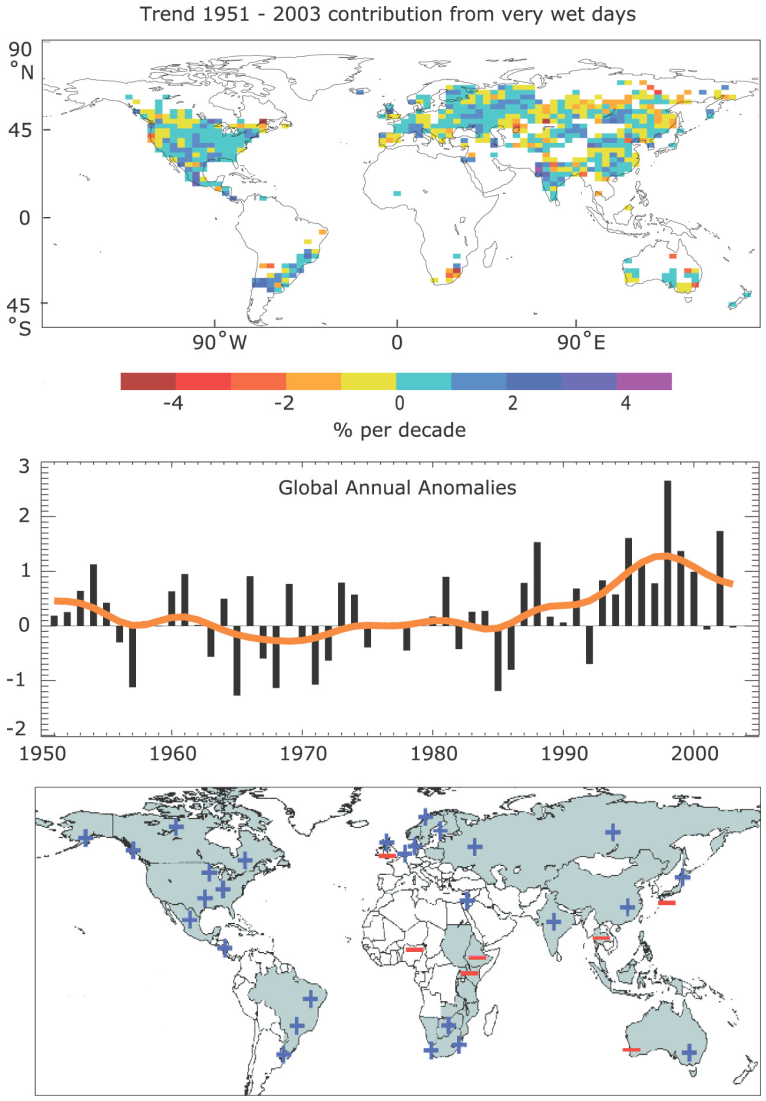

Figure 4.8. *Top:* Observed trends (% per decade) for 1951 to 2003 in the contribution to total annual precipitation from very wet days (95th percentile). Trends were only calculated for grid boxes where both the total and the 95th percentile had at least 40 years of data during this period and had data until at least 1999. *Middle:* Anomalies (%) of the global annual time series (with respect to 1961 to 1990) defined as the percentage change of contributions of very wet days from the base period average (22.5%). The smooth orange curve shows decadal variations. From Alexander et al. (2006). *Bottom:* Regions where disproportionate changes in heavy and very heavy precipitation during the past decades were documented as either an increase (+) or decrease (–) compared to the change in the annual and/or seasonal precipitation (updated from Groisman et al., 2005). Thresholds used to define "heavy" and "very heavy" precipitation vary by season and region. However, changes in heavy precipitation frequencies are always greater than changes in precipitation totals and, in some regions, an increase in heavy and/or very heavy precipitation occurred while no change or even a decrease in precipitation totals was observed. *Source:* AR4-WGI, Figure 3.39.

A notable increasing frequency of wet days in recent decades is seen in the eastern United States, southeastern South America, central Europe, western Russia and India. Fewer wet days have been recorded in the western U.S. and throughout much of central and eastern Russia. As is evident from the bottom panel of Fig. 4.8, however, many more regions display increasing than decreasing trends in very wet days. Data quality in the tropics and most of the Southern Hemisphere is insufficient to be able to draw any firm conclusions regarding changes in precipitation extremes in those areas.

Increases in days with heavy precipitation are also evident in the U.S. and Canada, as depicted in **Figure 4.9**. From 1958 to 2007, there are clear trends toward more very heavy precipitation for the U.S. as a whole, particularly in the Northeast and Midwest. While total precipitation in the U.S. increased by about 7 percent over the past century, the heaviest 1 percent of rain events increased by nearly 20 percent (Bull et al., 2007). In Canada, the results are more mixed regionally, but the number of days with heavy precipitation increased by 1.8 days nationally, a statistically significant change (Vincent and Mekis, 2006).

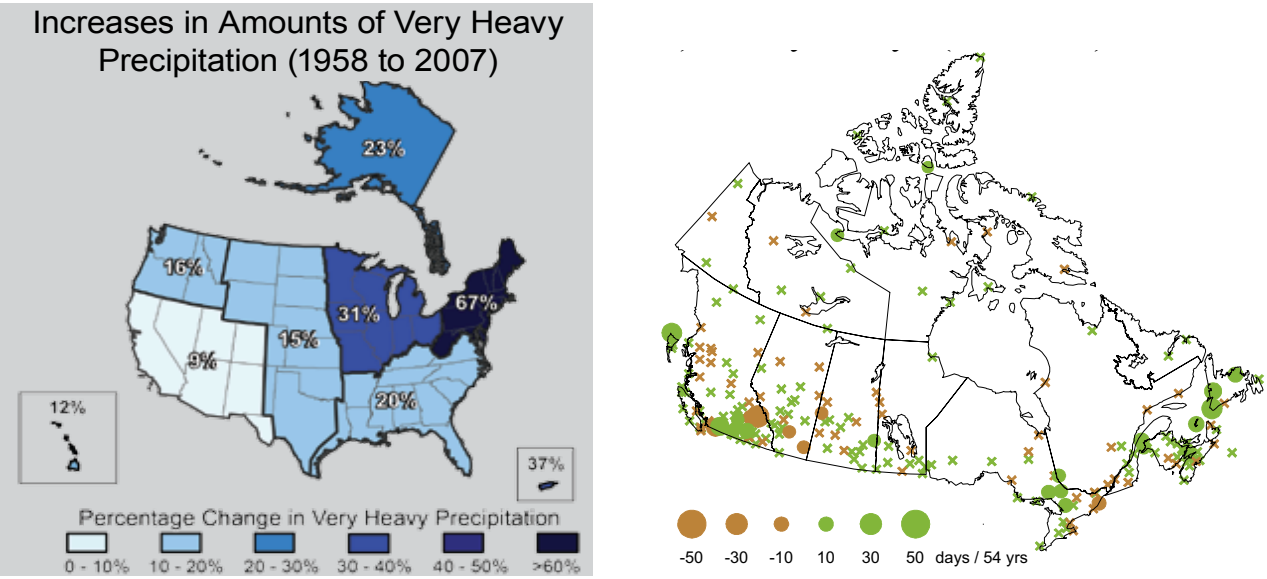

Figure 4.9. *Left:* Percent increases in the amount falling in very heavy precipitation events (defined as the heaviest 1 percent of all daily events). *Source:* Karl et al. (2009), updated from Groisman et al. (2005). *Right:* Trend in days with heavy precipitation (>10 mm/day) in Canada between 1950 and 2003. Brown and green dots indicate trends significant at the 5% level. The size of the dots is proportional to the magnitude of the trend (in units of days per 54 years). Crosses denote non-significant trends. *Source:* Vincent and Mekis (2006).

4.3 Storms and hurricanes

4.3.1 Tropical storms and hurricanes

The term "tropical cyclone" (TC) is here employed as a catch-all for a "non-frontal low-pressure system with a closed circulation over tropical or subtropical oceans" (Grossmann and Morgan, 2011). The strongest form of TC, characterized by sustained (10-min. average) wind speeds in excess of 74 miles per hour (119 km/h), is termed a "hurricane" in the Northeast Pacific and

North Atlantic Ocean, "typhoon" in the Northwest Pacific, and "severe cyclonic storm/TC" in other ocean basins[1].

Detection of a trend in hurricane activity is hindered by the fact that hurricanes are fairly rare events whose numbers vary significantly from year to year (**Figure 4.10**). Also, the observational record is not particularly long as climate observations are concerned. The long-term (1970-2005) average, annual, global TC frequency is 84 ± 7 (Webster et al., 2005). In the Atlantic basin, the long-term average annual TC number is 10, of which 6 are typically hurricane strength (WMO 2006). According to Mendelsohn, Emanuel and Chonabayashi (2011), only 111 hurricanes have struck the United States in the 50-year period up to 2009. Moreover, only eight storms account for more than half of all damage done by hurricanes in the U.S. since 1870, normalized for changing population, wealth and currency value (Pielke et al., 2008). Observing systems have also changed significantly since the first intrepid airplane reconnaissance missions in the late 1940s. Nevertheless, this research area has been extremely active over the last two decades, and a few secure results are beginning to emerge.

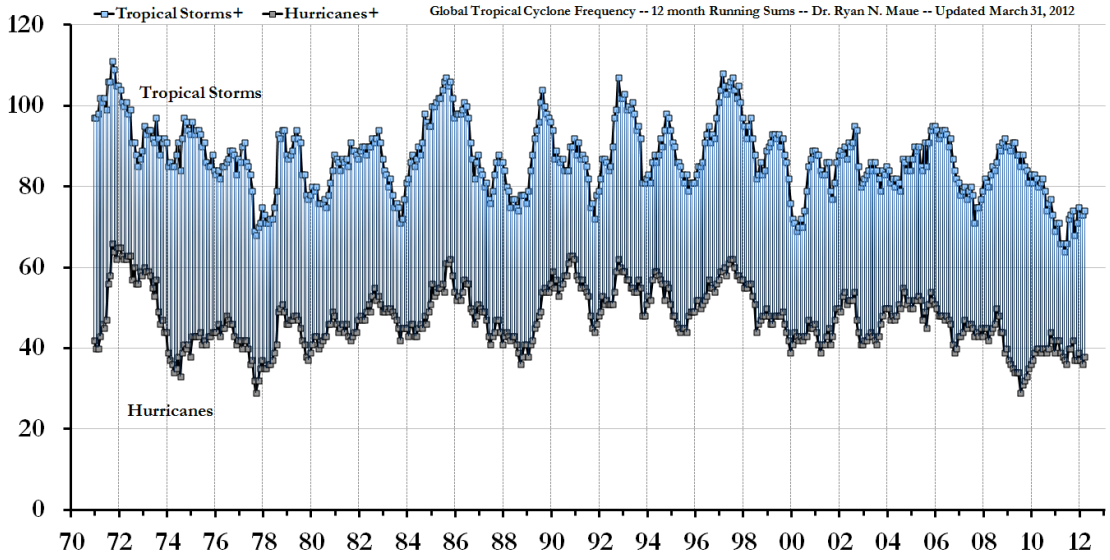

Figure 4.10. The last four decades of global TC and hurricane frequency, expressed as 12-month running sums. The top time series is the number of TCs that reach at least tropical storm strength (maximum lifetime wind speed exceeds 34 knots). The bottom time series is the number of hurricane strength (>64 knots) TCs. *Source:* Maue (2011).

The IPCC AR4 was issued at a time when intensive research efforts were underway to correct for the known undercounting bias of TCs prior to the advent of satellite observations (circa 1966). The AR4 also followed on the heels of the most active hurricane season on record in the tropical Atlantic basin (2005), with 27 named storms and seven major hurricanes (Saffir-Simpson Category 3-5; see Appendix A) making landfall. The decade prior to 2005 displayed a notably higher than average number of North Atlantic TCs and hurricanes, as shown in **Figure 4.11**. The consensus view expressed in the AR4-WGI in 2007 was as follows:

[1] National Hurricane Center, http://www.aoml.noaa.gov/hrd/tcfaq/A1.html. Retrieved on 2012-01-19.

Globally, estimates of the potential destructiveness of hurricanes show a substantial upward trend since the mid-1970s, with a trend towards longer storm duration and greater storm intensity, and the activity is strongly correlated with tropical sea surface temperature. These relationships have been reinforced by findings of a large increase in numbers and proportion of strong hurricanes globally since 1970 even as total numbers of cyclones and cyclone days decreased slightly in most basins. Specifically, the number of (Saffir-Simpson) category 4 and 5 hurricanes increased by about 75% since 1970. The largest increases were in the North Pacific, Indian and Southwest Pacific Oceans. However, numbers of hurricanes in the North Atlantic have also been above normal in 9 of the last 11 years, culminating in the record-breaking 2005 season.

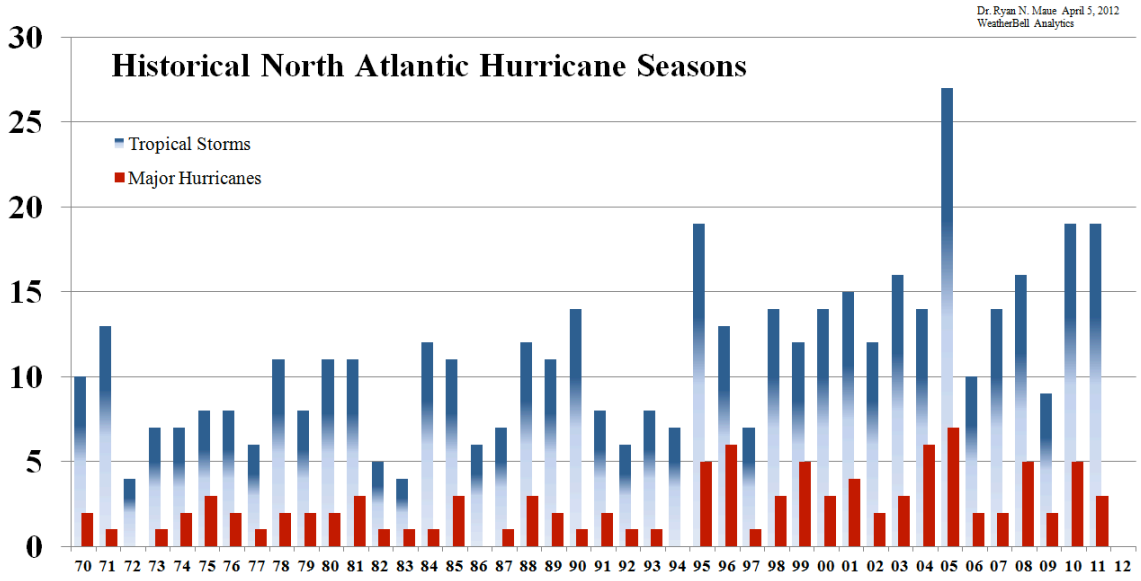

Figure 4.11. Historical North Atlantic tropical storm and major hurricane frequency since 1970 from the HURDAT best-track dataset, which should be complete for the period shown. Since 1970, there have been 465 tropical storms including 102 major hurricanes (22%). Since 1995, the ratio is slightly higher (26%) or 64 major hurricanes out of a total of 250 storms. *Source:* Maue (2012).

Shortly after the AR4, some of the above conclusions were challenged, insofar as important limitations in the observed data record prior to 1966 that might lead to spurious trends were brought to light (Vecchi and Knutson, 2008; Landsea et al., 2009; Vecchi and Knutson, 2011). However, the AR4-WGI conclusion regarding increased intensity (e.g., as gauged by maximum wind speed) of the most powerful hurricanes still appears valid, based on global, satellite-derived results for the 1981-2006 period (**Figure 4.12**; Elsner et al. 2008). The destructive potential of a hurricane is usually approximated as the product of its duration and either the second or third power of the maximum wind speed (corresponding to kinetic energy or wind power, respectively; see, e.g., Drews [2007], Emanuel [2005]). Hence, the results shown in Fig. 4.12 suggest that the destructive potential of the most intense tropical hurricanes (i.e., those in the uppermost quantile) is also on the rise.

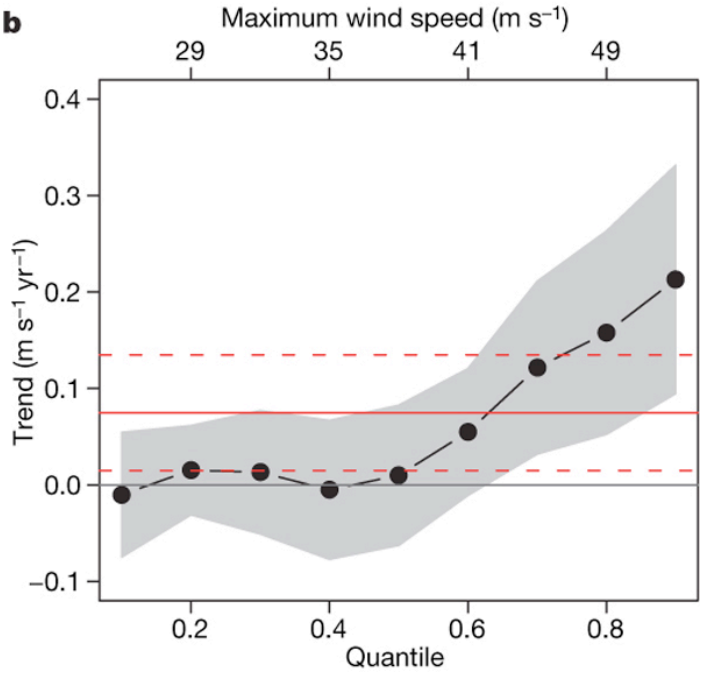

Figure 4.12. Trends in global satellite-derived tropical cyclone maximum wind speeds by quantile, from 0.1 to 0.9 in increments of 0.1, over the period 1981-2006. Trends are estimated coefficients from quantile regression in units of metres per second per year. The point-wise 90% confidence band is shown in grey, under the assumption that the errors are independent and identically distributed. The solid red line is the trend from a least-squares regression of wind speed as a function of year and the dashed red lines delineate the 90% point-wise confidence band about this trend. *Source:* Elsner et al. (2008).

Two recent comprehensive reviews of the topic, Knutson et al. (2010) and the IPCC-SREX Report (2012), came up with considerably weaker conclusions concerning global historical TC trends. As summarized by Knutson et al.:

> It remains uncertain whether past changes in any tropical cyclone activity (frequency, intensity, rainfall, and so on) exceed the variability expected through natural causes, after accounting for changes over time in observing capabilities.

In individual ocean basins (Atlantic, Pacific, Indian), the still smaller sample of historical TCs available in the historical record makes trend detection even more challenging. However, Elsner et al. (2008) discovered upward trends in TC lifetime-maximum wind speeds over the period 1981-2006 in three ocean basins—the southern Indian, northern Indian, and North Atlantic—as shown in **Figure 4.13**. Only in the North Atlantic basin, however, was the trend statistically significant. Also, in the Atlantic it has been demonstrated that both annual TC counts and total power dissipated by TCs are correlated with August-October SSTs in the tropical Atlantic over the last century (Fig. 5.10; Emanuel 2005).

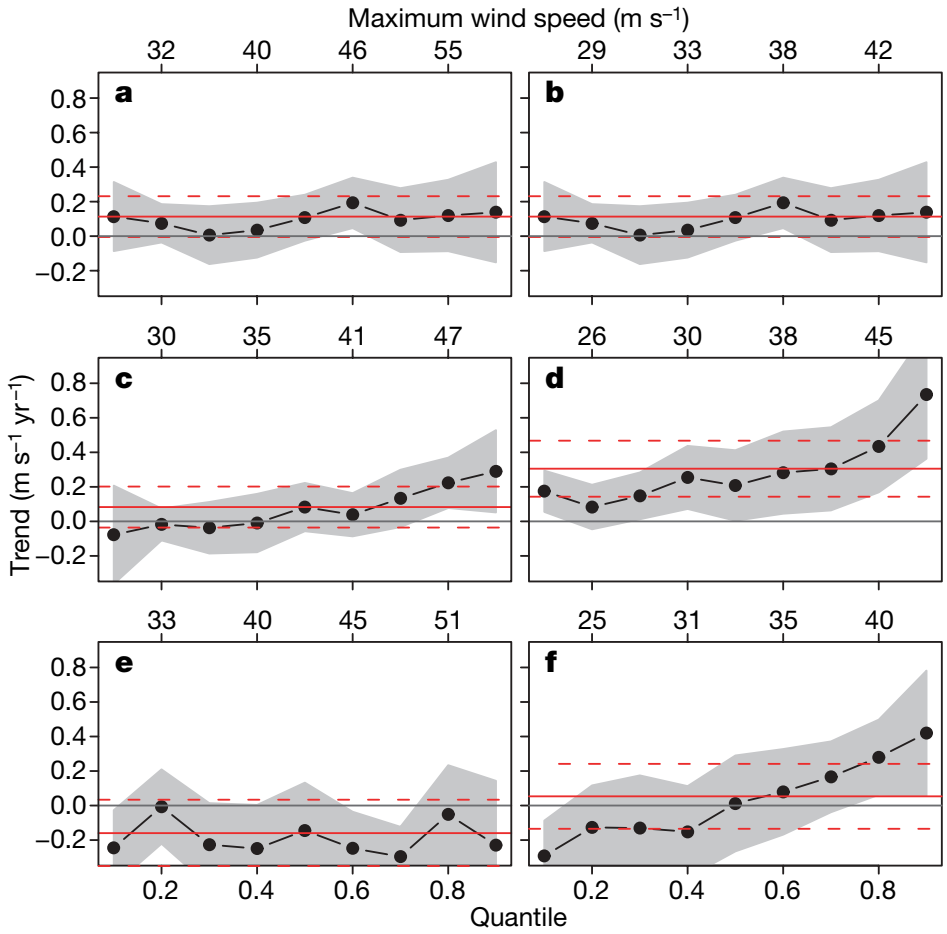

Figure 4.13. Trends in satellite-derived tropical cyclone lifetime-maximum wind speeds over the period 1981-2006, as in Fig. 4.12. (a) Western North Pacific Ocean cyclones (cyclone count, 698); (b) eastern North Pacific Ocean cyclones (423); (c) southern Indian Ocean cyclones (413); (d) North Atlantic Ocean cyclones (291); (e) South Pacific Ocean cyclones (157); (f) northern Indian Ocean cyclones (115). *Source:* Elsner et al. (2008).

Although the topic of model-based projections of TC activity is deferred to Section 6, it is worth mentioning that nearly all climate models project some increase in the mean maximum wind speed and lower central pressure of TCs under continued twenty-first century warming. This is because the type of environment in which TCs are typically born, regions of the tropics with a moist atmosphere overlying a warm ocean (usually with SST > 26°C), becomes generally more common under global warming. However, while nearly all models agree on this point, most do not predict a noticeable effect until the mid-21st century. As emphasized by Knutson et al.:

> The intensity changes projected by various modelling studies of the effects of greenhouse-gas-induced warming … are small in the sense that detection of an intensity change of a magnitude consistent with model projections should be very unlikely at this time, given data limitations and the large interannual variability relative to the projected changes.

Therefore, it is not surprising that the detection of a more significant and widespread trend in TC intensities due to global warming remains elusive.

When considering hurricane data, it is important to distinguish between trends in hurricane *activity* (which can be evaluated from measurements) and hurricane *damage* or *losses*, which are primarily economic. If populations and property shift towards TC-exposed coastal areas over time, as has been documented on the Atlantic coast of the U.S. (Collins and Lowe 2001), hurricane damages will increase even if the frequency and intensity of landfalling TCs remain unchanged. Thus, Pielke Jr. et al. (2008), Peduzzi et al. (2012) and others have pointed out that trend analyses based on TC-caused losses as opposed to some direct measure of TC activity or strength are biased by the effect of increased exposure of assets and populations with time. Although the economic loss data can be "normalized" by the use of corresponding socioeconomic data (as was done by both Pielke Jr. et al. and Collins and Lowe, who found this eliminated the aforementioned positive trend), such a method is not ideal since errors in the latter may compound those already present in the former. Thus the economic loss data adjusted in this way should not be considered even roughly equivalent to results inferred from climate data directly, however imperfect the latter may be. Nevertheless, the sociological trend highlighted by these authors shows little sign of slowing, leading Pielke Jr. et al. to conclude:

> Unless action is taken to address the growing concentration of people and properties in coastal areas where hurricanes strike, damage will increase, and by a great deal, as more and wealthier people increasingly inhabit these coastal locations.

The implications of this conclusion and those from the scientific studies summarized above for construction of a hurricane destructive index linked to climate change will be discussed in Section 5.

4.3.2 Extratropical cyclones and storms

Extratropical cyclones (hereafter ECs) exist throughout the mid-latitudes in both hemispheres and mainly develop over the oceanic basins, either as TCs continuing away from the tropics or as a result of flow over mountains. ECs do not include all regional smaller-scale storms, but are the main transporters of heat and moisture away from the tropics and are often accompanied by windstorms, storm surges, and extreme precipitation events.

According to the AR4-WGI, there has likely been an increase in both the frequency and intensity (depending on the specific region) of Northern Hemisphere extreme extratropical cyclones and a poleward shift in storm tracks since the 1950s (Trenberth et al., 2007, Table 3.8). The evidence for this comes mostly from observations over the North Pacific and the North Atlantic storm track regions. As related in the SREX (p.164):

> North American cyclone numbers have increased over the last 50 years, with no statistically significant change in cyclone intensity (X.D. Zhang et al., 2004)….Canadian stations showed that winter cyclones have become significantly more frequent, longer lasting, and stronger in the lower Canadian Arctic over the last 50 years (1953-2002), but

> less frequent and weaker in the south, especially along the southeast and southwest Canadian coasts (Wang et al., 2006). Further south, a tendency toward weaker low-pressure systems over the past few decades was found for U.S. East Coast winter cyclones … but no statistically significant trends in the frequency of occurrence of systems (Hirsch et al., 2001).

Several studies using observational reanalyses indicate a northward and eastward shift in Atlantic EC activity during the last 60 years with more frequent and intense wintertime cyclones at high-latitudes (Weisse et al., 2005; Wang et al., 2006; Schneidereit et al., 2007; Raible et al., 2008; Vilibic and Sepic, 2010), and fewer ECs occurring in the mid-latitudes (Wang et al., 2006; Raible et al., 2008). Consistent with these studies, Donat et al. (2011) discovered significant upward trends in wind storm frequency and extreme wind speeds from 1870 to present over central, northern, and western Europe. These authors found that 1.4-6.8 additional storm days per year are being recorded, depending on the exact region.

4.3.3 Trends in tornadoes and wind speed

A considerable amount of data exists on tornado occurrence in the U.S., where around three-quarters of tornadoes occur (NOAA Storm Prediction Center; Appendix B). Although some trend analysis has been conducted (Simmons and Sutter, 2011), there are two principal problems with drawing conclusions from these data. First, the data are certain to be incomplete, since tornadoes are small-scale phenomena (~100 m to a few km across, 500 ft or 150 m on average) and their tracks 5 miles (8.0 km) long on average, although some can persist for hundreds of km. Second, the scale commonly used for tornado intensity, the Fujita scale, rates tornadoes by damage caused, not by maximum wind speed, central pressure, or some other meteorological property (although wind speeds are available from radar observations). Thus trend analyses of tornado intensity based on either frequency or intensity are even more subject to non-climatic (socioeconomic) factors than is the case for hurricanes.

With regard to winds in general, one recent study found that annual mean wind speeds have declined by 5%-15% at approximately three-quarters of surface stations in the Northern Hemisphere over the past 30 years (Vautard et al., 2010). The authors hypothesized that the declines were due to a combination of atmospheric circulation changes and transformations in land cover over recent decades.

According to SREX (p.150-152), evidence for robust and widespread trends in extreme wind speed and tornadoes is not strong at this time:

> Regarding other phenomena associated with extreme winds, such as thunderstorms, tornadoes, and mesoscale convective complexes, studies are too few in number to assess the effect of their changes on extreme winds. As well, historical data inhomogeneities mean that there is low confidence in any observed trends in these small-scale phenomena. … A number of recent studies have addressed observed changes in wind speed across different parts of the globe, but due to the various shortcomings associated with anemometer data and the inconsistency in anemometer and reanalysis trends in some regions, we have *low confidence* in wind trends and their causes at this stage. We also have *low confidence* in how the observed trends in mean wind speed relate to trends in extreme winds.

4.4 Drought

At a given location on land, the annual amount of precipitation or its decadal trend is not likely to be as important as the cumulative amount of rain or snow that falls in a given time. Episodes of heavy rainfall can cause flooding, while little rain falling over long time periods can produce drought conditions, both of which can have dire consequences in agricultural areas and population centers.

The description of such conditions requires information beyond that for precipitation alone. One must consider the entire water balance in a given location, which comprises: (1) precipitation; (2) evaporation, which depends on air temperature and available water (evapotranspiration on land, which includes uptake of moisture by plants); and (3) on land, pre-existing amounts of water on the surface and in the soil, in addition to soil/surface properties (e.g., a simple 10 cm deep "bucket" of soil is often assumed). On land, local water balance is expressed as "precipitation minus evapotranspiration equals runoff," and thus the situation is more complicated than for temperature.

The simplest description encompassing these effects is the *moisture anomaly*, Z, defined as the difference between the sum of precipitation and available soil moisture minus potential evapotranspiration (the evaporation that would occur both directly to the atmosphere and through plants, if an unlimited supply of water were available). A negative moisture anomaly is a water deficit, a measure of the stress affecting vegetation in the event of meteorological drought, while a positive anomaly is characterized by saturated soils and runoff. A *standardized moisture anomaly*, i.e., $Z/\sigma(Z)$, was constructed by Hansen et al. (1998), and applied to climate time series from New York City. We examine this along with other climate indices in detail in Section 5.

Severe meteorological drought in continental regions invariably precedes both "hydrologic" and "agricultural" drought. The former is manifested by below-normal streamflow, lake and groundwater levels, while the latter relates to moisture deficits in the topmost one meter or so of soil (the root zone) that impact crops and other vegetation. By increasing evaporation, anomalously high temperatures exacerbate the problem of precipitation deficits, thus hastening the transition to agricultural drought.

The most commonly used quantitative definition of drought severity is the Palmer Drought Severity Index (PDSI), which includes information about air temperature, precipitation, and also soil moisture, which is affected by plant transpiration and soil properties. The calculation of PDSI is somewhat involved (see Alley [1984] for details), but it is basically the sum of the moisture anomaly Z described above and a term which accounts for the persistence of a given state. Specifically, the PDSI at month m is related to that at the preceding month by $\mathrm{PDSI}(m) = 0.9\,\mathrm{PDSI}(m\text{-}1) + (1/3)Z(m)$. Thus the PDSI is a cumulative index, i.e., one in which each successive value is based on the previous value. The first term represents the current climate state, while the second incorporates the long-term "memory" of soil moisture compared to precipitation, which indicates how wet or dry it has been in previous months. Thus, the PDSI is better suited than either the Standardized Precipitation Index (SPI; Sec. 2.2) or moisture anomaly to a description of a longer term climatic event such as drought. This can be seen in **Figure 4.14**, a comparison of the SPI and PDSI during 1929-40, a period of extensive drought in the U.S., and 1946-56, which was characterized by more or less normal climatic conditions over most of the

country (see also Fig. 6.13).

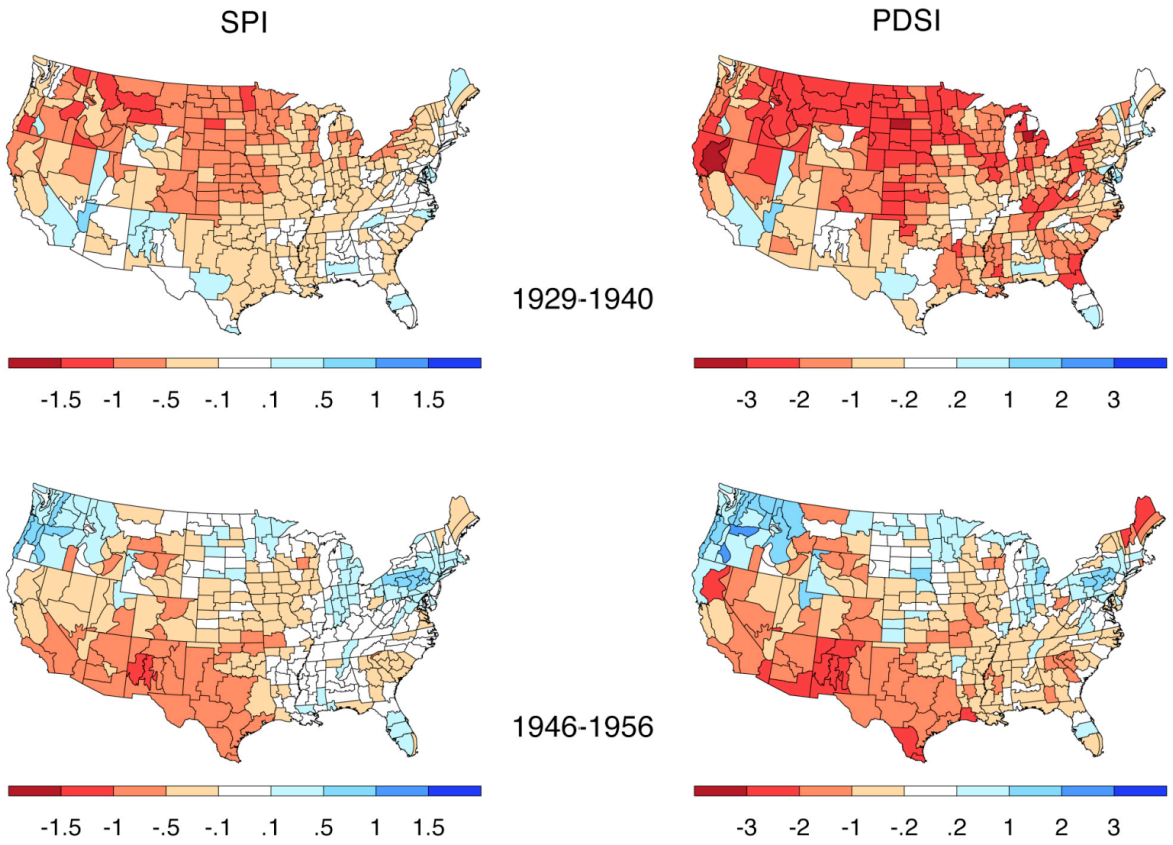

Figure 4.14. The observed Standardized Precipitation Index (SPI, 12-month period; *left*) and self-calibrated Palmer Drought Severity Index (PDSI; *right*) averaged for the period 1929-1940 (*top*) and 1946-1956 *(bottom)*. Negative indicies denote abnormally low surface moisture conditions. *Source:* M. Hoerling, X.-W. Quan, and J. Eischeid (2009).

Despite its explicit reference to drought, the PDSI is a useful characterization of both dry and wet periods, as the moisture index can be either positive (moisture excess) or negative (moisture deficit). The scale of the PDSI is nominally -10 to +10, where 0 represents normal conditions, values less than -1 denote the onset of drought, and values +1 and larger indicate abnormally wet periods[1]. The top panel of **Figure 4.15** shows the spatial pattern of PDSI over the globe for the entire 20th century. The index captures the extensive and severe drought that characterized much of the century in Africa, the North American Prairies, the Mediterranean, eastern Australia and the Brazilian interior. Wetter than average conditions characterize eastern North and South America and northern Eurasia. The lower part of Fig. 4.15 indicates that globally, drought conditions are becoming more prevalent with time.

[1] Palmer (1965) originally calibrated his index against data from the 13 driest intervals recorded in central Iowa and western Kansas, finding that these "extreme droughts" corresponded to a PDSI = -4.0.

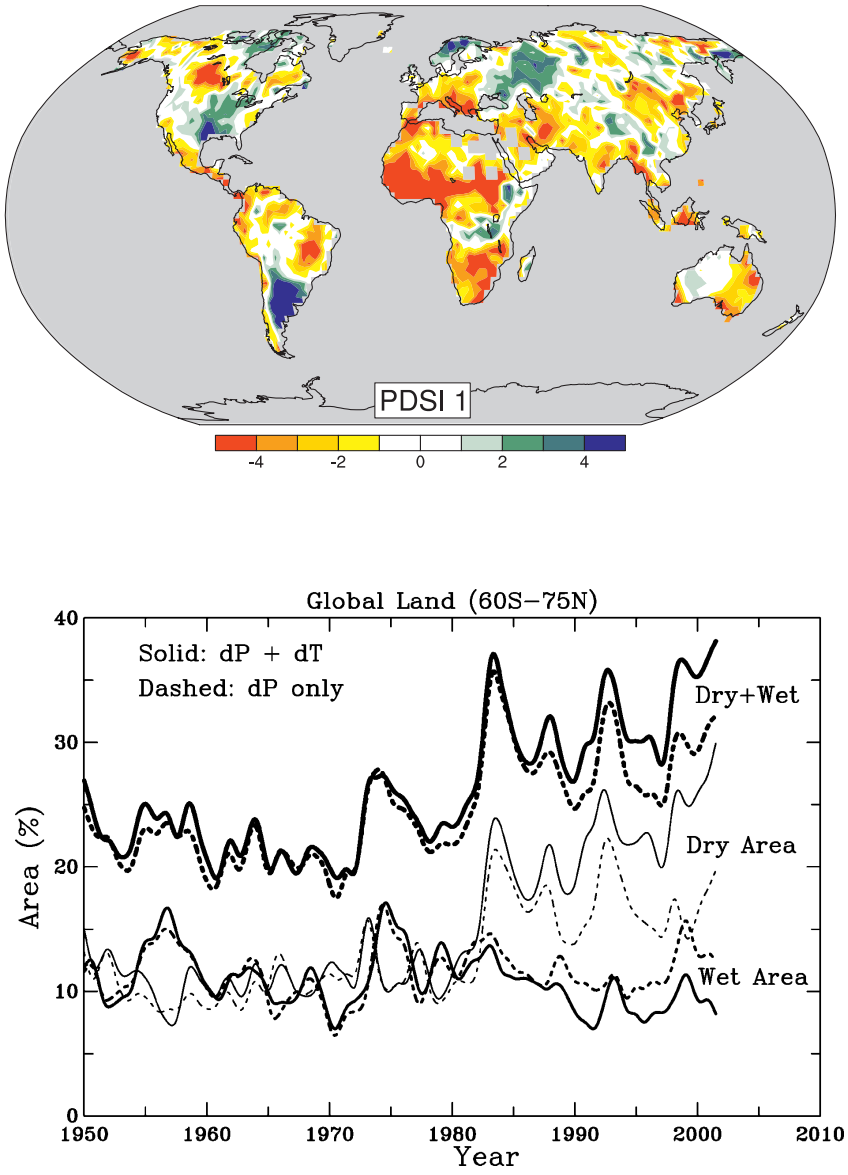

Figure 4.15. *Top:* The most important spatial pattern of the monthly Palmer Drought Severity Index (PDSI) for 1900 to 2002. The PDSI is a prominent index of drought and measures the cumulative deficit (relative to local mean conditions) in surface land moisture by incorporating previous precipitation and estimates of moisture drawn into the atmosphere (based on atmospheric temperatures) into a hydrological accounting system. *Source:* AR4-WGI. FAQ 3.2, Fig. 1 (lower panel removed), adapted from Dai et al. (2004). *Bottom:* Smoothed time series of the percentage of the total land areas within 60°S–75°N that were in very dry (PDSI < -3.0; thin lines), very wet (PDSI > +3.0; medium lines), and very dry or wet (thickest lines at the top) conditions from 1950 to 2002. The solid lines are based on the PDSI calculated with both precipitation and temperature changes, while the dashed lines are without temperature changes (i.e., due to precipitation alone). *Source:* Dai et al. (2004).

Comparing the regional trends in PDSI with those in temperature (Fig. 3.1) and precipitation (Fig. 3.4), the AR4-WGI concluded that "decreases in land precipitation, especially since the early

1980s are the main cause for the drying trends, although large surface warming during the last two to three decades has also likely contributed to the drying."

A detailed view of the behavior of the PDSI thresholds in the western United States is shown in **Figure 4.16**, where one sees that the area of extremely dry surface conditions has significantly exceeded that of extremely wet regions since the mid-1980s. However, the areal coverage at the peak of the two most recent droughts (~80% in 1990 and 2002) is by no means unprecedented; similarly dry episodes occurred in the early 1930s and mid-1970s.

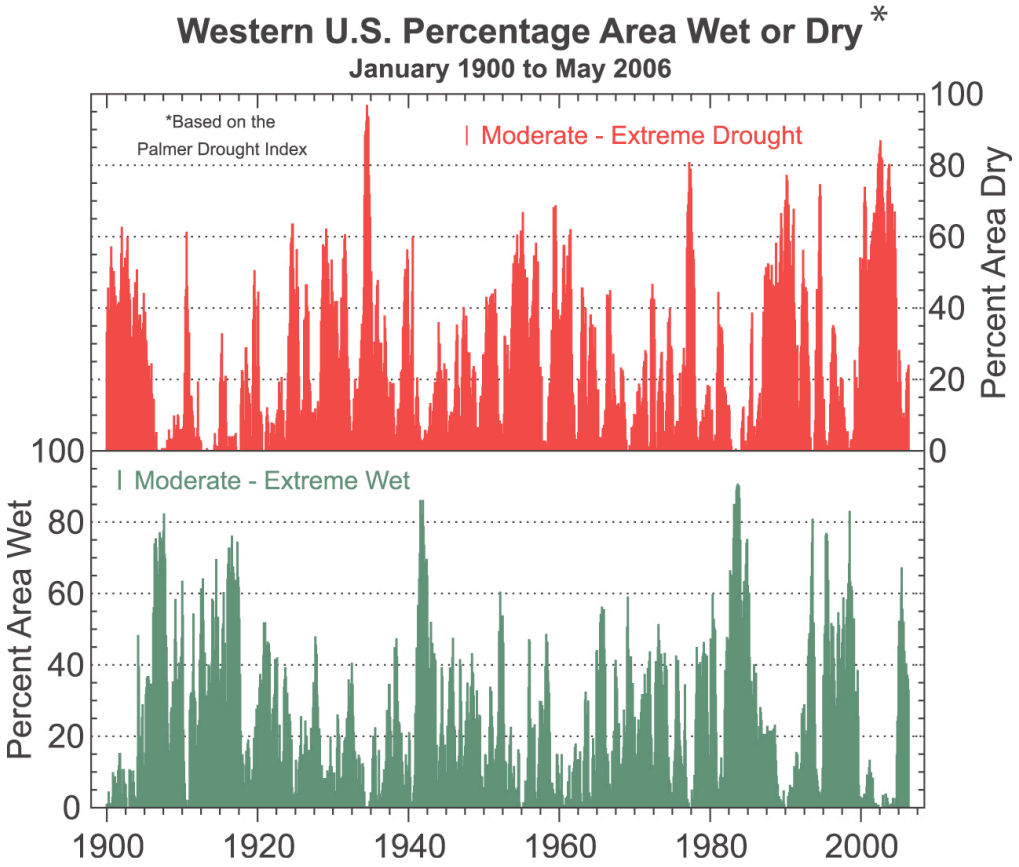

Figure 4.16. Percentage of the USA west of the Rocky Mountains (the 11 states west of and including Montana to New Mexico) that was dry (*top*) or wet (*bottom*) based on the PDSI for classes of moderate to extreme drought (PDSI < -1) or wet (PDSI > +1). From NOAA, NCDC. *Source:* AR4-WGI, Box 3.6, Fig. 1.

4.5 Flooding

The same water balance that governs drought also applies to flooding, but the time scale for floods is much shorter and external triggers play a larger role. For that reason, the PDSI is not as robust an indicator of flood conditions, although it does convey information on whether a given region may be predisposed to flooding if subjected to an external trigger such as a storm surge or river overflow. For example, the devastating summer 2002 floods in central Europe were triggered by a few high-intensity, short-duration precipitation events but compounded by the

fact that "the soils were completely saturated and the river water levels were already high because of previous rain (Rudolf and Rapp, 2003; Ulbrich et al., 2003a,b)" (AR4). Hence, while a single index for flood risk is difficult to formulate, statistical and modelling studies have been useful in placing recently observed floods in historical context and in investigating possible links to climate change.

Over the last decade or so, mounting economic losses from large floods in northern and central Europe (summer 1997, spring 1998, autumn 2000, summer 2002, winter 2003, and summer 2007) have prompted a number of analyses of whether these events are becoming more frequent or intense compared to previous decades. Although extreme floods with return periods of 100 years and 500 years occurred in central Europe in July 1997 (Oder River) and August 2002 (Elbe River), respectively, Mudelseeet al. (2003) found no significant trend in the occurrence of extreme summer (May–October) floods in the two major rivers over the past few decades. Prompted by an increasing trend in economic losses due to flooding in Europe over the 1970-2006 period, Barredo (2009) normalized the losses for socioeconomic factors (as done for hurricane losses by Pielke Jr. et al. [2008]; Sec. 3.3.1), finding no residual trend. However, as mentioned in Sec. 4.3.1, trend analysis of normalized economic data should not be placed on an equal footing to a description of actual climatic phenomena.

The trend analyses mentioned above are prone to fairly large sampling errors; that is, the events in question are so rare that the lack of statistically significant trends may be due more to the small number of events composing the sample, than to the lack of actual physical changes. For example, aside from the aforementioned multi-century level flood levels achieved in central Europe in recent years, we should acknowledge the possible significance of the maximum 24-hour precipitation total of 353 mm observed at the German station Zinnwald-Georgenfeld during the 2002 event, which set a new record for Germany. Also, increased precipitation variability at a majority of German precipitation stations during the last century (Trömel and Schönwiese, 2005) indicates an increased likelihood of both floods and droughts (AR4).

One way to avoid the sampling error issue mentioned above is to employ models that can generate arbitrarily large numbers of statistical or deterministic realizations of a given phenomenon. As a reality check, these models can then be validated against observed distributions. As a case in point, Pall et al. (2011) simulated the conditions surrounding the autumn 2000 floods in England and Wales using GCM experiments. Specifically, the authors ran two types of simulations. In the first (labeled A2000), realistic autumn 2000 conditions were represented in the model by prescribing concentrations of greenhouse gases and atmospheric pollutants (sulphate aerosol and ozone), as well as patterns of observed SSTs and sea ice for April-November 2000. The second type of simulation (A2000N) was conducted in the same manner except greenhouse gas concentrations, SST and sea ice patterns were replaced with best-guess year 1900 levels. Thus, differences between the two simulations could be attributed to the human-caused component of climate change.

The first notable result of the Pall et al. study was that, for four different climate models and several thousand one-year simulations, the occurrence frequency of high-runoff events in the region was always largest (or the return period always lowest) in the simulations including anthropogenic greenhouse gas forcings and their effects. Equivalently, daily runoff rates were

always larger in the A2000 simulations for a given occurrence frequency (return period). If R and R_N are the fraction of runoff events in the A2000 and A2000N climates, respectively, that exceed the actually observed runoff rates during the flood, then the fraction of risk attributable to human-caused warming is FAR = 1 - R_N/R. **Figure 4.17** shows the results, which the authors summarize as follows:

> the increase in risk of occurrence of floods in England and Wales in autumn 2000 that is attributable to twentieth-century anthropogenic greenhouse gas emissions is very likely (nine out of ten cases) to be more than 20%, and likely (two out of three cases) to be more than 90%.

There are, however, various caveats associated with any particular study; but this example illustrates a general means of making the most of imperfectly sampled data, and such methods do provide insight into mechanisms in the climate system that may be changing in response to human influences.

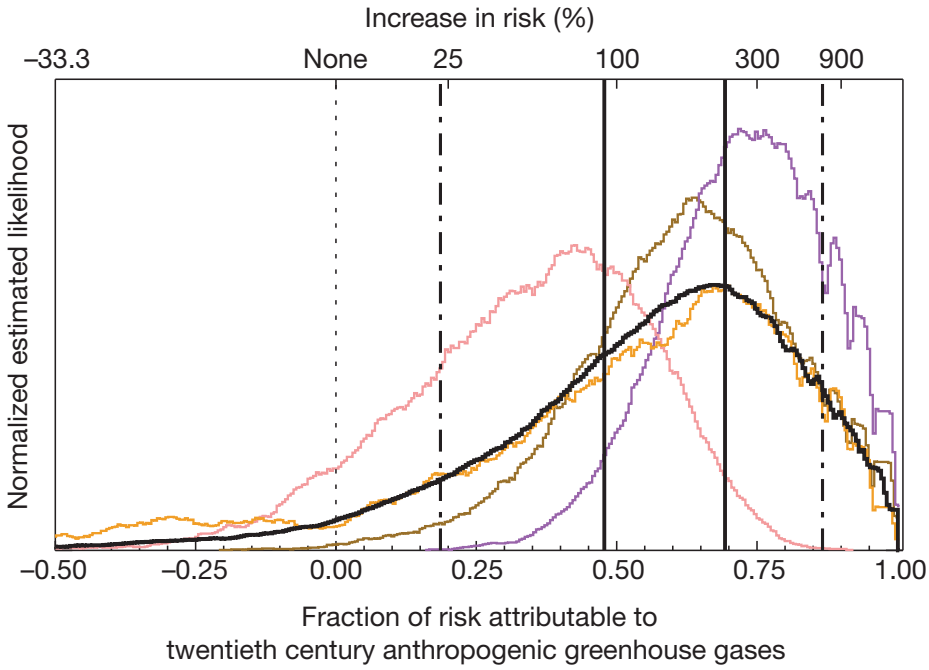

Figure 4.17. Smoothed histograms of the fraction of risk of severe synthetic runoff in the A2000 climate that is attributable to twentieth-century anthropogenic greenhouse gas emissions, i.e., fraction of attributable risk (FAR). The aggregate histogram (black) represents the FAR relative to the A2000N climate, while each colored histogram shows the FAR for a particular climate model. The dot-dashed (solid) pair of vertical lines marks the 10th and 90th (33rd and 66th) percentiles. The top axis shows the equivalent increase in risk. *Source:* Pall et al. (2011).

5. The Construction of Climate Indices

Climate indices offer a useful means of summarizing and communicating the vast amount of research reviewed in the previous three sections. An index can be constructed for a single climate variable, or as a composite of many variables. It is in the composite form that the index achieves its real utility, since it is not obvious from the information presented in previous sections how one might express changes in, say, surface air temperature (SAT), sea ice, and drought frequency using a single measure.

There are numerous ways to construct an index, and for this reason we consider each index and its components separately in the subsections that follow. However, all indices share a few desirable features:

(1) An index of a single variable should be a relative or normalized measure, and therefore a dimensionless number.

(2) The chosen normalization should reflect something that is easily understood, for example, the mean value or standard deviation over a base period, or total land area.

(3) The index should be easy to update, allowing more recent data to be included, and should not depend on specialized measurements that may be specific to a given instrument or technology.

(4) The averaging time used for the index (e.g., daily, monthly, annual) should not be too short or too long. For example, the use of a monthly index may result in spurious trends in certain variables due to the sinusoidal nature of the seasonal cycle (unless the climatology is subtracted). Portraying short-term variations could end up making the index too difficult to interpret, while averaging over too long a period might lead to misleading trends. As decadal and longer-term trends are often of interest, an index constructed from annual mean data would be appropriate in most cases, with additional smoothing applied if interannual variability is especially evident.

(5) A composite climate index, constructed of climate indices for single variables, should use an equal weighting for each individual index in the sum, or have a clear justification for any weightings applied.

(6) When constructing a composite index, the choice of individual variables should suit the intended application. Exposed populations and stakeholders directly affected by climate change and variability, such as insurers, will presumably be most concerned with changes occurring in regions where those interests are concentrated, rather than in more remote locations. For example, while an index for sea ice area could be one component of a composite index, it may have little direct relevance for human socioeconomic affairs, at least on the time scale of most interest to property insurers, i.e., a few years. On the other hand, the feedback to climate that occurs upon the disappearance of Arctic ice has global-scale effects, and so may affect long-term trends in other variables and indices. Thus, while the choice of variables comprising the index is a subjective matter, it may be helpful to keep track of the relative contribution of different component indices.

Readers should also be alerted to the fact that the term "climate index" in the research literature usually has a somewhat different meaning than the object of this report. The climate indices most often discussed in the research literature are specific defining quantities of atmospheric and joint atmosphere-ocean variability, such as the NINO3.4 index, Pacific Decadal Oscillation index, Southern Annular Mode index, and a handful of others. While such indices are used by researchers to summarize a wealth of spatially varying information in a single number, they are mainly designed to study internal climate variability and not longer-term trends.

We begin in Section 5.1 with a short description of some simple climate indices in use or under development that were formulated to communicate climate change science to a general audience. They aim to be as accessible to the public and policy makers as the GDP or Dow Jones Industrial Index is to business-minded audiences. In Section 5.2, we outline some of the advantages of standardized climate indicies, which incorporate the key features of climate variability. Section 5.3 describes two index methodologies focused on extremes, while Sections 5.4, 5.5, and 5.6 describe specialized indicies used for agriculture, health, and hurricane activity and damage, respectively. While some examples of constructing a composite index from indices for individual variables are given in Sec. 5.2 and 5.3, a more comprehensive strategy for doing so, that includes socioeconomic impacts as well as climate indicators, is deferred to Section 7.

5.1 Available Climate Indicies

The International Geosphere-Biosphere Program (IGBP), a body that funds and coordinates international research on Earth system science, publishes an annually updated climate index based on four global climate indicators, described as follows:

> Each parameter (carbon dioxide, sea level, temperature, Arctic sea-ice minimum) is normalised between -100 and +100. Zero is no annual change. One hundred is the maximum-recorded annual change since 1980. Each year, we take the average of the normalised parameters. This gives the index for the year. The value for each year is added to that of the previous year to show the cumulative effect of annual change.

In their online description, the IGBP describes the index as analogous to the Dow Jones Industrial Index, which summarizes the performance of the complex U.S. equities markets in a single number. The IGBP index from 1980-2009 (**Figure 5.1**) resembles a straight line or slightly concave-upward parabola, with little interannual variability; this is not surprising since it is a cumulative index. By including carbon dioxide concentration as one of the four component indices, it is essentially guaranteed to rise year after year. However, as explained in Sec. 2.3, carbon dioxide is more of a climate driver than an indicator, and has a delayed effect on the climate, so its inclusion in the index pushes it beyond a description of climate per se.

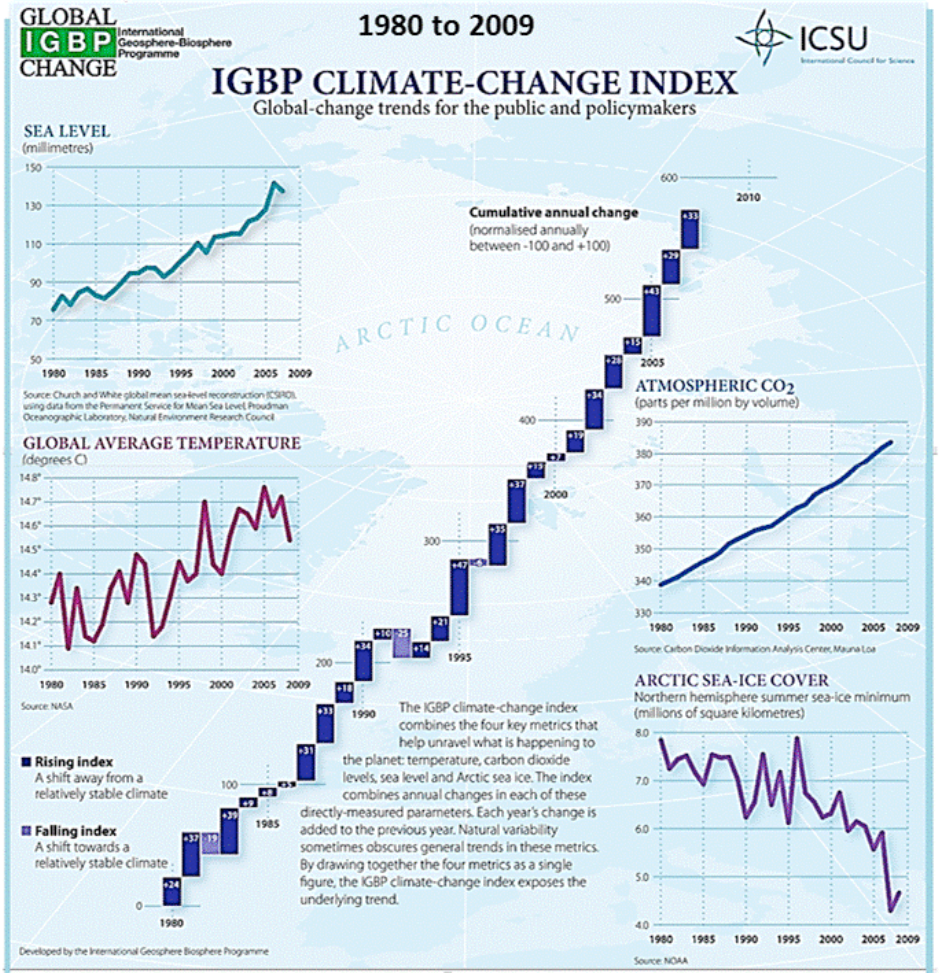

Figure 5.1. The IGBP climate change index and its component indices. *Source:* http://www.igbp.net/5.1b8ae20512db692f2a680008616.html. Accessed 04/25/2012.

Two ocean-related indices, both focused on marine ecosystems, are also under development. The first, known as IndiSeas, tracks eight primary indicators of ocean ecosystems with a specific focus on implications for the management of fisheries. Indicators include total biomass of key species, mean life span, and proportion of predatory fish. A description of this project is given by Cury and Christensen (2005).

The second project, the Ocean Health Index (OHI), a collaborative effort between Conservation International and a number of other marine-oriented groups, is still under development. The OHI attempts to measure the ability of oceanic ecosystems to thrive and to support human livelihoods—goals that are often in tension. The index aggregates complex data into a single, annual numerical score for every country, which allows an intercomparison of that nation's marine conditions and management practices. Factors comprising the index include climate change indicators, ocean acidification, fisheries, eutrophication (prevalence of oxygen-deprived "dead zones"), chemical contamination, decline in biodiversity and habitat destruction, invasive species, and other problems such as plastics pollution and sound (e.g., sonar and explosives). Further information on both ocean index projects may be found at the links provided in Appendix B.

5.2 Standardized Climate Index

5.2.1 Standardized temperature index

Hansen et al. (1998) introduced a unitless temperature index defined as the anomaly of SAT compared to a baseline period divided by the standard deviation over the same period: the *standardized temperature index* (*STI*)[1]. In their case, the baseline period was 1951-80, so the standard deviation is calculated as: $\sigma = [\text{Sum } ((T_i - T')^2) / 30]^{1/2}$, where T' is the mean SAT over the baseline period, and T_i is a single seasonal mean. The STI is precisely what is plotted in the previously discussed Fig. 4.1. At a particular location of interest, it may be more useful to examine the time series of such an index (e.g., for trend detection); an example is shown in **Figure 5.2**.

The upper left panel Fig. 5.2A shows the time series of seasonal mean STI, while panels B and C show two other measures of warming: heating and cooling degree days (H+CDD; Appendix A), and frequency of unusually hot summer days and cold winter days (HS+CWD). Since each of these quantities is normalized by the interannual standard deviation in the same quantity, each index is dimensionless. Plotted on the same graph, the individual indices are not substantially different (Fig. 5.2D, lower), but a higher degree of variability is evident in the H+CDD and HS+CWD indices. Thus, a composite index calculated as the simple average of the three individual indices (Fig. 5.2D, upper) incorporates information about both seasonal SAT variations and extremes. This is important, as we have seen that the most statistically significant trends in SAT and precipitation, for example, are those for extremes (Sec. 4.1, 4.2). They are also the features of climate change that are most likely to be noticed by the general public (Hansen et al., 2012).

The data shown in Fig. 5.2 for New York City extend only up to the mid-1990s. Although a warming phase is apparent during the last decade of the record, the composite STI is only ~ 1 over that period (Fig. 5.2D). Other locations have updated data to 2012, and some examples are shown in **Figure 5.3**. At these locations, the composite index indicates the emergence of a distinct warming signal (composite STI ~ 1.5–2.0) from the background noise of temperature variability, consistent with the results of previous sections.

[1] Hansen et al. (1998) referred to this index as the "common sense climate index," explaining that the average adult's perceptions of climate change arise from an informal comparison of the current season's temperatures, say, with those they experienced in prior decades at the same location. Further, a "significant" seasonal temperature difference would be noticed as one that differs by $\pm 1\sigma$ or more from the long-term mean, since anomalies of that magnitude are comparatively rare.

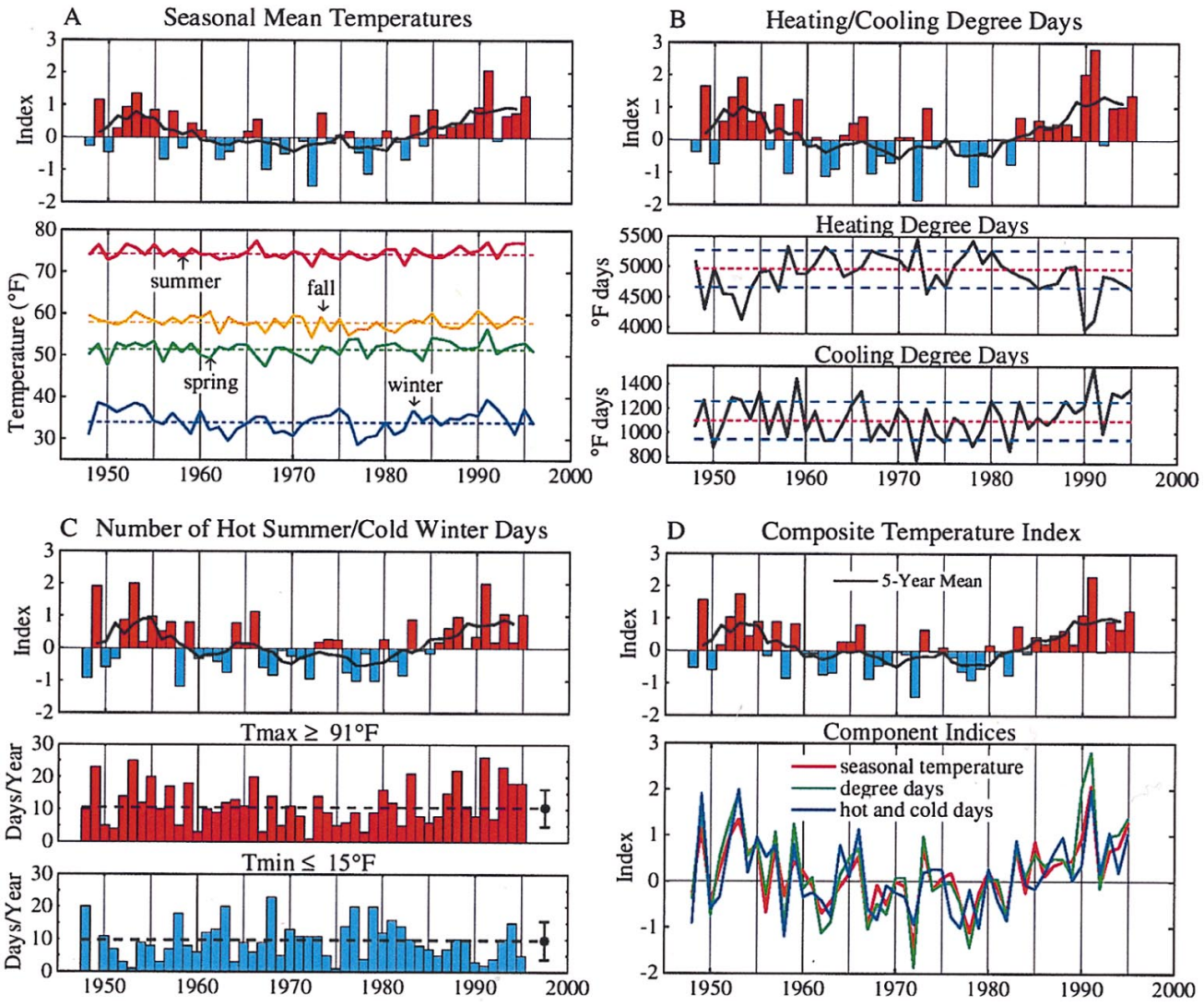

Figure 5.2. Components of the temperature index for New York (La Guardia Airport), based on (A) seasonal mean temperatures, (B) heating and cooling degree days, and (C) frequency of unusually hot summer days and cold winter days. (D) The net temperature index. The lower part of each panel shows the input data for that index. *Source:* Hansen et al., (1998).

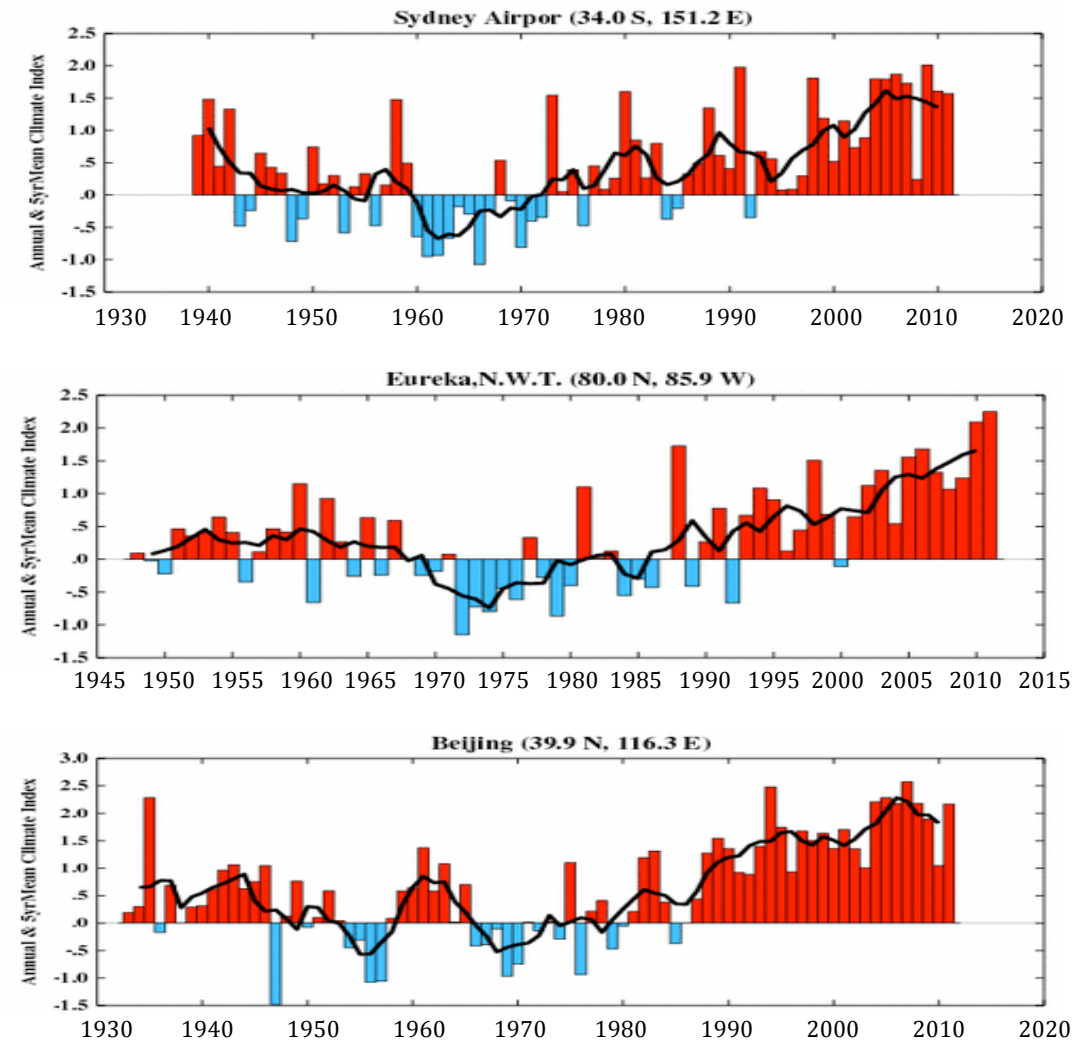

Figure 5.3. Examples of the composite SAT index at locations with complete data up to 2012. Sydney, Australia and Beijing, China station temperatures have been corrected for urban heat island effects. *Source:* NASA-Goddard Institute for Space Studies, http://data.giss.nasa.gov/csci/stations/.

One caveat with the choice of σ as a normalization for a climate index is that, like means and extremes, σ may also change under global warming. In the case of SAT, for example, using a base period of 1951-1980 to plot the distribution of normalized SAT anomalies gives the results shown in **Figure 5.4**, from Hansen et al., (2012). The leftmost panel of the figure shows a notable increase in SAT variability, with a shift towards higher extreme temperature anomalies in successive decades. Using 1981-2010 as a base period instead produces a normalized SAT distribution that does not reflect this change in variability, because the increased σ in the last decade has been divided out in the normalization (Fig. 5.4b). Thus, the choice of a base period for normalized anomalies, and therefore a climate index, must be carefully considered. Hansen et al., (2012) prefer 1951-80 as the period closest to preindustrial, "unperturbed" climate conditions for which data of sufficient quality are available.

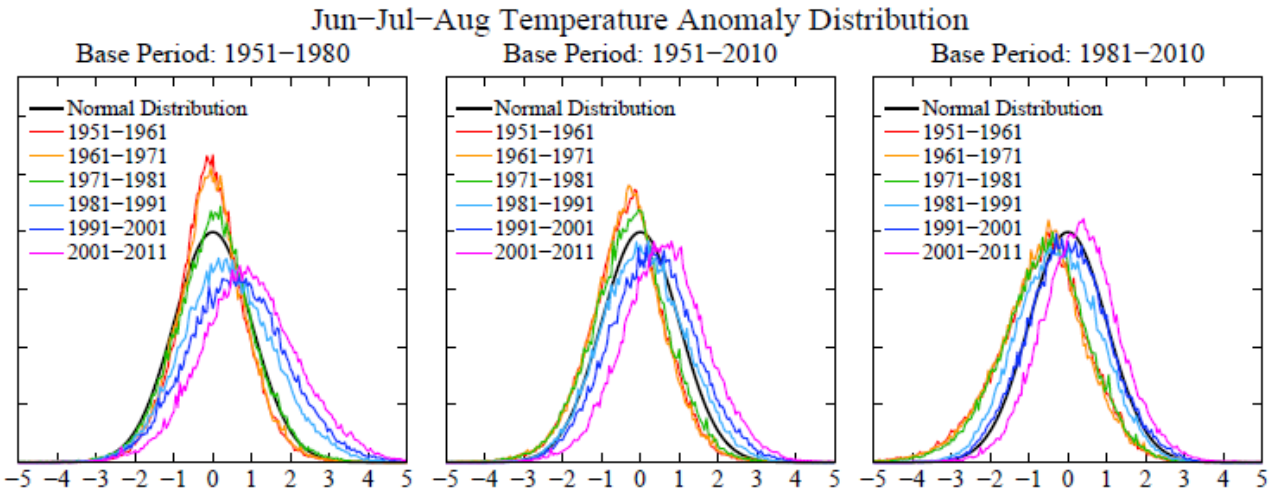

Figure 5.4. Frequency of occurrence (y-axis) of local temperature anomalies divided by local standard deviation (x-axis) obtained by binning all local results for 11-year periods into 0.05 intervals. The area under each curve is normalized to a value of 1. *Source:* Hansen et al., (2012).

5.2.2 Standardized precipitation, moisture, and drought indices

Just as for temperature, precipitation may be normalized by its standard deviation. The *standardized precipitation index* (SPI) is defined as the number of standard deviations that observed cumulative precipitation deviates from the climatological average (McKee 1993)[1]. The SPI for New York City on the seasonal time scale is shown in **Figure 5.5A**. As mentioned in Sec. 4.4, the overall water balance on land is better described by the standardized moisture anomaly, the normalized difference of precipitation and evapotranspiration. The negative of this quantity, termed the "annual water deficiency" by Hansen et al., [1998], is shown in Fig. 5.5B. The opposite sign is adopted so that the composite index will be large and positive when there is either too much precipitation or too little soil moisture. An index for extreme precipitation events, shown in Fig. 5.5C, is formed as the normalized sum of "heavy" and "rare" precipitation events. The latter are defined as those amounts occurring on average five times per year (heavy) and once every five years (rare) in the base period. For the climatology of New York City over 1951-80, this implies a daily rainfall amount of > 1.4 inches and > 3.6 inches for heavy and rare events, respectively.[2]

[1] The global SPI for the last 12 months is periodically updated at http://iridl.ldeo.columbia.edu/maproom/.Global/.Precipitation/SPI.html.

[2] While these thresholds are arbitrarily chosen, Hansen et al. (1998) found little sensitivity of their extreme precipitation index to other values.

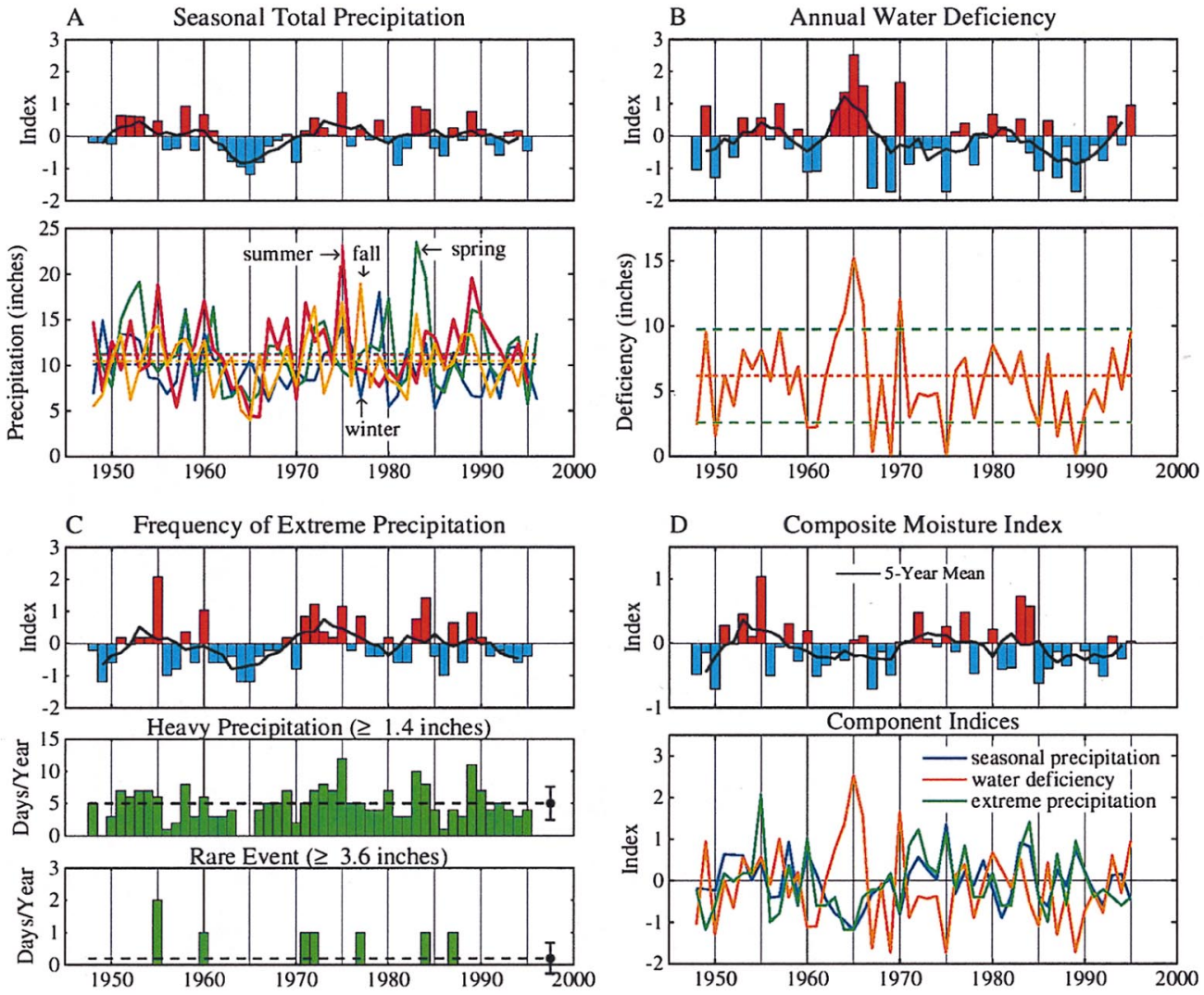

Figure 5.5. Components of the moisture index for New York, based on (A) seasonal total precipitation, (B) annual water deficiency, and (C) frequency of extreme precipitation. Panel (D) shows the net moisture index. Lower panels show the input data for each index component. *Source:* Hansen et al., (1998).

The composite moisture index, again constructed as a simple average of the three individual measures, is shown in Fig. 5.5D. This composite index most resembles the extreme precipitation index, since some cancellation occurs between the SPI and annual water deficiency.

The Palmer Drought Severity Index (PDSI), defined in Sec. 4.4, is a more sophisticated measure of persistent abnormally dry or wet land surface conditions, and is widely used to monitor drought worldwide. As pointed out by scientists at NOAA in the U.S., which issues a monthly drought forecast, the PDSI is better suited to describing long-term drought—on the order of several months—rather than conditions prevailing for a few weeks or less. One caveat of the PDSI is that it does not account for the supply of water locked up as snow, and so tends to overestimate the frequency of drought in mountainous areas and high northern latitudes.

The Crop Moisture Index (CMI) (Palmer 1968), a variant of the PDSI, places less weight on the data from previous weeks and more weight on the most recent week, meaning that it responds more rapidly than the PDSI to changing soil moisture conditions and thus is better suited to the description of short-term dry or wet anomalies affecting agriculture. The CMI is designed to indicate normal conditions at the beginning and end of the growing season, and uses the same [-4, 4] scale as the PDSI.

5.2.3 Composite standardized indices

If desired, a comprehensive climate index for a given location can be constructed as a simple average of composite, standardized temperature, moisture, and other individual variable indices. The meaning of such a comprehensive index needs to be carefully considered, however, since individual indicators are not independent. For example, a composite temperature index displaying a strong positive trend may often coincide with a moisture index showing a trend of opposite sign (since drying often accompanies heating), and thus significant cancellation may occur. A better strategy in this case might be to take absolute values of the individual indicator indices before averaging.

Another issue is that the standardized indices discussed so far were constructed for individual locations. There is no difficulty, in principle, to averaging results from different locations together; but over large areas, station inhomogeneity becomes an issue. For example, metropolitan areas tend to have many stations, while much larger rural areas have few. Thus, a simple averaging procedure will bias the results toward densely populated regions which, as was mentioned in Sec. 3.1, contain urban heat island and other effects. One means of avoiding such biases when constructing an index representative of a large area is discussed in the following subsection.

5.3 Indices based on climate extremes

While the standardized indices described in Sec. 5.2 provide a view of the entire range of anomalies, one may be more interested in the changing behavior of the extremes exhibited by a particular climate variable. As the anomaly distributions in Fig. 5.4 show, temperature extremes are rare events, and tracking the changing frequency of such exceptional events is another way to define a climate index.

An example of such an approach is that of Baettig et al., (2007), who focused on a “1 in 20 year” annual mean climate anomaly, which for a normally distributed variable such as SAT corresponds to values lying above the 95th or below the 5th percentile of the entire distribution of anomalies from a chosen base period. They then investigated how the frequency of such anomalies changed subsequent to the base period, quantifying this as the number of additional occurrences of an extreme event, *N*, per 20 year period. For example, a “1 in 20 year” warm extreme SAT event at a specific location in the base period 1951-80 might become a “3 in 20

year" event in a later period in which the distribution of SAT is shifted to the right (Fig. 5.4, leftmost panel)[1]. In that case, $N_{hot,ANN} = 2$.

The authors also tracked annual extremes of precipitation and seasonal extremes of both temperature and precipitation, which they combined into a single composite index as follows:

$$\text{CCI} = (N_{hot,ANN} + [N_{dry} + N_{wet}]_{ANN} + [0.5\, N_{hot,JJA} + 0.5\, N_{hot,DJF}] + [0.5\, (N_{dry} + N_{wet})_{JJA} + 0.5\, (N_{dry} + N_{wet})_{DJF}])/4.$$

Several subjective choices were made in the formulation of the CCI: (1) the mean of winter (DJF) and summer (JJA) extremes is given equal weight to annual extremes; (2) the sum of excessively wet and dry events is weighted equally to hot events; (3) as precipitation data are not normally distributed (rather, they are positively skewed, with a longer tail towards heavy precipitation events), a more suitable distribution function was fitted to the data before assessing percentiles; and (4) cold temperature extremes are neglected. This raises the issue of the intended application of the CCI. If the function of the CCI is to quantify the emergence of *all* extreme events over and above the usual 1 in 20 expectation, then cold SAT extremes should be included. If, instead, the intent of the CCI is to reflect prevailing climatic conditions expected in a warmer world, then cold SAT extremes should enter into the formula with a negative sign, e.g., as the extra terms $-N_{cold,ANN} - [0.5\, N_{cold,JJA} + 0.5\, N_{cold,DJF}]$. In either case, however, it seems clear from Fig. 5.4, left, that the number of such extremes recorded in recent decades is likely to be small.

A somewhat different approach was used to define a climate extremes index for the United States, the U.S. Climate Extremes Index (CEI) (Gleason et al., 2008). The CEI is a composite index that expresses the percentage of the total area of the continental U.S. that experienced extreme climate conditions at a given time, where "extreme" in this case signifies observations lying outside the 90th and 10th percentiles of the base period (1931-90) distribution[2]. Monthly mean data from individual GHCN stations were screened for 90% completeness over the interval from 1910 to present, leaving ~1100 stations over the entire country. A 1° × 1° grid is superimposed, and only grid boxes containing one or more stations are included in the analysis[3]. The problem of station density mentioned in Sec. 4.1 above was addressed by dividing the country into nine regions (**Figure 5.6**) and calculating the CEI on single regions first, then weighting each regional CEI according to its fraction of total U.S. area in the national CEI.

Examples of the U.S. CEI for annual minimum SAT and days with and without precipitation are shown in **Figure 5.7**. The top panel of the graph indicates that the area of the U.S. experiencing above-normal minimum SAT has been increasing since about 1980, while the bottom panel shows the same tendency in wet versus dry days, but only over the ~100 year time scale. For both variables, approximately opposite behavior is seen in the early part of the 20th century.

---

[1] Baettig et al. used model-simulated climates in their study, the results of which are summarized in Sec. 6; however, the same analysis could be applied to the observational record.

[2] Note that the 90th and 10th percentiles of a normal distribution correspond to $\pm 1.3\sigma$, and thus are not particularly extreme compared to some of the observations considered in Sec. 4, for example.

[3] That is, areas without stations are not counted in the total area. Doing so would systematically underestimate the CEI (K. Gleason, private communication).

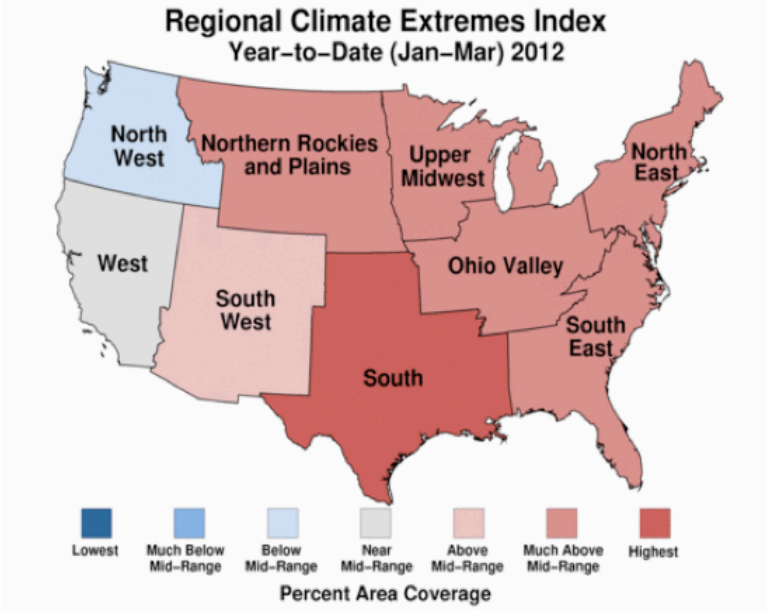

Figure 5.6. The regional definitions used in the calculation of the U.S. Climate Extremes Index. The color scale corresponds to the top row results in the CEI example shown in Fig. 5.8 below.

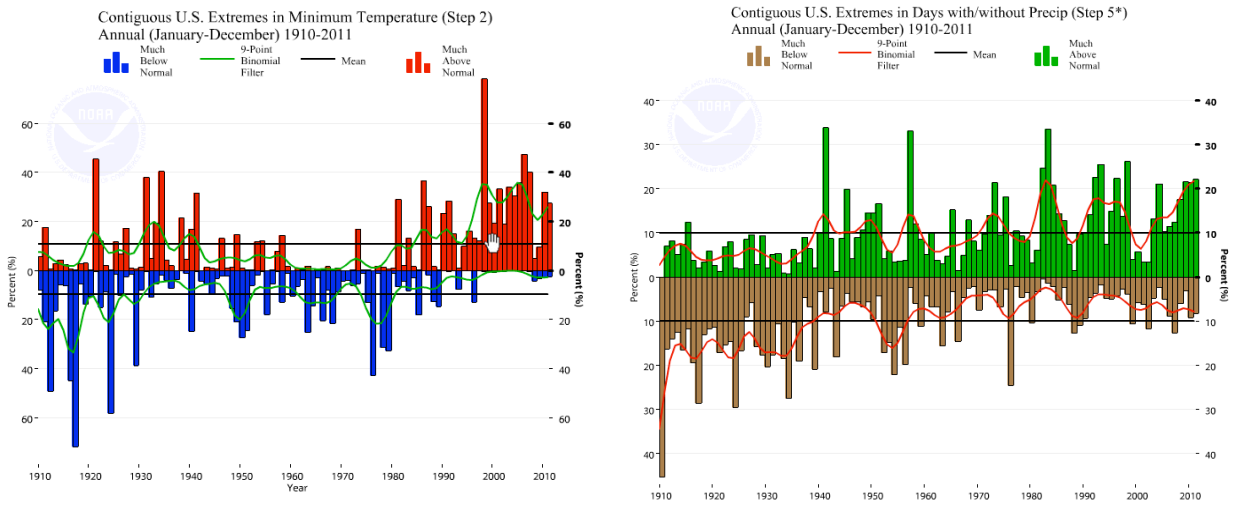

Figure 5.7. *Top:* Percentage of the contiguous U.S. area with much above-normal (*red*) and much below-normal (*blue*) minimum SAT, compared to the base period 1931-90. Green curves are five-year moving averages and straight black lines show the corresponding averages over the entire period. *Bottom:* Same as for top panel, but for the number of wet (*green*) and dry (*brown*) days. *Source:* http://www.ncdc.noaa.gov/extremes/cei/.

Other variables included in the CEI are listed in the table shown in **Figure 5.8**, which records values of the CEI by region for the January-March 2012 period. For each variable, observations lying outside the 90th and 10th percentiles of the base period (1931-90) distribution are used to calculate the index. The recent North American heat wave of March 2012 (Sec. 2.1) is reflected in

both the CEI and its components, particularly in the south and eastern two-thirds of the U.S. (Figs. 5.6 and 5.8). Thus, the CEI appears to fulfill the criterion of highlighting climate variations that are noticeable to the general population.

The composite U.S. CEI expressed as a time series is shown in **Figure 5.9**. Despite the relatively larger values of the index seen in the last two decades, similar behavior occurred between 1910-35.

Percent Area Coverage of Indicator by Region

Year-to-Date 2012

	Contig-uous U.S.	North East	Upper Mid-west	Ohio Valley	South East	South	N'rn Rockies and Plains	South West	West	North West
CEI	39%	54%	46%	47%	47%	51%	38%	30%	14%	10%
Max Temp (Warm)	74%	1%	1%	1%	97%	80%	79%	58%	42%	8%
Max Temp (Cold)	0%	0%	0%	0%	0%	0%	0%	0%	0%	0%
Min Temp (Warm)	63%	1%	1%	97%	82%	90%	69%	19%	0%	0%
Min Temp (Cold)	0%	0%	0%	0%	0%	0%	0%	0%	3%	0%
PDSI (Wet)	11%	25%	3%	32%	0%	0%	20%	0%	13%	1%
PDSI (Dry)	18%	3%	13%	0%	50%	30%	0%	39%	12%	0%
1-Day Precip	11%	8%	6%	0%	0%	27%	10%	11%	0%	17%
Days w/ Precip	4%	17%	3%	8%	6%	0%	3%	0%	0%	9%
Days w/out Precip	3%	8%	0%	0%	0%	3%	0%	11%	0%	0%

Occurrence within the Historical Distribution:

Coldest	Bottom Tenth	Bottom Third	Mid-Range	Top Third	Top Tenth	Warmest
Driest	Bottom Tenth	Bottom Third		Top Third	Top Tenth	Wettest

Figure 5.8. Breakdown of the U.S. CEI by region, for the period January-March, 2012. Results in the top row of the table are represented graphically in Fig. 5.6.
Source: http://www.ncdc.noaa.gov/extremes/cei/regional_overview/ytd.

A slightly modified form of the CEI was applied to climate data over Australia by Gallant and Karoly (2010), with the same qualitative results as in the U.S., namely, an increase in the extent of hot and wet extremes and a decrease in the extent of cold and dry extremes, both annually and in each season.

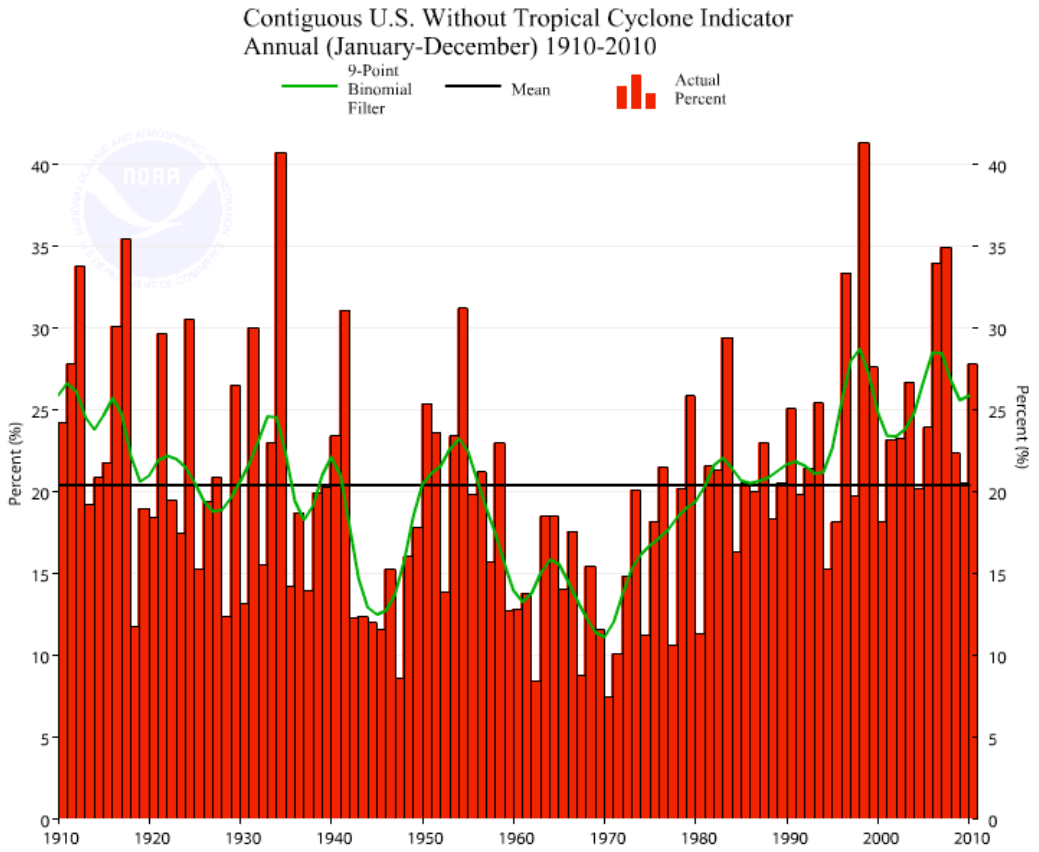

Figure 5.9. Composite U.S. CEI constructed from an average of all individual CEI's listed in Fig. 5.8.

5.4 Agriculture-related indices

Three types of agro-climate indices are commonly encountered: frost days, growing degree-days (GDD), and the heat stress index (HSI). Days when the minimum temperature drops below 0°C are frost days, which can damage crops if they occur during the growing season. GDD are the number of accumulated degrees within certain SAT thresholds over a given time period. The HSI is defined similarly, but with only an upper temperature threshold. Temperatures above this threshold can disrupt key plant processes such as grain filling, resulting in reduced production, as mentioned in the example discussed in Sec. 4.1. Trends in each of these indices over the period 1951-2010 over North America show continuing declines in the number of frost days and increases in GDD, while increases in HSI are largely confined to the western half of the continent (Terando, Easterling, Keller, and Easterling 2012).

5.5 Health-related indices

As mentioned in Sec. 4.1, heat stress and heat-related mortality are sensitive not only to temperature but also to humidity, which raises the apparent temperature perceived by humans, livestock, etc. Several quantities are in common use, and although they are termed indices, most, like temperature, are measured in degrees. Two closely related and widely used measures are the *humidex*, developed by the Meteorological Service of Canada and the *heat index* (or *humiture*),

used by the National Weather Service in the U.S. The two differ mainly by the use of dew-point temperature in the humidex[1] and relative humidity in the heat index (Hartz et al., 2012). Although not in general use, it would be straightforward to construct a normalized heat index from either of these quantities using their respective standard deviations. Alternatively, one could quantify the occurrence frequency of humidex/humiture threshold values by examining the underlying distribution, as was done by Baettig et al., (2007), or define an areal coverage of extremes as used for the CEI.

5.6 Hurricane indices

Several specialized indices have been formulated to characterize hurricane activity. The occurrence frequency of TCs and hurricanes is of course the simplest choice, although as mentioned in Sec. 4.3, it does not display any statistically significant historical trend. Trends were detected in the upper quantiles of lifetime-maximum hurricane wind speed, however. As these strong storms are of most concern to stakeholders, an index that accounts for both hurricane intensity and duration is preferable.

The U.S. Climate Prediction Center uses the *accumulated cyclone energy* (ACE) in its forecasts and reports on seasonal hurricane activity (Bell et al., 2000). The ACE for an individual storm is calculated by summing the square of the maximum wind speed, $V_{\max}$, measured at six-hour intervals over the entire time when the cyclone is classified as at least a tropical storm (i.e., while the maximum wind speed is at least 39 miles per hour). Therefore, the ACE accounts for both cyclone strength and duration. Summing the ACE values for all TCs over the hurricane season gives the annual ACE, as shown in **Figure 5.10**. In this figure, the median value of the ACE over the 1951-2000 period has been "indexed" to a value of 100, as a matter of convention (note, however, that the ACE has units of m^2/s^2, and so is not a standardized index by the definition used for other variables above). Further, as shown in the figure, NOAA has defined thresholds to indicate whether this indexed ACE for a given year is close to normal, or significantly above or below normal.

[1] http://climate.weatheroffice.gc.ca/prods_servs/normals_documentation_e.html

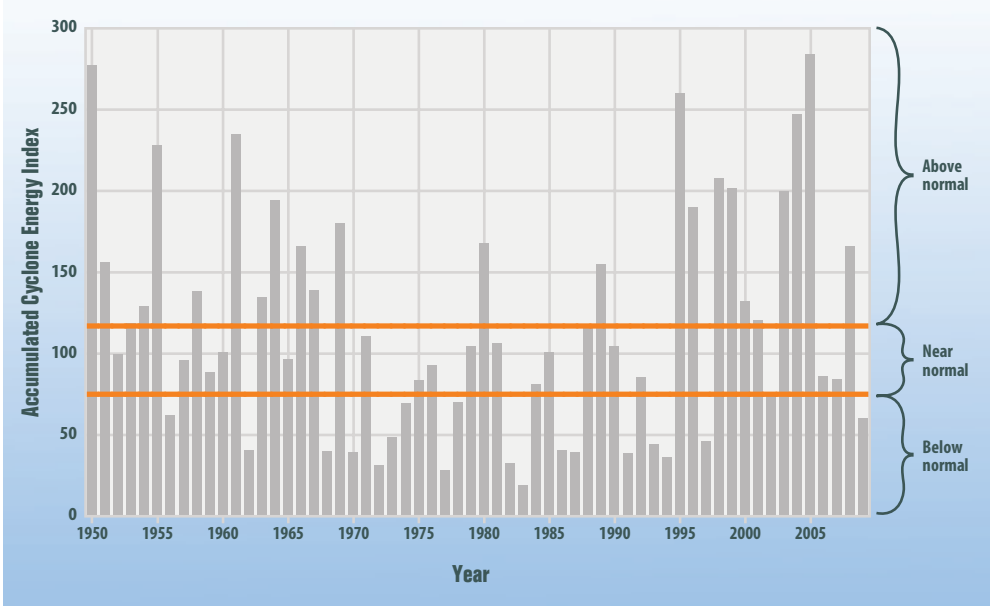

Figure 5.10. Total annual accumulated cyclone energy (ACE) index values from 1950 through 2009 for tropical cyclones in the North Atlantic. A value of 100 corresponds to the median value of the ACE over the 1951-2000 period. *Source:* NOAA, 2010.

While the ACE is proportional to the square of the wind speed and so the kinetic energy packed by TCs, another quantity, known as the power dissipation index (PDI) is defined as the integrated effect of the maximum wind power (proportional to V_{max}^3) in a storm or for all TCs in a given season (Emanuel 2005). It has also been argued that hurricane damage should scale with wind power, rather than with V_{max} or V_{max}^2 (Emanuel 2011). As shown in **Figure 5.11**, the PDI in the Atlantic Ocean is highly correlated with the SST averaged over the region where most hurricanes form, suggesting that warmer (cooler) oceans can lead to more (less) intense hurricanes. Just such a relation was in fact predicted in earlier theoretical work on TCs (Emanuel 1987). While it has been argued that the decadal variations of the subtropical Atlantic SST seen in Fig. 5.10 are driven mostly by anthropogenic changes in greenhouse gases and aerosols (Mann and Emanuel 2006; Emanuel 2008), other studies stop short of attributing changes in the PDI to human influence (Knutson et al., 2010).

One shortcoming of both the ACE and PDI is that neither accounts for the size of the storm. For two TCs achieving the same maximum wind speed (and therefore of the same Saffir-Simpson category), the larger of the storms covers a wider area with damaging winds, increasing its destructive potential. In order to reflect this, the *integrated kinetic energy* (IKE), was proposed by Powell and Reinhold (2007). The IKE is defined as the integral of kinetic energy over a range of specified wind speeds within a large volume surrounding the TC. Hence, calculation of the IKE requires detailed observations of the wind field of the TC, which are not available for most hurricanes prior to the satellite era.

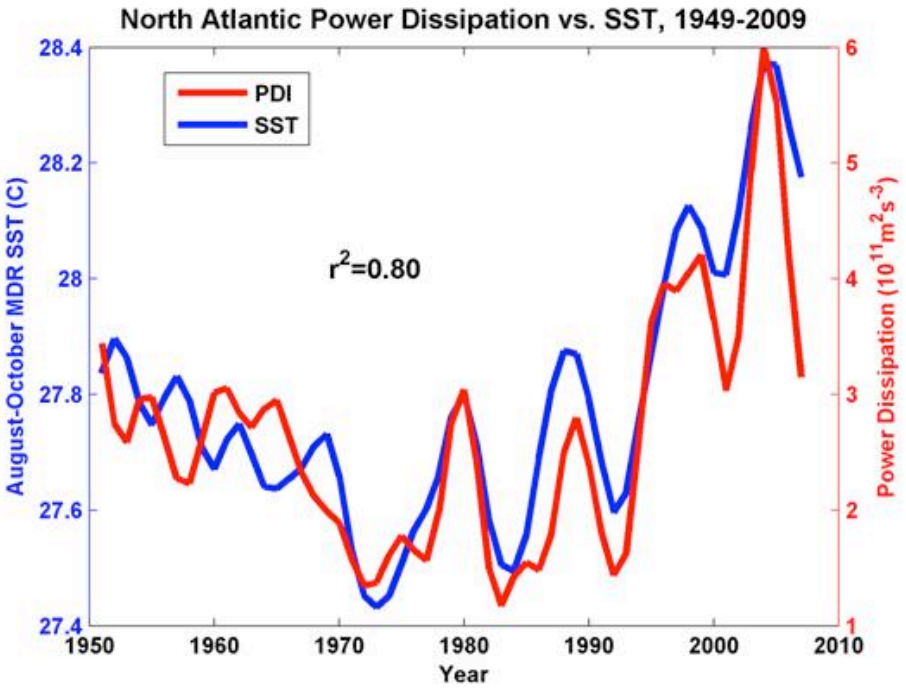

Figure 5.11. Atlantic tropical cyclone Power Dissipation Index (PDI, in red) and main development region (MDR) sea surface temperature (SST, in blue) from 1949 to 2009, inclusive. The MDR is defined as the region bounded by 6N and 18N, and 20W and 60W; the SST data is the HADISST1 data set from the U.K. Hadley Center, averaged from August through October of each year. The two time series are correlated with a correlation coefficient $r^2 = 0.80$. *Source:* Homepage of Prof. Kerry Emanuel, http://eaps4.mit.edu/faculty/Emanuel/publications/tropical_cyclone_trends, updated from Emanuel (2005).

Following on Emanuel's work, Kantha (2006) suggested a further variation on the PDI, noting that hurricane damage potential depends on properties other than V_{max}. First, the area of a hurricane at landfall, proportional to R^2, where R is the radius to which hurricane-force winds extend from the center of the storm, affects the amount of damage. Second, the translational speed S of the TC along both ocean and land surfaces is also important, as hurricanes that move more slowly tend to produce more damage (for a given V_{max}), via both extreme winds and storm surge. Both R and S can be obtained from satellite observations of storm radius and tracks.

Kantha's suggested metric, the *Hurricane Hazard Index* (HHI), includes all three of the above factors: i.e., $HHI = (V_{max}/ V_{max,0})^3 (R/R_0)^2 (S_0/S)$ (where $V_{max,0}$, R_0, and S_0 are constant reference values). The HHI reflects the observed features that: 1) small hurricanes may cause significant damage, but over a more limited area than larger hurricanes of roughly the same intensity category, and; 2) slow-moving hurricanes can produce heavier precipitation, higher storm surges, and more flooding than faster-moving storms. Comparing the HHI at landfall for Hurricanes Andrew (Saffir-Simpson category 5, 1992) and Katrina (category 3, 2005), Kantha found that although its V_{max} was 25% smaller, Katrina was twice the size of Andrew (both had about the same overland speed), leading to an HHI that was 85% larger. This result is consistent with Katrina's significantly larger normalized damage estimate (Pielke Jr. et al., 2008)[1].

[1] Kantha claims that Katrina's damage (in adjusted dollars) outstrips that due to Andrew even ignoring the devastating effect of the levee failures in New Orleans caused by the hurricane. However, we know of no independent verification of this claim.

Based on these results from the scientific literature, two additional measures of hurricane destructive potential have been suggested by insurance industry analysts interested in TC impacts. The *Carvill Hurricane Index*, developed by Carvill, Inc., a reinsurance intermediary in the U.S., is of the following form: $CHI = (V/V_0)^3 + (3/2)(R/R_0)(V/V_0)^2$. Thus, the CHI is an additive combination of a modified ACE and the PDI. The *Willis Hurricane Index* (WHI; Willis Research Network, 2009), developed by G. J. Holland (NCAR, U.S.) and Brian F. Owens (Willis Research Network, UK), incorporates the same factors as the HHI but in a different form: i.e., $WHI = (V/V_0)^3 + C_1 (R/R_0) + C_2(S_0/S)^2$, where C_1 and C_2 are constants fitted from data. Thus, the WHI places more weight on the inverse of translational speed and less weight on hurricane size than the HHI.

Holland and Owens (2009) found a high correlation ($R^2 > 0.9$) of the WHI with inflation-adjusted (to 1998 $U.S. values) economic losses for seven U.S. landfalling hurricanes in the Gulf of Mexico between 1992 (Andrew, category 5) and 2008 (Ike, category 4). The small sample size is due to limited data on storm size and translational speed, which are only available for a small subset of recent TCs. As the sample size should increase with improved data recovery in the future, further validation of the HHI, CHI, and WHI should determine their usefulness as meteorology-based damage indices for hurricanes.

Finally, two additional considerations are worth mentioning for the particular case of hurricane indices. First, in order to be combined with indices for other climate variables into a composite climate index, each of the hurricane indices described above should be standardized (i.e., divided by their standard deviations). Second, unlike the CEI or other comparable indices that utilize data available from a majority of land-based meteorological stations, incorporating spatial information into the above-described TC indices would appear impractical, since only certain hurricanes track over a limited number of land stations. However, as the historical occurrence frequency of hurricanes over fairly large regions (e.g., the southeastern and northeastern U.S.) is known, other indices taking exposed population and property assets into account could conceivably be constructed, as will be discussed in Section 7.

6. Future Climate Projections

Historical trends in certain key climate indicators discussed above (e.g., global and regional temperatures) and the increased occurrence of climate extremes (e.g., heat waves, extreme precipitation) have been attributed in many cases to the warming effect of increased amounts of greenhouse gases in the atmosphere (Secs. 2.3, 4.1, 4.5). Greenhouse gas emissions, in turn, evolve in lock-step with human industrial development and population growth, particularly in urban centres (Raupach et al., 2007). Thus, projections of emissions rely, first, on understanding past patterns of industrial development, and second, on educated guesses as to future changes in these patterns. According to the International Geosphere-Biosphere Program:

> Unless development patterns change, by 2030 humanity's urban footprint will occupy an additional 1.5 million square kilometres - comparable to the combined territories of France, Germany and Spain … [United Nations] estimates show human population growing from 7 billion today to 9 billion by 2050, translating into some 1 million more people expected on average each week for the next 38 years, with most of that increase anticipated in urban centres. And ongoing migration from rural to urban living could see world cities receive yet another 1 billion additional people. Total forecast urban population in 2050: 6.3 billion (up from 3.5 billion today).[1]

The links between population growth and economic development, especially in urban centers, and industrial emissions are well established (Raupach et al., 2007). Hence, the U.N. range of population projections translates into an envelope of possible future emissions scenarios, as quantified by the IPCC explicitly for use as input to time-evolving global climate models (GCMs). These were presented in a dedicated IPCC report in 2000, the IPCC Special Report on Emissions Scenarios (SRES; Nakicenovic et al., 2000). The three most commonly used scenarios, referred to as SRES B1, A1B and A2, describe low, moderate, and high cumulative emissions at year 2100, respectively[2].

Projections of future climate change are largely based on GCMs, global-scale numerical models of the coupled atmosphere-ocean-land system driven by estimated changes in anthropogenic factors. GCMs are most sensitive to changing concentrations of greenhouse gases and sulfate aerosols, but other factors are also important, such as black carbon emissions and land-use change. Most simulations cover the period from the present until 2100, the final year of the SRES scenarios.[3]

---

[1] http://www.igbp.net/5.705e080613685f74edb8000470.html. Accessed 04/30/2012.

[2] Note that annual CO_2 emissions in the A1B scenario actually exceed those in the high growth A2 scenario until the mid-21st century. After that, development of low-carbon emitting energy sources in A1B leads to a sharp decline in annual emissions, while emissions in the A2 scenario continue to grow.

[3] In advance of the upcoming IPCC AR5, a new set of scenarios were developed based on projected concentrations of greenhouse gases, as opposed to emissions. These are known as Representative Concentration Pathways (RCPs). Nevertheless, the SRES scenarios are still widely used for climate projections, partly because they are reasonably consistent with actual global emissions over the last decade (Van Vuuren and O'Neill 2006).

A process is in place to evaluate and intercompare results from these models (the Coupled Model Intercomparison Project, or CMIP, coordinated by the World Climate Research Program), and summaries of the model formulations and their projections are available from many different sources, including the comprehensive reports mentioned at the beginning of Section 2 (see also Appendix B). A very useful addition to the next IPCC Assessment Report AR5 is a new "atlas" presenting a series of figures showing global and regional patterns of climate change computed from global climate model output gathered as part of the 5th Coupled Model Intercomparison Project (CMIP5). This will no doubt constitute a valuable resource for the study of climate change impacts around the world.

In the remainder of this section, we focus on the climate indicators highlighted in earlier sections, and present examples of projected changes in those variables of greatest concern. We also focus specifically on projections for climate indices, where available.

6.1 Global climate models: Utility and limitations

Before turning to a selection of key results from GCMs, it is important to review what sort of information they can, and can't, provide. Provided the appropriate input data, the models are designed to output physical variables that are roughly equivalent to observed quantities such as temperature, humidity, precipitation, sea ice extent and thickness, etc., albeit in a 3D, gridded version of the real world. A wide variety of GCM simulations have been run by research groups worldwide, and further, it is increasingly common for the results to be made freely available to any interested party via the internet. But ease of access and subsequent use belies the complex underpinnings of these models, whose results must be interpreted with caution.

There are three primary types of uncertainty embedded within all GCM simulations of the type just described (Hawkins and Sutton 2011):

> First, there is model uncertainty: for the same radiative forcings, different models produce different projections (shown by the spread between similarly coloured lines in Fig. [5.1]). Secondly, there is scenario uncertainty: uncertainty in future radiative forcing causes uncertainty in future climate (demonstrated by the spread [amongst different] coloured lines in Fig. [5.1]).

Hawkins and Sutton also refer to a third property of GCM simulations, "the random, internal fluctuations in climate, which are the 'wiggles' superimposed on the long term trends in each projection," as a type of uncertainty; but that appellation is debatable since this is a well-known feature of the real climate system. The first source of uncertainty results from the independence of model formulations: each GCM is constructed according the same physical principles, but scientists differ in how particular processes are modeled mathematically. This is not, in fact, an undesirable state of affairs. The alternative, that all GCMs be somehow constrained to produce identical results, implying convergence to a "perfect" model in which all processes are modeled in the same way, would not represent much of an improvement. Since such a model could not include all real-world processes, it will still disagree with observations. But over time, the hope is that climate indicators simulated by different GCMs will converge somewhat around the observed values, representing a reducible uncertainty of the type discussed in Sec. 1.3. The

second type of uncertainty, in future scenario, is irreducible in the sense described there: the future evolution of important climate forcings can only be guessed. These features, common to all GCM simulations irrespective of the climate indicator of interest, are worth bearing in mind for the results that follow.

6.2 Projections of surface temperature and precipitation

Global average, future temperature projections made by different GCMs are unanimous in projecting positive, increasing surface air temperature (SAT) change over the coming decades. However, there is a considerable range of projected SAT changes across models, even under the same greenhouse gas forcing scenario, as shown in **Figure 6.1**.

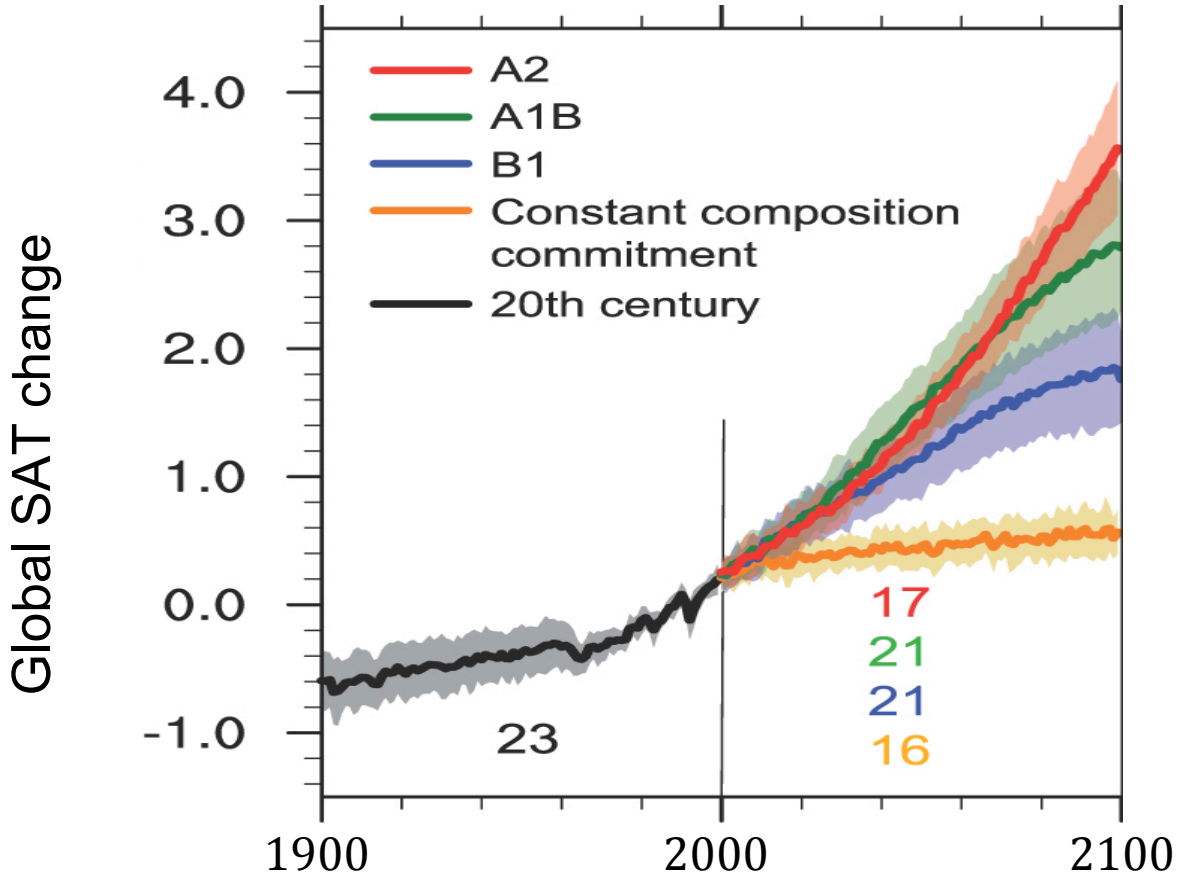

Figure 6.1. GCM (CMIP3) projections of changes in global mean SAT change (degrees Celsius), relative to the mean of 1971–2000, for historical forcings (*grey*) and three different future emission scenarios: low (B1; *blue*), moderate (A1B; *green*), and high (A2; *red*). One additional scenario (*orange*) is shown with greenhouse gas concentrations stabilized at year 2000 levels. The number of CMIP3 models whose output is available for the historical period and each SRES scenario is indicated. The thick lines represent the multi-model means for each scenario, while shading denotes the ±1 standard deviation range of individual model annual means. The mean SAT of the moderate growth scenario slightly exceeds that of the high growth scenario until about 2060; this is due to the corresponding emissions pathways, as described in footnote 22. *Source:* Adapted from IPCC AR4-WGI, Fig. 10.4.

The corresponding geographic patterns of surface warming, shown in **Figure 6.2**, do not depend strongly on the emissions scenario until the middle of the 21st century, by which time the considerable amount of accumulated CO_2 in the moderate and high growth scenarios, and the associated enhanced greenhouse effect, becomes evident. For example, by the 2090s, the projected SAT change over high northern latitudes in the high emissions scenario exceeds 8°C in some locations, about a factor of two larger than in the low emissions scenario (Fig. 6.2, *right*).

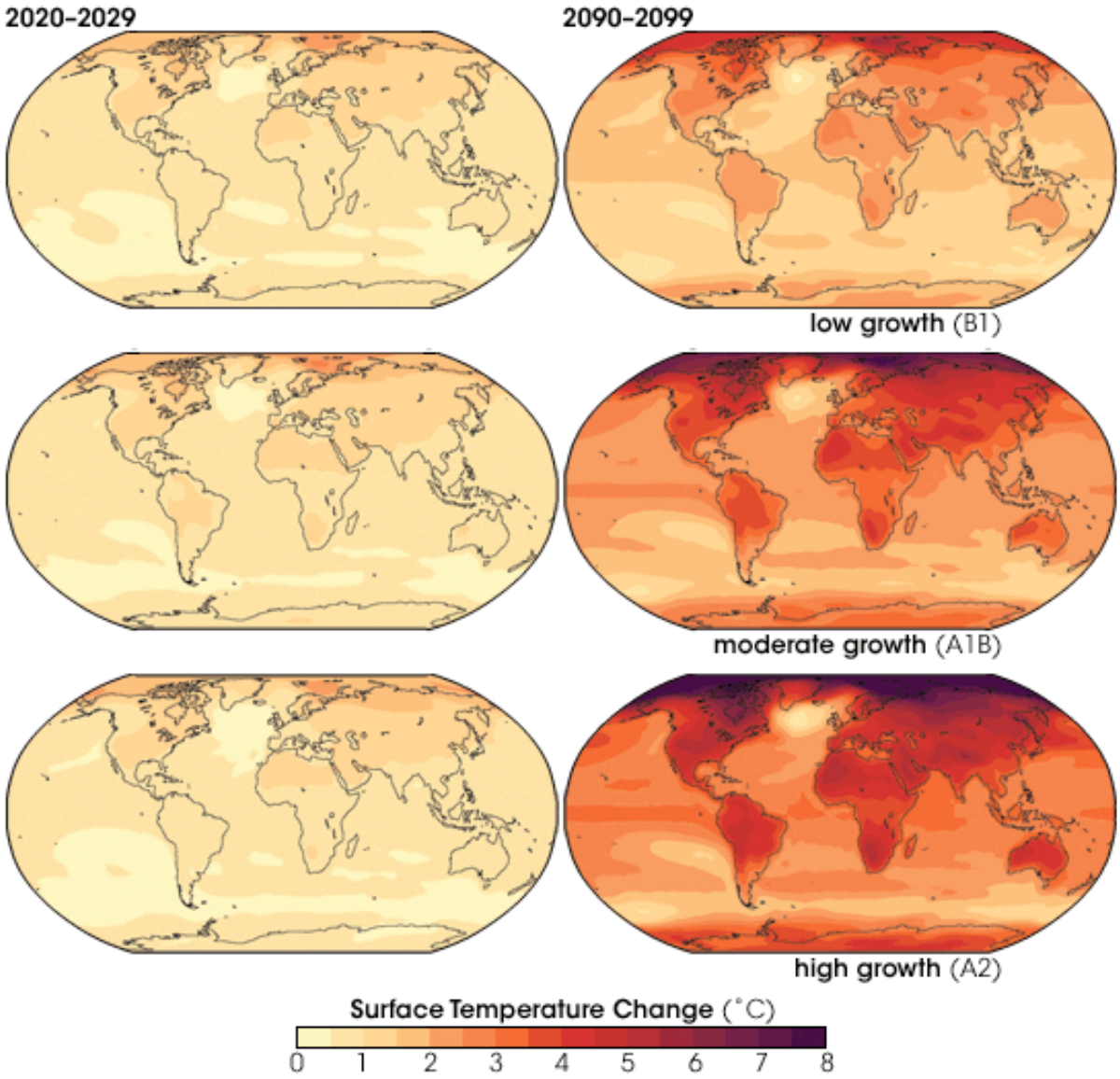

Figure 6.2. Projected future patterns of surface warming under three different emissions scenarios (low, moderate, and high growth). *Source:* NASA Earth Observatory, based on the IPCC AR4-WGI.

Precipitation changes simulated by GCMs are also unanimous with respect to their global mean projections, as shown in **Figure 6.3**. The models project an increase in global mean precipitation with global warming, which is expected according to the basic physics of the hydrological cycle (Sec. 2.4). Regionally, the precipitation projections are much more varied, as can be seen in

Figure 6.4. Generally, as the world warms, regions that are typically wet today will get wetter while those that are dry today will get drier. When it rains or snows there is a greater likelihood of the rain or snow falling in heavier amounts. Also, the likelihood of the precipitation falling as rain instead of snow increases as the century progresses. So while we will never be able to say that global warming caused the 2010 record-breaking floods in Pakistan, we can say that according to GCM projections, the likelihood of similar-magnitude flooding events will increase in certain regions (e.g., Russia and northern China; Fig. 6.4) as the century progresses.

Specifically, by the end of this century, most models project drying in the tropics and subtropics and increased precipitation at mid- to high latitudes, particularly in NH winter. Annual precipitation decreases exceeding -20% of 1980-99 levels are expected in the Mediterranean and North Africa, while winter precipitation increases of more than +20% are projected in Alaska, Canada, Northern Europe, and the bulk of Asia. Global warming will create an issue of water storage, not water availability, for these regions, as rainfall will come more frequently when it is not needed. By and large, precipitation decreases coincide with the dry season in most drought-prone areas, meaning that droughts are likely to worsen (Sec. 6.4.2).

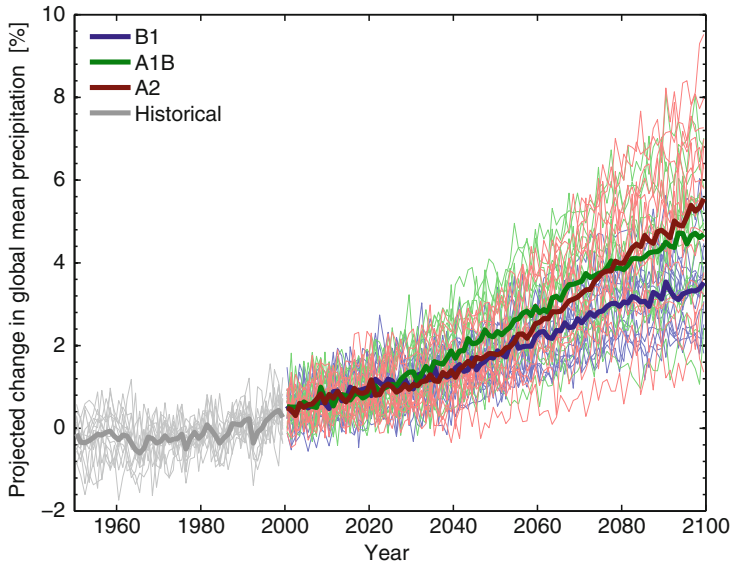

Figure 6.3. As in Fig. 6.1, but for GCM-projected changes in global mean precipitation (in percent). Here the thin lines represent individual model results. *Source:* Hawkins and Sutton (2011).

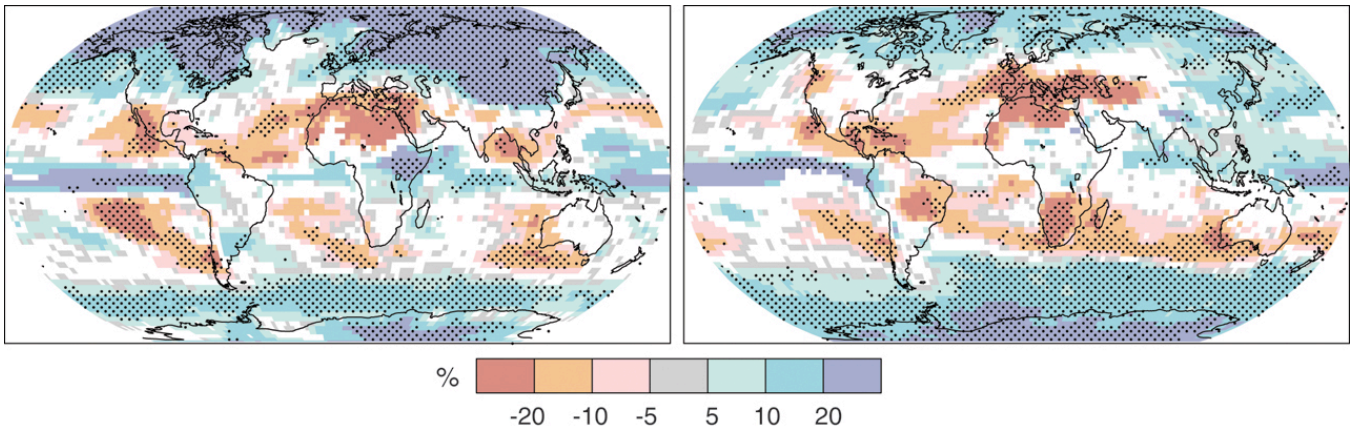

Figure 6.4. Relative changes in precipitation (in percent) for the period 2090-2099, relative to 1980-1999. Values are multi-model averages based on the moderate growth (SRES A1B) scenario for December to February (*left*) and June to August (*right*). White areas are where less than 66% of the models agree in the sign of the change and stippled areas are where more than 90% of the models agree in the sign of the change. *Source:* AR4-WGI Figure 10.9, SPM.

Projections of mean precipitation for North America specifically are shown in **Figure 6.5**.

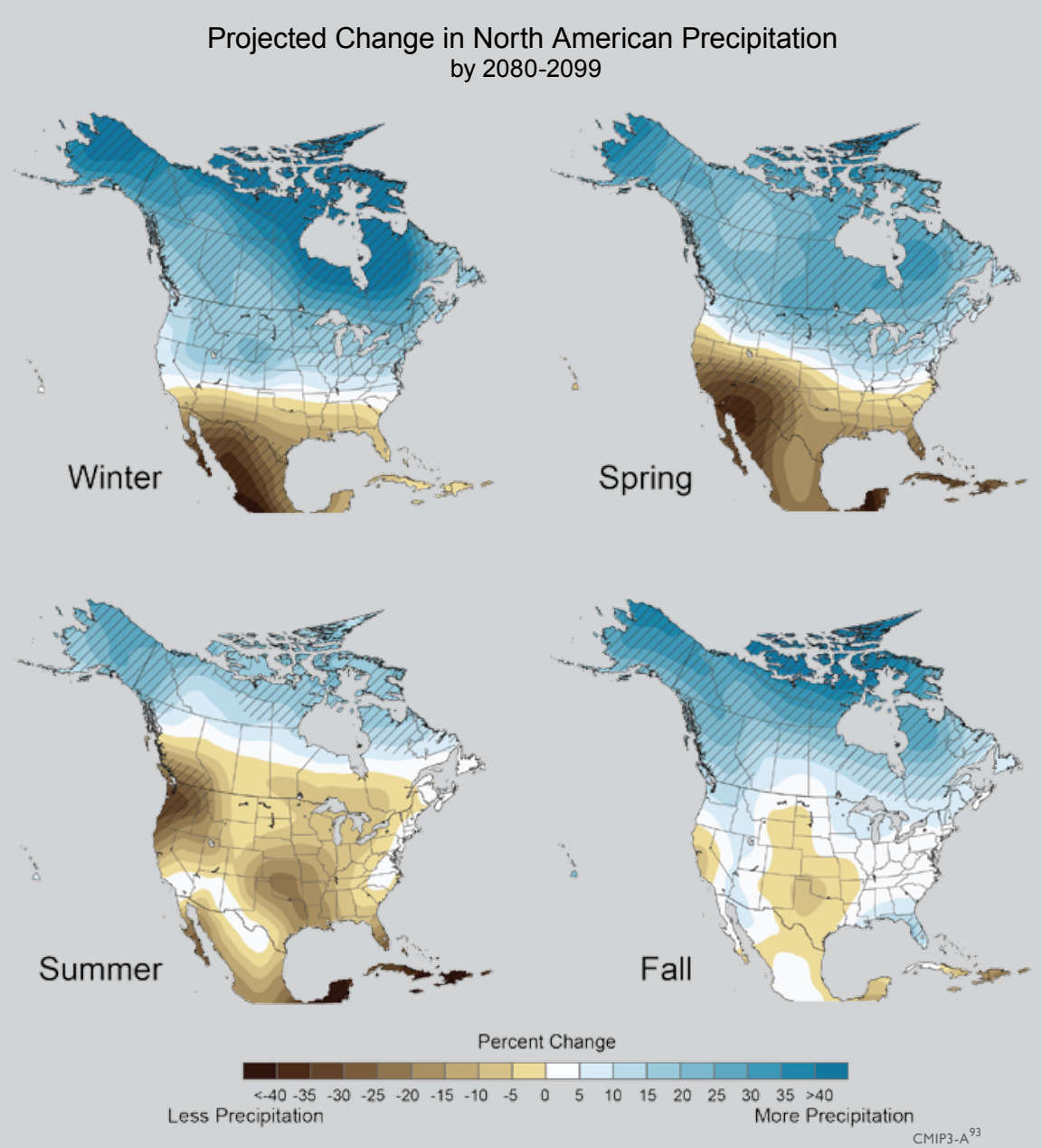

Figure 6.5. Projected future changes in precipitation relative to the recent past (in percent) as simulated by 15 CMIP3 models. The simulations are for late this century, under a higher emissions scenario (SRES-A2). Inter-model agreement in the projected changes is highest in the hatched areas. *Source:* Karl et al., (2009).

Generally speaking, Canada and the northern U.S. are expected to get wetter and southern areas drier. The transition zone between the two roughly follows the band of latitudes between 40-45°N, but moves northward in summer and southward in winter. However, climate models cannot predict with confidence exactly where the transition between wetter and drier areas will occur. Precipitation will be skewed more towards the winter months. Most models agree that the amount of spring and summer rainfall in the western U.S. will decrease by up to 40% of present-day values by the 2090s, while winter precipitation over Alaska and eastern Canada could increase by approximately the same amount. As summer drought becomes more common (Sec.

6.4.2), there may be pressure on national governments to transport water from northern regions of North America to the drier, southern regions.

Comparing Fig. 6.5 with the historical trend in annual mean precipitation shown in Fig. 3.6, one sees that projected precipitation trends in Canada represent a reinforcement of the historical pattern, in which the largest increases, ~30% or more, are seen at high latitudes, mostly in the form of increased snowfall in winter. More moderate increases in rainfall are projected nearly everywhere in the country, except in summer, when less rainfall is projected in the southern, more populated areas. In the U.S., as in the observed record, significantly less rainfall is projected in the U.S. southeast and southwest, except in fall. The model projections for the south-central U.S., however, which feature prominent drying, are opposite to the observed trends there (Fig. 3.6, lower).

6.3 Projections of surface temperature and precipitation extremes

According to the SREX Summary for Policymakers (SREX-SPM, 2012) (see Sec. 4 for a precise definition of italicized terms):

> **Models project substantial warming in temperature extremes by the end of the 21st century**. It is *virtually certain* that increases in the frequency and magnitude of warm daily temperature extremes and decreases in cold extremes will occur in the 21st century at the global scale. It is *very likely* that the length, frequency, and/or intensity of warm spells or heat waves will increase over most land areas. Based on the A1B and A2 emissions scenarios, a 1-in-20 year hottest day is *likely* to become a 1-in-2 year event by the end of the 21st century in most regions, except in the high latitudes of the Northern Hemisphere, where it is *likely* to become a 1-in-5 year event … Under the B1 scenario, a 1-in-20 year event would *likely* become a 1-in-5 year event (and a 1-in-10 year event in Northern Hemisphere high latitudes). The 1-in-20 year extreme daily maximum temperature (i.e., a value that was exceeded on average only once during the period 1981–2000) will *likely* increase by about 1°C to 3°C by the mid-21st century and by about 2°C to 5°C by the late 21st century, depending on the region and emissions scenario (based on the B1, A1B, and A2 scenarios).

In the previous sections, historical changes in SAT were expressed in terms of the standardized temperature index, STI, defined as the SAT anomaly divided by the standard deviation, with the latter reflecting natural variability. Thus, the STI, like other standardized indexes, is essentially the signal-to-noise ratio of the SAT observations. It was noted in Sec. 4.1 (Fig. 4.2) that globally over land, values of STI > 2 are being experienced in the summer season somewhat regularly (~30% of the time) over the last decade. Inasmuch as these heat waves are likely to be noticed by the population at large, they can be considered true climate change signals. We can then ask the following question: *Can climate model projections determine when and where to first expect the emergence of a climate change signal, as diagnosed by STI > 2?*

This issue was addressed using the CMIP3 models by Hawkins and Sutton (2012), who refer to the time when STI exceeds a given threshold as the time of emergence (ToE). Their results are summarized in **Figure 6.6**.

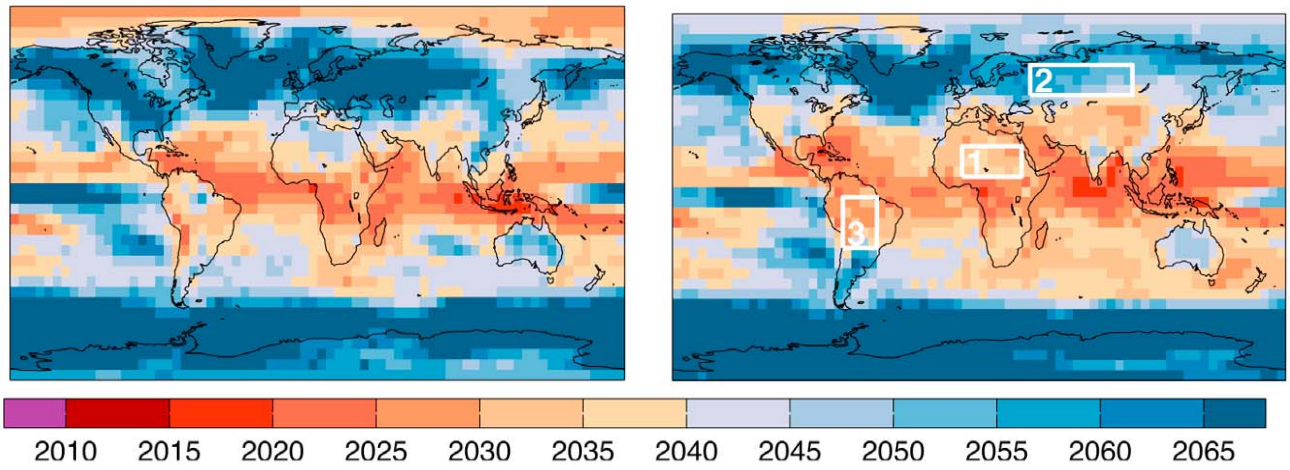

Figure 6.6. Median Time of Emergence, i.e., the first year when SAT has an expected STI > 2, for October-March (*left*) and April-September (*right*) derived from CMIP3 results for 15 GCMs under the moderate (A1B) emissions scenario. The regions indicated by the white boxes were the topic of further discussion by the authors. *Source:* Hawkins and Sutton (2012).

Fig. 6.6 shows that the median time of emergence occurs several decades sooner in low latitudes, particularly in boreal spring/summer, than in mid-latitudes. Also, the median ToE in the Arctic occurs 5–10 years sooner in boreal autumn/winter than in boreal spring/summer. This is likely related to the rapid reduction of sea ice and the associated ice-albedo feedback that occurs in the models. It should be noted that Fig. 6.6 shows median values of ToE, and that there is a considerable spread of estimates. The authors note, "There is a very large uncertainty in ToE arising from the inter-model differences in simulating both signal and noise. This uncertainty is at least 30 years in all three regions shown and as much 60 years in some regions." They also point out that the variability of SAT (i.e., σ) in the climate models is generally higher than observed, meaning that STI = $\Delta T/\sigma$ is underestimated, and hence ToE overestimated. Thus the values appearing in Fig. 6.6 should be taken as illustrative, although the qualitative differences between regions should be robust.[1]

The conclusions of the SREX-SPM with regard to precipitation extremes are the following (italics as in the original):

> **It is *likely* that the frequency of heavy precipitation or the proportion of total rainfall from heavy falls will increase in the 21st century over many areas of the globe.** This is particularly the case in the high latitudes and tropical regions, and in winter in the northern mid-latitudes. Heavy rainfalls associated with tropical cyclones are *likely*

[1] This also helps to explain how it is that these model-projected results could be consistent with the observational findings of Hansen et al. (2012), who contend that STI > 2 has already occurred in summertime in a number of locations in recent years (Sec. 4.1). That is, the models' underestimate of STI implies that they may be missing climate signals that have already emerged.

to increase with continued warming. There is *medium confidence* that, in some regions, increases in heavy precipitation will occur despite projected decreases in total precipitation in those regions. Based on a range of emissions scenarios (B1, A1B, A2), a 1-in-20 year annual maximum daily precipitation amount is *likely* to become a 1-in-5 to 1-in-15 year event by the end of the 21st century in many regions, and in most regions the higher emissions scenarios (A1B and A2) lead to a stronger projected decrease in return period.

As for surface air temperature, the ToE for future noticeable changes in precipitation may also be derived; but due to its larger natural variability, the ToE generally occurs further into the future. As depicted in **Figure 6.7**, which uses a less stringent ToE definition of SPI > 1 (indicating one standard deviation or a 84% likelihood of emergence), noticeable increases in precipitation are expected by 2040 in North America, northern Europe, eastern Asia, and equatorial east Africa, while rainfall deficits will be noticeable in southern Europe and North Africa. Similar magnitude increases are expected up to two decades later in India, east China and Japan, while decreases are projected around the same time in Central America and the Caribbean. Precipitation decreases over Southern Hemisphere land areas are expected to emerge near the end of the century.

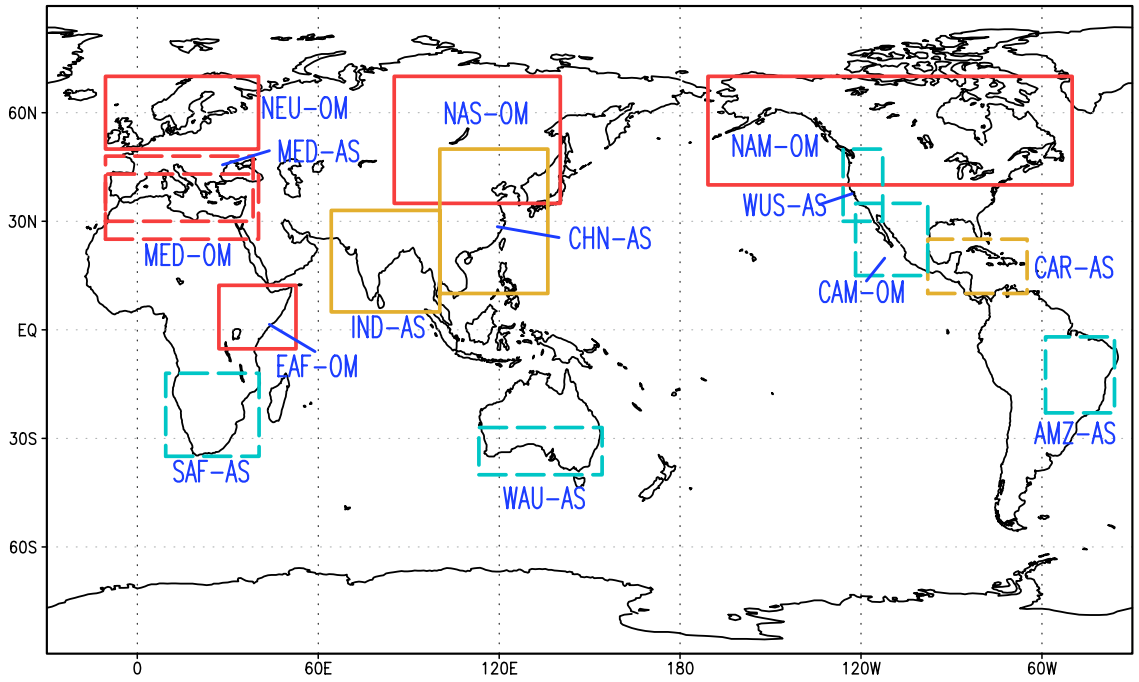

Figure 6.7. Summary of the ToE for a 1σ change in precipitation in selected world regions, derived from 14 CMIP3 models for the moderate growth (A1B) emissions scenario. Red, yellow, and light blue colors indicate early (up to 2040), mid (2040–2080) and late (beyond 2080) 21st century decade ToE, respectively. Boxes with solid (dashed) contours indicate regions with a positive (negative) precipitation change. In region labels, the "-AS" suffix is April–September, while "-OM" is October–March. *Source:* Giorgi & Bi (2009).

As reviewed in Sec. 4.2, the historical increase in North American precipitation was distributed unevenly between light and heavy precipitation events. There has been little change or a decrease in the frequency of light and moderate precipitation during the past 30 years, while

heavy precipitation has increased. In future climate simulations over North America, as shown in **Figure 6.8**, the observed trend is expected to continue, with the lightest precipitation projected to decrease, while the heaviest will increase, by up to 45% in the high emission scenario (A2). This means that, in the absence of any target adaptation measures to handle increased runoff from heavy rainfall events, there will be an increased risk of flooding.

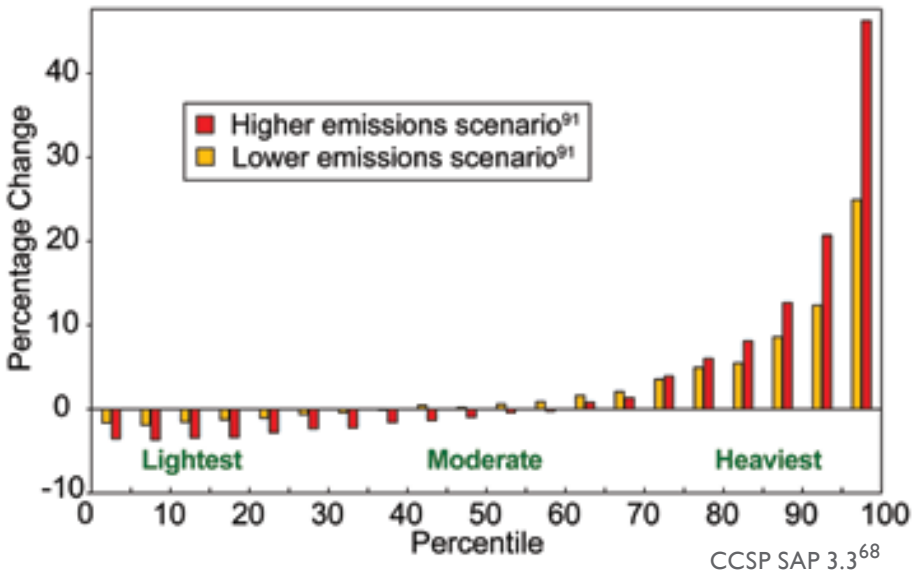

Figure 6.8. Projected changes from the 1990s to the 2090s in the amount of precipitation falling in light, moderate, and heavy events in North America. Projected changes are displayed in 5 percent increments from the lightest drizzles to the heaviest downpours. Projections are based on the models used in the IPCC AR4-WGI. *Source:* Karl et al., (2009), after Gutowski et al., (2008).

As mentioned in Sec. 4.1, an alternative means of expressing changes in extremes is via the occurrence frequency of rare events. **Figure 6.9** shows results from the work of Baettig et al., (2007) described in that section. Specifically, the figure shows the *additional* frequency of occurrence of a "1 in 20" (5th or 95th percentile) present-day event assessed using GCM simulations of a future climate. For example, the top left panel contains a striking conclusion: worldwide, the frequency of a 1 in 20 "hottest" year is projected to increase by a factor of 10 to 19 by the end of this century. A value of 18 in Fig 6.9a means that the "1 in 20 year" event will happen 18 more times in the 2090s, becoming a "19 in 20 year" event. The lower panels show that most of this projected increase in frequency occurs in boreal summer, except in Antarctica, which shows a larger change in austral summer. The upper right panel reflects the precipitation projections discussed above in Sec. 6.2: that is, an increasing occurrence of 1 in 20 driest years in the tropics and subtropics and of 1 in 20 wettest years mainly at mid- to high latitudes, both by a factor of 2-13.

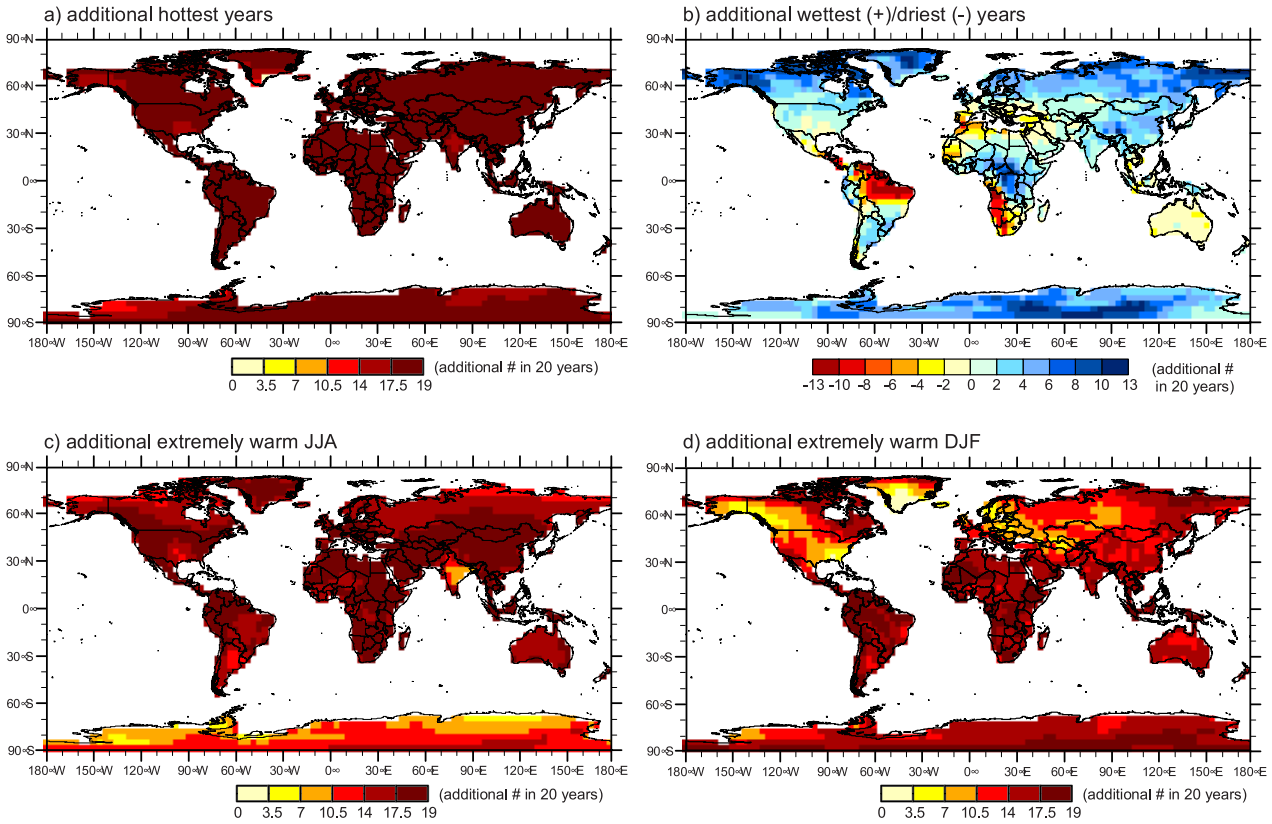

Figure 6.9. Individual CCI indicators. Each indicator is a multi-model mean of a high- and low-emissions scenario (i.e., SRES A2 and B2). Changes are between the control period 1961–1990 and the scenario period 2071–2100. JJA denotes the mean of June-July-August, while DJF is for December-January-February. *Source:* Baetttig et al., (2007).

As discussed in Section 4.3, a composite climate index (CCI) may be constructed from the excess occurrences in individual climate extremes, using the equation presented there. The results of doing so are shown in **Figure 6.10**, which shows the composite CCI aggregated by country for the 2071-2100 period. The largest CCI values are in South America and Africa, where the ToE for temperature is only a few decades away and where projected annual mean precipitation deficits are largest (Fig. 6.9b). Large CCI values are also projected for Antarctica and much of Asia and Canada. Combining these results with corresponding maps of projected population and socioeconomic data would be expected to give some insight into climate change impacts (see also Section 7).

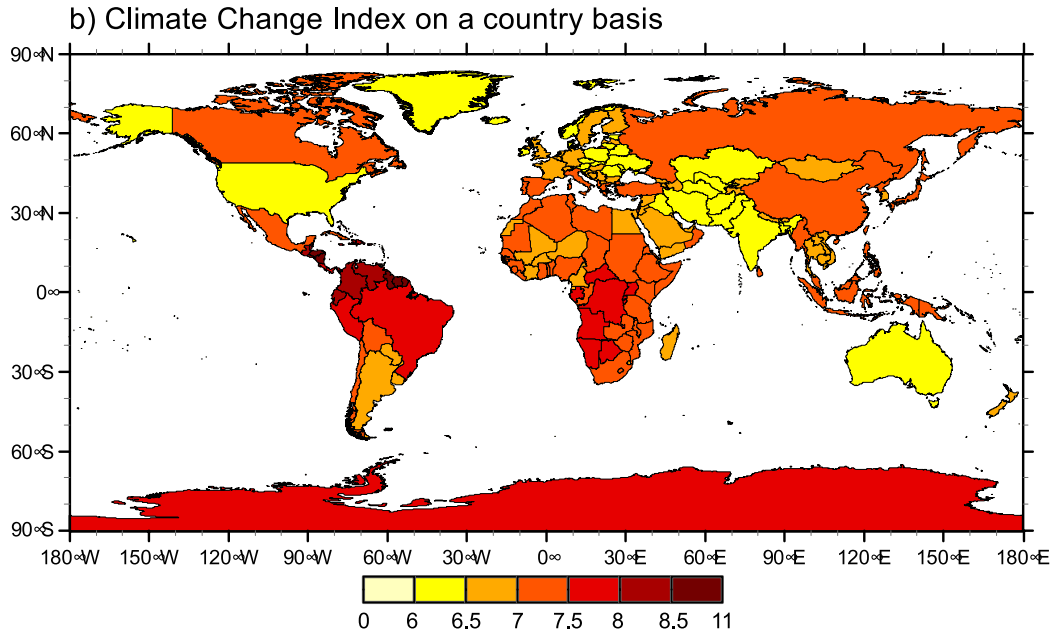

Figure 6.10. The aggregated CCI, formed from the individual CCI indicators in Fig. 6.9, on a country basis for 2071–2100. The country value is the mean of all grid values over the surface area of each country. *Source:* Baettig et al., (2007).

6.4 Selected additional impacts of climate change

The implications of the projected increases in temperature and precipitation can be anticipated, to some extent, by the results for other climate indicators summarized for the historical period in Sections 2-4. Detailed projections for these indicators, derived from a variety of model approaches and simulation techniques, are available in the sources reviewed at the beginning of Sec. 2. In the remainder of this section, we focus instead on some of the projected impacts of excessive heat, drought, and flooding.

6.4.1 Agriculture

Agricultural production is highly sensitive to weather, which occurs against the backdrop of a changing climate. In addition, plant growth is stimulated by increased atmospheric CO_2 concentrations, the so-called CO_2 fertilization effect. When exposed to higher CO_2, leaf pores (stomata) are able to shrink, which results in reduced water stress for crops. For a CO_2 concentration increase from 370 to 580 parts per million, yields of photosynthetic crops like rice and wheat were found to increase by as much as 14% (Ainsworth et al., 2008).

However, increasing SAT and reduced soil moisture under global warming work against the gains achieved by CO_2 fertilization, and even short duration heat stress events can damage photosynthetic cells and result in sharply decreased yields (Schlenker and Roberts, 2009; Wassmann et al., 2009). Both global simulations and experimental studies have shown that although crop yields may rise initially due to CO_2 fertilization, the effect is soon overwhelmed by the detrimental effects of heating and moisture stress, as shown in **Figure 6.11**. Some form of adaptation is therefore required to avoid such impacts, which would lead to decreased food supply, increased food prices, and thus more hunger and starvation in poorer countries.

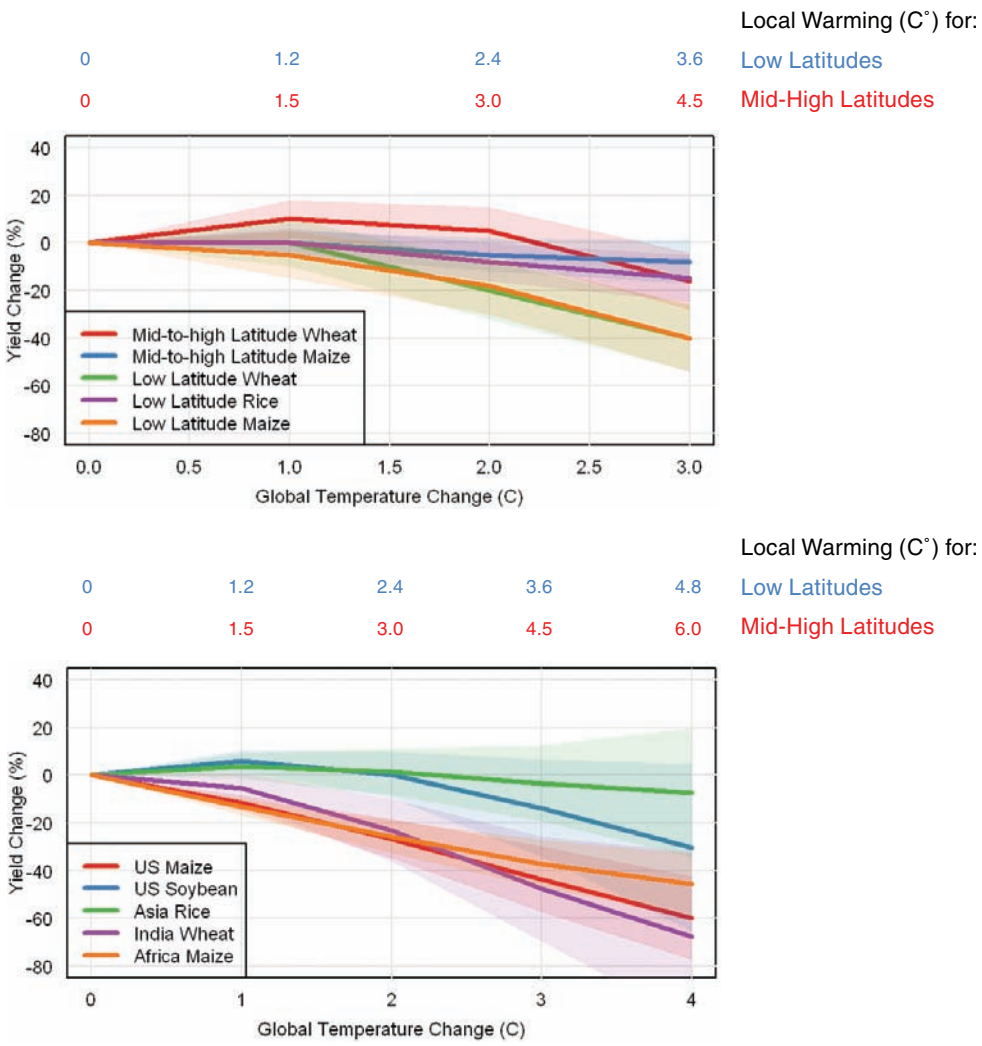

Figure 6.11. Expected impact of combined warming and CO_2 increase on crop yields, without adaptation, for broad regions summarized in IPCC AR4-WGII (*top*) and for selected crops and regions with detailed studies (*bottom*). The shaded areas show the likely range (67% confidence interval or 1 standard error). Impacts are averages for current growing areas within each region and may be higher or lower for individual locations within regions. Temperature and CO_2 changes for the IPCC summary (*top*) are relative to late 20th century, while those estimated for regions (*bottom*) were computed relative to pre-industrial. *Sources: Climate Stabilization Targets*, NRC (2011); top panel is after Figure 5.2 in the AR4-WGII report (Easterling et al., 2007), while bottom panel estimates were derived from various sources (Matthews et al., 1995; Lal et al., 1998; Easterling et al., 2007; Schlenker and Roberts, 2009; Schlenker and Lobell, 2010).

The increased incidence of crop diseases and parasites are also a concern under global warming. Earlier springs and warmer winters permit the proliferation and higher survival rates of disease pathogens and parasites (Hatfield et al., 2008; Frumhoff et al., 2007), and a longer growing season allows some insects to produce more generations in a single season, increasing their populations.

The future availability of moisture is also a key uncertainty. **Figure 6.12** (*top*) is a map indicating suitability of world regions for rain-fed crops in the present climate. Soil moisture availability, or runoff, is the difference of precipitation and evaporation (Sec. 4.4). Future projections of runoff change (2100-present) are shown in **Fig. 6.12** (*lower left*) and **Fig. 6.12** (*lower right*) for the U.S.A. specifically**.**

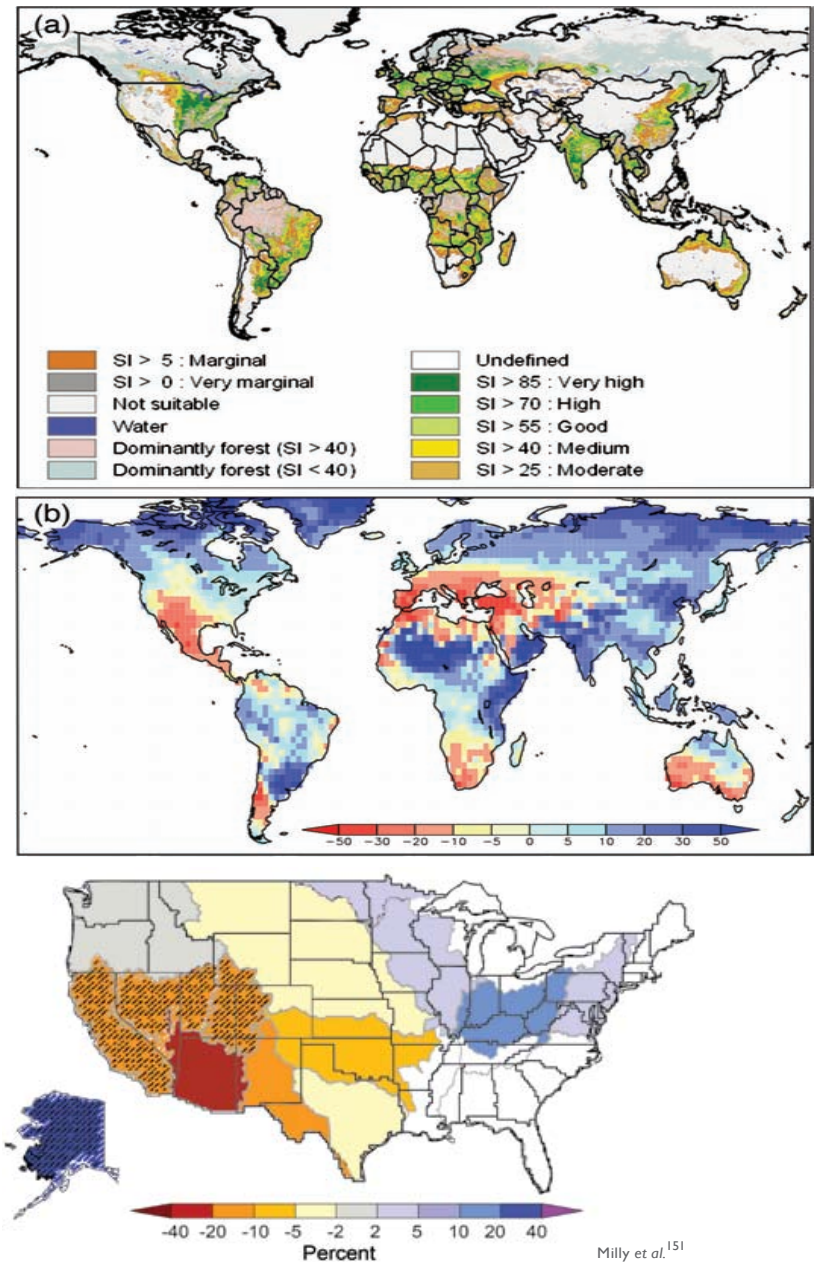

Figure 6.12. *Top:* Current suitability for rain-fed crops (excluding forest ecosystems) (after Fischer et al., 2002b). SI = suitability index. *Middle:* Ensemble mean percentage change of annual mean runoff between present (1981 to 2000) and 2100. *Source:* AR4-WGII, Figure 5.1, after original in Nohara et al., (2006). *Bottom:* Projected percentage changes in U.S. median runoff for 2041-2060, relative to a 1901-1970 baseline, mapped by water-resource region. Hatched areas indicate better agreement among model projections. White areas indicate divergence among model projections. Results are based on the mean of low and high emissions scenarios. *Source:* Karl et al., (2009).

Comparing the top two panels of Fig. 6.12, one sees that many regions of moderate (e.g., Turkey, North Africa, Mexico, and southeast Australia) and high (e.g., Europe, western Russia) crop suitability, are projected to experience strong decreases in runoff while others of low suitability may experience runoff increases in future (e.g., northern Europe, Russia, and western China). Thus, efforts at agricultural adaptation might consider taking these shifting patterns into account.

6.4.2 Drought

The projected decrease in precipitation in certain regions, in concert with enhanced evaporation from warming, is expected to increase the incidence of severe drought. One particularly susceptible area is the U.S. Southwest, which is projected to receive about 20%-40% less rainfall by the 2090s than at present (Fig. 6.5). CMIP3 model historical and future-simulated values of the Palmer Drought Severity Index (PDSI) in this region are shown in **Figure 6.13**, taken from Gutzler and Robbins (2011). Several features of this figure are worth noting. First, the excessively dry conditions of the Dust Bowl period (1929-40; Fig. 4.14) are well simulated (Fig. 6.13b), and also the return to more normal PDSI values in subsequent decades (Fig. 6.13c). Second, in the present and near-future epoch, the PDSI in many western U.S. states is at or below its Dust Bowl values. Finally, by the end of the 21st century (Fig. 6.13h), the projected extent and severity of the drought is unprecedented in the simulated period.

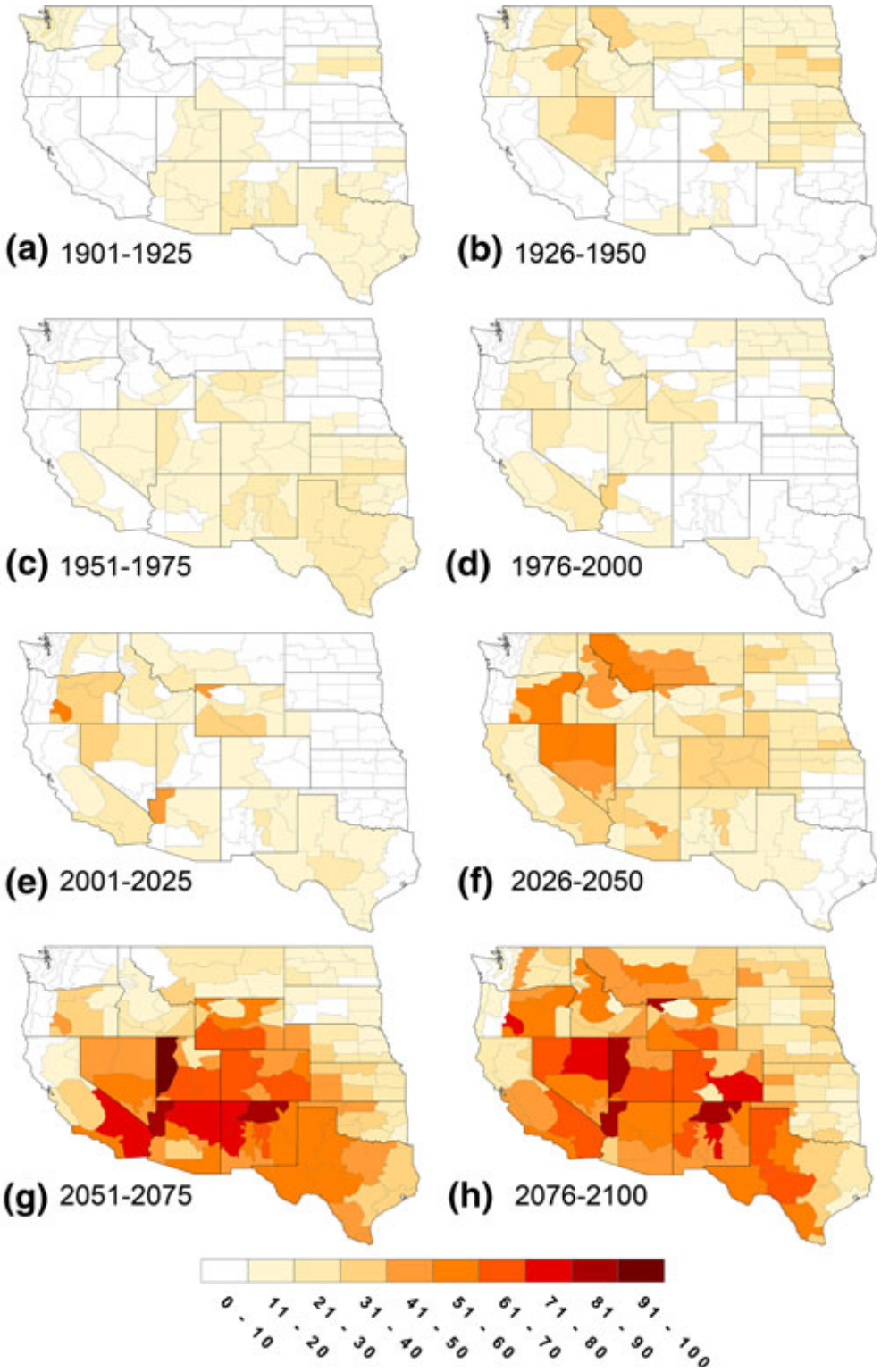

Figure 6.13. Percentage of months in successive 25-year epochs with PDSI < -3. Such values represent "severe drought" in the current climate (Heim, 2002). *Source:* Gutzler and Robbins (2011).

6.4.3 Wildfires

As discussed in Sec. 2.8, the incidence of forest fires under global warming is expected to increase for a number of reasons, and large wildfires in the western U.S. display a correlation with temperature anomalies during the fire season (Fig. 2.17). Coupled climate-forest fire models have been used to simulate future changes in area burned, with an example from one such study for the western U.S. shown in **Figure 6.14**. Under a simulated 1°C increase in SAT, decreases in area burned (~25 percent) are projected for some semi-desert regions, but large increases are anticipated for nearly all forested areas, with 3 to 6 times as much area burned in the warmer climate.

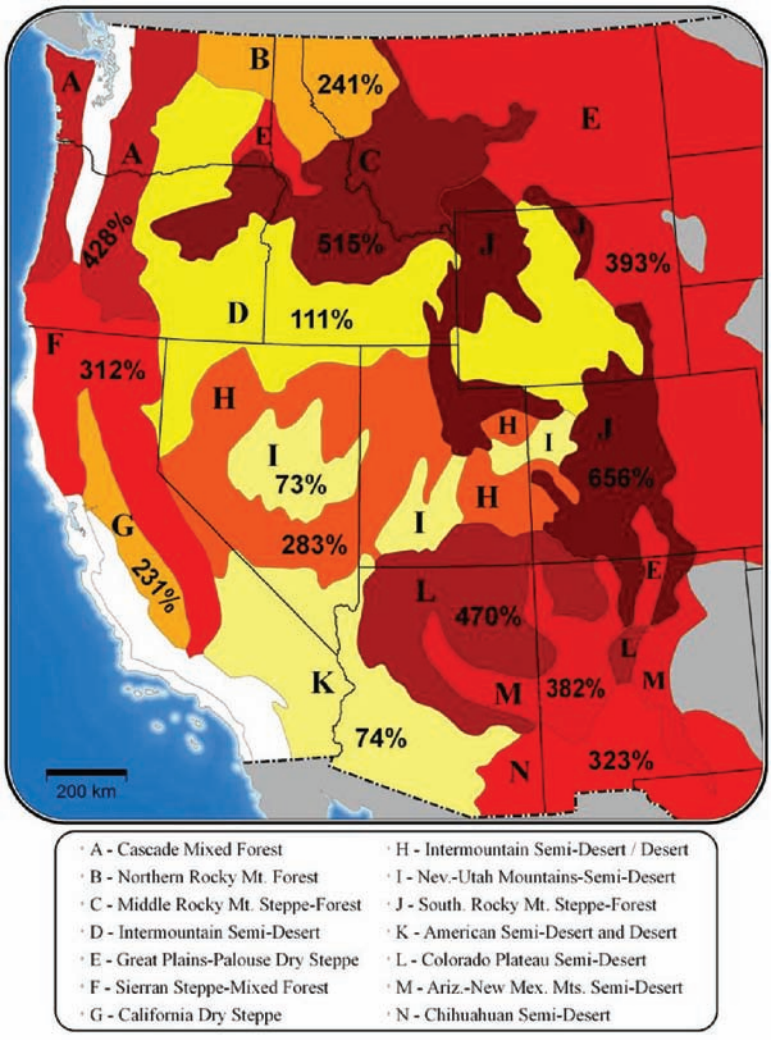

Figure 6.14. Map of changes in area burned over the western U.S. for a 1°C increase in global average temperature, shown as the percentage change relative to the median annual area burned during 1950-2003. Results are aggregated to ecoprovinces (Bailey, 1995) of the western U.S. Changes in temperature and precipitation were aggregated to the ecoprovince level. Climate-fire models were derived from NCDC climate division records and observed area burned data following methods described in Littell et al., (2009). *Source:* NRC (2011), after original figure by Rob Norheim.

6.4.4 Human and mammalian health impacts

In general, an overall increase in heat-related deaths is expected to accompany the projected excess of high temperature extremes noted over much of the Earth's land area in Sec. 6.1. This expectation is supported by historical data: in an analysis of long-term weather records for 50 U.S. cities from 1989-2000, Medina-Roman and Schwartz (2007) found that mortality rates associated with high temperature extremes exceed those due to low temperature extremes by a factor of 3.6.

Meteorological conditions recorded during the severe Paris heat wave of 2003—in particular, the standard deviations for the meteorological variables—formed the basis of a novel "analog city" approach by Kalkstein et al., (2008) to estimate the number of heat-related deaths that might occur in U.S. cities under similarly extreme conditions. Specifically, the time series of the standardized temperature index (STI; Sec. 5.1) for Paris was used in each U.S. city, then converted back to actual temperature using the known local climatology (for 1971-2000), yielding a unique time series of SAT specific to that city. Daily mortality data for each U.S. city over the same period, along with meteorological data were used to look for coincidences of temperature extremes and elevated mortality, and regression formulae were developed to relate excess mortality rates to temperature, humidity, heat wave duration, and time of season.

The results of the study are summarized in **Table 6.1**. Compared to the hottest summers on record, heat-related deaths in St. Louis and New York were projected to increase by 29% and 155%, respectively, under the analog heat wave scenario. Other cities, including Washington, Philadelphia, and Detroit, could experience 2%-11% more heat-related deaths, compared to their hottest summers on record. Hayhoe et al., (2010) carried out an identical analysis for Chicago, finding that city would experience 17% more heat-related deaths than in its hottest previous summer on record (1995). The same authors also used temperatures from GCM projections over the region along with the same mortality-temperature relationship to project a doubling of current heat wave mortality rates by 2050 under a low-emissions scenario, and a quadrupling under a high-emissions scenario.

Table 6.1. Heat-related mortality using an "analog city" approach. *Source:* Kalkstein et al., (2008).

TABLE 3.Heat-related mortality (expressed as excess deaths) during the average, analog, and hottest historical summer. The rules for lower-limit and revised mortality estimates are discussed in text.					
	Detroit	**New York**	**Philadelphia**	**St. Louis**	**Washington**
Metropolitan area population[a]	4.4 million	9.3 million	5.1 million	2.6 million	4.9 million
Avg summer heat-related mortality[b]	47	470	86	216	81
Avg summer mortality rate per 100,000 population	1.07	5.05	1.69	8.30	1.65
Analog summer heat-related mortality	342	3253	432	688	191
Analog summer mortality rate per 100,000 population	7.77	34.98	8.47	26.46	3.89
Hottest historical summer mortality[c]	308	1277	412	533	188
Hottest historical summer mortality rate per 100,000 population	7.00	13.73	8.08	20.50	3.84
Year of hottest historical summer occurrence	1988	1995	1995	1988	1980
Analog percent deaths above hottest historical summer	11.0	154.7	4.9	29.1	1.6

[a]Based on U.S. Census Bureau data (see online at www.census.gov/population/cen2000/phc-t3/tab01.txt).
[b]Numbers represent revised values.
[c]Based on the period from 1961 to 1995.

The range of responses among cities seen in Table 6.1 highlights their variable sensitivity to extreme heat, which might stem from factors such as baseline climate conditions (cooler cities may be more susceptible to heat), demographic patterns, and acclimatization measures such as air conditioning (NRC, 2011). By the same token, the increased frequency of warmer winters and overall decreases in cold extreme temperatures (Figs. 4.3, 4.4) would be expected to result in reduced cold-season mortality in high-latitude nations.

It is worth mentioning that the more frequent occurrence of SATs exceeding 35°C or so (and their persistence during heat waves) raises a concern about a basic physiological threshold: specifically, that associated with the need of mammals, including humans, to dissipate body heat. This can happen only if the temperature to which the skin is exposed is lower than the skin temperature itself. Sherwood and Huber (2010) considered future statistics of annual maximum wet bulb temperature[1] exceeding average human skin temperature of 35°C as a measure of heat stress on humans and other mammals. Under a rather extreme future scenario reaching a global temperature change of 10°C relative to 1999-2008, these authors came to the remarkable conclusion that the area of land that could become uninhabitable due to heat stress could be greater than that lost to sea-level rise over the same time frame.

6.4.5 Sea-level rise and coastal flooding

According to the AR4-WGI, the global mean projected SLR between the present and the 2090s due to thermal expansion of seawater ranges from 0.10 m to 0.41 m, depending on the emissions scenario. Adding to this the highly uncertain contribution from land ice sheet melting, which assumes no catastrophic ice sheet loss, one arrives at a total SLR of 0.18 m to 0.59 m. However, as discussed in Sec. 3.3, local SLR can be considerably higher or lower than the global average—of order ±0.2 m for the thermal expansion component alone. A recent study by Slangen et al., (2011) quantified these local changes as predicted by the CMIP3 GCMs, with the results shown in **Figure 6.15**. Under the moderate (A1B) emissions scenario, the local relative sea level change projections range from -3.91 m to 0.79 m, with a global mean of 0.47 m. New York City is notable amongst the locations listed in Fig. 6.15, *right*, for having the largest projected relative SLR projection of 0.63 m ± 0.12 m.

[1] Wet bulb temperature is the temperature experienced when one's skin is wet and exposed to moving air, so that the moisture evaporates. Since evaporation has a cooling effect, the wet bulb temperature is always less than the usual (dry bulb) temperature, but higher than the "dew point" temperature at which atmospheric water vapor condenses.

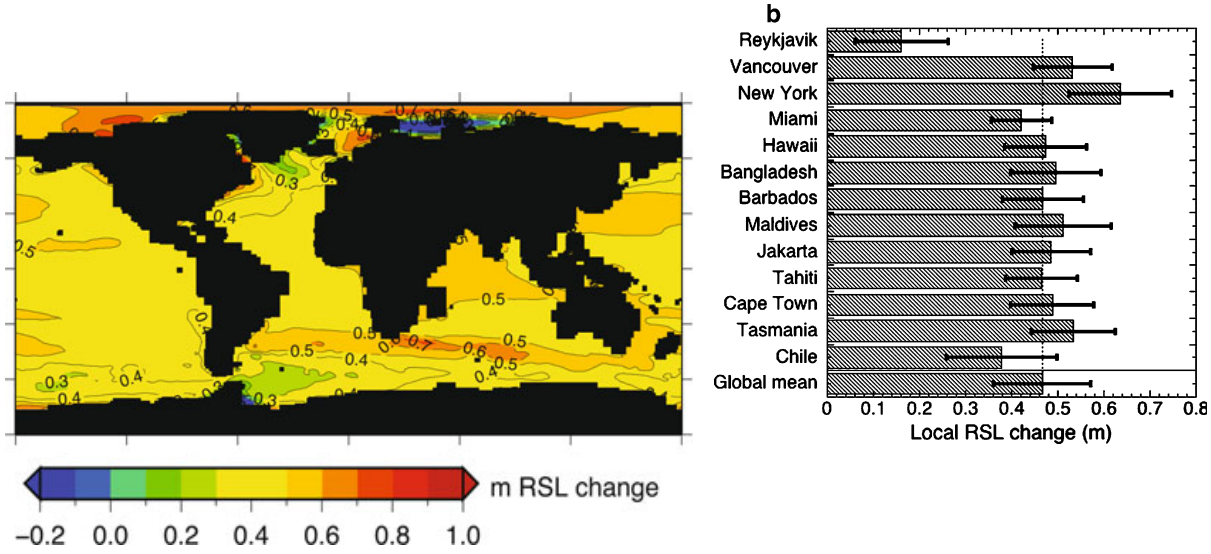

Figure 6.15. *Left:* Total relative sea level change (in meters) between 1980–1999 and 2090–2099 for scenario A1B, based on the mean of 12 GCMs used in the IPCC AR4-WGI. *Right:* Corresponding projections of local relative sea level change for selected coastal cities. Error bars are the associated 1σ uncertainty. *Source:* Slangen et al., (2011).

These regional SLR projections, along with historical records of coastal areas susceptible to flooding and future population projections, allow a relative ranking of areas most vulnerable to future floods. As shown in **Figure 6.16**, the highest-risk areas are densely populated, broad river deltas, mostly in the tropics and sub-tropics. **Figure 6.17** shows the estimated effects of varying levels of adaptation to coastal flooding, including flood embankments and barrages. Flood impacts vary with emissions scenario, socioeconomic situation and adaptation assumptions. In the absence of adaptation, an estimated more than 100 million people are flooded per year above a 0.40 m rise for all scenarios.

Figure 6.16. Relative vulnerability of coastal deltas according to estimated population displaced by current sea-level trends to 2050 (Extreme=>1 million; High=1 million to 50,000; Medium=50,000 to 5,000; following Ericson et al., 2006). *Source:* AR4-WGII, Nicholls et al., (2007), Fig. 6.6.

Fig. 6.17 shows that the adoption of flood defenses reduces the impacts substantially, in some cases by a factor of 10 for a given scenario. Increased storm intensity would exacerbate these impacts, as would larger rises in sea level (Nicholls, 2004). Estimates of the total vulnerable populations (occupying an area below the 1 in 1,000 year flood level) in the 2080s by continent, ignoring any adaptation measures, are given in **Table 6.2**.

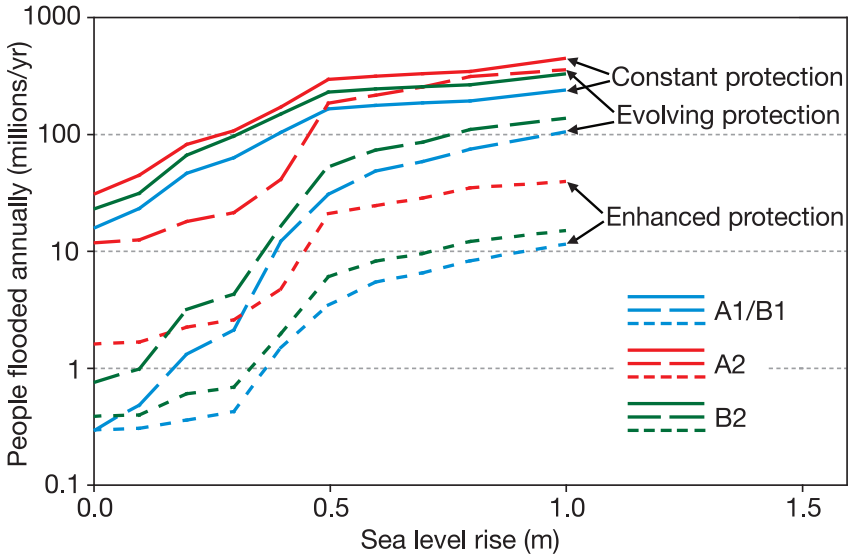

Figure 6.17. Estimates of people flooded in coastal areas due to sea level rise, SRES socio-economic scenario and protection response in the 2080s (following Nicholls and Lowe, 2006; Nicholls and Tol, 2006). *Source:* AR4-WGII, Chapter 6.

Table 6.2. Estimates of the population (in millions) of the coastal flood plain* in 1990 and the 2080s.

Region	1990 (baseline)	SRES scenarios (and sea-level rise scenario in metres)			
		A1FI (0.34)	A2 (0.28)	B1 (0.22)	B2 (0.25)
Australia	1	1	2	1	1
Europe	25	30	35	29	27
Asia	132	185	376	180	247
North America	12	23	28	22	18
Latin America	9	17	35	16	20
Africa	19	58	86	56	86
Global	197	313	561	304	399

*Area below the 1 in 1,000 year flood level. Assumes uniform population growth; net coastward migration could substantially increase these numbers. Following Nicholls (2004). *Source:* AR4-WGII, Chapter 6.

In the United States in particular, a recent report by Climate Central based on peer-reviewed research by Tebaldi et al., (2012) and Strauss et al., (2012b) contains detailed projections of current rates of SLR out to 2050. These projections use only the global mean SLR as projected by GCMs along with historical data on relative SLR at tidal gauge stations to estimate future SLR at those locations. **Figure 6.18** shows the results of this procedure.

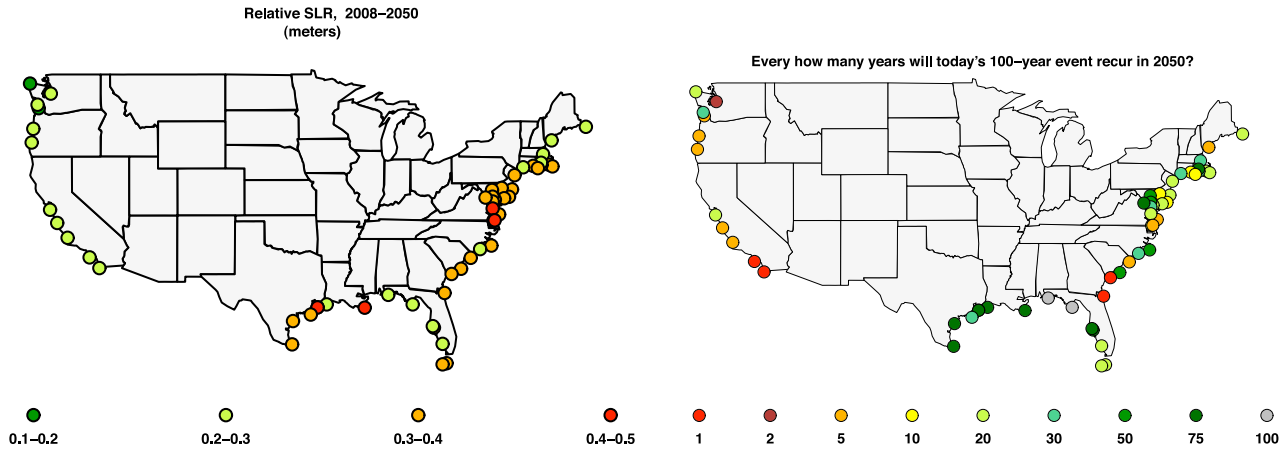

Figure 6.18. *Left:* Sea level rise (mean estimate from 19 models temperature projections, under six scenarios and for three carbon cycle parameter settings) over the period 2008–50 at 55 tide gauges, in units of meters. *Right:* For the ensemble average estimate of relative SLR at each gauge, projected return periods, by 2050, for floods currently qualifying as 100-year events. *Source:* Tebaldi et al., (2012).

6.4.6 Storms and hurricanes

The compact structure of tropical and extratropical cyclones makes their simulation with global climate models challenging. The typical grid cell size of the CMIP3 GCMs used in the AR4-WGI, approximately 250 × 250 km, is about five times larger than the radius of maximum wind for an average hurricane. However, model resolution has been steadily improving, and other types of simulation strategies, including regional climate and weather prediction models, have allowed hurricane researchers to gain insight into the effect of atmosphere-ocean warming on tropical cyclone (TC) genesis and development. A result that has emerged from many of these studies, which is robust to a variety of boundary conditions and model parameters used, is that the distribution of intensities for a large number of events shifts to higher intensity in a warmer climate (Knutson and Tuleya 2004; Emanuel 2005).

As mentioned in Sec. 5.6, the PDI, a measure of TC power and duration, displays a high correlation with tropical sea surface temperature (Fig. 5.10). Thus, as SSTs warm along with SAT, one might expect an increase in PDI based on this empirical relation. However, it is known that TC intensity also depends on the state of the atmosphere, specifically the vertical profiles of temperature and wind shear (Emanuel 2008). Work by Emanuel and co-workers showed that knowledge of the "potential intensity," a function of the SST and the vertical temperature gradient, is enough to establish an upper bound on the intensity of actual TCs (Bister and Emanuel 2002). This points to a role for GCMs in TC projections after all, as a means of judging when and where the conditions are right (in a model) for TCs to originate in the first place.

Along these lines, a novel approach was developed: the construction of large *synthetic* TC event sets driven by large-scale climate data obtained from reanalysis data sets or GCMs. In several studies by Emanuel and co-authors (Emanuel et al., 2006; Emanuel 2006), this Coupled

Hurricane Intensity Prediction System (CHIPS) is described and used to simulate hurricane behavior in the western Atlantic basin. In a first step, the points of origin for thousands of synthetic TC tracks were generated by randomly drawing from a probability distribution estimated from the post-1970 best track Atlantic hurricane data. These synthetic TCs were then moved according to a set of prescribed winds varying in space and time (**Figure 6.19**). In a final step, local environmental conditions (SSTs, wind shear, etc.) were then used to calculate the intensity of each hurricane along its path.

Using this method, Emanuel (2006b) showed: (1) that the frequency distribution of synthetic TCs in the current simulated climate as a function of peak wind speed, V_{max}, is very similar to the corresponding distribution for observed TCs (**Figure 6.20**, *left*); (2) that a 10% increase in potential intensity, corresponding to a future SST increase of approximately 2.5°C, leads to a noticeable increase in the relative number of intense hurricanes (as characterized by peak wind speed along the synthetic track; **Figure 6.20**, *right*), and; (3) the PDI increases by 65% in response to the 10% increase in potential intensity.

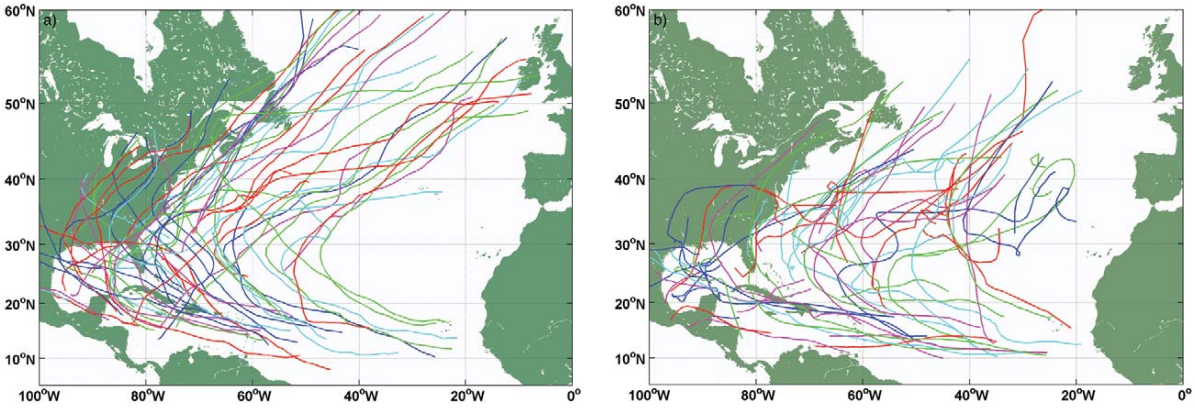

Figure 6.19. Sixty random tracks from the synthetic hurricane generator (*left*), and (*right*) historical TC (HURDAT) data. *Source:* Emanuel et al., (2006).

As noted in Sec. 4.3.1, most TC modeling studies spanning the historical and future periods do not predict noticeable trends in number, intensity, and other properties until the mid-21st century. This is consistent with the above results, which are representative of conditions projected for the late 21st century. Based on these studies and many others addressing TCs and extratropical cyclones, the recent literature reviews by Knutson et al., (2010) and the IPCC-SREX Report (2012) found remarkable consistency with regard to projected TC properties. According to the SREX-SPM (emphasis in the original):

> Average tropical cyclone maximum wind speed is *likely* to increase, although increases may not occur in all ocean basins. It is *likely* that the global frequency of tropical cyclones will either decrease or remain essentially unchanged. … There is *medium confidence* that there will be a reduction in the number of extratropical cyclones averaged over each hemisphere. While there is *low confidence* in the detailed geographical projections of extratropical cyclone activity, there is *medium confidence* in a projected poleward shift of extratropical storm tracks.

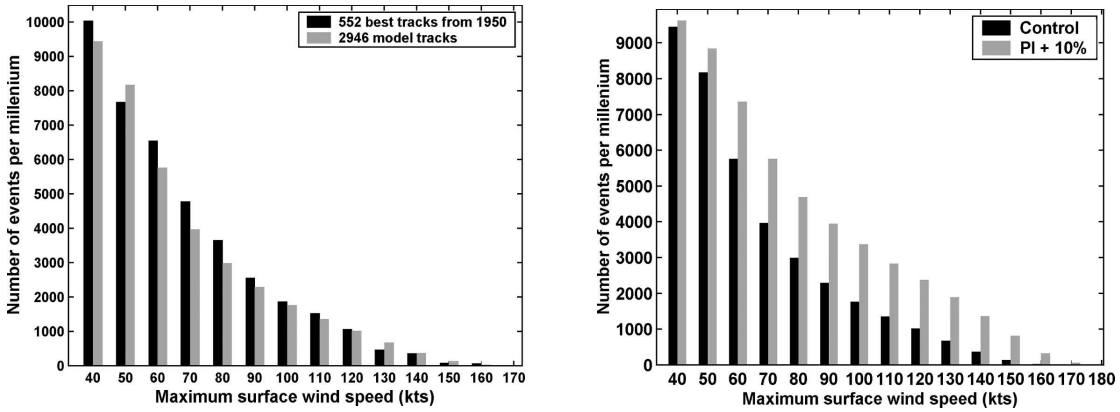

Figure 6.20. Cumulative frequency distribution, expressed as the number of events per millennium whose peak wind speed (knots) exceeds the value on the horizontal axis, for North Atlantic TCs. *Left:* The black bars are taken from Atlantic historical tropical cyclone data, encompassing all 552 events from 1950 to 2004, while the gray bars are calculated by running the CHIPS model on 3000 synthetic storm tracks. *Right:* As in left panel, but comparing the control experiment (*black bars*) with an experiment in which the CHIPS model was run using the same 3000 tracks but with the potential intensity increased everywhere by 10%. (*grey bars*). All other input variables, such as shear and ocean properties, were the same as in the control. *Source:* Emanuel (2006).

According to both reviews, models in which TC precipitation rates have been examined are highly consistent in projecting increased rainfall within 100 km of the TC center under 21st century warming, with increases of 3% to 37% and a mean value of +20%. Thus, rainfall rates associated with TCs are also *likely* to increase. It is worth noting that TC trajectory models such as that used by Emanuel et al., (2006) are sufficiently detailed to provide appropriate input to the hurricane indices summarized in Sec. 5.6, particularly those that track wind speed, radius, and translation speed (i.e., the HHI, CHI and WHI). Finally, the SREX expresses *low confidence* in projections of small spatial-scale phenomena such as tornadoes and hail, for the reasons outlined in Sec. 4.3.3, and also because current GCMs cannot simulate such phenomena.

6.4.7 Ecological change and hotspots

Plant species survive, compete, and reproduce within the range of climatic conditions to which they are physiologically suited and evolutionarily adapted. In response to changes in climate outside this range, plants must either "migrate"—i.e., adapt, if the change is not too rapid—or perish. A recent NASA study by Bergengren et al. (2011) employed a vegetation model driven by GCM climate projections to estimate the degree of species turnover that must occur for ecosystems to be in equilibrium with changing local climates. The authors used two different metrics of ecological sensitivity to assess potential changes in worldwide plant communities in different future climate scenarios. The first metric registers life form changes, such as a change from one species of tree to another, which might be prompted by a transition towards a drier local climate, for example. The second metric tracks biome-scale changes, such as the entire disappearance of trees from a given region, to be replaced by grasses, for example.

Using the mean projections from 10 GCMs under the moderate (A1B) emissions scenario (median global ΔSAT = +2.6°C at 2100), the authors found that 49% of the Earth's land surface will see at

least some changes in plant species, while 37% of the land area will transform from one major ecosystem zone, or biome, into another (**Figure 6.21**). The results shown in Fig. 6.21 reveal the existence of ecological "hotspots," that is, areas projected to undergo the greatest degree of species turnover. These include areas around the Himalayas and the Tibetan Plateau, eastern equatorial Africa, Madagascar, the Mediterranean region, southern South America, and the Great Lakes and Great Plains areas of North America. Much of the sub-Arctic land area also stands out, mainly due to pervasive northward expansion of the boreal forest.

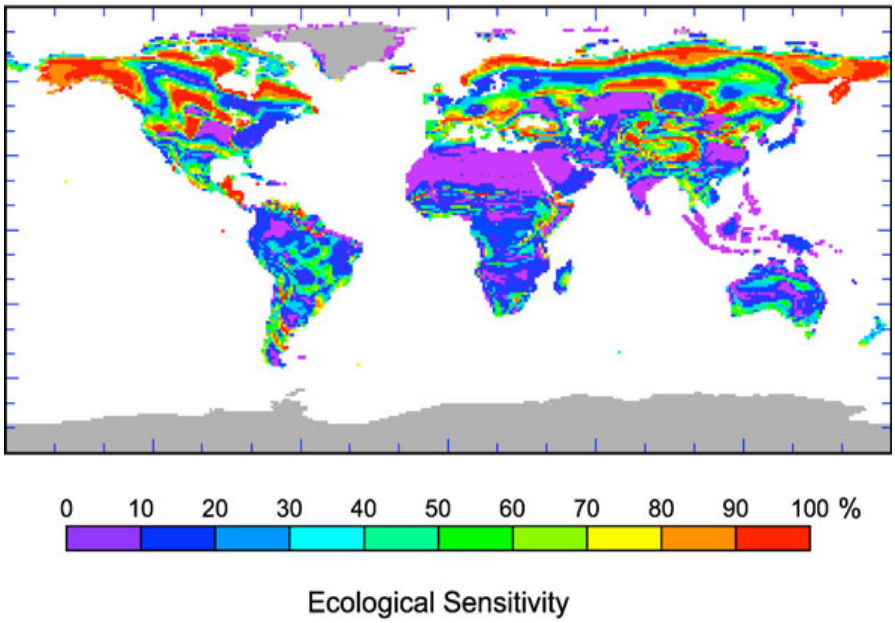

Figure 6.21. Twenty-first century ecological sensitivity to entire biome shifts derived from the 110 plant life form fractional cover maps generated by the equilibrium vegetation model of Bergengren et al., (2011) from climate change projections averaged across10 GCM simulations. Percentages refer to the relative area of a 1° × 1° grid cell that is simulated to undergo some biome change.

After the work was published, Jon Bergengren, an ecologist and lead author on the study, remarked in an interview that some wildlife will not survive these transformations. "Obviously, it is much easier for plants and animals to migrate or adapt to this level of climatic change over 10,000 years than it is over 100 years," he said.[1]

In a related study, Sommer et al., (2010) attempted to quantify the rate of local and regional turnover of species and net changes in plant species richness (PSR). The distribution of species is highly constrained by climate variability and extremes, and in particular by plants' physiological level of tolerance, for example, their ability to deal with frost and drought. A net decline in PSR under future warming would be cause for concern, since less diverse ecosystems subjected to still harsher environmental conditions may lead to local and even global extinction events (Thomas et al., 2004; Thuiller et al., 2005).

[1] http://www.cbc.ca/news/canada/manitoba/story/2012/01/12/mb-nasa-ecological-change-canada-manitoba.html.

Sommer et al., used relationships obtained from present-day data to construct a model of PSR response to climate, and then applied projected future warming rates in the model. The authors found that between now and 2100, the global average PSR is projected to remain similar to today under the low emissions scenario B1 (global ΔSAT = +1.8°C in 2100), but decreases significantly (by 29%) under a high emissions scenario (A1FI; global ΔSAT = 4.1°C). For all scenarios, the magnitude and direction of PSR change are geographically highly non-uniform, as shown in **Figure 6.22**. While a PSR increase is expected in most temperate and arctic regions, the projections indicate a strong decline in most tropical and subtropical regions.

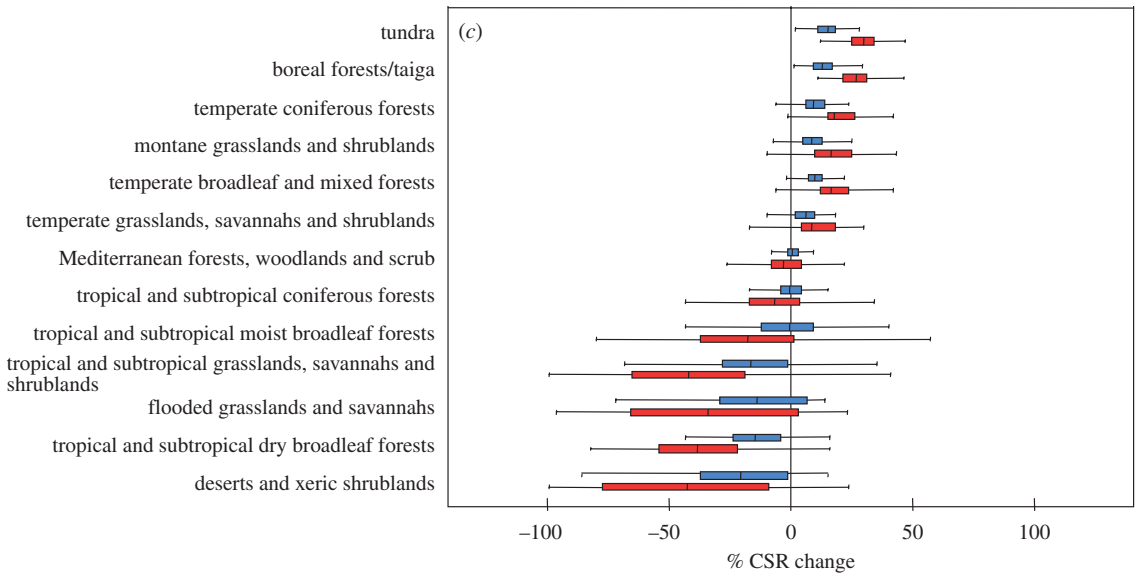

Figure 6.22. Modeled changes in the capacity for plant species richness (PSR; species number per 1° × 1° grid cell) between today and the year 2100 under the low-emissions B1 scenario (*blue*) and the high-emissions A1FI scenario (*red*). PSR change is shown across all 13 terrestrial biomes. Bold lines indicate the mean value, boxes indicate second and third quartiles and whiskers indicate the 10th and 90th percentiles. *Source:* Sommer et al. (2011).

7. From Climate Indices to Impacts and Risk Assessment

7.1 Defining climate-related risk

In this final section, we consider the assessment of insurance risk due to climate change. In Sec. 5, we reviewed several quantities already in use that satisfy the criteria for a climate index. Here the goal is to point the way toward an index or indices incorporating both the changes in the climate indicators summarized in previous sections and the risk component into a single measure. For definiteness, we refer to this more complex quantity as the *Actuaries Climate Risk Index*, or ACRI for short. The desired features of the ACRI echo those listed at the beginning of Sec. 5, augmented by the addition of socioeconomic information, which should be subject to the same constraints (such as, be available at the desired frequency and be easily updatable). Above all, the ACRI should be constructed to allow both ready interpretation by actuaries, and be modular enough that any of its components can be easily separated out from the main index.

It is important to acknowledge at the outset that there is a range of terminology with respect to climate-related risk assessment as it relates to the broader literature on risk. For our purpose, it is most convenient to adopt the definition of risk used by the United Nations Disaster Relief Office (Cardona 2005) and by two recent quantitative studies of climate-related risk (Peduzzi et al., 2009, 2012). By this definition (see **Figure 7.1**) *risk may be estimated quantitatively as the product of separate functions of hazard (intensity and frequency), exposure of assets (e.g., human populations, property, crops), and vulnerability (the degree of loss to each asset should a hazard occur).* This may be expressed mathematically as

$$K = C\, f(H)\, g(P)\, s(V), \qquad (1)$$

where K is risk, C is a proportionality constant, H is the frequency of a given hazard (possibly weighted by intensity), P is the exposed human population or assets, and V is vulnerability, which is comprised of socioeconomic variables.[1] The functions f, g, and s could be chosen on theoretical grounds, or determined empirically if data are available (see, e.g., Sec. 7.2). The separation of the hazard function $f(H)$ as a distinct factor is useful, since it allows the direct substitution of a climate index such as those considered in Sec. 5. In general, the variables H, P, V, and hence K as well, each depend on both location and time.

Note that the above definitions of risk and vulnerability differ somewhat from the same terms used by the IPCC-WGII, which did not make a quantitative assessment of climate-related risk. For example, as stated in Chapter 19 of the AR4-WGII, "Assessing key vulnerabilities and the risk from climate change":

> The concept of risk, which combines the magnitude of the impact with the probability of its occurrence, captures uncertainty in the underlying processes of climate change, exposure, impacts and adaptation. … Adaptation can significantly reduce many potentially dangerous impacts of climate change and reduce the risk of many key vulnerabilities.

[1] A widely used resource for global socioeconomic data is the Socioeconomic Data and Applications Center (SEDAC), http://sedac.ciesin.columbia.edu/.

The AR4 definition of risk is equally valid, but does not lend itself as readily to a quantitative treatment. According to our definition, the introduction of adaptive measures would reduce vulnerability, which in turn, reduces risk (instead of reducing the "risk of many key vulnerabilities"). Also, in some studies, vulnerability is itself a function of climate change (e.g., Yohe et al., 2006), thus conflating hazard and vulnerability by our definition.

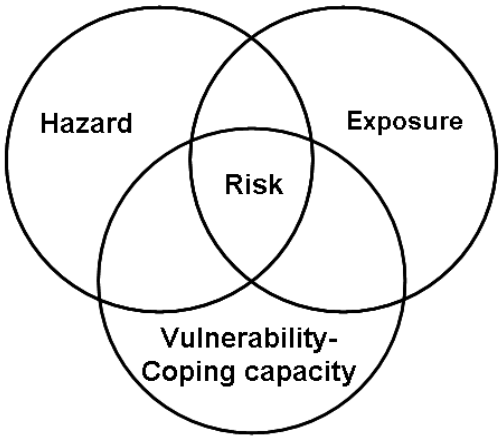

Figure 7.1. The relation of risk to its component factors: hazard, exposure, and vulnerability.

Climate extremes of all kinds represent natural hazards, and either or both the increasing frequency or the intensity of many types of extreme events, documented in Sec. 4, indicate positive trends in several climate-related hazards (heat waves, heavy precipitation, etc.). In the face of this reality, maintaining or reducing current levels of risk requires that society either: (1) slow or reverse present trends in climate indicators that lead to increased hazard; or (2) find some means of reducing exposure and vulnerability in future. To the extent that observed trends in climate indicators are due to anthropogenic influences, goal (1) could be achieved via *mitigation* measures, such as significant reductions in global greenhouse gas emissions. The means of accomplishing goal (2) is widely referred to as *adaptation*.

As the results of previous sections demonstrate, the climate hazard varies with geographic location. This is equally true of exposure and vulnerability. For the purpose of illustration, **Figure 7.2** shows examples of this geographic variation within the United States alone. Note that the effect of climate variability will be included in the hazard factor if a composite standardized index such as that discussed in Sec. 5.2.3 is used, or if *f(H)* is based on extremes of the probability distribution, as in the case of the CCI or CEI (Sec. 5.3).

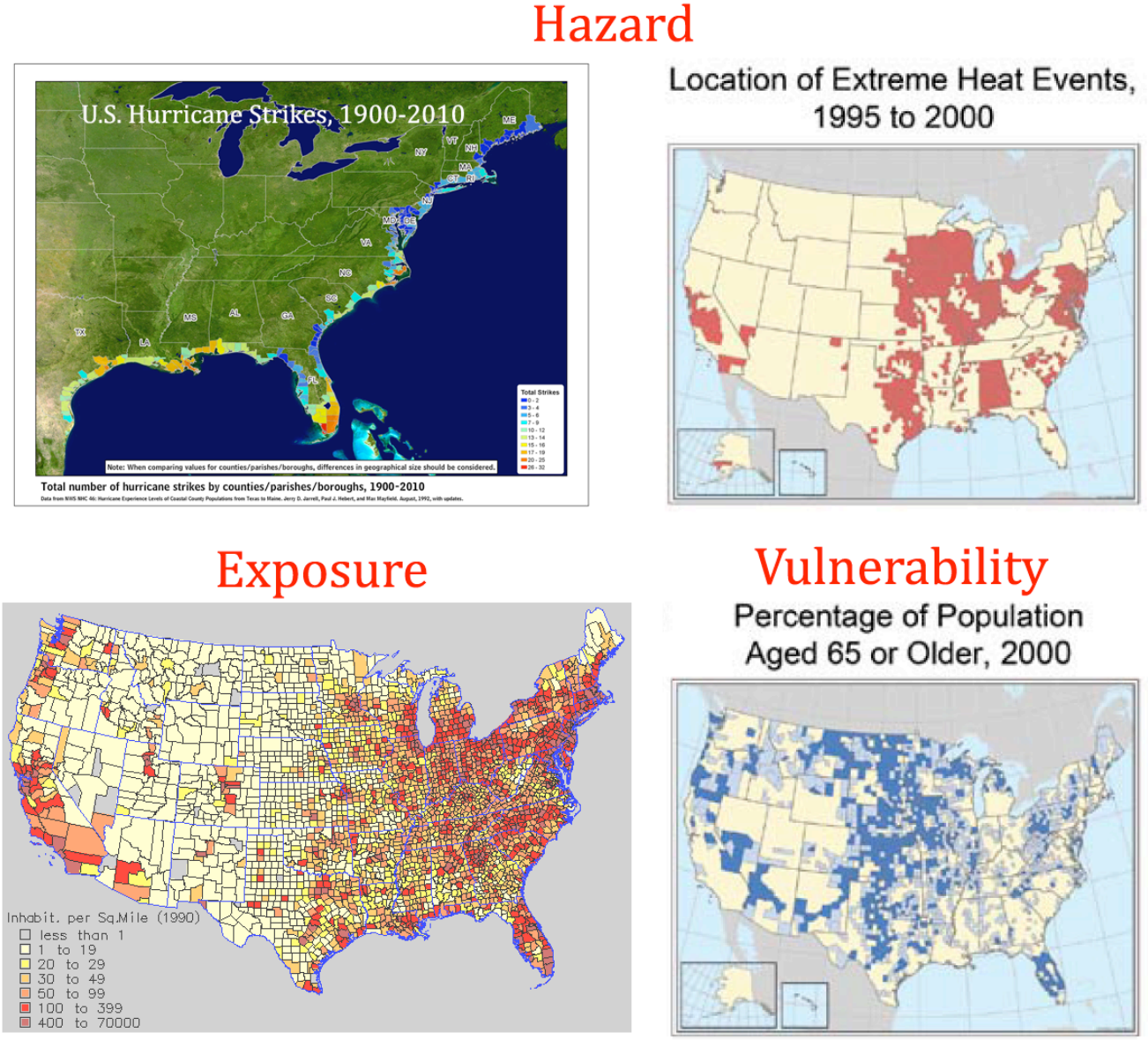

Figure 7.2. Examples of climate-related hazard, exposure and vulnerability for the United States, using data from the county level. The upper two panels show the geographic distributions of two climate-related hazards, hurricane strikes (*left)* and extreme heat events (*right*). The map at lower left shows U.S. population density according to 1990 census data, which gives a measure of overall exposure to all types of hazards. The map at lower right shows the percentage of population aged 65 or older, giving an indication of vulnerability to heat stress and ailments that have a larger impact on the elderly. *Sources: Upper left panel:* NWS NHC 46, with updates to 2010; *lower left panel:* Map Gallery of North America, Univ. of Omaha, http://maps.unomaha.edu/Peterson/geog1000/MapLinks/NAmerica/gallery.html; *other panels:* Karl et al., (2009).

Exposure varies in direct proportion to population or assets, while research shows that much of the global-scale variation in vulnerability is inversely proportional to the level of economic development. In a 2009 study focused on human casualties due to natural hazards, Peduzzi et al.,

pointed out the important effect of a region's development on the death toll from natural disasters:

> According to available global statistics, least developed countries represent 11% of the population exposed to hazards but account for 53% of casualties (Peduzzi et al., 2002). On the other hand, the most developed countries represent 15% of human exposure to hazards, but account only for 1.8% of all victims. Obviously, similar exposures with contrasting levels of development lead to drastically different tolls of casualties (Peduzzi et al., 2009).

7.2 Risk under constant hazard

Although many of the climate indicators discussed earlier in this report display historical trends, those that do not may be amenable to a simpler treatment of climate-related risk. Let us reconsider the case of tropical cyclones (TCs), first discussed in Sec. 4.3.1. Peduzzi et al., (2012) drew attention to the mismatch between the characteristics of TC events as recorded by instruments and those reported in the widely used Emergency Disasters Data Base (EMDAT; **Table 7.1**)[1]. Specifically, while none of the TC physical characteristics displays a notable trend over the last 40 years (lines A-D of Table 7.1)[2], TC disasters as reported in EMDAT have tripled since 1970 (line E). This highlights the danger of attempting to estimate trends in TC physical properties from socioeconomic data (Sec. 4.3.1). Thus, although TCs represent a highly spatially variable hazard, historical data support the notion that they are roughly stationary with time.

Table 7.1. TC events as recorded by instruments versus estimates based on mortality and economic loss.

Table 1 | Events as recorded by instruments (lines A–D) versus trend of reported TC disasters (lines E and F, average per year).

		1970s	1980s	1990s	2000s
A	Number of TC physical events (recorded)[15]	88.4	88.2	87.2	86.5
B	Number of TC events making landfall (recorded)	34.4	34.4	35.6	35.2
C	Weighted average intensity over landfall*	1.7	1.8	1.8	1.8
D	Number of times that TCs hit countries (recorded)	142.1	144.0	155.0	146.3
E	TC disasters in EM-DAT (reported)	21.7	37.5	50.6	63.0
F	Killed (×1,000) by TCs in EM-DAT (reported)	35.7	4.7	21.1	17.4
G	Percentage of reported disasters versus countries hit by TCs	15%	26%	33%	43%

The percentage of reported disasters increased threefold, whereas the number of TCs remained stable. *Weighted average is the sum of all maximum intensity, divided by the number of observed TCs.

Source: Peduzzi et al., (2012).

According to equation (1), at constant hazard *H*, risk is the product of exposure and vulnerability. Using data from EMDAT, Peduzzi et al., (2012) examined the dependence of risk, in the form of TC-induced mortality, on these purely socioeconomic variables for different world regions over the 1970-2010 period. Their results are shown in **Figure 7.3.**

[1] EMDAT (Centre for Research on the Epidemiology of Disasters, http://www.em-dat.net/) reports casualty and economic loss data for events with estimated losses above US$100,000 and greater than 10 casualties. Thus, it misses some damaging events in developing countries.

[2] Note that the category of TCs which does display a historical (increasing) trend—namely, the most intense hurricanes (Sec. 4.3, Fig. 4.12)—is not considered separately in Table 7.1.

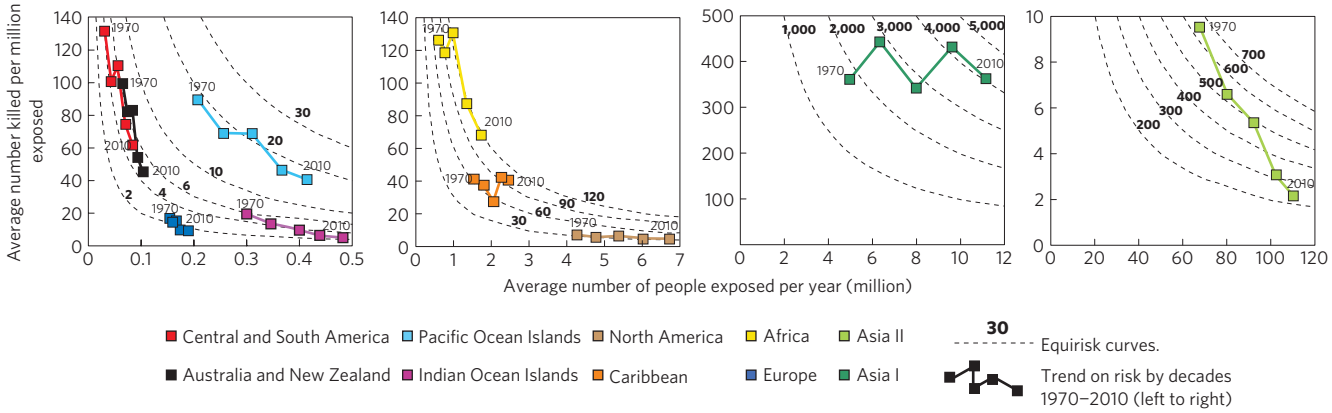

Figure 7.3. Trends in TC exposure, vulnerability, and risk by IPCC regions from 1970 to 2010. The *y*-axis represents the vulnerability (in number killed per million exposed); the *x*-axis represents the number exposed (in million). The area of the virtual rectangles where the bottom left corner is the origin (0, 0) and each colored square is the top right corner is equal to the level of risk. The dashed lines represent levels of equal risk. *Source:* Peduzzi et al., (2012).

The dashed curves in each panel of Fig. 7.3 represent equal risk under the simple assumption that the functions $g(P) = P$ and $s(V) = V$. In that case, reduced vulnerability (vertical axis, number of fatalities per million exposed) in combination with increased exposure (horizontal axis, number exposed) maintains approximately constant risk. As shown in panels 1 and 2 of the figure, this is precisely what has occurred in many world regions: although population has grown in these areas, vulnerability was reduced, through adaptation, standard of living increases, and other means. Two exceptions are the Caribbean and Asia I (India, Bangladesh, and Myanmar), where vulnerability remains high due to lack of adaptation (e.g., relocation from active TC zones and lack of storm shelters) and widespread poverty. A third exception are the Asian countries on the Pacific Rim (Asia II), which despite increasing exposure have managed to reduce their vulnerability by a factor of 5, lowering their risk by a factor of 3. These advances are largely due to rapid economic growth in China.

Peduzzi et al., (2012) (following on the work of Peduzzi et al., [2009]; see Sec. 7.3) also provide a global map of mortality risk based on the aforementioned exposure and vulnerability data, along with historical information on observed TC frequencies and tracks over world oceans, as shown in **Figure 7.4**. This map clearly illustrates the potential for risk estimates based upon a combination of socioeconomic data and spatially and temporally varying climate indicators.

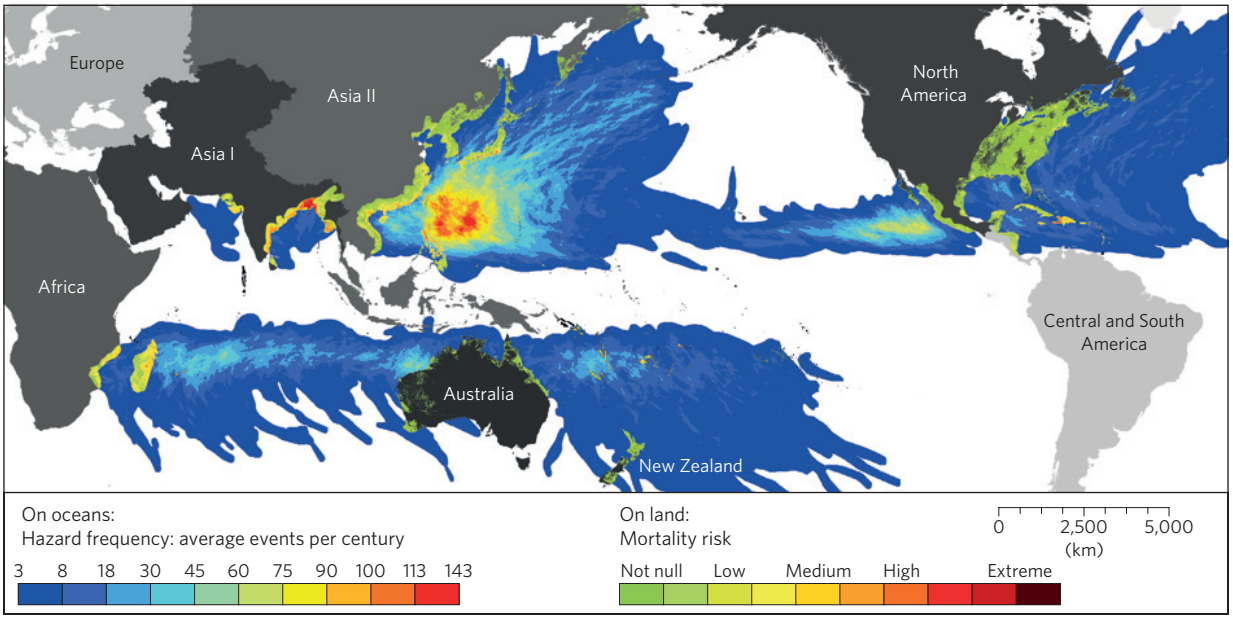

Figure 7.4. Map showing distribution of hazard frequency and mortality risk from TCs for the year 2010. Estimates are applied to all pixels on a geographic grid. Mortality risk is categorized from low to extreme. *Source:* Peduzzi et al., (2012).

7.3 Risk under changing hazard

In order to cope with the more general situation of changing hazard, one needs to come up with a specific formulation for the factor *f(H)* in equation (1). Many of the climate change indices discussed in Sec. 5 would suffice for this purpose. However, a reasonable estimate of risk *K* (with respect to mortality or property) requires estimation of the proportionality constant *C* and other non-climatic parameters appearing in the vulnerability factor. This can be achieved in a straightforward manner using a regression-based method, as we now describe.

Under the auspices of the United Nations Development Program, Peduzzi et al., (2009) developed a composite index, the *Disaster Risk Index* (DRI), to monitor the evolution of mortality risk due to natural hazards. The authors combined the variables *H* and *P* in equation (1) into a quantity called *physical exposure*, $PE = H \times P$, and further, assumed that *K* varied according to arbitrary powers of *PE* and each socioeconomic variable, i.e.,

$$K = C \times (PE)^{\alpha} \times V_1^{\alpha 1} \times V_2^{\alpha 2} \times V_3^{\alpha 3} \times \ldots$$

where *C* is an arbitrary constant and $\alpha, \alpha_1, \alpha_2, \ldots$, etc. are exponents to be determined. Taking the logarithm of both sides of this equation, one obtains

$$\ln(K) = \ln(C) + \alpha \ln(PE) + \alpha_1 \ln(V_1) + \alpha_2 \ln(V_2) + \ldots$$

Using data from EMDAT for *K*, and various other data sources for *PE* and the V_i, an initial exploratory analysis was used to determine which socioeconomic variables were most important

for a given region (e.g., by performing regression of each single variable V_i on K). Once the V_i were chosen, multiple linear regression was used to determine the intercept and coefficients α_i.

The *PE* term for TCs was constructed by Peduzzi et al., (2009) as depicted in **Figure 7.5**. First, historical data on individual cyclone tracks and associated wind speeds are plotted on a gridded region of the globe for the period of interest (panel 1). Counting the number of wind measurements exceeding a given threshold in each grid cell then gives the frequency; this constitutes the hazard factor, *H* (panel 2). The product of *H* and the population distribution (panel 3) is the physical exposure, *PE* (panel 4). Since TCs are primarily a coastal hazard, *PE* reflects this localized exposure. For the regression analysis, *PE* was aggregated at the national level so that socioeconomic data may be more easily applied.

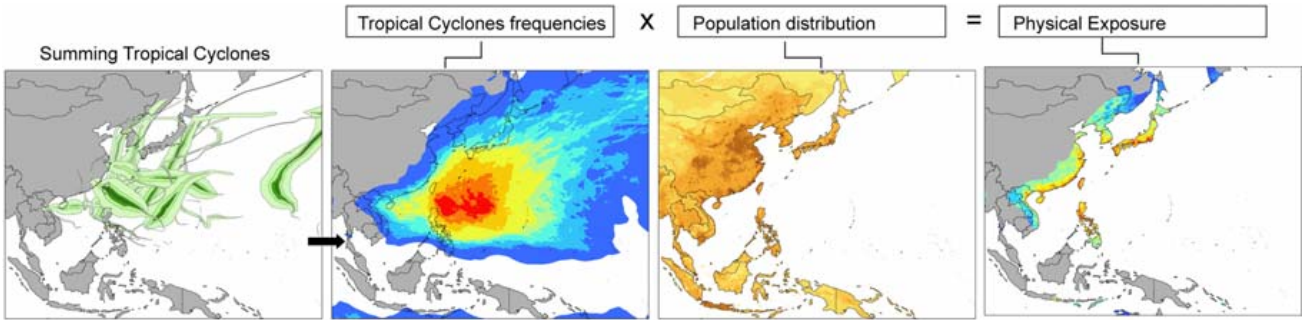

Figure 7.5. Schematic of the calculation of physical exposure (PE) for tropical cyclones in the Asia-Pacific region. *Source:* Peduzzi et al., (2009).

Over the period 1980-2000, Peduzzi et al., (2009) found that *K* was significantly correlated with PE for TCs affecting coastal nations worldwide. In addition, they found that the Gross Domestic Product per capita, GDP, and the relative fraction of country area dedicated to cropland, CRP, were also good predictors, and led to a total explained variance of $R^2 = 0.80$ ($N = 35$). The regression relation obtained was the following:

$$\ln(K) = 0.62 \ln(PE) - 0.53 \ln(GDP) + 0.35 \ln(CRP) - 0.49.$$

Casualties are positively correlated with PE (i.e., population exposed to the hazard) and CRP (with domestic food supplies adversely affected following a TC), and negatively correlated with GDP, echoing the conclusions regarding development level made in Sec. 7.1.

The authors also considered mortality due to droughts, floods, and earthquakes, deriving analogous regression relations for each. Modeled mortality risk from multiple hazards was obtained as the sum of *K* over all hazards, and aggregated to the county level. In order to formulate the DRI, both absolute (number killed) and relative mortality (number killed per country population) risk measures were used. This was done in order to avoid biasing results toward more populous countries that have high absolute mortality in any case (e.g., China and India) and especially vulnerable nations having low populations (e.g., Caribbean island nations), which feature high fatalities per capita due to disasters. Hence, the scale for the DRI is chosen as

the product of absolute and relative mortality, as illustrated in **Figure 7.6**, with the final DRI represented as a value ranging from 1 (mild risk) to 7 (severe risk). Further details on the procedure may be found in Peduzzi et al., (2009). A spatial map of DRI for all countries is shown in **Figure 7.7**.

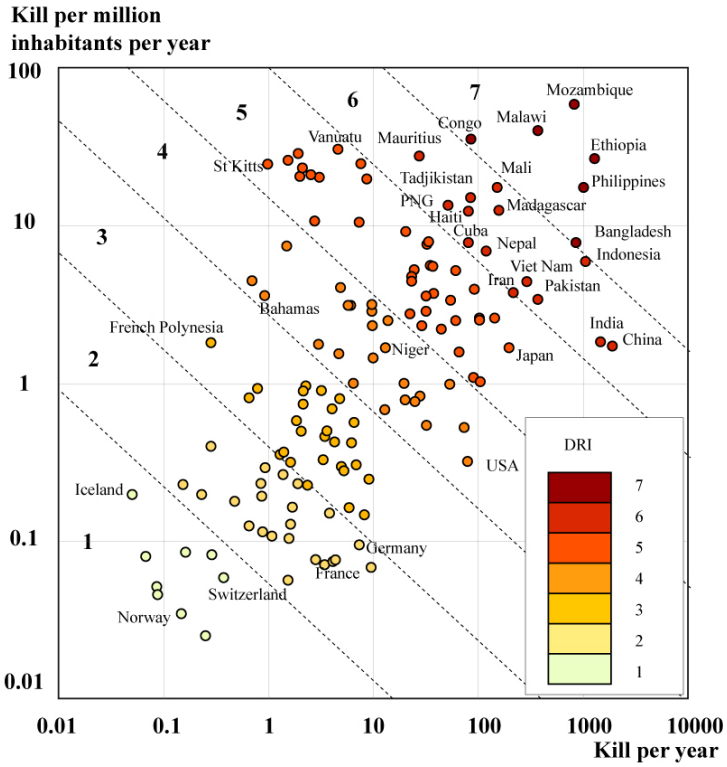

Figure 7.6. Calibration of the Disaster Risk Index (DRI) for all natural hazards worldwide. Note the logarithmic scale on both axes, which implies that the dotted diagonal lines represent equirisk levels. *Source:* Peduzzi et al., (2009).

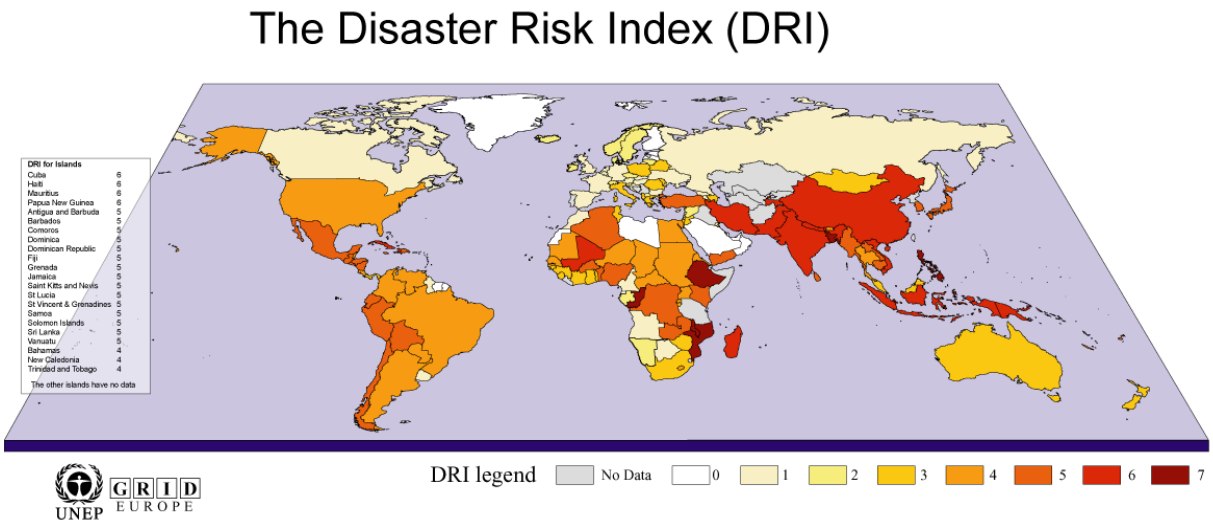

Figure 7.7. Spatial distribution of the DRI worldwide. *Source:* Peduzzi et al., (2009).

It is worth noting that an exceptional online resource is available based on the DRI framework. Hosted by the United Nations Environment Program (UNEP), the Global Resource Information Database (GRID) contains publicly available, gridded data on a host of environmental and socioeconomic variables potentially entering into the calculation of the DRI. An interface platform, PREVIEW, allows users to specify a number of risk factors simultaneously and produce geographical plots of the factors and of the resulting risk.[1] Information on sources of data is also provided. An example of multiple mortality risk due to all hazards as generated by the program is shown in **Figure 7.8**. The specific hazards included are: TCs, droughts, floods, storm surges, fires, tsunamis, earthquakes and landslides. The mortality index categories used in this figure differs from the DRI, but translates into the following figures for casualties over the 2001-2010 period:

Low: 1-1000
Moderate: 1000 - 10 000
Medium: 10 000 - 100 000
High: 100 000 – 1 000 000
Extreme: Over 1 000 000

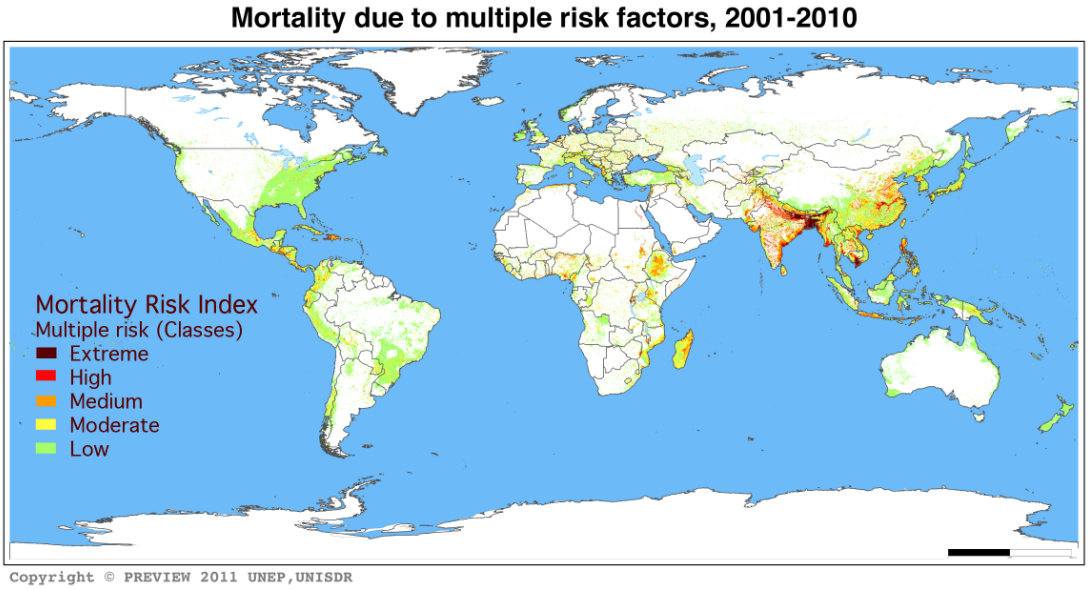

Figure 7.8. An example of user-generated output from the PREVIEW Global Risk Data platform. *Source:* Adapted from original available at UNEP-GRID.

Although mainly useful for illustrative or exploratory purposes, this user-friendly platform could serve as a starting point for a more detailed risk assessment of a specific hazard and/or region. The proposed ACRI could follow the same general approach as the DRI, but extend beyond mortality risk to include the areas of property loss, economic disruption, and even natural capital (e.g., agriculture, forests, and other ecosystems).

[1] http://preview.grid.unep.ch/index3.php?preview=data&lang=eng. Note that this tool may be incomplete in some respects. For example, an attempt to display exposure to the devastating 2004 tsunami in the Indian Ocean near Sumatra did not show any effect; however, results did show up under "Earthquakes."

A first step in this direction would be to locate and assemble socioeconomic data of sufficient quality and detail to make this possible. An example of this kind of information is the compilation of Collins and Lowe (2001), who assembled a dataset of aggregated insured losses from hurricanes affecting the continental U.S. from 1900-99. As one means of isolating economic losses, the authors accounted for growth in the number of housing units in affected areas over the time period of interest, rather than changes in population. This is indicative of the type of data that might be needed for formulating a comprehensive ACRI.

7.4 Conclusions

In this section a definition of climate-related risk that lends itself naturally to a quantitative treatment was introduced. It is also modular, in the sense that climate hazards, exposure, and vulnerability are represented as separate factors. Any of the climate indices introduced in Sec. 5 could be used in formulating the hazard factor *f(H)*, and this would represent a significant advance over existing approaches, which cover only a limited array of climate hazards, and are not standardized to reflect the key role of climate variability. The formulation of the DRI in terms of a multiple linear regression model that accepts spatially and temporally varying risk factors as input points one way forward to a more comprehensive approach.

Extensions of the method that would facilitate the formulation of the more targeted ACRI, which better serves the interests of actuaries might include:

(1) introduction of a wider array of climate hazards, as outlined in previous sections of this report;
(2) inclusion of detailed geographic data on insured or uninsured property assets, where data are available;
(3) exploration of future climate-related risk, using projections of climate change (Sec. 6), patterns of population and economic development, and evolving vulnerability (where any one of these could be held constant in the event that confidence in its projected change is poor).

While only a rough framework has been sketched here, it seems clear that further investigation in any of these areas would reap significant rewards in terms of estimating the threat of hazards arising from climate change on life, property, and natural capital.

Appendix A: Glossary of Terms and Acronyms

ACE: accumulated cyclone energy, a measure of hurricane strength.

anomaly: difference between a measurement over a given period (e.g., a single month) and a longer-term mean (e.g., a decade).

anthropogenic: of or pertaining to human influence.

apparent temperature: A measure of how hot it really feels when relative humidity is factored with the actual air temperature. The apparent temperature usually exceeds the surface air temperature, except at low values of relative humidity (< 50%). Also referred to as the *heat index* or *humiture,* or, using the dew point instead of relative humidity, the *humidex.*

AR4: Fourth Assessment Report of the IPCC published in 2007. Separate volumes were produced by three different working groups, WGI, WGII, and WGIII.

CHIPS: Coupled Hurricane Intensity Prediction System.

CMI: Crop Moisture Index. Related to the Palmer Drought Severity Index (PDSI – see below).

CMIP: Coupled Model Intercomparison Project. A periodic evaluation and intercomparison of Global Climate Models.

DRI: Disaster Risk Index.

EC: extratropical (i.e., mid- to high-latitude) cyclone.

ENSO: The El Niño-Southern Oscillation. See text of Sec. 2.1 of the report for a description of this phenomenon.

GCM: Global Climate Model; also General Circulation Model.

GHCN: Global Historical Climatology Network.

GISS: NASA's Goddard Institute for Space Studies.

GRACE: Gravity Recovery and Climate Experiment.

heating/cooling degree days: A practical measure used by utility companies and others to quantify total energy use over high-demand periods for heating (i.e., winter) and cooling (i.e., summer). Heating (cooling) degree days (units: degrees × days) are the product of the number of degrees that the daily mean surface air temperature falls below (above) a specified threshold temperature (e.g., 65°F in Hansen et al., [1998]) multiplied by the number of days in the heating (cooling) season.

IKE: integrated kinetic energy, a measure of hurricane strength.

IPCC: The Intergovernmental Panel on Climate Change. The IPCC was established in 1988 by the World Meteorological Organization (WMO) and the United Nations Environment Programme (UNEP) as a means to assess global climate change.

NOAA: National Ocean and Atmospheric Administration, a U.S. federal agency focused on the condition of the oceans and the atmosphere, and a major provider of global climate data to the worldwide scientific community.

NSIDC: National Snow & Ice Data Center, Boulder, Colorado, U.S.A.

PDI: power dissipation index, a measure of hurricane strength.

PDSI: Palmer Drought Severity Index, a measure of soil water that accounts for persistence of a previous soil moisture state.

phenology: The study of cyclic and seasonal natural phenomena, especially in relation to climatic influences on plant and animal life.

PSR: plant species richness.

quantile: Data values marking the boundaries between equal-size subsets of a cumulative probability distribution. For example, the 2-quantile is called the median, while 4-quantiles are referred to as quartiles.

radiative forcing: The rate of change of energy flowing into or out of the Earth system per unit area of the globe as measured at the top of the atmosphere. The IPCC uses a more precise, but somewhat technical, definition in its Assessment Reports. Radiative forcing results from changes in the amount of absorbed and reflected solar energy, as well as the amounts of volcanic aerosol and greenhouse gases present in the atmosphere.

reanalysis data: A data analysis method in which observations of climate variables are interpolated onto the 3D grid of a GCM and used to constrain the subsequent model simulation. The output is a hybrid of observational and model-generated information, and is often available at six-hourly, daily, and monthly time steps for all climate variables simulated by the GCM.

return period/recurrence interval: A statistical estimate of the interval of time between events of a certain intensity or size, often used in risk analysis.

SAT: surface air temperature, usually measured at a standard height of two meters above the ground.

Saffir-Simpson hurricane scale: A discrete rating scale categorizing hurricanes from 1 to 5 according to their maximum sustained (1-min) wind speed. The following table defines the categories, which also includes less damaging events known as Tropical Depressions and Storms (Simpson and Riehl 1981). The scale, developed by Herbert Saffir and Robert Simpson in 1969, is intended to provide a rough estimate of a hurricane's potential for property damage, including storm surge.

Tropical Cyclone Type	*Max. Sustained 1-min. Wind Speed (m.p.h.)*	*Storm Surge (ft)*	*Damage*
Tropical Depression	*< 39*	*n/a*	*n/a*
Tropical Storm	*39 to 73*	*n/a*	*n/a*
Category 1	*74 to 95*	*4 to 5*	*Minimal*
Category 2	*96 to 110*	*6 to 8*	*Moderate*
Category 3	*111 to 130*	*9 to 12*	*Extensive*
Category 4	*131 to 155*	*13 to 18*	*Extreme*
Category 5	*> 156*	*> 19*	*Catastrophic*

SCE: snow cover extent, measured in units of area (e.g., square miles or kilometers).

sea ice area, or cover, versus sea ice extent: Ice area is the best estimate of actual ice covering the ocean, not including any gaps or holes. Extent is a more liberal term, in that it designates any satellite grid cell that is at least 15% ice-covered as "100% ice" for the purpose of calculating extent. Thus, extent is always a larger number than area. It is extent that is reported by NSIDC, because it is somewhat less prone to observational errors (e.g., distinguishing surface melt on top of sea ice as open ocean, which is challenging for satellites).

SLR: sea-level rise.

SPI: standardized precipitation index, a dimensionless quantity defined as the precipitation anomaly divided by its standard deviation.

SPM: Summary for Policymakers.

SRES: IPCC Special Report on Emissions Scenarios (2000).

SREX: IPCC Special Report on Climate Extremes (2012).

SST: sea surface temperature.

standard deviation: A commonly used measure of the variability of a population or a sample thereof, equal to the square root of the variance, and expressed in the same units as the data. For example, a normal distribution of a random variable has 68 percent of the anomalies falling within $\pm 1\sigma$ of the mean value, where σ is the standard deviation. The tails of the normal distribution decrease rapidly so there is only a 2.3% chance of the temperature exceeding $+2\sigma$, and a 2.3% chance of being colder than -2σ. The chance of an anomaly lying beyond $\pm 3\sigma$ is only 0.26% for a normal distribution of variability.

STI: standardized temperature index, a dimensionless quantity defined as the temperature anomaly divided by its standard deviation.

TC: tropical cyclone.

ToE: time of emergence, referring to the time when a climate signal significantly exceeds the background variability.

WGMS: World Glacier Monitoring Service.

Appendix B: Unit Conversions

Note: Attention is restricted to units actually cited in the report.

I. Temperature conversion: To convert from degrees Celsius (°C) to Fahrenheit (F), first multiply by 9/5, then add 32. To convert from F to °C, first subtract 32, then multiply by 5/9.

II. Length and area

U.S. or Imperial		**Metric (S.I.)**
1 inch [in]		2.54 cm
1 foot [ft]	12 in	0.3048 m
1 yard [yd]	3 ft	0.9144 m
1 mile [mi]	1760 yd	1.6093 km
1 nautical mile	2025.4 yd, 1.151 mi	1.853 km
1 acre	4840 yd^2	4046.9 m^2
1 square mile [mi^2]	640 acres	2.59 km^2

Metric (S.I.)		**U.S. or Imperial**
1 millimeter [mm]		0.03937 in
1 centimeter [cm]	10 mm	0.3937 in
1 meter [m]	100 cm	1.0936 yd
1 kilometer [km]	1000 m	0.6214 mi 0.540 nautical mi
1 hectare [ha]	10,000 m^2	2.4711 acres
1 square kilometer [km^2]		0.3861 mi^2

III. Other

U.S. or Imperial		**Metric (S.I.)**
1 pound [lb]		0.4536 kg
1 short ton [US]		0.9072 t
1 long ton [UK]		1.0160 t
1 nautical mile per hour [kt]	1.151 mph	1.853 km/h
1 pound per square inch		703.1 kg/m^2

Metric (S.I.)		**U.S. or Imperial**
1 kilogram [kg]		2.2046 lb
1 tonne [t]	1000 kg	1.1023 short ton 0.9842 long ton
1 gigaton [Gt]	10^9 t	1.1023×10^9 short ton 0.9842×10^9 long ton
1 kilometer per hour [km/h]		0.540 kt
1 kilogram per m^2 [kg/m^2]		0.001422 lb/in^2

Appendix C: Online Resources

I. Observed climate data

NOAA and the National Climatic Data Center (NCDC) are exceptional resources for quality-controlled and frequently updated (monthly) climatic data of various types, especially (but not exclusively) for the U.S.A. Data for a month are typically made available by the 15th of the following month. Some of the available products follow.

Annual State of the Climate: An overview of all climatic variables for the year, with a description of notable events placed in a longer-term climatological context.
http://www.ncdc.noaa.gov/sotc

Global Surface Temperature Anomalies:
http://www.ncdc.noaa.gov/cmb-faq/anomalies.php

20th Century Reanalysis:
http://www.esrl.noaa.gov/psd/data/20thC_Rean/

North American Regional Reanalysis:
http://www.esrl.noaa.gov/psd/cgi-bin/data/narr/plotmonth.pl

Atmospheric response associated with El Nino and La Nina events from 1948 - present:
http://www.esrl.noaa.gov/psd/enso/compare/

North American Drought Monitor:
http://www.ncdc.noaa.gov/temp-and-precip/drought/nadm/

U.S. Storm Prediction Center Tornado Database:
http://www.spc.noaa.gov/wcm/index.html#jmc

Interactive online map of U.S. relative sea level, with links to data for each tidal gauge:
http://tidesandcurrents.noaa.gov/sltrends/slrmap.html

Other useful and accessible global climate data products are the following:

Global Surface Temperature Anomalies (NASA-GISS): An interactive menu-based tool allowing the user to choose the dataset, base period, anomaly period, and type (monthly/seasonal/annual), etc.
http://data.giss.nasa.gov/gistemp/maps/

International Research Institute (IRI) for Climate and Society at Columbia University:
Miscellaneous climate data maps from around the world, updated monthly.
http://iridl.ldeo.columbia.edu/

European Centre for Medium-Range Weather Forecasts European Reanalysis (ERA-40) Atlas:
http://www.ecmwf.int/research/era/ERA-40_Atlas/

II. Climate model output (e.g., future projections)

IPCC Data Distribution Centre:
http://www.ipcc-data.org/

Climate System Visualizations:
http://www.vets.ucar.edu/vg/categories/climate.shtml

International Research Institute (IRI) for Climate and Society at Columbia University:
http://iridl.ldeo.columbia.edu/maproom/

III. Socioeconomic data for risk assessment

U.S. Climate Change Research Program, Synthesis and Assessment Products:
http://www.globalchange.gov/publications/reports/scientific-assessments/saps

EM-DAT International Disaster Database: A fully searchable online catalogue of global disasters associated with substantial losses.
http://www.emdat.be/

Socioeconomic Data and Applications Center (SEDAC):
http://sedac.ciesin.columbia.edu/

UNEP Global Risk Data Platform:
http://preview.grid.unep.ch/index3.php?preview=data&lang=eng

World Bank Climate Change Portal:
http://sdwebx.worldbank.org/climateportal/

IV. Climate Indices

Yale Online Forum on Climate Change and the Media:
http://www.yaleclimatemediaforum.org/2010/05/climate-index-reporting-projects/

IGBP Climate Change Index:
http://www.igbp.net/4.1b8ae20512db692f2a680001647.html

Common Sense Climate Index: Results similar to those presented in Sec. 5.1 can be viewed at numerous stations worldwide. Note that only a composite temperature index is provided, and that the data are not up-to-date at a majority of locations:
http://data.giss.nasa.gov/csci/stations/

Standardized Precipitation Index:
http://iridl.ldeo.columbia.edu/maproom/.Global/.Precipitation/SPI.html

Palmer Drought Severity and Crop Moisture Indices:
http://www.drought.noaa.gov/palmer.html
http://drought.unl.edu/Planning/Monitoring/ComparisonofIndicesIntro/CMI.aspx

North American Drought Monitor:
http://www.ncdc.noaa.gov/temp-and-precip/drought/nadm/nadm-maps.php

U.S. Climate Variability Index:
http://gis.ncdc.noaa.gov/map/cdo/?thm=themeIndices

U.S. Percentage Areas Very Warm/Very Cold:
http://www.ncdc.noaa.gov/temp-and-precip/uspa/?area=warm-cold&year=2012&month=2

References

Adams, H. D., M. Guardiola-Claramonte, G. A. Barron-Gafford, J. C. Villegas, D. D. Breshears, C. B. Zoug, P. A. Troch, and T. E. Huxman (2009). Temperature sensitivity of drought-induced tree mortality portends increased regional die-off under global-change-type drought, *PNAS*, **106**, 17, 7063–7066.

Ainsworth, E. A. , A. Rogers, and A. D. B. Leakey (2008), Targets for Crop Biotechnology in a Future High-CO2 and High-O3 World. *Plant Physiology*,**147**, 1, 13-19. DOI 10.1104/pp.108.117101.

Alexander, L. V., X. Zhang, T. C. Peterson, J. Caesar, B. Gleason, A. M. G. Klein Tank, M. Haylock, D. Collins, B. Trewin, F. Rahimzadeh, A. Tagipour, K. Rupa Kumar, J. Revadekar, G. Griffiths, L. Vincent, D. B. Stephenson, D.B. J. Burn, E. Aguilar, M. Brunet, M. Taylor, M. New, P. Zhai, M. Rusticucci, and J. L. Vazquez-Aguirre (2006). Global observed changes in daily climate extremes of temperature and precipitation. *Journal Of Geophysical Research*, **111**, D05109. DOI 10.1029/2005JD006290.

Alley, W. M.(1984). The Palmer Drought Severity Index: Limitations and Assumptions. *Journal of Climate and Applied Meteorology*, **23**, 1100-1109.

Allison, I., N. L. Bindoff, R. A. Bindschadler, P. M. Cox, N. de Noblet, M. H. England, J. E. Francis, N. Gruber, A. M. Haywood, D. J. Karoly, G. Kaser, C. Le Qu.r., T. M. Lenton, M. E. Mann, B. I. McNeil, A. J. Pitman, S. Rahmstorf, E. Rignot, H. J. Schellnhuber, S. H. Schneider, S. C. Sherwood, R. C. J. Somerville, K. Steffen, E. J. Steig, M. Visbeck, and A. J. Weaver (2009). *The Copenhagen Diagnosis, 2009: Updating the World on the Latest Climate Science.* The University of New South Wales Climate Change Research Centre (CCRC), Sydney, Australia, 60pp.

Anderegg, W. R. L., J. W. Prall, J. Harold, and S. H. Schneider (2010). Expert credibility in climate change: *Proceedings of the National Academy of Sciences*, **107,** 27, 12107-12109. DOI 10.1073/pnas.1003187107.

Baettig, M. B., M. Wild, and D. M. Imboden (2007). A climate change index: Where climate change may be most prominent in the 21st century. *Geophysical Research Letters*, **34**, L01705. DOI 10.1029/2006GL028159.

Bailey, R. G. (1995). Description of the ecoregions of the United States. *Miscellaneous Publication 1391*. USDA Forest Service, Washington, D.C., USA.

Bamber J. L., R. E. M. Riva, B. L. A. Vermeersen, and A. M. LeBroq (2009). Reassessment of the potential sea-level rise from a collapse of the West Antarctic Ice Sheet (Supporting Online Material)". *Science,* **324**, 5929 901–3. DOI 10.1126/science.1169335.

Barredo, J.I. (2009). Normalised flood losses in Europe: 1970–2006. *Natural Hazards and Earth System Sciences*, **9**, 97–104. DOI 10.5194/nhess-9-97-2009.

Barriopedro, D., E. M. Fischer, J. Luterbacher, R. M. Trigo, R. García-Herrera (2011). The Hot Summer of 2010: Redrawing the Temperature Record Map of Europe. *Science,* **332**, 220. DOI 10.1126/science.1201224.

Bell, G. D., M. S. Halpert, R. C. Schnell, R. W. Higgins, J. Lawrimore, V. E. Kousky, R. Tinker, W. Thiaw, M. Chelliah, and A. Artusa (2000). Climate assessment for 1999, *BAMS*, **81** 6, 1328.

Bergengren, J.C., D. E. Waliser, and Y. L. Yung (2011). Ecological sensitivity: a biospheric view of climate change. *Climatic Change*, **107**, 3-4, 433-457. DOI 10.1007/s10584-011-0065-1.

Bister, M., and K. A. Emanuel (2002). Low frequency variability of tropical cyclone potential intensity. Climatology for 1982–1995. *Journal Of Geophysical Research*, **107**, 4621, 4. DOI 10.1029/2001JD000780.

Borick, C. P., E. Lachapelle, and B. G. Rabe (2011). Climate compared: Public opinion on climate change in the United States & Canada. *Issues in Governance Studies*, **39**, April 2011, The Brookings Institution, Washington DC.

Borick, C. P., and B. G. Rabe (2012). Fall 2011 National Survey of American Public Opinion on Climate Change. *Issues in Governance Studies*, **45**, February 2012, The Brookings Institution, Washington DC.

Boykoff, M., and J. Boykoff (2004). Balance as bias: Global warming and the U.S. prestige press. *Global Environmental Change*, **14,** 2, 125-136.

Breshears, D. D., N. S. Cobb, P. M. Rich, K. P. Price, C. D. Allen, R. G. Balice, W. H. Romme, J. H. Kastens, M. L. Floyd, J. Belnap, J. J. Anderson, O. B. Myers, and C. W. Meyer (2005). Regional vegetation die-off in response to global-change-type drought. *PNAS*, **102**, 42, 5144–15148.

Brohan, P., J. J. Kennedy, I. Harris, S. F. B. Tett, P. D. Jones (2006). Uncertainty estimates in regional and global observed temperature changes: A new dataset from 1850. *Journal of Geophysical Research*, **111**, D12106. DOI 10.1029/2005JD006548.

Brown, R. D., and D. A. Robinson (2011). Northern Hemisphere spring snow cover variability and change over 1922–2010 including an assessment of uncertainty. *The Cryosphere*, **5**, 219-229. DOI 10.5194/tc-5-219-2011.

Bull, S. R., D. E. Bilello, J. Ekmann, M. J. Sale, and D. K. Schmalzer (2007). Effects of climate change on energy production and distribution in the United States. In: *Effects of Climate Change on Energy Production and Use in the United States* [Wilbanks, T. J., V. Bhatt, D. E. Bilello, S. R. Bull, J. Ekmann, W. C. Horak, Y. J. Huang, M. D. Levine, M. J. Sale, D. K. Schmalzer, and M. J. Scott (eds.)]. Synthesis and Assessment Product 4.5. U.S. Climate Change Science Program, Washington, DC, pp. 45-80.

Canadian Council of Forest Ministers (2011), http://nfdp.ccfm.org/.

Cardona, O.D. (2005). Indicators of Disaster Risk and Risk Management, *IDB Publications 14478*, Inter-American Development Bank.

Cazenave, A. and F. Remy (2011). Sea level and climate: measurements and causes of changes. *WIREs Climate Change*, **2**, 647–662. DOI 10.1002/wcc.139.

Choi, G., D. A. Robinson, S. Kang (2010). Changing Northern Hemisphere Snow Seasons. *Journal of Climate*, **23**, 5305-5310.

Church, J. A., N. J. White (2006). A 20th century acceleration in global sea-level rise. *Geophysical Research Letters*, **33**, L01602. DOI 10.1029/2005GL024826.

Church, J. A., N. J. White (2011). Sea-Level Rise from the Late 19th to the Early 21st Century. Surveys in Geophysics, **32**, 585–602. DOI 10.1007/s10712-011-9119-1.

Ciais, Ph., M. Reichstein, N. Viovy, A. Granier, J. Ogée, V. Allard, M. Aubinet, N. Buchmann, Chr. Bernhofer, A. Carrara, F. Chevallier, N. De Noblet, A. D. Friend, P. Friedlingstein, T. Grünwald, B. Heinesch, P. Keronen, A. Knohl, G. Krinner, D. Loustau, G. Manca, G. Matteucci, F. Miglietta, J. M. Ourcival, D. Papale, K. Pilegaard, S. Rambal, G. Seufert, J. F. Soussana, M. J. Sanz, E. D. Schulze, T. Vesala, and R. Valentini (2005). Europe-wide reduction in primary productivity caused by the heat and drought in 2003. *Nature,* **437**, 529-533. DOI 10.1038/nature03972.

Collins, D. J., Lowe, S. P. (2001). A macro validation dataset for U.S. hurricane models, Casualty Actuarial Society Forum, Casualty Actuarial Society, Arlington, Va., http://www.casact.org/pubs/forum/01wforum/01wf217.pdf. Accessed March 29, 2012.

Comiso, J. and C., F. Nishio (2008). Trends in the sea ice cover using enhanced and compatible AMSR-E, SSM/I, and SMMR data, *Journal of Geophysical Research*, **113**, C02S07. DOI 10.1029/2007JC004257.

Comiso, J. C. (2012). Large Decadal Decline of the Arctic Multiyear Ice Cover. *Journal of Climate*, **25**, 1176-1193. DOI 10.1175/JCLI-D-11-00113.1.

Confalonieri, U., B. Menne, R. Akhtar, K. L. Ebi, M. Hauengue, R. S. Kovats, B. Revich, and A. Woodward (2007). Human health. In: Parry, M. L., O. F. Canziani, J. P. Palutikof, P. J. van der Linden, C. E. Hanson (eds) *Climate change 2007: impacts adaptation and vulnerability. Contribution of working group II to the fourth assessment report of the intergovernmental panel on climate change*. Cambridge University Press, Cambridge, UK, 391–431.

Cook, A. J., A. J. Fox, D. G. Vaughan, and J. G. Ferrigno (2005). Retreating Glacier Fronts on the Antarctic Peninsula over the Past Half-Century. *Science*, **308**, 5721, 541-544. DOI 10.1126/science.1104235.

Cury, P. M., and V. Christensen (2005). Quantitative Ecosystem Indicators for Fisheries Management. *ICES Journal of Marine Science*, **62**, 307-310. DOI 10.1016/j.icesjms.2005.02.003.

Dai, A., K. E. Trenberth, and T. Qian (2004). A Global Dataset of Palmer Drought Severity Index for 1870–2002: Relationship with Soil Moisture and Effects of Surface Warming. *Journal of Hydrometeorology*, **5**, 1117-1130.

DeGaetano, A. T., and R. J. Allen (2002). Trends in Twentieth-Century Temperature Extremes across the United States. *Journal of Climate*, **15**, 3188–3205.

Devictor, V., C. van Swaay, T. Brereton, L. Brotons, D. Chamberlain, J. Heliölä, S. Herrando, R. Julliard, M. Kuussaari, Å. Lindström, J. Reif, D. B. Roy, O. Schweiger, J. Settele, C. Stefanescu, A. Van Strien, C. Van Turnhout, Z. Vermouzek, M. WallisDeVries, I. Wynhoff, and F. Jiguet (2012) Differences in the climatic debts of birds and butterflies at a continental scale. *Nature Climate Change*, **2**, 121-124. DOI 10.1038/NCLIMATE1347.

Donat, M. G., D. Renggli, S. Wild, L. V. Alexander, G. C. Leckebusch, and U. Ulbrich (2011). Reanalysis suggests long-term upward trends in European storminess since 1871, *Geophysical Research Letters*, **38**, L14703. DOI 10.1029/2011GL047995.

Drews, C. (2007). Separating the ACE Hurricane Index into Number, Intensity, and Duration, http://acd.ucar.edu/~drews/hurricane/SeparatingTheACE.html.

Durre, I., M.J. Menne, B.E. Gleason, T.G. Houston, and R.S. Vose (2010). Comprehensive automated quality assurance of daily surface observations. *Journal of Applied Meteorology Climatology*, **49**, 1615–1633.

Dyurgerov, M.B., and M. F. Meier (2005). Glaciers And The Changing Earth System: A 2004 Snapshot. INSTAAR, University of Colorado at Boulder.

Easterling, W. E., P. K. Aggarwal, P. Batima, K. M. Brander, L. Erda, S. M. Howden, A. Kirilenko, J. Morton, J. -F. Soussana, J. Schmidhuber, and F. N. Tubiello (2007): Food, fibre and forest products. Climate Change 2007: Impacts, Adaptation and Vulnerability. Contribution of Working Group II to the Fourth Assessment Report of the Intergovernmental Panel on Climate Change, M.L. Parry, O.F. Canziani, J.P. Palutikof, P.J. van der Linden and C.E. Hanson, Eds., Cambridge University Press, Cambridge, UK, 273-313.

Eby, M., K. Zickfeld, A. Montenegro, D. Archer, K. J. Meissner, and A. J. Weaver (2009). Lifetime of Anthropogenic Climate Change: Millennial Time-scales of Potential CO2 and Surface Temperature Perturbations. *Journal of Climate*, **22**, 2501-2511.

Elsner, J. B., J. P. Kossin, and T. H. Jagger (2008). The increasing intensity of the strongest tropical cyclones. *Nature*, **455**, 92-95. DOI 10.1038/nature07234.

Emanuel, K. A. (1987). The dependence of hurricane intensity on climate. *Nature*, **326**, 483-485.

Emanuel, K. (2005). Increasing destructiveness of tropical cyclones over the past 30 years. *Nature*, **436**, 686-688. DOI 10.1038/nature03906.

Emanuel, K. (2006). Climate and Tropical Cyclone Activity: A New Model Downscaling Approach. *Journal of Climate*, **19**, 4797-4802.

Emanuel, K. (2008). The Hurricane—Climate Connection. *BAMS*, **89**, 5, ES10-ES20. DOI 10.1175/BAMS-89-5-Emanuel.

Emanuel, K. (2011). Global Warming Effects on U.S. Hurricane Damage. *Weather, Climate, and Society*, **3**, 4, 261-268. DOI 10.1175/WCAS-D-11-00007.1.

Emanuel, K., S. Ravela, E. Vivant, and C. Risi (2006). A Statistical Deterministic Approach to Hurricane Risk Assessment. *BAMS*, March 2006, DOI:10.1175/BAMS-87-3-299.

Environmental Protection Agency (EPA) (2010). *Climate Change Indicators for the United States.* Available at http://www.epa.gov/climatechange/science/indicators/download.html.

Ericson, J. P., C. J. Vorosmarty, S. L. Dingman, L. G. Ward, and M. Meybeck (2006). Effective sea-level rise and deltas: causes of change and human dimension implications. *Global Planet Change*, **50**, 63-82.

Feng, S., and Q. Hu (2007) Changes in winter snowfall/precipitation ratio in the contiguous United States. *Journal of Geophysical Research*, **112**, D15109. DOI 10.1029/2007JD008397.

Fetterer, F., K. Knowles, W. Meier, and M. Savoie (2002), updated 2012. Sea Ice Index. Boulder, CO: National Snow and Ice Data Center. Digital media.

Flannigan, M. D., and J. B. Harrington (1988). A study of the relation of meteorological variables to monthly provincial area burned by wildfire in Canada (1953-80). *Journal of Applied Meteorology*, **27**, 441-452.

Folland, C., and T. Karl, et al., (2001). Observed Climate Variability and Change. Climate Change 2001: The Scientific Basis. Contribution of Working Group I to the Third Assessment Report of the Intergovernmental Panel on Climate Change. H. JT, Y. Ding, D. Griggset al. Cambridge, UK, Cambridge University Press.

Frumhoff, P. C., J. J. McCarthy, J. M. Melillo, S. C. Moser, and D. J. Wuebbles (2007) Confronting Climate Change in the U.S. Northeast: Science, Impacts and Solutions. Synthesis report of the Northeast Climate Impacts Assessment. Union of Concerned Scientists, Cambridge, MA, 146 pp.

Gallant, Ailie J. E., and D. J. Karoly (2010). A Combined Climate Extremes Index for the Australian Region. *Journal of Climate*, **23**, 6153–6165. DOI 10.1175/2010JCLI3791.1.

García-Herrera, R., J. Díaz, R. M. Trigo, J. Luterbacher, and E. M. Fischer (2010). A Review of the European Summer Heat Wave of 2003, *Critical Reviews in Environmental Science and Technology*, **40**, 4. DOI 10.1080/10643380802238137.

Gillett, N. P., A. J. Weaver, F. W. Zwiers, and M. D. Flannigan (2004) Detecting the effect of climate change on Canadian forest fires. *Geophysical Research Letters*, **31**, L18211. DOI 10.1029/2004GL020876.

Giorgi, F., and X. Bi (2009), Time of emergence (TOE) of GHG-forced precipitation change hot-spots, Geophys. Res. Lett., 36, L06709, doi:10.1029/2009GL037593.

Gleason, K. L., J. H. Lawrimore, D. H. Levinson, T. R. Karl, and D. J. Karoly (2008). A Revised U.S. Climate Extremes Index. *Journal of Climate*, **21**, 2124–2137. DOI 10.1175/2007JCLI1883.1.

Groisman, P. Y., R. W. Knight, D. R. Easterling, T. R. Karl, G. C. Hegerl, and V. N. Razuvaev (2005). Trends in Intense Precipitation in the Climate Record. *Journal of Climate*, **18**, 1326-1350.

Grossmann, I., M. and G. Morgan (2011). Tropical cyclones, climate change, and scientific uncertainty: what do we know, what does it mean, and what should be done? *Climatic Change*, **108**, 3, 543-579. DOI 10.1007/s10584-011-0020-1.

Gutzler, D.S., and T. O. Robbins (2011). Climate variability and projected change in the western United States: regional downscaling and drought statistics. *Climate Dynamics*, **37**, 835–849. DOI 10.1007/s00382-010-0838-7.

Hatfield, J. L., K. J. Boote, B. A. Kimball, D. W. Wolfe, D. R. Ort, R. C. Izaurralude, A. M. Thomson, J. A. Morgan, H. W. Polley, and P. A. Fay (2008). Agriculture. In The Effects of Climate Change on Agriculture, Land Resources, Water Resources, and Biodiversity in the United States. U.S. Climate Change Science Program and Subcommittee on Global Change Research, Washington, DC.

Hawkins, E., and R. Sutton (2011). The potential to narrow uncertainty in projections of regional precipitation change. *Climate Dynamics,* **37**, 407–418. DOI 10.1007/s00382-010-0810-6.

Hawkins, E., and R. Sutton (2012). Time of emergence of climate signals. *Geophysical Research Letters*, **39**, L01702. DOI 10.1029/2011GL050087.

Haughian, S. R., P. J. Burton, S. W. Taylor, and C. L. Curry (2012). Expected Effects of Climate Change on Forest Disturbance Regimes in British Columbia. *BC Journal of Ecosystems and Management*, **13**, 1.

Hansen, J., M. Sato, J. Glascoe, and R. Ruedy (1998). A common-sense climate index: Is climate changing noticeably? *Proceedings of the National Academy of Science*, **95**, 4113–4120.

Hansen, J., R. Ruedy, M. Sato, M. Imhoff, W. Lawrence, D. Easterling, T. Peterson, and T. Karl (2001) A closer look at United States and global surface temperature change. *Journal of Geophysical Research*, **106**, 23947–23963.

Hansen, J., R. Ruedy, M. Sato, and K. Lo (2010), Global surface temperature change, *Reviews of Geophysics*, **48**, RG4004. DOI 10.1029/2010RG000345.

Hansen, J., M. Sato, and R. Ruedy (2012). Perceptions of Climate Change: The New Climate Dice, http://arxiv.org/abs/1204.1286.

Hartz, D. A., J. S. Golden, C. Sister, W.-C. Chuang, and A. J. Brazel (2012). Climate and heat-related emergencies in Chicago, Illinois (2003–2006). *International Journal of Biometeorology*, **56**, 71–83. DOI 10.1007/s00484-010-0398-x.

Hayhoe, K. M. Robson, J. Rogula, M. Auffhammer, N. Millere, J. VanDorn, and D. Wuebbles (2010). An integrated framework for quantifying and valuing climate change impacts on urban energy and infrastructure: A Chicago case study. *Journal of Great Lakes Research*, **36**, 94–105. DOI 10.1016/j.jglr.2010.03.011.

Hebert, P. J., and G. Taylor (1983). The deadliest, costliest, and most intense United States hurricanes of this century (and other frequently requested hurricane facts), NOAA Technical Memorandum NWS NHC 18.

Heim Jr., R. R. (2002). A review of twentieth-century drought indices used in the United States. *BAMS*, **83**, 1149–1165.

Hengeveld, H., B. Whitewood, and A. Fergusson (2005). *An Introduction to Climate Change: A Canadian Perspective.* Environment Canada. Available at http://www.fcm.ca/Documents/reports/PCP/An_Introduction_to_Climate_Change_a_Canadian_perspective_EN.pdf

Hoerling, M., X.-W. Quan, and J. Eischeid (2009). Distinct causes for two principal U.S. droughts of the 20th century, *Geophysical Research Letters*, **36**, L19708. DOI 10.1029/2009GL039860.

Hoerling, M., J. Eischeid, J. Perlwitz, X. Quan, T. Zhang, and P. Pegion (2011). On the Increased Frequency of Mediterranean Drought, *Journal of Climate*, **25**, 2146-2161. DOI 10.1175/JCLI-D-11-00296.1.

Huber, M., and R. Knutti (2012). Anthropogenic and natural warming inferred from changes in Earth's energy balance. *Nature Geoscience,* **5**, 1, 31-36.

IPCC (2007). *Climate Change 2007: The Physical Science Basis. Contribution of Working Group I to the Fourth Assessment Report of the Intergovernmental Panel on Climate Change (AR4-WGI),* Solomon, S., D. Qin, M. Manning, Z. Chen, M. Marquis, K.B. Averyt, M. Tignor, and H.L. Miller *(*eds.*).* Cambridge University Press (Cambridge, UK and New York, USA).

IPCC (2007). *Climate Change 2007: Impacts and Adaptation. Contribution of Working Group II to the Fourth Assessment Report of the Intergovernmental Panel on Climate Change (AR4-WGII),* M.L. Parry, O.F. Canziani, J.P. Palutikof, P.J. van der Linden and C.E. Hanson *(eds).* Cambridge University Press (Cambridge, UK and New York, USA).

IPCC (2012). *Special Report: Managing the Risks of Extreme Events and Disasters to Advance Climate Change Adaptation (SREX). Contribution of Working Groups I & II,* Cambridge University Press, 594 pp. Available at http://ipcc-wg2.gov/SREX/.

Jacobs, S. S., A. Jenkins, C. F. Giulivi, and P. Dutrieux (2011). Stronger ocean circulation and increased melting under Pine Island Glacier ice shelf. *Nature Geoscience*, **4**, 519-523.

Kalkstein, L. S., J. S. Greene, D. M. Mills, A. D. Perrin, J. P. Samenow, and J.-C. Cohen (2008). Analog European Heat Waves For U.S. Cities To Analyze Impacts On Heat-Related Mortality. *BAMS*, **89**, 75-85. DOI 10.1175/BAMS-89-1-75.

Kantha, L. (2006). Time to Replace the Saffir-Simpson Hurricane Scale? *EOS*, **87**, 1, 3-6.

Karl, T. R., J. M. Melillo, and T. C. Peterson, (eds.) (2009). *Global Climate Change Impacts in the United States* (U.S. Global Change Research Program). Cambridge University Press.

Knutson, T. R., and R. E. Tuleya (2004). Impact of CO2-Induced Warming on Simulated Hurricane Intensity and Precipitation: Sensitivity to the Choice of Climate Model and Convective Parameterization. *Journal of Climate*, **17**, 18, 3477-3495.

Knutson, T. R., J. L. McBride, J. Chan, K. Emanuel, G. Holland, C. Landsea, I. Held, J. P. Kossin, A. K. Srivastava, and M. Sugi (2010). Tropical cyclones and climate change. *Nature Geoscience*, **3**, 157-163. DOI 10.1038/NGEO779.

Krawchuk, M. A., and M. A. Moritz (2011). Constraints on global fire activity vary across a resource gradient. *Ecology*, **92**, 1, 2011, pp. 121–132.

Kunkel, K. E., P. D. Bromirski, H. E. Brooks, T. Cavazos, A. V. Douglas, D. R. Easterling, K. A. Emanuel, P. Ya. Groisman, G. J. Holland, T. R. Knutson, J. P. Kossin, P. D. Komar, D. H. Levinson, and R. L. Smith (2008). Observed changes in weather and climate extremes. In: Weather and Climate Extremes in a Changing Climate: Regions of Focus: North America, Hawaii, Caribbean, and U.S. Pacific Islands [Karl, T. R., G. A. Meehl, C. D. Miller, S. J. Hassol, A. M. Waple, and W. L. Murray (eds.)]. Synthesis and Assessment Product 3.3. U.S. Climate Change Science Program, Washington, DC, pp. 35-80.

Kurz, W. A., C. C. Dymond, G. Stinson, G. J. Rampley, E. T. Neilson, A. L. Carroll, T. Ebata, and L. Safranyik, 2008. Mountain pine beetle and forest carbon feedback to climate change. *Nature,* **452**, 987-990. DOI 10.1038/nature06777.

Kwok, R., and D. A. Rothrock (2009). Decline in Arctic sea ice thickness from submarine and ICESat records: 1958–2008. *Geophysical Research Letters*, **36**, L15501. DOI 10.1029/2009GL039035.

Kwok, R., G. F. Cunningham, M. Wensnahan, I. Rigor, H. J. Zwally, and D. Yi (2009). Thinning and volume loss of the Arctic Ocean sea ice cover: 2003 – 2008. *Journal of Geophysical Research*, **114**, C07005. DOI 10.1029/2009JC005312.

Lal, M., K. K. Singh, L. S. Rathore, G. Srinivasan, and S. A. Saseendran (1998). Vulnerability of rice and wheat yields in N.W. India to future changes in climate. *Agricultural and Forest Meteorology*, **89**, 101-114.

Landsea, C. W., G. A. Vecchi, L. Bengtsson, and T. R. Knutson (2010). Impact of duration thresholds on Atlantic tropical cyclone counts. *Journal of Climate*, **23**, 2508–2519. DOI 10.1175/2009JCLI3034.1.

Lee, T., and M. J. McPhaden (2010). Increasing intensity of El Niño in the central-equatorial Pacific. *Geophysical Research Letters*, **37**, L14603. DOI 10.1029/2010GL044007.

Lehikoinen, E. S. A, T. H. Sparks, and M. Zalakevicius (2004). Arrival and Departure Dates. *Advances in Ecological Research*, **35**, 1–31. DOI 10.1016/S0065-2504(04)35001-4.

Lenton, T. M., H. Held, E. Kriegler, J. W. Hall, W. Lucht, S. Rahmstorf, and H. J. Schellnhuber (2008). Tipping elements in the Earth's climate system. *PNAS*, 1**05**, 6, 1786-1793. DOI 10.1073/pnas.0705414105.

Lim, Y-H., A. K. Park, and H. Kim (2012). Modifiers of diurnal temperature range and mortality association in six Korean cities. *International Journal of Biometeorology*, **56**, 33–42. DOI 10.1007/s00484-010-0395-0.

Littell, J. S., D. Mckenzie, D. L. Peterson, and A. L. Westerling (2009). Climate and wildfire area burned in western U.S. ecoprovinces, 1916–2003. *Ecological Applications*, **19**, 4, pp. 1003–1021.

Lobell, D. B., A. Sibley, and J. I. Ortiz-Monasterio (2012). Extreme heat effects on wheat senescence in India. *Nature Climate Change*, **2**, 186-189. DOI 10.1038/NCLIMATE1356.

Lugina, K. M., P. Ya. Groisman, K. Ya. Vinnikov, V. V. Koknaeva, and N. A. Speranskaya (2005). Monthly surface air temperature time series area-averaged over the 30-degree latitudinal belts of the globe, 1881- 2004. In: Trends: A Compendium of Data on Global Change. Carbon Dioxide Information Analysis Center, Oak Ridge National Laboratory, U.S. Department of Energy, Oak Ridge, TN, http://cdiac.esd.ornl.gov/ trends/temp/lugina/lugina.html.

Mann, M., and K. Emanuel (2006). Atlantic hurricane trends linked to climate change, *EOS Transactions of the AGU*, **87**, 24, 233, 238, 241.

Markus, T., J. C. Stroeve, and J. Miller (2009), Recent changes in Arctic sea ice melt onset, freezeup, and melt season length, *Journal of Geophysical Research*, **114**, C12024. DOI 10.1029/2009JC005436.

Matthews, R. B., M. J. Kropff, D. Bachelet, and H. H. Van Laar (1995). The impact of global climate change on rice production in Asia: a simulation study, CAB International, Wallingford and IRRI, Los Baños, Philippines.

Matthews, H. D., and K. Caldeira (2008), Stabilizing climate requires near-zero emissions, *Geophysical Research Letters*, **35**, L04705. DOI 10.1029/2007GL032388.

Maue, R.N. (2011). Recent historically low global tropical cyclone activity. *Geophysical Research Letters*, **38**, L14803. DOI 10.1029/2011GL047711.

Maue, R.N. (2012). National Research Council, *AMS 30th Conference on Hurricanes and Tropical Meteorology*, April 16, 2012.

McKee, T.B., N.J. Doesken, and J. Kleist (1993). The relation of drought frequency and duration to time scales. *Proceedings of the Eighth Conference on Applied Climatology*, 179–84. American Meteorological Society, Boston.

Mendelsohn, R., K. Emanuel, and S. Chonabayashi (2011). The Impact of Climate Change on Global Tropical Storm Damages. The World Bank, Finance Economics and Urban Department, Global Facility for Disaster Reduction and Recovery. Policy Research Working Paper 5562.

Meier, W. (2012). NSIDC: http://nsidc.org/cryosphere/sotc/sea_ice.html. Accessed March 26, 2012.

Menzel, A., T. H. Sparks, N. Estrella, E. Koch, A. Aasa, R. Ahas, K. Alm-Kübler, P. Bissolli, O. Braslavská, A. Briede, F.M. Chmielewski, Z. Crepinsek, Y. Curnel, Å. Dahl, C. Defila, A. Donnelly, Y. Filella, K. Jatczak, F. Måge, A. Mestre, Ø. Nordli, J. Peñuelas, P. Pirinen, V. Remišová, H. Scheifinger, M. Striz, A. Susnik, A.J.H. van Vliet, F.-E. Wielgolaski, S. Zach, and A. Zust, (2006). European phenological response to climate change matches the warming pattern. *Global Change Biology*, **12**, 1969-1976.

Mudelsee, M., M. Börngen, G. Tetzlaff, and U. Grünewald (2003). No upward trends in the occurrence of extreme floods in central Europe. *Nature*, **425**, 166-169. DOI 10.1038/nature01928.

Munich Re (2011). Database Methodology, NatCatSERVICE, Munich, Germany. Available at http://www.munichre.com/touch/naturalhazards/en/natcatservice/database.aspx. Accessed June 12, 2012.

Munich Re (2012). Topics Geo: Natural Catastrophes 2011, Analyses, Assessments, Positions. Münchener Rückversicherungs-Gesellschaft, Geo Risks Research, NatCatSERVICE, Munich, Germany. Available at http://www.munichre.com/publications/302-07225_en.pdf

Mouillot, F., and C. B. Field (2005). Fire history and the global carbon budget: a 1 x 1 fire history reconstruction for the 20th century. *Global Change Biology,* **11**, 398–420 DOI 10.1111/j.1365-2486.2005.00920.x

National Research Council (2011). *Climate Stabilization Targets: Emissions, Concentrations, and Impacts over Decades to Millennia.* Washington, DC: National Academies Press. Available at http://www.nap.edu/catalog.php?record_id=12877.

Nicholls, R. J. (2004). Coastal flooding and wetland loss in the 21st century: changes under the SRES climate and socio-economic scenarios. *Global Environmental Change*, **14**, 69-86.

Nicholls, R. J., and J. A. Lowe (2006). Climate stabilisation and impacts of sea-level rise. Avoiding Dangerous Climate Change, H. J. Schellnhuber, W. Cramer, N. Nakićenović, T. M. L. Wigley and G. Yohe, Eds., Cambridge University Press, Cambridge, 195-202.

Nicholls, R. J., and R. S. J. Tol (2006). Impacts and responses to sea-level rise: a global analysis of the SRES scenarios over the twenty-first century. *Philosophical Transactions of the Royal Society A*, **364**, 1073-1095.

Nicholls, R. J., P. P. Wong, V. R. Burkett, J. O. Codignotto, J. E. Hay, R. F. McLean, S. Ragoonaden, and C. D. Woodroffe (2007). Coastal systems and low-lying areas. *Climate Change 2007: Impacts, Adaptation and Vulnerability. Contribution of Working Group II to the Fourth Assessment Report of the Intergovernmental Panel on Climate Change*, M. L. Parry, O. F. Canziani, J. P. Palutikof, P. J. van der Linden and C. E. Hanson, Eds., Cambridge University Press, Cambridge, UK, 315-356.

Nohara, D., A. Kitoh, M. Hosaka, and T. Oki (2006). Impact of climate change on river runoff. *Journal of Hydrometeorology*, **7**, 1076–1089.

Oreskes, N. (2004). Beyond the ivory tower: The scientific consensus on climate change. *Science*, **306**, 5702, 1686. DOI 10.1126/science.1103618.

PAGES News (2012). **20**, No 1, February 2012. Available at http://www.pages-igbp.org/products/2011-03-28-16-23-06/522-pages-news-vol-20-no1.

Pall, P., T. Aina, D. A. Stone, P. A. Stott, T. Nozawa, A. G. Hilberts, and M. R. Allen (2011). Anthropogenic greenhouse gas contribution to flood risk in England and Wales in autumn 2000, *Nature*, **470**, 7334, 382-385. DOI 10.1038/nature09762.

Palmer, W. C., 1968. Keeping Track of Crop Moisture Conditions, Nationwide: The New Crop Moisture Index, Weatherwise, **21**, 4, 156-161. DOI 10.1080/00431672.1968.9932814.

Peduzzi, P., H. Dao, and C. Herold (2002). Global Risk and Vulnerability Index Trends per Year (GRAVITY), Pages II: Development, Analysis and Results, Geneva, UNDP/BCPR.

Peduzzi, P., H. Dao, C. Herold, and F. Mouton (2009). Assessing global exposure and vulnerability towards natural hazards: the Disaster Risk Index. Natural Hazards and Earth System Sciences, **9**, 1149–1159.

Peduzzi, P., B. Chatenoux, H. Dao, A. De Bono, C. Herold, J. Kossin, F. Mouton, and O. Nordbeck (2012). Global trends in tropical cyclone risk. *Nature Climate Change*, **2**, 4, 289-294. DOI 10.1038/NCLIMATE1410.

Pielke Jr., R.A., J. Gratz, C. W. Landsea, D. Collins, M. A. Saunders, and R. Musulin (2008). Normalized Hurricane Damage in the United States: 1900–2005. *Natural Hazards Review*, **9**, 1, 29-42. DOI 10.1061/(ASCE)1527-6988(2008)9:1(29).

Powell, M. D., and T. A. Rheinhold (2007). Tropical Cyclone Destructive Potential By Integrated Kinetic Energy. *BAMS*, **88**, 513-526. DOI 10.1175/BAMS-88-4-513.

Raible, C. C., P. M. Della-Marta, C. Schwierz, H. Wernli, and R. Blender (2008). Northern Hemisphere Extratropical Cyclones: A Comparison of Detection and Tracking Methods and Different Reanalyses. *Monthly Weather Review*, **136**, 880–897. DOI 10.1175/2007MWR2143.1.

Rampal, P., J. Weiss, C. Dubois, and J.-M. Campin (2011). IPCC climate models do not capture Arctic sea ice drift acceleration: Consequences in terms of projected sea ice thinning and decline, *Journal of Geophysical Research*, **116**, C00D07. DOI 10.1029/2011JC007110.

Raupach, M. R, G. Marland, P. Ciais, C. Le Quéré, J. G. Canadell, G. Klepper, and C. B. Field (2007). Global and regional drivers of accelerating CO2 emissions. *PNAS*, **104**, 10288-10293. DOI 10.1073/pnas.0700609104.

Rignot, E., I. Velicogna, M. R. van den Broeke, A. Monaghan, and J. Lenaerts (2011). Acceleration of the contribution of the Greenland and Antarctic ice sheets to sea level rise, *Geophys. Res. Lett.*, **38**, L05503, doi:10.1029/2011GL046583.

Robine, J-M., S. L. Cheung, S. Le Roy, H. Van Oyen, C. Griffiths, J.-P. Michel, and F. R. Herrmann (2008). Death toll exceeded 70,000 in Europe during the summer of 2003. *Comptes Rendus Biologies*, **331**, 2, 171–178.

Root, T. L., J. T. Price, K. R. Hall, S. H. Schneider, C. Rosenzweig, and J. A. Pounds (2003). Fingerprints of global warming on wild animals and plants. *Nature,* **421**, 57–60.

Rothrock, D. A., D. B. Percival, and M. Wensnahan (2008). The decline in arctic sea-ice thickness: Separating the spatial, annual, and interannual variability in a quarter century of submarine data, *Journal of Geophysical Research*, **113**, C05003. DOI 10.1029/2007JC004252.

Rudolf, B., and J. Rapp (2003). The century flood of the River Elbe in August 2002: Synoptic weather development and climatological aspects. *Quarterly Report of the Operational NWP-Models of the Deutscher Wetterdienst*, Special Topic July 2002, Offenbach, Germany, 7-22.

Schlenker, W., and M. J. Roberts (2009). Nonlinear temperature effects indicate severe damages to U.S. crop yields under climate change. *PNAS*, **106**, 37, 15594–15598. DOI 10.1073/pnas.0906865106.

Schlenker, W., and D. B. Lobell (2010). Robust negative impacts of climate change on African agriculture. *Environmental Research Letters,* **5**, 014010. DOI 10.1088/1748-9326/5/1/014010.

Schneidereit, A., R. Blender, K. Fraedrich, and F. Lunkeit (2007). Icelandic climate and North Atlantic cyclones in ERA-40 reanalyses. *Meteorologische Zeitschrift*, **16**, 1, 17-23(7). DOI 10.1127/0941-2948/2007/0187.

Shakhova, N., I. Semiletov, A. Salyuk, D. Yusupov, and O. Gustafsson (2010). Extensive methane venting to the atmosphere from sediments of the East Siberian Arctic Shelf. *Science*, **327**, 1246-1250. DOI: 10.1126/science.1182221.

Sherwood, S. C., and M. Huber (2010). An adaptability limit to climate change due to heat stress. *PNAS*, **107**, 21, 9552-9555.

Simmons, K. M., and D. Sutter (2011). Economic and societal impacts of tornadoes. ISBN: 9781878220998.

Slangen, A. B. A., C. A. Katsman, R. S. W. van de Wal, L. L. A. Vermeersen, and R. E. M. Riva (2012). Towards regional projections of twenty-first century sea-level change based on IPCC SRES scenarios. *Climate Dynamics,* **38**, 1191–1209. DOI 10.1007/s00382-011-1057-6.

Smith, T. M., and R. W. Reynolds (2005). A global merged land and sea surface temperature reconstruction based on historical observations (1880–1997). *Journal of Climate*, **18**, 2021–2036.

Sommer, J. H., H. Kreft, G. Kier, W. Jetz, J. Mutke, and W. Barthlott (2010). Projected impacts of climate change on regional capacities for global plant species richness. *Proceedings of the Royal Society B,* **277**, 2271-2280. DOI 10.1098/rspb.2010.0120.

Stewart, I. T., D. R. Cayan, and M. D. Dettinger (2005). Changes toward Earlier Streamflow Timing across Western North America, *Journal of Climate*, **18**, pp. 1136-1155.

Stott, P. A., D. A. Stone, and M. R. Allen (2004). Human contribution to the European heatwave of 2003. *Nature*, **432**, 610-613.

St-Pierre, N. R, B. Cobanov, and G. Schnitkey (2003). Economic losses from heat stress by US livestock industries. *Journal of Dairy Science*, **86**, E52–E77, 10.3168/jds.S0022-0302(03)74040-5.

Strauss, B., C. Tebaldi, and R. Ziemlinski (2012a). *Surging Seas: Sea level rise, storms & global warming's threat to the US coast. A Climate Central Report, March 14, 2012.* Available at http://sealevel.climatecentral.org/research/reports/surging-seas/.

Strauss, B.H., R. Ziemlinski, J. L. Weiss, and J. T. Overpeck (2012b). Tidally adjusted estimates of topographic vulnerability to sea level rise and flooding for the contiguous United States. *Environmental Research Letters,* **7**, 014033. DOI 10.1088/1748-9326/7/1/014033

Stroeve, J., M. M. Holland, W. Meier, T. Scambos, and M. Serreze (2007). Arctic sea ice decline: Faster than forecast. *Geophysical Research Letters*, **34**, L09501. DOI 10.1029/2007GL029703.

Tebaldi, C., B. H Strauss, and C. E. Zervas (2012). Modelling sea level rise impacts on storm surges along US coasts. *Environmental Research Letters,* **7**, 014032. DOI 10.1088/1748-9326/7/1/014032.

Terando, A., W. E. Easterling, K. Keller, and D. R. Easterling (2012). Observed and Modeled Twentieth-Century Spatial and Temporal Patterns of Selected Agro-Climate Indices in North America. Journal of Climate, **25**, 2, 473-490. DOI 10.1175/2011jcli4168.1.

Thomas, C. D., A. Cameron, R. E. Green, M. Bakkenes, L. J. Beaumont, Y. C. Collingham, B. F. N. Erasmus, M. Ferreira de Siqueira, A. Grainger, L. Hannah, L. Hughes, B. Huntley, A. S. van Jaarsveld, G. F. Midgley, L. Miles, M. A. Ortega-Huerta, A. T. Peterson, O. L. Phillips, and S. E. Williams (2004). Extinction risk from climate change. *Nature,* **427**, 145-148. DOI 10.1038/nature02121.

Thuiller, W., S. Lavorel, M. B. Araújo, M. T. Sykes, and I. C. Prentice (2005). Climate change threats to plant diversity in Europe. *PNAS*, **102**, 23, 8245-8250. DOI 10.1073/pnas.0409902102.

Trenberth, K. E., L. Smith, T. Qian, A. Dai, and J. Fasullo, 2007: Estimates of the Global Water Budget and Its Annual Cycle Using Observational and Model Data. *Journal of Hydrometeorology*, **8**, 758–769. DOI 10.1175/JHM600.1.

Trömel, S., and C.-D. Schönwiese (2005). A generalized method of time series decomposition into significant components including probability assessments of extreme events and application to observational German precipitation data. *Meteorologische Zeitschrift*, **14**, 417-427.

Ulbrich, U., T. Brücher, A. H. Fink, G. C. Leckebusch, A. Krüger, and J. G. Pinto (2003a). The Central European Floods in August 2002 , Part II: Synoptic causes and considerations with respect to climatic change, *Weather*, **58**, 434-441.

Ulbrich, U., T. Brücher, A. H. Fink, G. C. Leckebusch, A. Krüger, and J. G. Pinto (2003b). The Central European Floods in August 2002, Part I: Rainfall periods and flood development, *Weather*, **58**, 371-376.

Vandentorren, S., and P. Empereur-Bissonnet (2005). Health Impact of the 2003 Heat-Wave in France in Extreme Weather Events and Public Health Responses, Part 2, 81-87. DOI 10.1007/3-540-28862-7_8.

Vautard, R., J. Cattiaux, P. Yiou, J.-N. Thépaut, and P. Ciais (2010). Northern Hemisphere atmospheric stilling partly attributed to an increase in surface roughness. *Nature Geoscience*, **3**, 756–761.

Vecchi, G. A., and T. R. Knutson (2008). On Estimates of Historical North Atlantic Tropical Cyclone Activity. *Journal of Climate*, **21**, 3580–3600. DOI 10.1175/2008JCLI2178.1.

Vecchi, G. A., and A. T. Wittenberg (2010). El Niño and our future climate: where do we stand? *Wiley Interdisciplinary Reviews: Climate Change*, **1**, 2, pages 260–270. DOI 10.1002/wcc.33.

Vecchi, G. A., and T. R. Knutson (2011). Estimating Annual Numbers of Atlantic Hurricanes Missing from the HURDAT Database (1878–1965) Using Ship Track Density. *Journal of Climate*, **24**, 1736-1746. DOI 10.1175/2010JCLI3810.1.

Velicogna, I. (2009). Increasing rates of ice mass loss from the Greenland and Antarctic ice sheets revealed by GRACE, *Geophysical Research Letters*, **36**, L19503. DOI 10.1029/2009GL040222.

Vilibić, I., and J. Šepić (2010), Long-term variability and trends of sea level storminess and extremes in European Seas. *Global and Planetary Change*, **71**, 1–12. DOI 10.1016/j.gloplacha.2009.12.001.

Vincent, L. A., and É. Mekis (2006). Changes in Daily and Extreme Temperature and Precipitation Indices for Canada over the Twentieth Century, *Atmosphere-Ocean*, **44,** 2, 177-193.

Volneya, W. J. A., and R. A. Fleming (2000). Climate change and impacts of boreal forest insects. *Agriculture, Ecosystems & Environment*, **82**, 1–3, 283–294. DOI 10.1016/S0167-8809(00)00232-2.

Wang, X.L., V. R. Swail, and F. W. Zwiers (2006). Climatology and Changes of Extratropical Cyclone Activity: Comparison of ERA-40 with NCEP–NCAR Reanalysis for 1958–2001. *Journal of Climate*, **19**, 3145–3166. DOI 10.1175/JCLI3781.1.

Wang, G., and H. H. Hendona (2007). Sensitivity of Australian Rainfall to Inter–El Niño Variations. *Journal of Climate*, **20**, 4211-4226.

Wassmann, R., S. V. K. Jagadish, K. Sumfleth, H. Pathak, G. Howell, A. Ismail, R. Serraj, E. Redona, R. K. Singh, and S. Heuer (2009). Chapter 3 Regional Vulnerability of Climate Change Impacts on Asian Rice Production and Scope for Adaptation, In: D. L. Sparks, Editor(s), *Advances in Agronomy*, Academic Press, 2009, **102**, 91-133. DOI 10.1016/S0065-2113(09)01003-7.

Webster, P. J., G. J. Holland, J. A. Curry, and H.-R. Chang (2005). Changes in Tropical Cyclone Number, Duration, and Intensity in a Warming Environment, *Science,* **309**, 1844; DOI 10.1126/science.1116448.

Weisse, R., H. von Storch, and F. Feser (2005). Northeast Atlantic and North Sea Storminess as Simulated by a Regional Climate Model during 1958–2001 and Comparison with Observations. *Journal of Climate*, **18**, 465–479. DOI 10.1175/JCLI-3281.1.

Weng, H., S. K. Behera, T. Yamagata (2009). Anomalous winter climate conditions in the Pacific Rim during recent El Niño Modoki and El Niño events, *Climate Dynamics*, **32**, 663–674. DOI 10.1007/s00382-008- 0394-6.

Westerling, A. L., H. G. Hidalgo, D. R. Cayan, and T. W. Swetnam (2006). Warming and Earlier Spring Increases Western U.S. Forest Wildfire Activity, *Science*, **313**, 940-943. DOI 10.1126/science.1128834.

Westerling, A. L., and B. P. Bryant (2008). Climate change and wildfire in California. *Climatic Change*, **87**, Supplement 1, 231-249. DOI 10.1007/s10584-007-9363-z.

Westerling, A. L., M. G. Turner, E. A. H. Smithwick, W. H. Romme, and M. G. Ryan (2011). Continued warming could transform Greater Yellowstone fire regimes by mid-21st century. *PNAS*, **108**, 32, 13165–13170.

Yeh, S.-W., J.-S. Kug, B. Dewitte, M.-H. Kwon, B. Kirtman, and F.-F. Jin (2009). El Niño in a changing climate, *Nature*, **461**, 511–514. DOI 10.1038/nature08316.

Yohe, G.W., E. Malone, A. Brenkert, M. Schlesinger, H. Meij, and X. Xing (2006). Global Distributions of Vulnerability to Climate Change. Integrated Assessment, **6**, 3.

Zemp, M., and J. van Woerden (Eds) (2008). Global glacial changes: facts and figures. World Glacier Monitoring Service, Zurich, Switzerland.

Zhang, T., R. G. Barry, K. Knowles, F. Ling, and R. L. Armstrong (2003). Distribution of seasonally and perennially frozen ground in the Northern Hemisphere, in Proc. 8th Int. Conf. Permafrost, 21–25 July 2003, Zurich, Switzerland, edited by M. Phillips, S. M. Springman, and L. U. Arenson, 1289–1294, A. A. Balkema, Lisse, Netherlands.

Zhang, X., L. A. Vincent, W. D. Hogg, and A. Niitsoo (2000). Temperature and Precipitation Trends in Canada During the 20th Century, *Atmosphere-Ocean,* **38**, 3, 395–429.

Authors of the Report

Charles Curry earned a B.Sc. in Mathematics and Physics at Saint Mary's University in 1988, an M.Sc. in Physics from Queen's University in 1990, and a Ph.D. in Physics from McMaster University in 1995. Since 2003, he has been engaged in global climate and Earth system modeling, and from 2008-2011 was a Research Scientist at the Canadian Centre for Climate Modelling and Analysis, a division of Environment Canada. He is currently Senior Research Associate in the Climate Modelling Group and Adjunct Professor in the School of Earth and Ocean Sciences at the University of Victoria.

Andrew Weaver received his B.Sc (Mathematics and Physics) from the University of Victoria in 1983, a Certificate of Advanced Studies in Mathematics from Cambridge University in 1984, and a PhD in Applied Mathematics from the University of British Columbia in 1987. He is the Lansdowne Professor and Canada Research Chair in climate modelling and analysis in the School of Earth and Ocean Sciences, University of Victoria. Dr. Weaver was a Lead Author in the United Nations Intergovernmental Panel on Climate Change 2nd, 3rd and 4th scientific assessments and is also a Lead Author in the ongoing 5th scientific assessment. He was the Chief Editor of the *Journal of Climat*e from 2005-2009. Dr. Weaver is a Fellow of the Royal Society of Canada, Canadian Meteorological and Oceanographic Society and the American Meteorological Society. He is the past recipient of a number of international, national and provincial science and leadership awards. In 2008 he was also appointed to the Order of British Columbia.

Ed Wiebe received a B.Sc in Physics and Ocean Science at the University of Victoria in 1996 and an M.Sc from the School of Earth and Ocean Science at the same institution in 1998. He has worked on a wide variety of climate research related projects with emphasis on computer modelling, data analysis and visualisation. Ed manages and maintains the Vancouver Island School-Based Weather Station network.